非線性港池振盪數值模式研究

執行單位　：　數學模式組

計畫召集人　：　蘇青和　研究員

第一子計畫主持人：　蘇青和　研究員

第二子計畫主持人：　劉立方　教授

共同主持人：　蔡丁貴　教授

第三子計畫主持人：　陳冠宇　助理研究員

行政助理　：　陳毓清

Numerical Modelling of Harbor Oscillations Induced by Nonliner Waves

Ching-Ho Su and Guan-Yu Chen

Mathematical Modelling Devision

Institute of Harbor & Marine Technology

Wuchi, Taichung District, Taiwan

Philip L.-F. Liu

School of Civil and Environmental Engineering

Hollister Hall

Cornell University

Ithaca ,New York ,U.S.A.

Ting-Kuei Tsay

Department of Civil Engineering

National Taiwan University

Taipei, Taiwan

摘 要

第一子計畫介紹本所現有之線性波浪模式,模式包括本所開發研究之邊界元素法模式(Model WH21)、有限元素法模式(Model WE21)、有限差分法模式(Model WP21)及由丹麥水工試驗所(DHI)引進之有限差分法模式MIKE 21 OSW,NSW,PMS及EMS等四個模組。

Model WP21主要應用於推算波浪從外海傳遞至近岸海域之波場分佈,如果海岸線爲平緩沙灘,反射波不明顯之情形,引用拋物線型態緩坡方程式建立之有限差分法模式甚爲適用。在應用貼壁座標轉換,其可取較大之網格點,將節省甚多之記憶體,遠較有限元素法模式爲佳。Model WH21主要應用於推算等水深或水深變化不明顯之不規則形狀港池之波場分佈或港池共振變化,因邊界元素法模式處理一維邊界之元素遠較有限元素法之二維之三角形元素方便。Model WE21主要應用於推算水深緩變化之不規則形狀港池之波場分佈或港池共振變化,在推算港池波場,則不宜使用有限差分法模式(拋物線型態方程式)。

Mike21 OSW模組主要應用於探討在外海深水地區之風浪之進行、成長及減衰等現象。OSW模組之功能包括波浪之產生(風力)、折射、淺化、不同頻率間波與波交互作用等,並以波譜型態完整的描述波浪特性,包括波向之擴展(方向波譜),不同頻率分量之擴展(能量波譜)等。MIKE 21 NSW主要應用於探討近海地區之風浪進行、成長及減衰等現象,NSW模組之功能包括波浪之產生(風力)、折射、淺化、碎波、底床摩擦、波與流交互作用等,並以不規則波譜型態完整描述波向之擴展及不同頻率分量之擴展等現象。因考慮碎波及底床摩擦等效應甚重要之近岸地區,因此也可推算幅射應力(radiation stress)。

MIKE 21 PMS基本方程式爲拋物線型態之緩坡方程式,緩坡方程式基本上可納入折射及繞射等效應,因此PMS模組主要應用於探討含有凸堤或離岸堤等結構物之近岸地區波場變化。MIKE 21 EMS基本方程式爲橢圓型態緩坡方程式,除考慮繞射、折射(淺化)效應,尙可納入波浪反射、部分反射、部份透射之效應。因此EMS模組主要應用於探討結構物複雜波浪繞射,及多次反射現象明顯之港區。

第二子計畫之研究主要建立新的非線性港池振盪有限元素法模式,新的模式包括二維連續方程式及運動方程式之垂直積分理論建立,而描

述弱非線性與弱分散波也爲本模式之基礎。本年度主要探討一維之問題,時間積分方面比較隱性及顯性兩種不同積分結果,而數值計算之穩定及正確爲比較重點。空間積分方面探討 Galerkin 與 Petrov-Galerkin 兩種不同方法之優劣結果,邊界條件則包括有 Dirichlet 邊界條件及 Neumann 邊界條件兩種。最後本文並計算七個應用例子,以探討模式可能之應用範圍及驗證模式之正確性。

第三子計畫針對海洋中四種常見的波，即深水Stokes波、赤道Kelvin波、海岸Kelvin波，與邊緣波(Edge Wave)的弱非線性演化方程進行探討。根據不同的尺度假設，這四種波可分別以Korteweg-de Vries(KdV)方程、Kadomtsev-Petviashvili(KP)方程,nonlinear Schroedinger(NLS)方程其中的一種或兩種來表示，因此本研究首先回顧這三個方程的推導及其特性。其次再就四種波的物理性質分別討論。

非線性演化方程之推得，固然是由基本的流體力學方程藉由尺度假設逐步演算的結果，但是也可以直接由頻散關係式及其他物理特性求得。這樣的方式較爲簡捷，其物理特性也比較容易明白。而且由於頻散關係式與演化方程的對應，吾人可以進一步由已知之演化方程倒推其頻散關係。其缺點則是結果不能涵蓋其他的波動，因此只適用在同一種波的交互作用。此外，頻散關係式通常也不容易求得。最後，本研究介紹幾種數值模式，並進行初步的數值實驗。這些數值實驗的結果可以與理論計算的結果互相印證。本研究部份公式之導得，並利用符號運算軟體Maple，以利爾後驗證與推廣。

線性波場推算數值模式

蘇青和

研究員

數學模式組

港灣技術研究所

Numerical Modelling of Linear Waves

Ching-Ho Su

Mathematical Modelling Devision

Institute of Harbor & Marine Technology

Wuchi, Taichung District, Taiwan

摘 要

本計畫擬介紹本所現有之線性波浪模式,模式包括本所開發研究之邊界元素法模式(Model WH21)、有限元素法模式(Model WE21)、有限差分法模式(Model WP21)及由丹麥水工試驗所(DHI)引進之有限差分法模式MIKE 21 OSW,NSW,PMS及EMS等四個模組。

Model WP21主要應用於推算波浪從外海傳遞至近岸海域之波場分佈,如果海岸線爲平緩沙灘,反射波不明顯之情形,引用拋物線型態緩坡方程式建立之有限差分法模式甚爲適用。在應用貼壁座標轉換,其可取較大之網格點,將節省甚多之記憶體,遠較有限元素法模式爲佳。Model WH21主要應用於推算等水深或水深變化不明顯之不規則形狀港池之波場分佈或港池共振變化,因邊界元素法模式處理一維邊界之元素遠較有限元素法之二維之三角形元素方便。Model WE21主要應用於推算水深緩變化之不規則形狀港池之波場分佈或港池共振變化,在推算港池波場,則不宜使用有限差分法模式(拋物線型態方程式)。

Mike21 OSW模組主要應用於探討在外海深水地區之風浪之進行、成長及減衰等現象。OSW模組之功能包括波浪之產生(風力)、折射、淺化、不同頻率間波與波交互作用等,並以波譜型態完整的描述波浪特性,包括波向之擴展(方向波譜),不同頻率分量之擴展(能量波譜)等。MIKE 21 NSW主要應用於探討近海地區之風浪進行、成長及減衰等現象,NSW模組之功能包括波浪之產生(風力)、折射、淺化、碎波、底床摩擦、波與流交互作用等,並以不規則波譜型態完整描述波向之擴展及不同頻率分量之擴展等現象。因考慮碎波及底床摩擦等效應甚重要之近岸地區,因此也可推算幅射應力(radiation stress)。

MIKE 21 PMS基本方程式爲拋物線型態之緩坡方程式,緩坡方程式基本上可納入折射及繞射等效應,因此PMS模組主要應用於探討含有凸堤或離岸堤等結構物之近岸地區波場變化。MIKE 21 EMS基本方程式爲橢圓型態緩坡方程式,除考慮繞射、折射(淺化)效應,尚可納入波浪反射、部分反射、部份透射之效應。因此EMS模組主要應用於探討結構物複雜波浪繞射,及多次反射現象明顯之港區。

線性波場推算數值模式

目 錄

壹、前 言

有關港池之水波數值推算問題，Miles及Mumk (1961)探討矩形港池開口連接外海，同時考慮由港口傳至外海之幅射效應，應用積分方程方法解析，其理論上可解任意形狀之港池，但積分方程以Green's函數表示，而Green's函數對不規則形狀港池甚難決定，其應用範圍僅討論矩形港池問題。其解析結果提出港池開口縮小反使港內共振情形加劇之港口矛盾論(Harbour paradox)。Ippen及Goda (1963)以富利葉轉換法及變數分離法分別處理矩形港池外海與港內之水位解，至於在港口處做二解之連續交接條件，其理論並與小型矩形港池模型試驗結果比較甚爲吻合。林及王(1982)引用Ippen及Goda (1963)之方法探討矩形港池共振問題，並考慮堤頭的摩擦損失及港口處的水流因收縮及擴張作用而引起的水頭損失，由理論與實驗證明Miles及Munk (1961)提出之港口矛盾論，在某些情形並不成立。

Chen (1986)及Tsay et al. (1989)分別探討包括海底摩擦效應及岸壁爲部份反射邊界之港池共振特性變化，因爲其岸壁部份反射之條件僅以一反射係數計算，所以僅能定性觀察共振點之波能消減變化，而無法實際瞭解透水性岸壁對共振之影響。Chwang at al. (1990)引用Chwang et al. (1989)剛性水面型態多孔岸壁之新觀念於港池內壁，分析比較多孔岸壁和一般不透水直立壁設計之矩形港池與圓形港池，因波浪引起之共振現象改變情形，在計算不同多孔影響參數G_0之共振曲線，他們發現共振點發生位置(共振週期)不因G_0值不同而有所改變，但G_0值之增加，共振點之擴大率快速的減小。此顯示剛性水面型態多孔岸壁設計之港池減振效果甚佳，而多孔影響參數爲決定共振大小之參數。

歐等(1990)探討水深變化對剛性水面型態多孔岸壁港池之共振影響，其模式將水深變化因素納入考慮，其實用範圍更廣泛。蘇等(1992)探討自由水面型態多孔岸壁設計之港池波能消散特性，並比較自由水面型態多孔岸壁與剛性水面型態多孔岸壁之矩形港池共振特性。當多孔影響參數G_0改變時，剛性水面型態多孔岸壁港池，除共振點之擴大率快速的減小，共振週期改變並不明顯，而自由水面型態多孔岸壁港池，當消波室寬度不爲四分之一波長時，考慮不同的多孔影響參數其共振週期改變則甚明顯，此現象表示多孔岸壁港池不但減小共振之強度，而且可能改變共振之週期。蘇(1993)解析剛性表面及自由水面兩種多孔岸壁設計港池之波能消散及共振週期改變情形，並針對計算港池共振之數值方法做深入的探討。消波體中之孔隙介值若引用多孔板理論時，消波岸壁港池之共振特性變化，多孔影響參數爲一重要參數，在不同水位時，消波室寬度也是一個重要決定因素。若消波體中之孔隙介值引用多孔牆理論時，消波岸壁港池之共振特性變化與多孔牆參數、消波室寬度之關係，也是值得深入探討之問題。

一般數學解析方法所能得到之共振正確解(exact solution)局限於某些特殊之港池，如

矩形或圓形港池，但在探討港池共振現象，因港池形狀不規則，近岸通常有結構物存在，波浪繞射爲一重要現象;如果地形又複雜變化，折射效亦爲考慮因素之一。而海底摩擦效應、邊界透水性、堤頭之水頭能量損失及碎波之能量損失皆增加解析之複雜性，因此使用數值方法，以求解波場爲必要之途徑。

在等水深或水深變化不明顯之港池或海域，考慮線性規則波浪條件，波浪繞射現象可以引用荷姆茲方程式(Helmholtz equation)描述。邊界元素法將二維區域問題，利用低維之邊界元素求解，對複雜之港池或海岸線，處理甚爲方便。Hwang及Tuck (1970)、Ho及Bomze (1975)、Lee (1969，1971)、Lee及Raichlen (1971，1972)、Chwang et al. (1990)等引用邊界元素法(boundary element method)或稱積分方程法(integral equation method)，在利用Weber解，由荷姆茲方程式求得積分方程式，將邊界分割爲有限個邊界元素，因而化積分方程式爲一矩陣方程式以求得解。Lee (1969)探討狹長型矩形港池共振問題，發現在共振點之擴大率(測點波高比入射波高)，數值計算結果與其模型試驗結果甚爲吻合，但其理論值則遠較數值結果爲大，其認爲其數值解較理論解正確。Chwang et al. (1990)引用類似Lee (1969)之數值計算方法，其模式則將Lee (1969)之不透性岸壁邊界條件推廣至透水性邊界條件。周宗仁等(1986，1989，1992a，1992b)應用邊界元素法解析任意地形及水深之港池水面波動，並延伸至任意反射率防波堤或岸壁的港池水面振動問題，其引用之控制方程式，則爲三維拉普拉氏方程式(Laplace equation)。

在地形變化不劇烈，即地形緩慢變化之海域或港池，Berkhoff (1972)提出緩坡方程式(mild-slope equation)，並引用有限元素法求解波浪之折繞射共同效應，在外海邊界上則以邊界元素法處理。Chen及Mei (1974)，Chen (1986)發展一混合元素法(hybrid finite element method)，分別求解淺水波方程式及緩坡方程式。其作法爲邊界內以一般有限元素法運算，而其港口外圍邊界則以解析解形式展開。Tsay及Liu (1983)、Tsay et al. (1989)、林及謝(1985)、林及許(1985)、歐等(1990)與蘇(1993)使用與Chen及Mei (1974)類似原理，以求解緩坡方程式。Chen (1986)、Tsay et al. (1989)之數值模式則包括海底摩擦效應及岸壁部份反射邊界及碎波之能量消散效應。歐等(1990)及蘇(1993)之數值模式則考慮港池爲多孔消波岸壁之透水性岸壁。

上述學者之波場推算模式,其理論在外海邊界無窮遠處應滿足Sommerfeld輻射邊界條件，即與港池或結構物作用產生之波浪，在無窮遠之外海處應僅有向外之消散進行波(outgoing progressive wave)存在。而爲滿足此項邊界條件，各種數值方法計算之海域，常分割爲有限港池區及半無限外海區二個區域，而且外海區域必假設爲等水深區(Chen及Mei (1974)、Tsay及Liu (1983)、歐等(1990))。若有海岸線存在之情形,則又必須滿足海岸線平直,且兩邊無限延伸之理想條件;但在沿岸地區，除非擴大數值計算區域，否則外圍鮮少

爲固定水深及海岸線平直等理想條件，因此實際計算非常不方便。

陳及蔡(1990)、蘇等(1991)在有限海域外圍設定局部型式之輻射條件，以取代原來標準型式之無窮遠處輻射條件，以避開外海區域必爲等水深區之假設。陳及蔡(1990)探討兩種輻射條件應用於計算圓形島之折繞射造成之差異。他們發現在考慮地形及波長等因素，適當設置外圍邊界，局部輻射邊界也可得到相近結果。蘇等(1991)探討局部型式輻射條件及原來標準型式輻射條件，應用在港池共振計算之差異。他們解析一等水深矩形港池共振問題，同樣發現在離1/5波長處，即近於滿足輻射條件。基本上滿足輻射條件位置應與相對波長、水深分佈、港池或結構物尺度大小等有關。而在較複雜不規則港池或地形，局部型式輻射條件於實際應用時得需再作進一步的探討。局部型式輻射條件之優點爲可避免外圍等水深之不方便假設。

在等水深或水深變化不明顯之港池或海域，考慮線性規則波浪條件，波浪繞射現象可以引用荷姆茲方程式(Helmholtz equation)描述。邊界元素法將二維區域問題，利用低維之邊界元素求解，對複雜之港池或海岸線，處理甚爲方便。Hwang及Tuck (1970)、Ho及Bomze (1975)、Lee (1969，1971)、Lee及Raichlen (1971，1972)、Chwang et al. (1990)、蘇等(1992)等引用邊界元素法(boundary element method)或稱積分方程法(integral equation method)，在利用Weber解，由荷姆茲方程式求得積分方程式，將邊界分割爲有限個邊界元素，因而化積分方程式爲一矩陣方程式以求得解。周宗仁等(1986，1989，1992a，1992b)應用邊界元素法解析任意地形及水深之港池水面波動，並延伸至任意反射率防波堤或岸壁的港池水面振動問題，其引用之控制方程式，則爲三維拉普拉氏方程式(Laplace equation)。

橢圓形態緩坡方程式，其微分方程屬封閉型態，在邊界必需給定適當的邊界值，才能求得解。以上所述之數值模式皆屬這類型問題，因此在有限海域外圍邊界上需給定適當的入射波條件，而爲了滿足入射波由無限遠進入計算區之條件，計算外圍必需向外深海區延伸，但此卻造成區域之擴大，增大計算所需之電腦記憶體容量。而且在有限元素法模式中解析之變數爲波場水位變化，爲達到合理描述波場分佈變化，網格間之距離不宜太長，一般一個特徵波長內至少取7～10個計算點，如向深海擴大計算區時，網格點數量大增，相對計算機之記憶體增加量，甚爲龐大，除非有較大型之電腦，否則一般電腦可能就無法執行。網格點間距離不宜太長之限制及外圍邊界無法內移之限制爲有限元素法模式在實際應用之重缺點。其次在這樣龐大的區域，切割元素也是一項甚爲費時費力之工作，而最後結點之最佳編號，以減少矩陣之帶寬，也是重要之工作。

波浪從深海區進入近海淺水區，因地形或結構物之影響，波向及波高皆將改變，如何推

算其能量分佈變化爲一重要工作。早期計算近海波場之折射及淺化現象,一般引用波向線理論(wave ray theory),波向線理論爲假設波能延著波向線進行,波向線可能因地形變化改變,因此波向線間之距離可能改變,但能量爲守恒,波向線間距減小,表示波高增大,但波向線理論上不能相交,因爲相交點之距離爲零,波高無限大爲不合理,因此波向線理論無法包容波浪繞射現象。

Booij(1981), Lozano and Liu(1980)及Radder(1979),等學者引用拋物線解析法(parabolic approximation)以解析包括析射及繞射現象之波場,在引用拋物線方程式(parabolic wave equation),改進波向線理論不能容納波向線相交之現象,其理論較完整的納入繞射效應, Liu(1986), Liu(1989), Liu et al (1980)等則納入海底摩擦,碎波和波流交互等效應,更完整的描述實際波場變化。

Liu and Tsay(1985), Tsay and Liu(1982), Tsay et al (1989)等則針對近岸地區之不規則地形及區域,引用曲線座標系統(curvilinear coordinate system),並以數值方法計算貼壁座標系統(boundary-fitted curvilinear coordinate) ,將不規則地區轉換爲長方形網格系統。原有之拋物線方程式經座標轉換新座標再以差分原理,化爲差分方程式。此種方法將可解決區域不規則形狀時之數值網格切割困擾。

拋物型態之波方程式,在微分方程屬拋物線型,因此一般引用有限差分法建立數值模式;而波場計算則由深海推算至近岸區。拋物線模式,其理論基本上無法納入波浪之反射效應,而與海岸線之夾角需爲小入射角($20^0 \sim 30^0$),也是一般之限制(Liu ,1989)。不過因爲拋物線模式所解之波場變數爲振幅及相位變化,因此網格點間距不必像有限元素法模式所要求之嚴格,將可減少甚多之電腦記憶體。

有關海域波場數值推算問題，如引用拋物線模式由深海處推算近岸地區至港口外適當之處,再引用計算結果做爲港內區有限元素法模式之入射波條件,以完整的解析整個近岸地區(包括港池)之波場。

有關線性波場推算數值模式,現有的模式包括本所合作研究之邊界元素法模式(Model WH21)、有限元素法模式(Model WE21)、有限差分法模式(Model WP21)、及由丹麥水工試驗所(DHI)引進之有限差分法模式四個模組: MIKE 21 OSW,NSW,PMS,EMS等。線式模式已甚爲完整，而且部份模組經引用於國內部份港口計算甚爲良好,此處將本所開發三個模組及自丹麥水工試驗所(DHI)引進之四個模組做一較完整之介紹、並列舉例子做使用說明。

—貳、波浪特性介紹—

2-1線性進行波

若線性進行波波向線與正 x 軸成α角度(如圖2-1-1)，水位變化ζ_0之複數表示式爲

$$\zeta_0(x,y,t) = ae^{i(kx\cos\alpha+ky\sin\alpha+\varepsilon)}e^{-i\sigma t} \tag{2.1.1a}$$

或

$$\zeta_0(x,y,t) = ae^{i(\vec{k}\cdot\vec{x}+\varepsilon)}e^{-i\sigma t} \tag{2.1.1b}$$

式中a爲振幅(wave ampltitude)，α爲波向角，$i=\sqrt{-1}$,波向量$\vec{k}=(k\cos\alpha, k\sin\alpha)$,位置向量$\vec{x}=(x,y)$, k爲波數(wave number)，$k=2\pi/L$,L爲波長(wave length)，$\sigma$爲週頻率(radian frequency)，$\sigma=2\pi/T$, T爲波浪週期(wave period), $c=L/T$稱波速(wave velocity)。

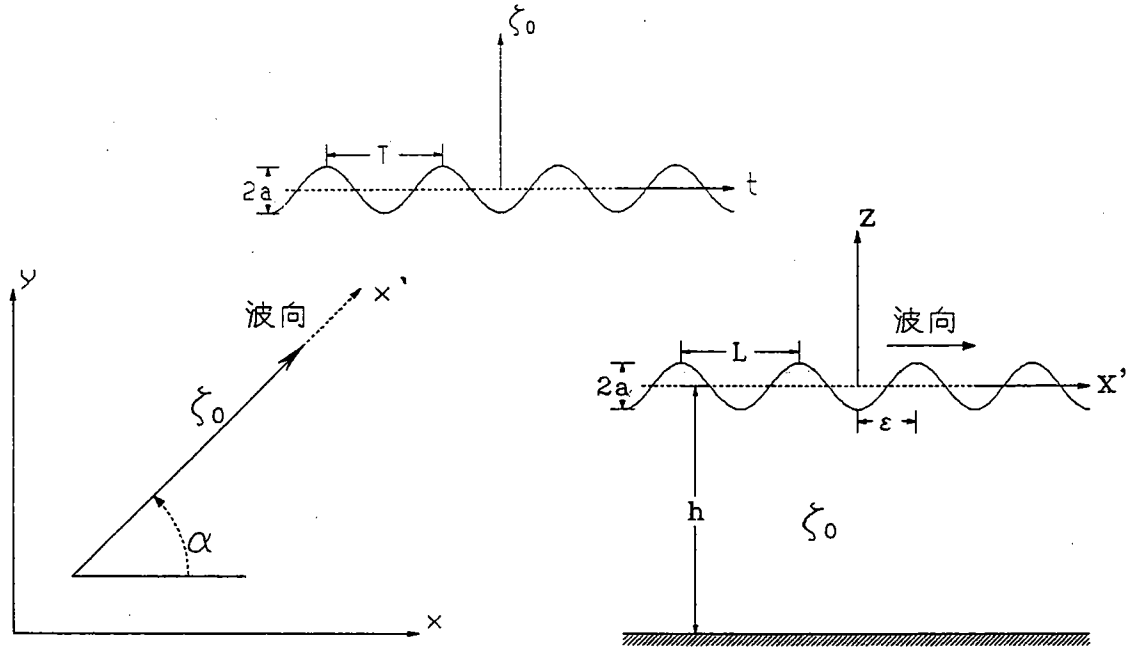

圖2-1-1進行波示意圖

定義

$$s(x,y) = kx\cos\alpha + ky\sin\alpha + \varepsilon \tag{2.1.2a}$$

式中$s(x,y)$稱爲相位，因此方程式(2.1.1)可表示爲

$$\zeta_0(x,y,t) = ae^{is}e^{-i\sigma t} \tag{2.1.2b}$$

若定義

$$\eta_0 = Real[\zeta_0(x,y,t)] = a\cos[kx\cos\alpha + ky\sin\alpha + \varepsilon - \sigma t] \tag{2.1.3}$$

式中η_0爲實際水位，a稱爲波浪振幅，α爲波向角，k爲波數，σ爲週頻率，ε爲相位差。

若$\alpha = 0^0, \varepsilon = 0$,則(由左向右,如附圖2-1-1)

$$\eta_0 = a\cos[kx - \sigma t] \tag{2.1.4a}$$

若$\alpha = 180^0, \varepsilon = 0$,則(由右向左)

$$\eta_r = a\cos[kx + \sigma t] \tag{2.1.4b}$$

η_r稱爲η_0之反射波(reflect wave)。

k,σ與水深h,並滿足下列分散關係式(dispersion relation)

$$\sigma^2 = gk\tanh(kh) \tag{2.1.5}$$

又根據線性波理論,線性進行波之流速勢(potential function)$\Phi_0(x,y,z,t)$與複數水位$\zeta_0(x,y,t)$滿足線性動力邊界條件之下列關係式:

$$\frac{\partial\Phi_0}{\partial t} + g\zeta_0 = 0, \qquad z = 0 \tag{2.1.6}$$

因此線性進行波之流速勢(potential function)$\Phi_0(x,y,z,t)$可表示爲:

$$\Phi_0(x,y,z,t) = \frac{ag}{i\sigma}e^{i(kx\cos\alpha + ky\sin\alpha + \varepsilon)}\frac{\cosh k(h+z)}{\cosh kh}e^{-i\sigma t} \tag{2.1.7}$$

令

$$\Phi_0(x,y,z,t) = \phi_0(x,y)\frac{\cosh k(h+z)}{\cosh kh}e^{-i\sigma t} \tag{2.1.8}$$

式中ϕ_0稱波函數(wave function)表示爲

$$\phi_0(x,y)=\frac{ag}{i\sigma}e^{i(kx\cos\alpha+ky\sin\alpha+\varepsilon)} \tag{2.1.9a}$$

或

$$\phi_0(r,\theta)=\frac{ag}{i\sigma}e^{i[kr\cos(\theta-\alpha)+\varepsilon]} \tag{2.1.9b}$$

(x,y)與(r,θ)滿足

$$x=r\cos\theta,\quad y=r\sin\theta,\quad r=\sqrt{x^2+y^2},\quad \theta=\tan^{-1}(\frac{y}{x}) \tag{2.1.10}$$

定義

$$\phi_0(x,y,z)=A_0e^{is} \tag{2.1.11}$$

$$A_0=\frac{ag}{i\sigma},\qquad s=kx\cos\alpha+ky\sin\alpha+\varepsilon \tag{2.1.12}$$

式中A_0爲波函數振幅,s爲相位。

又根據線性波理論,線性進行波之壓力(presure)$p(x,y,z,t)$與複數水位$\zeta_0(x,y,t)$滿足Bernoulli equation,有下列關係式:

$$p=-\rho gz+\rho\frac{\partial\Phi_0}{\partial t} \tag{2.1.13a}$$

或

$$p=-\rho gz+\rho gK_p\eta \tag{2.1.13b}$$

其中$-\rho gz$爲靜水壓,而動態壓或稱波壓(wave pressure) p_d爲

$$p_d=\rho gK_p\eta \tag{2.1.14a}$$

其中壓力反應因子(the pressure response factor)K_p定義爲

$$K_p=\frac{\cosh k(h+z)}{\cosh kh} \tag{2.1.14b}$$

波力(wave force) F(x,y)定義爲

$$F(x,y)=\int_{-h}^{\eta}p(x,y,z)dz=\frac{1}{2}\rho g(h^2+\eta^2)+\rho gh\frac{\tanh kh}{kh}\eta \tag{2.1.15}$$

水粒子速度$u(x,y,z,t),v(x,y,z,t),w(x,y,z,t)$定義爲

$$u(x,y,z,t)=-\frac{\partial\Phi_0}{\partial x} \tag{2.1.16a}$$

$$v(x,y,z,t)=-\frac{\partial\Phi_0}{\partial y} \tag{2.1.16b}$$

$$w(x,y,z,t)=-\frac{\partial\Phi_0}{\partial z} \tag{2.1.16c}$$

水粒子位移(displacement)(假設$v=0$) $X(x,z,t),Z(x,z,t)$定義爲

$$X(x,z,t)=\int u dt \tag{2.1.17a}$$

$$Z(x,z,t)=\int w dt \tag{2.1.17b}$$

水粒子位移運動爲一橢圓可表示爲:

$$\left(\frac{X}{A}\right)^2+\left(\frac{Z}{B}\right)^2=1 \tag{2.1.18}$$

其中

$$A=a\frac{\cosh k(h+z)}{\sinh kh} \tag{2.1.19a}$$

$$B=a\frac{\sinh k(h+z)}{\sinh kh} \tag{2.1.19b}$$

波浪之平均位能(potential energy) (假設$v=0$)爲

$$\overline{PE}=\frac{1}{L}\int_z^{x+L} d(PE)=\frac{1}{L}\int_z^{x+L}\frac{1}{2}\rho g(h+\eta)^2dx-\frac{1}{2}\rho gh^2=\frac{1}{4}\rho ga^2 \tag{2.1.20}$$

波浪之平均動能(kinetic energy) (假設$v=0$)爲

$$\overline{KE}=\frac{1}{L}\int_z^{x+L}\int_{-h}^{\eta} d(KE)=\frac{1}{L}\int_z^{x+L}\int_{-h}^{\eta}\frac{1}{2}\rho(u^2+w^2)dxdz=\frac{1}{4}\rho ga^2 \tag{2.1.21}$$

波浪之平均總能(Total energy) (假設$v=0$)爲

$$E = \overline{PE} + \overline{KE} = \frac{1}{2}\rho g a^2 \tag{2.1.22}$$

波浪週期能量通(energy flux)爲

$$\Im = \frac{1}{T}\int_t^{t+T}\int_{-h}^{\eta} p_d \cdot u dz dt = C_g E \tag{2.1.23}$$

式中C_g稱群波速(group velocity)或稱能量傳遞速度表示爲

$$C_g = nC = \frac{1}{2}\left(1 + \frac{2kh}{\sinh 2kh}\right)C \tag{2.1.24}$$

式中n稱爲淺化因子(shoaling factor)表示爲

$$n = \frac{1}{2}\left(1 + \frac{2kh}{\sinh 2kh}\right) \tag{2.1.25}$$

群波速(group velocity)也可定義爲

$$C_g = \frac{d\sigma}{dk} \tag{2.1.26}$$

重要參數說明:

@ 波高(wave height) $H = 2a$ 。

@ 波數(wave number) $k = 2\pi/L$ 。

@ 週頻率(radian frequency) , $\sigma = 2\pi/T$ 。

@ 波速(wave velocity) $c = L/T$ 。

@ 相對振幅(relative wave amplitude) : $\epsilon = \frac{a}{h}$ $(=\frac{H}{h})$.

@ 尖銳度(wave slope ,steepness) : $\delta = \frac{a}{L}$ $(=\frac{H}{L})$.

@ Ursell parameter : $U_r = \frac{aL^2}{h^3}$.

@ 相對水深(relative depth) : $\mu = \frac{h}{L}$.

@ 淺水波(shallow-water wave,long wave): $\mu(kh) << 1$, $\cosh kh = 1, \sinh kh = kh$ 。

@ 深水波(deep-water wave,short wave): $\mu(kh) >> 1$, $\cosh kh = \sinh kh = 1/2e^{kh}$ 。

波長L、週期T、波速C、群波速C_g與水深h之關係:

@ 深水波(Deep Water Wave), $\mu = h_0/L_0 > 0.5$,$L_0 = 1.57T_0^2$,$C_0 = 1.57T_0$,$\sigma^2 = gk_0$,$n = 1/2$,$C_g = 1/2C$ 。

@ 淺水波(Shallow Water Wave), $\mu = h/L < 0.05$, $C = \sqrt{gh}$,n=1,$C_g = C$ 。

表2-1-1 μ, h, T, L, C之關係值

$\mu = h/L$	h(m)	T(sec)	L(m)	C(m/s)
0.21	1000	10	157	15.7
0.21	10	6	48.4	8.1
0.14	10	8	70.8	8.9
0.11	10	10	92.3	9.2
0.09	10	12	113.2	9.4
0.36	20	6	55.0	9.2
0.23	20	8	88.7	11.1
0.17	20	10	121.1	12.1
0.13	20	12	152.3	12.7
0.00001	10	12.4hr	440km	10.0

2.2 波浪之反射及透射

若線性進行波波向線與正 x 軸成α角度(如圖2-1-1)，水位變化ζ_0之複數表示式爲

$$\zeta_0(x,y,t) = ae^{i(kx\cos\alpha+ky\sin\alpha)}e^{-i\sigma t} \tag{2.2.1}$$

當線性進行波作用於一垂直結構物，則反射波之水位變化ζ_r之複數可表示式爲

$$\zeta_r(x,y,t) = a_re^{i(kx\cos\alpha-ky\sin\alpha+\varepsilon_r)}e^{-i\sigma t} \tag{2.2.2}$$

式中a_r稱爲反射波波浪振幅，，ε_r爲相位差。

若$\alpha = 0^0, \varepsilon = 0$,則

$$\eta_0 = a\cos[kx - \sigma t] \tag{2.2.3a}$$

$$\eta_r = a_r\cos[kx + \sigma t + \varepsilon_r] \tag{2.2.3b}$$

假設結構物爲完全反射體則$a = a_r$,且$\varepsilon_r = 0$。即

$$\eta_0 = a\cos[kx - \sigma t] \tag{2.2.4a}$$

$$\eta_r = a\cos[kx + \sigma t] \tag{2.2.4b}$$

$$\eta_s = \eta_0 + \eta_r = a\cos kx\cos\sigma t \tag{2.2.4c}$$

η_s稱駐波(standing wave)。

若結構物可部分穿透則透射波之水位變化ζ_t之複數可表示式爲

$$\zeta_t(x,y,t) = a_te^{i(kx\cos\alpha+ky\sin\alpha+\varepsilon_r)}e^{-i\sigma t} \tag{2.2.5}$$

式中a_t稱爲透射波波浪振幅，，ε_t爲相位差。

一般反射係數定義爲

$$C_r = \frac{a_r}{a} \tag{2.2.6a}$$

透射係數定義爲

$$C_t = \frac{a_t}{a} \tag{2.2.6b}$$

考慮多孔消波體(porous wave absorber)爲由厚度2b之垂直多孔牆(porous structure)位於x-軸方向爲半無限長之等水深區域,如圖2-2-1所示,

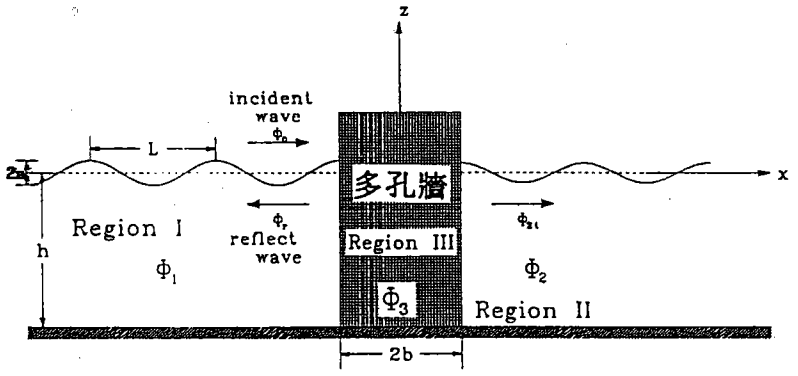

圖2-2-1多孔消波體設計側視示意圖

(其中心面置於x=0平面上)。座標定義如示意圖，xy平面置於平均海平面上，軸原點置於多孔牆中央處，正x軸與入射波傳播方向相同，且波向線與正x-軸成θ_0角，y軸方向爲無限長，垂直進入書面爲正，z軸向上爲正，h爲平均水深，多孔牆前水域(稱水域I，$x \le -b$)及消波室內水域(稱水域II，$b \le x \le b+d$)之流體運動，假設滿足不可壓縮、無黏性及非旋流之條件，因此存在流速勢(velocity potential) $\Phi_j(x,y,z,t), j=1,2$ 分別滿足拉普拉氏方程式(Laplace equation)：

$$\frac{\partial^2 \Phi_j}{\partial x^2}+\frac{\partial^2 \Phi_j}{\partial y^2}+\frac{\partial^2 \Phi_j}{\partial z^2}=0, \qquad j=1,2 \tag{2.2.7}$$

Φ_1, Φ_2分別表示在水域I及水域II內之流速勢，水域I及水域II內之壓力P_j在小振幅波之條件下滿足線性伯努力方程式(Bernoulli equation)：

$$\frac{\partial \Phi_j}{\partial t}+\frac{P_j}{\rho}+gz=0, \qquad -h \le z \le 0, \qquad j=1,2 \tag{2.2.8}$$

式中ρ爲水之密度，g爲重力加速度。

關於多孔牆體內流體運動及波動之現象，引用Sollitt及Cross(1972)孔隙介質流體運動理論，假設在多孔牆內介質爲剛體結構，流體在孔隙內之運動爲不可壓縮，非旋轉流,存在多孔流速勢Φ_3 (pore velocity potential)與滲流速度$\vec{U}_{3s}$ (seepage velocity)之關係爲$\nabla \Phi_3 = \vec{U}_{3s}$，因此拉普拉氏方程式同樣表示爲：

$$\frac{\partial^2 \Phi_3}{\partial x^2}+\frac{\partial^2 \Phi_3}{\partial y^2}+\frac{\partial^2 \Phi_3}{\partial z^2}=0 \tag{2.2.9}$$

根據線性Lorentz's等功原理(Lorentz's condition of equivalent work) (Sollitt及Cross 1972)，即在一週期內以線性機構取代非線性機構,並確定兩者具有相等能量條件下，在多孔介質內之波動頻率與作用於介質外之波浪頻率σ相同，並引用無因次摩擦係數f (dimensionless friction coefficient)及慣性係數s (inertial coefficient)兩個參數，描述流體在多孔牆內之阻尼效應，得到多孔介質流體伯努力方程式:

$$s\frac{\partial \Phi_3}{\partial t}+\frac{P_3}{\rho}+gz+f\sigma\Phi_3=0, \qquad -h\le z\le 0 \tag{2.2.10}$$

式中P_3爲波浪引起之孔隙壓力(pore pressure)，σ爲波浪週頻率,慣性係數s (Sollitt及Cross, 1972)定義爲

$$s=1+\frac{1-\varepsilon}{\varepsilon}C_M \tag{2.2.11a}$$

式中ε爲孔隙率，C_M爲透水結構物產生之附加質量係數,需由試驗決定。s之值理論上取決於孔隙率ε及多孔結構物之孔隙形狀，一般實際計算取1,例如Sollitt及cross (1972) ,Madsen (1974) , Dalrymple et al. (1991)等，而Le Méhaute (1957)及Sulisz(1985)由實驗探討拋石堆結構體(rubble-mound porous structure)，則認爲s值較接近於2。s值有待進一步探討,本文僅以理論值s=1從事計算。摩擦係數f與作用波浪之特性、介質內流體之水量流速(discharge velocity) $\vec{U}_3(\vec{U}_3=\varepsilon\vec{U}_{3s})$、流體運動滯性係數$\nu$及透水結構物之孔隙率$\varepsilon$、透水度$K_p$(intrinsic permeability)、亂流阻尼係數C_f(turbulent resistance coefficient)等有關,在線性理論中不易決定，一般由多孔體參數(ε, K_p, C_f)及流體參數$(\nu, \vec{U}_3)$,在一多孔體積V內一週期平均以下列表示式計算而得(Sollitt及Cross, 1972)

$$f=\frac{1}{\sigma}\frac{\int_V dV\int_t^{t+T}(\frac{\nu|\vec{U}_3|^2}{K_p}+\frac{C_f\varepsilon}{K_p}|\vec{U}_3|^3)dt}{\int_V dV\int_t^{t+T}\varepsilon|\vec{U}_3|^2dt} \tag{2.2.11b}$$

摩擦係數f值在實際應用需經多次複雜疊代計算決定，此處在考慮均勻透水結構物，爲簡化計算則取常數。f值理論上可由零至無限大，一般多孔型態防波堤之數量級爲O(1)。假設多孔牆之流體運動爲無阻泥(f=0)及無虛擬質量影響(s=1)則多孔介質流體伯努力方程式(2.2.10)可退化爲線性波伯努力方程式(2.2.8)。

若入射波波向線與正x軸成θ_0角度(如圖2-2-2)，水位變化η_0之複數表示式爲

$$\eta_0(x,y,t)=a_0e^{-i[\sigma t+k_0(x+b)\cos\theta_0+k_0y\sin\theta_0]} \tag{2.2.12}$$

式中a_0爲振幅(wave ampltitude) , $i=\sqrt{-1}$, k_0爲波數(wave number) ,$k_0=2\pi/L$,L爲波長(wave length), σ爲週頻率(radian frequency)，$\sigma=2\pi/T$, T爲波浪週期(wave period)。

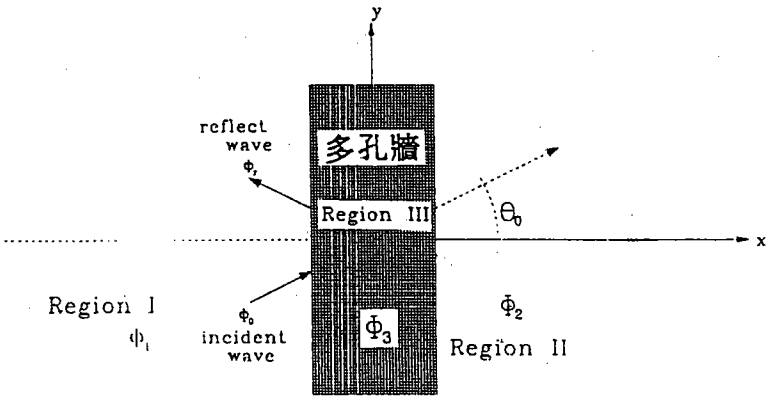

圖 2-2-2 多孔消波體設計上視示意圖

類似聲波在穿過不同介值傳播(Morse及Ingard ,1968)或電磁波通過導引介面(Yeh ,1988)之穿透和反射特性，我們假設線性入射波在多孔牆體內，或通過多孔牆進入消波室，其穿透波進行之週期不改變及 y 軸方向波長不改變(Snell's law)(Dalrymple et al. , 1991)，則在區域 I 、II 及III之流速勢Φ_j可表示爲:

$$\Phi_j(x,y,z,t) = \phi_j(x,z)e^{-i(\sigma t + k_0 y sin\theta_0)} \qquad j = 1,2,3 \tag{2.2.13}$$

將(2.2.13)式代入(2.2.7)或(2.2.9)式化簡可得

$$\frac{\partial^2 \phi_j}{\partial x^2} + \frac{\partial^2 \phi_j}{\partial z^2} - k_0^2 sin^2\theta_0 \phi_j = 0, \qquad j = 1,2,3 \tag{2.2.14}$$

水域 I 及室內水域 II 分別滿足線性自由動力邊界(DBC)及運動邊界條件(KBC):

$$\frac{\partial \Phi_j}{\partial t} + g\eta_j = 0, \qquad z = 0, \qquad j = 1,2 \tag{2.2.15a}$$

$$\frac{\partial \eta_j}{\partial t} - \frac{\partial \Phi_j}{\partial z} = 0, \qquad z = 0, \qquad j = 1,2 \tag{2.2.15b}$$

上二式可合併爲

$$\frac{\partial^2 \Phi_j}{\partial t^2} + g\frac{\partial \Phi_j}{\partial z} = 0, \qquad z = 0, \qquad j = 1,2 \tag{2.2.15c}$$

式中$\eta_1(x,y,t), \eta_2(x,y,t)$分別表示水域 I 及水域II之水位變化。

當入射波斜向作用於消波體，波浪與結構物交互作用產生之成份波$\overline{\Phi}_1$，定義爲$\overline{\Phi}_1 = \Phi_1 - \Phi_0$，其中$\Phi_0$爲入射波，$\overline{\Phi}_1$在無窮遠處$(x \to -\infty)$，應滿足下列輻射條件(radiation condition):

$$\lim_{x\to-\infty}(\frac{\partial\overline{\Phi}_1}{\partial x}-ik_0\overline{\Phi}_1)=0 \tag{2.2.16}$$

即$\overline{\Phi}_1$爲向外傳遞波(out-going wave)。

在多孔牆內(區域III)之假想自由表面$\eta_3(x,y,t)$，滿足線性動力邊界條件及運動邊界條件：

$$s\frac{\partial\Phi_3}{\partial t}+g\eta_3+f\sigma\Phi_3=0, \qquad z=0 \tag{2.2.17a}$$

$$\frac{\partial\eta_3}{\partial t}-\frac{\partial\Phi_3}{\partial z}=0, \qquad z=0 \tag{2.2.17b}$$

同樣二式可合併爲

$$s\frac{\partial^2\Phi_3}{\partial t^2}+g\frac{\partial\Phi_3}{\partial z}+f\sigma\frac{\partial\Phi_3}{\partial t}=0, \qquad z=0 \tag{2.2.18}$$

而不透水海底邊界條件爲

$$\frac{\partial\Phi_j}{\partial z}=0, \qquad z=-h, \qquad j=1,2,3 \tag{2.2.19}$$

$\overline{\Phi}_2$在無窮遠處$(x\to\infty)$,應滿足下列輻射條件(radiation condition)：

$$\lim_{x\to\infty}(\frac{\partial\Phi_2}{\partial n}+ik_0\Phi_2)=0 \tag{2.2.20}$$

基於入射波條件及線性理論，我們可知波壓皆爲週期性函數表示爲

$$P_j(x,y,z,t)=p_j(x,z)e^{-i(\sigma t+k_0 y sin\theta_0)}, \qquad j=1,2,3 \tag{2.2.21}$$

在多孔牆左側(x=-b)及右側(x=+b)分別爲區域I與區域III，區域II與區域III之界面處，必滿足壓力連續條件：

$$\Phi_1=-i\gamma\Phi_3, \qquad x=-b \tag{2.2.22a}$$

$$\Phi_2=-i\gamma\Phi_3, \qquad x=+b \tag{2.2.22b}$$

及流體質量連續條件:

$$\frac{\partial \Phi_1}{\partial x} = \varepsilon \frac{\partial \Phi_3}{\partial x}, \qquad x = -b \tag{2.2.22c}$$

$$\frac{\partial \Phi_2}{\partial x} = \varepsilon \frac{\partial \Phi_3}{\partial x}, \qquad x = +b \tag{2.2.22d}$$

式中ε爲孔隙率(porosity),表示多孔體孔隙所佔全體積之比率，$\gamma = f + is$爲阻抗係數(impedence)。

若多孔牆之厚度極薄($b = \Delta b \to 0$)，多孔牆退化爲多孔板(porous plate)，根據方程式(2.2.22)之壓力連續條件仍然滿足

$$\Phi_1 = -i\gamma \Phi_3, \qquad x = -\Delta b \tag{2.2.23a}$$

$$\Phi_2 = -i\gamma \Phi_3, \qquad x = +\Delta b \tag{2.2.23b}$$

及流體質量連續條件:

$$\frac{\partial \Phi_1}{\partial x} = \varepsilon \frac{\partial \Phi_3}{\partial x}, \qquad x = -\Delta b \tag{2.2.23c}$$

$$\frac{\partial \Phi_2}{\partial x} = \varepsilon \frac{\partial \Phi_3}{\partial x}, \qquad x = +\Delta b \tag{2.2.23d}$$

方程式(2.2.23)顯示只要多孔板厚度不爲零,基本上不管板厚度如何的薄,板左右兩側之壓力及流速並不一定相同。但若左右兩側孔隙率ε相同,則因滿足勢能流(potential flow)之流量守衡原理,板左右兩側流速應相等,但兩側壓力不相等。

Chwang (1983)認爲多孔板(數學上以零厚度處理,即$\Delta b = 0$)滿足線性達西定律，即通過板之流體垂直速度U與板兩側壓力差成正比關係，且因板之存在，其兩側流體質量應滿足連續條件，但兩側則應存在壓力差表示爲

$$U = \frac{b_0}{\mu}(P_1 - P_2), \qquad x = 0^{\pm} \tag{2.2.24a}$$

$$U = \frac{\partial \Phi_1}{\partial x} = \frac{\partial \Phi_2}{\partial x}, \qquad x = 0^{\pm} \tag{2.2.24b}$$

式中μ爲流體動力滯性係數，b_0爲波浪作用下之多孔板特性係數(爲長度單位)，應理解爲在固定板厚度及固定入射波頻率下之常數。

比較Sollitt及Cross (1972)有厚度多孔牆退化之多孔板介面條件(2.2.23)及Chwang (1983)之多孔板介面條件(2.2.24)兩者之形式及表示物理意義並不完全相同，我們將深入比較二者之關係。

將方程式(2.2.10)兩邊取$\frac{\partial}{\partial x}$可得到

$$\frac{s}{\varepsilon}\frac{\partial U_3}{\partial t}+\frac{1}{\rho}\frac{\partial P_3}{\partial x}+\frac{f}{\varepsilon}\sigma U_3=0, \tag{2.2.25}$$

式中$U_3=\varepsilon\frac{\partial \Phi_3}{\partial x}$爲通過板流速$\vec{U}_3$之垂直速度分量。

考慮到$U_3=u_3e^{i\sigma t}$,方程式(2.2.25)可化爲:

$$U_3=\frac{-\varepsilon}{\rho\sigma\gamma}\frac{\partial P_3}{\partial x}, \qquad -\Delta b<x<\Delta b \tag{2.2.26}$$

當$b=\Delta b$很小時,可以認爲在$-\Delta b<x<\Delta b$範圍$\frac{\partial P_3}{\partial x}$用以下差分式近似

$$\frac{\partial P_3}{\partial x}=\frac{1}{2\Delta b}(P_2-P_1), \qquad -\Delta b<x<\Delta b \tag{2.2.27}$$

因此

$$U_3=\frac{b_0'}{\mu}(P_1-P_2), \qquad -\Delta b<x<\Delta b \tag{2.2.28a}$$

且

$$U_3=\frac{\partial \Phi_1}{\partial x}|_{x=-\Delta b}=\frac{\partial \Phi_2}{\partial x}|_{x=\Delta b}, \qquad -\Delta b<x<\Delta b \tag{2.2.28b}$$

式中$b_0'=\frac{\varepsilon\mu}{2\rho\sigma\Delta b\gamma}$爲波浪做用下之多孔板特性係數(爲長度單位)，與孔隙率ε、阻抗係數γ(包括慣性係數s及摩擦係數f)有關，同樣應理解爲在固定板厚度及固定入射波頻率下之常數，b_0'爲複數。

比較由多孔牆退化之多孔板介面條件(2.2.28)式及Chwang(1983)之多孔板介面條件(2.2.24)兩者之形式相似，但二者之多孔板特性係數b_0及b_0'表達之物理特性不同,b_0爲實數(阻抗係數γ僅有摩擦阻力之影響),b_0'爲複數(阻抗係數γ包括摩擦阻力及慣性力效應)。在多孔板相對波長甚薄時,板兩側之相位差不明顯,慣性力效應不顯著,摩擦阻力之影響遠大於慣性力(此乃達西定理之條件)即$f>>s$,則介面條件(2.2.28)式退化爲Chwang(1983)之多孔板介面條件(2.2.24)式。此則顯示Sollitt及Cross (1972)之原理與Chwang(1983)是相通一致的。Chwang(1983)引用多孔板特性係數b_0及μ,而多孔牆之特性係數有牆厚度2b、孔隙率ε、慣性係數s及摩擦係數f等,基本上多孔板之理論是多孔牆原理之簡易退化型態。多孔牆理論較週延,多孔板則使用簡易方便,後者分析之結果可非常清楚看出一

些基本特性,有其實用上價值。Chwang(1983)提出之多孔板特性表示式(2.2.24),一般由多孔板引用爲界面邊界條件,其原理滿足基本物理特性,數學上板以零厚度處理,簡易方便。

因入射波之作用，多孔牆前後水域及牆體內水域皆存在自由水面波動。由控制方程式(2.2.14)及入射波條件(2.2.12)式，邊界條件(2.2.15)、(2.2.16)、(2.2.18)、(2.2.19)、(2.2.20)式及週期函數特性條件(2.2.13)，區域I, II及III之波函數ϕ_j (wave function)可分別表示爲：

$$\phi_1(x,z) = A\cosh[k_0(h+z)]e^{-i\overline{k}_0(x+b)} + R_0 A\cosh[k_0(h+z)]e^{i\overline{k}_0(x+b)} + \sum_{n=1}^{\infty} R_n A\cos[k'_n(h+z)]e^{\overline{k}'_n(x+b)}$$
$$x \le -b, \quad -h \le z \le 0 \tag{2.2.29}$$

$$\phi_2(x,z) = \sum_{n=0}^{\infty} T_n A\cosh[k_n(h+z)]e^{-i\overline{k}_n(x-b)}$$
$$b \le x, \quad -h \le z \le 0 \tag{2.2.30}$$

$$\phi_3(x,z) = \sum_{m=1}^{\infty}\{A_m A\cosh[K_m(h+z)]e^{-i\overline{K}_m(x+b)} + B_m A\cosh[K_m(h+z)]e^{i\overline{K}_m(x-b)}\}$$
$$-b \le x \le +b, \quad -h \le z \le 0 \tag{2.2.31}$$

表示式(2.2.29)等號右邊第一項ϕ_0爲區域I入射波:

$$\phi_0 = A\cosh[k_0(z+h)]e^{-i\overline{k}_0(x+b)} \tag{2.2.32a}$$

其中常數A定義爲

$$A = \frac{iga}{\sigma\cosh(k_0 h)} \tag{2.2.32b}$$

$\overline{k}_0$稱爲修正波數

$$\overline{k}_0 = k_0\cos\theta_0 \tag{2.2.32c}$$

k_0並滿足下列分散關係式(dispersion relation)

$$\sigma^2 = gk_0\tanh(k_0 h), \qquad k_0 > 0 \tag{2.2.33a}$$

或

$$\frac{1}{C_0} = k_0 h \tanh(k_0 h), \qquad k_0 > 0 \tag{2.2.33b}$$

其中$C_0 = g/\sigma^2 h$稱爲無因次波浪影響參數(dimensionless wave-effect parameter)。

(2.2.29)式等號右邊第二項ϕ_{1r}爲區域 I 反射波(reflected wave)：

$$\phi_{1r} = R_0 A \cosh[k_0(z+h)] e^{i\bar{k}_0(x+b)} \tag{2.2.34}$$

式中R_0爲未定係數。

(2.2.29)式等號右邊第三項ϕ_{1s}爲區域 I 之衰減波(evanescent waves)：

$$\phi_{1s} = \sum_{n=1}^{\infty} R_n A \cos[k'_n(h+z)] e^{\bar{k}'_n(x+b)} \tag{2.2.35}$$

式中R_n爲未定係數,n=1,2,3...，k_n滿足下列特徵方程式

$$\sigma^2 = -g k'_n \tan(k'_n h), \qquad n = 1, 2, 3... \tag{2.2.36a}$$

或

$$\frac{-1}{C_0} = k'_n h \tan(k'_n h) \tag{2.2.36b}$$

且

$$\bar{k}'_n = \sqrt{k'^2_n + k_0^2 \sin^2\theta_0} \tag{2.2.37}$$

ϕ_{1s}之振幅隨水平距離增加呈指數遞減,在無窮遠處,應滿足下列條件

$$\lim_{x \to -\infty} \phi_{1s} = 0 \tag{2.2.38}$$

(2.2.30)式等號右邊第一項當n=0爲多孔牆右側之透過進行波ϕ_{2t}：

$$\phi_{2t} = T_0 A \cosh[k_0(h+z)] e^{-i\bar{k}_0(x-b)} \tag{2.2.39a}$$

T_0爲未定係數。

(2.2.30)式等號右邊第一項當$n \geq 1$爲多孔牆右側之透過消散波ϕ_{2s}：

$$\phi_{2s} = \sum_{n=1}^{\infty} T_n A \cosh[k_n(h+z)] e^{-i\bar{k}_n(x-b)} \tag{2.2.39b}$$

T_n為未定係數,ϕ_{2s}其特性水深方面爲週期振盪，水平方向則呈指數遞減。

表示式(2.2.31)等號右邊第一項ϕ_{3r}定義爲

$$\phi_{3r}=\sum_{m=1}^{\infty}A_m A\cosh[K_m(h+z)]e^{-i\overline{K}_m(x+b)} \tag{2.2.40a}$$

此項成份波代表在多孔牆內向右進行並呈指數消散之透過消散進行波(exponentially damped sinusoidal propagating waves)。

(2.2.31)式等號右邊第二項ϕ_{3l}定義爲

$$\phi_{3l}=\sum_{m=1}^{\infty}B_m A\cosh[K_m(h+z)]e^{i\overline{K}_m(x-b)} \tag{2.2.40b}$$

則代表在多孔牆內向左進行並呈指數消散之反射消散進行波。所謂消散進行波,表示波浪爲進行波,但其振幅則隨水平距離之增加呈指數衰減。一般m愈大之成份波振幅愈小,衰減愈快。而複數特微值K_m爲下列特徵方程式之根

$$-i\sigma^2\gamma=gK_m\tanh(K_m h) \qquad ,m=1,2,3... \tag{2.2.41a}$$

或

$$\frac{-i\gamma}{C_0}=K_m h\tanh(K_m h) \tag{2.2.41b}$$

K_m爲複數,K_m之實部$K_{mr}\geq 0$，虛部$K_{mi}\leq 0$，根據Dalrymple et al. (1991)之解析,一般在阻尼係數f不大(小於1.2以下),或波長較長時皆爲一個特徵值K_m對應式(2.2.31)中一個特徵函數,但在一些特別情形時,如阻尼係數f較大,且波長較短時一個特徵值可能對應式(2.2.31)中兩個以上之特徵函數,此時表示式則爲不完全解,需另行處理,本文主要探討之問題範圍皆滿足完整性。

$$\overline{K}_m=\sqrt{K_m^2-k_0^2\sin^2\theta_0} \tag{2.2.42}$$

$\overline{K}_m$爲複數,$\overline{K}_m$之實部$\overline{K}_{mr}\geq 0$，虛部$\overline{K}_{mi}\leq 0$。

爲方便k_0, k_n'及K_m等符號統一,定義$k_n=-ik_n'$及$\overline{k}_n'=-i\overline{k}_n$,n=1,2,3...,則有滿足下列$\cosh(k_n z)=\cos(k_n' z)$, $\tanh(k_n z)=-\tan(k_n' z)$之關係式存在。

在低水位時，使用正交序列$\cosh[k_n(h+z)], n=0,1,2,3...$及$\cosh[K_m(h+z)], m=1,2,3...$在水深區(-h,0)之正交性，將表示式(2.2.29)、(2.2.30)及(2.2.31)代入界面連續條件(2.2.22a)、(2.2.22b)、(2.2.22c)及(2.2.22d)，每個項分別做積分運算$\int_{-h}^{0}(\,)\cosh K_m(z+h)dz$,則分別可得

$$N_{0m}+\sum_{n=0}^{\infty}N_{nm}R_n=(s-if)M_{mm}A_m+(s-if)M_{mm}E_m^-B_m \tag{2.2.43a}$$

$$\sum_{n=1}^{\infty}N_{nm}T_n=(s-if)M_{mm}E_m^-A_m+(s-if)M_{mm}B_m \tag{2.2.43b}$$

$$-\overline{k}_0N_{0m}+\sum_{n=0}^{\infty}\overline{k}_nN_{nm}R_n=-\varepsilon\overline{K}_mM_{mm}A_m+\varepsilon\overline{K}_mM_{mm}E_m^-B_m \tag{2.2.43c}$$

$$-\sum_{n=0}^{\infty}N_{nm}\overline{k}_nT_n=-\varepsilon\overline{K}_mM_{mm}E_m^-A_m+\varepsilon\overline{K}_mM_{mm}B_m \tag{2.2.43d}$$

式中

$$N_{nm}=\int_{-h}^{0}\cosh[k_n(h+z)]\cosh[K_m(h+z)]dz$$

$$=\frac{1}{k_n^2-K_m^2}[k_n\sinh(k_nh)\cosh(K_mh)-K_m\sinh(K_mh)\cosh(k_nh)]$$

$$n=0,1,2,3... \qquad m=1,2,3... \tag{2.2.44a}$$

$$M_{mm}=\int_{-h}^{0}\cosh^2[K_m(h+z)]dz=h[\frac{1}{2}+\frac{\sinh(2K_mh)}{4K_mh}]$$

$$m=1,2,3... \tag{2.2.44b}$$

$$E_m^{\pm}=e^{\pm i2b\overline{K}_m}, \qquad m=1,2,3... \tag{2.2.44c}$$

首先分別由式(2.2.43a)、(2.2.43b)消去A_m、B_m係數及由式(2.2.43c)、(2.2.43d)消去A_m、B_m係數可得下列包含未知變數R_n，T_n之方程組：

$$\sum_{n=0}^{\infty}\frac{N_{nm}}{N_{0m}}(\overline{k}_n+\frac{\varepsilon}{s-if}\overline{K}_m)R_n+\sum_{n=0}^{\infty}E_m^-\frac{N_{nm}}{N_{0m}}[\overline{k}_n-\frac{\varepsilon}{s-if}\overline{K}_m]T_n$$

$$=(\overline{k}_0-\frac{\varepsilon}{s-if}\overline{K}_m), \qquad m=1,2.,3... \tag{2.2.45a}$$

$$\sum_{n=0}^{\infty}\frac{N_{nm}}{N_{0m}}(\overline{k}_n-\frac{\varepsilon}{s-if}\overline{K}_m)R_n+\sum_{n=0}^{\infty}E_m^+\frac{N_{nm}}{N_{0m}}[\overline{k}_n+\frac{\varepsilon}{s-if}\overline{K}_m]T_n$$

$$=(\overline{k}_0+\frac{\varepsilon}{s-if}\overline{K}_m), \qquad m=1,2.,3... \tag{2.2.45b}$$

而分別由式(2.2.43a)、(2.2.43c)消去B_m係數及由式(2.2.43b)、(2.2.43d)消去A_m係數可得下列包含未知變數A_m及B_m如下:

$$A_m = \frac{1}{2\varepsilon(s-if)M_{mm}}\{\sum_{n=0}^{\infty} N_{nm}[\varepsilon-(s-if)\overline{k}_n/\overline{K}_m]R_n + N_{0m}[\varepsilon+\overline{k}_0(s-if)/\overline{K}_m]\}$$

$$m = 1,2,3..... \qquad (2.2.46a)$$

$$B_m = \frac{1}{2\varepsilon(s-if)M_{mm}} \sum_{n=0}^{\infty} N_{nm}[\varepsilon-(s-if)\overline{k}_n/\overline{K}_m]T_n$$

$$m = 1,2,3..... \qquad (2.2.46b)$$

多孔牆前反射係數定義爲

$$C_r = |R_0| \qquad (2.2.47)$$

表示多孔牆前(x=-b)反射波振幅與入射波振幅比值。

多孔牆透射係數定義爲

$$C_t = |T_0| \qquad (2.2.48)$$

表示透過波在多孔牆右側(x=+b)之振幅與入射波振幅比值。

在多孔牆體內第m個透過係數C'_{mt}與第m個反射係數C'_{mr}，我們分別定義爲

$$C'_{mt} = |(s-if)A_m \cosh(K_m h)|/\cosh k_0 h \qquad (2.2.49a)$$

$$C'_{mr} = |(s-if)B_m \cosh(K_m h)|/\cosh k_0 h \qquad (2.2.49b)$$

C'_{mt}及C'_{mr}分別表示在多孔牆體內，多孔牆前端(x=-b)處第m個透過消散波振幅與入射波振幅比值，及在多孔牆後端(x=b)處第m個反射消散波振幅與入射波振幅比值。

波函數無窮級數(2.2.29)、(2.2.30)及(2.2.31)爲收斂級數，在實際計算，可依收斂之速度取有限項，m=1,2,3....M，n=0,1,2,3....N-1。

在多孔牆前(水域Ⅰ)及多孔牆後(水域Ⅱ)之水位變化η_1, η_2可由線性自由動力邊界之表示式(2.2.15a)及週期函數特性條件(2.2.13)式求得

$$\eta_j(x,y,t) = \frac{-i\sigma}{g}\Phi_j, \qquad z=0, \qquad j=1,2 \qquad (2.2.50)$$

在多孔牆前(x=-b)之水位變化η_1則可表示爲

$$\frac{\eta_1(-b,y,t)}{a} = \mathbf{D_1} e^{-i(\sigma t + k_0 y sin\theta_0)} \tag{2.2.51a}$$

式中無因次振幅係數$\mathbf{D_1}$爲

$$\mathbf{D_1} = 1 + \sum_{n=0}^{\infty} R_n \frac{\cosh(k_n h)}{\cosh(k_0 h)} \tag{2.2.51b}$$

在多孔牆後(x=+b)之水位變化η_2可表示爲

$$\frac{\eta_2(+b,y,t)}{a} = \mathbf{D_2} e^{-i(\sigma t + k_0 y sin\theta_0)} \tag{2.2.52a}$$

式中無因次振幅係數$\mathbf{D_2}$爲

$$\mathbf{D_2} = \sum_{n=0}^{\infty} T_n \frac{\cosh(k_n h)}{\cosh(k_0 h)} \tag{2.2.52b}$$

若入射波之水位變化取複數入射波表示式(2.2.12)之實數部分,則可表示爲

$$\eta_0(x,y,t) = a\cos[\sigma t - k_0 \cos\theta_0 (x+b) - k_0 \sin\theta_0 y] \tag{2.2.53}$$

在多孔牆前(x=-b)水位變化η_1可由表示式(2.2.51)取實數部分求得

$$\frac{\eta_1(-b,y,t)}{a} = D_1 \cos(\sigma t - k_0 \sin\theta_0 y + \varepsilon_1) \tag{2.2.54a}$$

式中無因次振幅係數D_1及相位差ε_1分別爲

$$D_1 = \left| 1 + \sum_{n=0}^{\infty} R_n \frac{\cosh(k_n h)}{\cosh(k_0 h)} \right|, \qquad \varepsilon_1 = \tan^{-1}\left(\frac{\mathbf{D_{1i}}}{\mathbf{D_{1r}}}\right) \tag{2.2.54b}$$

其中$\mathbf{D_{1r}}$及$\mathbf{D_{1i}}$分別爲$\mathbf{D_1}$之實部及虛部。

在多孔牆後(x=+b)之水位變化η_2可由表示式(2.2.52)取實數部分求得

$$\frac{\eta_2(+b,y,t)}{a} = D_2 \cos(\sigma t - k_0 \sin\theta_0 y + \varepsilon_2) \tag{2.2.55a}$$

式中無因次振幅係數D_2及相位差ε_2分別爲

$$D_2 = \left| \sum_{n=0}^{\infty} T_n \frac{\cosh(k_n h)}{\cosh(k_0 h)} \right|, \qquad \varepsilon_2 = \tan^{-1}\left(\frac{\mathbf{D_{2i}}}{\mathbf{D_{2r}}}\right) \tag{2.2.55b}$$

其中$\mathbf{D_{2r}}$及$\mathbf{D_{2i}}$分別爲$\mathbf{D_2}$之實部及虛部。

在多孔牆內(區域III)之假想自由表面$\eta_3(x,y,t)$，可由線性動力邊界條件(2.2.17a)及週期函數特性條件(2.2.13)式求得

$$\eta_3(x,y,t)=\frac{\sigma}{g}\gamma\Phi_3, \qquad -b\le x\le b, \qquad z=0 \tag{2.2.56}$$

各區域之波函數皆爲無窮級數,雖然可依收斂之速度取必要的項階求解,但仍是一個甚爲複雜之聯立方程組求解矩陣問題。在未以一般解探討受不同型態波浪作用下之波能消散特性之前,擬於下節先觀察一些較簡易問題,對多孔消波體之反射特性及波壓分佈狀況做初步的了解。

假如多孔牆內摩擦係數f較小，慣性係數s接近理論值1,多孔介質流體伯努力方程式(2.2.10)與線性伯努力方程式(2.2.8)相差不大,則預期衰減波成份相對甚小，所有區域內之波浪僅考慮平面波(包括行進波及駐波)，因此N=1,M=1，則式(2.2.29)、(2.2.30)、(2.2.31)化簡爲：

$$\phi_1(x,z)=A\cosh[k_0(h+z)]e^{-i\overline{k}_0(x+b)}+R_0A\cosh[k_0(h+z)]e^{i\overline{k}_0(x+b)}$$

$$x\le -b, \quad -h\le z\le 0 \tag{2.2.57}$$

$$\phi_2(x,z)=T_0A\cosh[k_0(h+z)]e^{-i\overline{k}_0(x-b)}$$

$$b\le x, \quad -h\le z\le 0 \tag{2.2.58}$$

$$\phi_3(x,z)=A_1A\cosh[K_1(h+z)]e^{-i\overline{K}_1(x+b)}+B_1A\cosh[K_1(h+z)]e^{i\overline{K}_1(x-b)}$$

$$-b\le x\le +b, \quad -h\le z\le 0 \tag{2.2.59}$$

未知變數R_0,T_0,A_1及B_1可由方程組(2.2.43)式之簡化求得如下:

$$R_0=\frac{i(1-\Omega^2)\sin(2\overline{K}_1b)}{2\Omega\cos(2\overline{K}_1b)+(1+\Omega^2)i\sin(2\overline{K}_1b)} \tag{2.2.60a}$$

$$T_0=\frac{2\Omega}{2\Omega\cos(2\overline{K}_1b)+(1+\Omega^2)i\sin(2\overline{K}_1b)} \tag{2.2.60b}$$

$$A_1 = \frac{N_{01}[\varepsilon - (s-if)\overline{k}_0/\overline{K}_1]R_0 + N_{01}[\varepsilon + \overline{k}_0(s-if)/\overline{K}_1]}{2\varepsilon(s-if)M_{11}} \tag{2.2.60c}$$

$$B_1 = \frac{N_{01}[\varepsilon\cos(\overline{k}_0 d) + i(s-if)\overline{k}_0\sin(\overline{k}_0 d)/\overline{K}_1]T_0}{2\varepsilon(s-if)M_{11}} \tag{2.2.60d}$$

式中

$$N_{01} = \frac{h}{(k_0h)^2 - (K_1h)^2}[k_0h\sinh(k_0h)\cosh(K_1h) - K_1h\sinh(K_1h)\cosh(k_0h)] \tag{2.2.61a}$$

$$M_{11} = h[\frac{1}{2} + \frac{\sinh(2K_1h)}{4K_1h}] \tag{2.2.61b}$$

$$\Omega = \frac{\varepsilon\overline{K}_1 h}{\overline{k}_0 h(s-if)} \tag{2.2.62a}$$

$$b^* = 2b/h\overline{K}_1 h \tag{2.2.62b}$$

$$\lambda_1^{\pm} = E_1^{+} = e^{\pm ib^*} \tag{2.2.62c}$$

$$\lambda_2^{\pm} = 1 \pm \Omega \tag{2.2.62d}$$

$$\lambda_3^{\pm} = -i\sin(\overline{k}_0 d) \pm \Omega\cos(\overline{k}_0 d) \tag{2.2.62e}$$

從R_0, T_0, A_1及B_1各係數表示式(2.2.60)、(2.2.61)及(2.2.62)可明顯看出各係數與θ_0,2b/h(b^*),ε, s-if(γ),C_0 ($\overline{k}_0 h$),$\overline{K}_1 h$等參數有關。而且反射係數R_0與透射係數T_0爲Ω及b^*參數之函數，Ω稱多孔牆之可穿透度(admittance of the porous structure),其物理意義表示作用於多孔牆上之正向流速與壓力比值,爲描述多孔牆特性參數,並且與入射波角度有關。b^*爲一無因次多孔牆厚度(dimensionless width of the structure)爲牆之厚度與多孔牆內特性波長之比值。當$\Omega = 1$時,反射係數R_0爲最小值,即作用於多孔牆之正向流速與壓力相等。首先將探討平面波條件下,多孔消波體前反射係數C_r,透過係數C_t及多孔牆內一階透過係數C'_{1t},一階反射係數C'_{1r}等與多孔牆厚度$2b/h$,入射波參數C_0等無因次物理量之關係。爲簡化數值計算,多孔牆之慣性係數s,摩擦係數f及孔隙率ε等參數皆假設爲常數,並取$\varepsilon = 0.4, s = 1, f = 0.5$(低摩擦係數)做爲計算值。

若入射波之水位變化取複數入射波表示式(2.2.12)之實數部分如(2.2.53)式,則區域 I 之波函數 ϕ_1 表示式(2.2.57)等號右邊第二項爲區域 I 反射波 ϕ_{1r} 之水位變化 η_r 可由(2.2.57)代入(2.2.50)式取實數部分第二項求得

$$\eta_r(x,y,t) = a|R_0|\cos[\sigma t + k_0\cos\theta_0(x+b) - k_0\sin\theta_0 y + \varepsilon_r], \tag{2.2.63a}$$

$$|R_0| = \sqrt{R_{0r}^2 + R_{0i}^2}, \qquad \varepsilon_r = \tan^{-1}\left(\frac{R_{0i}}{R_{0r}}\right) \tag{2.2.63b}$$

式中 R_{or} 及 R_{0i} 分別爲 R_0 之實部及虛部。

區域 I 之水位變化 η_1 可表示爲

$$\eta_1 = \eta_0 + \eta_r \tag{2.2.64}$$

因此在多孔牆前(x=–b)之水位變化可表示爲

$$\frac{\eta_1(-b,y,t)}{a} = D_1\cos(\sigma t - k_0\sin\theta_0 y + \varepsilon_1) \tag{2.2.65}$$

式中無因次振幅係數 D_1 及相位差 ε_1 分別爲

$$D_1 = \sqrt{1 + |R_0|^2 + 2|R_0|\cos\varepsilon_r} \tag{2.2.66a}$$

$$\varepsilon_1 = \tan^{-1}\left(\frac{|R_0|\sin\varepsilon_r}{1+|R_0|\cos\varepsilon_r}\right) \tag{2.2.66b}$$

區域 II 之波函數 ϕ_2 其水位變化 η_2 可由(2.2.58)代入(2.2.50)式取實數部分求得

$$\eta_2(x,y,t) = a|T_0|\cos(\sigma t - k_0\sin\theta_0 y + \varepsilon_2), \tag{2.2.67a}$$

$$|T_0| = \sqrt{T_{0r}^2 + T_{0i}^2}, \qquad \varepsilon_2 = \tan^{-1}\left(\frac{T_{0i}}{T_{0r}}\right) \tag{2.2.67b}$$

式中 T_{or} 及 T_{0i} 分別爲 T_0 之實部及虛部

在多孔牆後(x= b)之水位變化可表示爲

$$\frac{\eta_2(b,y,t)}{a} = D_2\cos(\sigma t - k_0\sin\theta_0 y + \varepsilon_2) \tag{2.2.68a}$$

式中無因次振幅係數 D_2 及相位差 ε_2 分別爲

$$D_2 = |T_0\cos(\overline{k}_0 d)|, \qquad \varepsilon_2 = \tan^{-1}\left(\frac{T_{0i}}{T_{0r}}\right) \tag{2.2.68b}$$

在多孔牆內(區域Ⅲ)之假想自由表面水位變化$\eta_3(x,y,t)$，可由(2.2.59)代入(2.2.56)式取實數部分求得

$$\eta_3(x,y,t) =$$

$$|A_1(s-if)\cosh(K_1h)|a\frac{e^{K_{1i}(x+b)}}{\cosh(k_0h)}\cos(\sigma t - K_{1r}\cos\theta_0(x+b) - k_0\sin\theta_0 y + \varepsilon_a)$$

$$+|B_1(s-if)\cosh(K_1h)|a\frac{e^{-K_{1i}(x-b)}}{\cosh(k_0h)}\cos(\sigma t + K_{1r}\cos\theta_0(x+b) - k_0\sin\theta_0 y + \varepsilon_b)$$

$$-b \le x \le b \qquad (2.2.69)$$

式中ε_a及ε_b分別爲相位差。

在平面波之假設條件下，複雜之矩陣問題，簡化爲反射係數、透過係數及多孔牆前或後之波壓分佈等皆可以(2.2.60a)、(2.2.60b)、(2.2.49a)及(2.2.51b)等解析表示式，在實際應用時甚爲方便。至於在何種條件時，可正確引用，或產生之誤差不甚大，則與特徵值K_m之特性有關。

式(2.2.74a)顯示當多孔牆穿透係數$\Omega = 1$時，反射係數R_0=0，反射波完全消散，多孔牆達到最佳消波能力。同理在多孔牆前(x=–b)之水位變化可表示爲(2.2.43)式，式中之R_0定義如(2.2.74a)。但在多孔牆後(x= b)之水位變化表示爲

$$\frac{\eta_2(b,y,t)}{a} = D_2\cos(\sigma t - k_0\sin\theta_0 y + \varepsilon_2) \qquad (2.2.70a)$$

$$D_2 = |T_0|, \qquad \varepsilon_2 = \tan^{-1}\left(\frac{T_{0i}}{T_{0r}}\right) \qquad (2.2.70b)$$

多孔牆後爲一寬擴的水域，波浪透過多孔牆後無阻礙的進行，一般透水性離岸堤可當做此種狀況之一種應用，其作用乃希望透過波愈小，以達到消波效用，但也不希望堤前反射波太大，像不透水堤於堤前產生全反射波造成堤址嚴重沖刷現象，因此適當的比例減低反射波及透過波爲一個重要的原則。圖2-2-3，取$C_0 = 0.5$時，顯示反射波隨厚度增加而增大，在厚度爲2倍水深時達到定數，透過波則因厚度之增大而減小，最後消失。與有限長消波室一樣，對同一入射波作用，例如取$C_0 = 0.5$或$C_0 = 5$，且固定消波室寬度$d/L = 0.4$，則增大多孔牆厚度，並不一定可減低反射係數C_r，而是存在一最佳厚度(如圖2-2-4)。消波室內透水係數C_t，則隨牆厚度之增大而減小，最後消失(圖2-2-5)，而且波長越短(C_0值較小)，衰減越快。消波室寬度無限長之消波特性，在正向作用部份可參考Sollitt及Cross(1972)，在斜向作用部份可參考Dalrymple et al. (1991)。

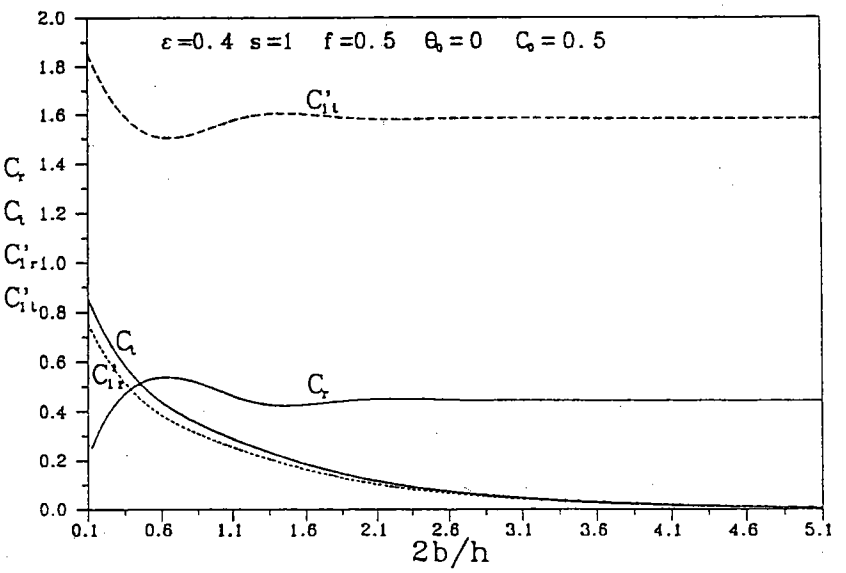

圖2-2-3多孔消波體各項係數$C_r, C_t,$
C'_{1r}, C'_{1t}與多孔牆厚度$2b/h$之相關曲線圖

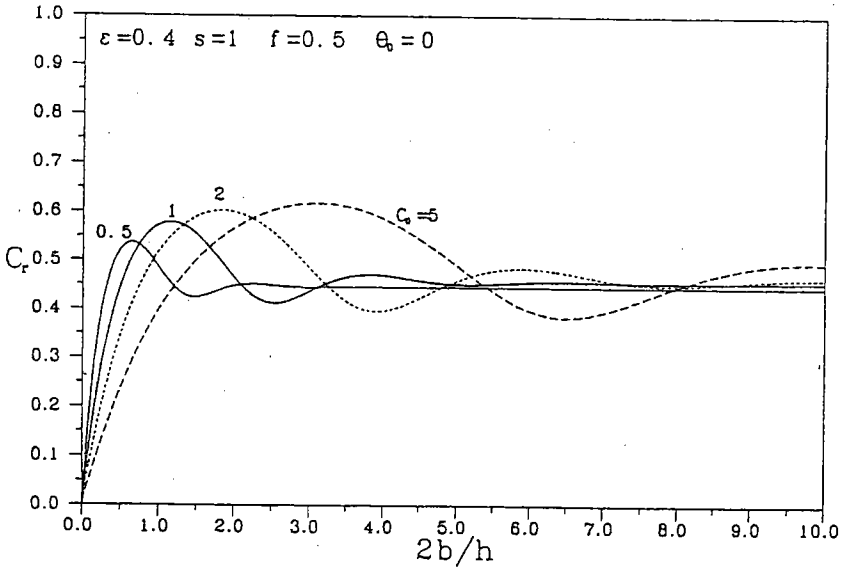

圖2-2-4多孔消波體在考慮不同波浪參數C_0
反射係數C_r與多孔牆厚度$2b/h$相關曲線圖

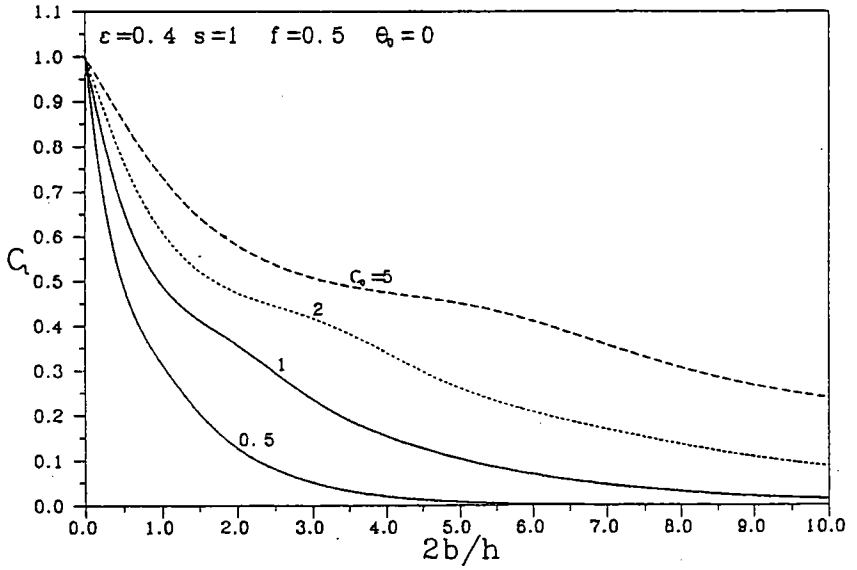

圖2-2-5多孔消波體在考慮不同波浪參數C_0透射係數C_t與多孔牆厚度$2b/h$相關曲線圖

2.3 波浪之淺化

假設近岸海域爲等坡度且等水線與海岸線(y軸)平行,若線性波自外海垂直進入海岸地區,則波浪波高及波速產生之變化稱淺化現象(shoaling)。因爲等深線平行海岸,所以波向不變,且週期不變。若不考慮底床摩擦或碎波現象,則波浪之能量通 EC_g 不因水深改變維持一定值,因此在不同水深之能量守恒可表示爲

$$E_1 C_{g1} = E_0 C_{g0} \tag{2.3.1}$$

或

$$(\frac{1}{8}\rho g H_1^2) n_1 C_1 = (\frac{1}{8}\rho g H_o^2) n_o C_o \tag{2.3.2}$$

式中 E_o, H_o, C_{g0} 分別代表在深水地區之能量,波高及群波速, E_1, H_1, C_{g1} 分別代表在近岸地區之能量,波及群波速,因此表示式(2.3.1)可化爲

$$K_s = \frac{H_1}{H_o} = \sqrt{\frac{n_o C_o}{n_1 C_1}} \tag{2.3.3}$$

K_s 稱淺化係數(shoaling coefficient),一般在深水區 $n_0 = 1/2$,在淺化水區n=1,而波速在深水區較淺水區爲大,波長在深水區也較淺水區爲長,因此淺化係數可能大於1,這表示波浪剛進入淺水區時波高變大,但再進入較淺水區因淺化因子n增大(趨近於1),波高可能再減小。

2.4 波浪之破碎

若不考慮碎波，則波浪之淺化係數在水深甚淺處趨向無窮大，但這與實際現場不符合。因此波浪由深水進入淺水區將因尖銳度之增大而產生碎波現象，根據Miche, Danel and Hamada所提出之淺水波鄰界尖銳度爲

$$(\frac{H}{L}) = (\mu)_{max} = 0.142 \tanh kh \tag{2.4.1}$$

而根據McCown由水分子流速等於波速，求得碎波水條件爲相對波高

$$(\varepsilon_b) = \frac{H_b}{h_b} \approx 0.78 \tag{2.4.2}$$

表水波浪在水深h之可能最大波高。

碎波因海底地形，流速強弱，入射波波形不同，碎波之外觀不同而分爲崩波型碎波(spilling breaker)，捲波型碎波(plunging breaker)及湧波型碎波(surging breaker)三種。

2.5 波浪之折射

波浪由深水區進入淺水區，因波速受水深影響，較淺處波速進行較慢，如波浪進行方向與等深線斜交時，波峰線因此產生彎曲現象，稱爲折射。與波峰線正交之曲線群稱波向線，波向線之切線方向即代表波浪進行方向。假設等水線與海岸線平行，則根據Snell定律波向角與波速滿足

$$\frac{\sin\alpha_1}{C_1} = \frac{\sin\alpha_2}{C_2} \tag{2.5.1}$$

若地形甚不規則，則滿足波數守恒即

$$\nabla \times \overrightarrow{K} = 0 \tag{2.5.2}$$

或

$$\frac{\partial}{\partial x}(k\sin\alpha) - \frac{\partial}{\partial y}(k\cos\alpha) = 0 \tag{2.5.3}$$

等深線如約略與海岸線平行，當波浪斜向進入淺水區，波向線會慢慢變成與海岸線垂直。根據能量守恒原理，當波浪斜向進入海岸時，若不考慮底床摩擦或碎波現象，則兩波向線間之能量不變，即

$$E_1 C_{g1} b_1 = E_2 C_{g2} b_2 \tag{2.5.4}$$

式中E_1, C_{g1}, b_1 (E_2, C_{g2}, b_2)分別代表不同位置能量，群速度及波向線之間距。

不同位置波高比則可表示爲

$$H_2/H_1 = \sqrt{\frac{C_{g1}}{C_{g2}}} \cdot \sqrt{\frac{b_1}{b_2}} = K_s \cdot K_r \tag{2.5.5}$$

式中$K_s = \sqrt{\frac{C_{g1}}{C_{g2}}}$爲淺化係數，$K_r = \sqrt{\frac{b_2}{b_2}}$稱折射係數(refration coefficient)。

2-6 波浪之繞射

波浪遭遇防波堤，在堤後水域，仍有部份波浪存在，此爲繞射(Diffraction)現象，一般同樣可以依光波繞射原理解析，防波堤對波浪之遮蔽(Sheltering)效果，繞射後之波高與入射波高比值稱爲繞射係數K_d(Diffraction coefficient)，繞射後之波向線同樣產生彎曲現象，一般以等繞射係數及波向線描述繞射現象。

波浪遭遇防波堤，在堤前部份波浪反射(稱爲反射波)，入射波與反射波因加成作用產生重複波，對防波堤近造成甚大影響。波浪由直角或斜向投射向防波堤之狀況，可按光波反射原理解析，反射角與入射角相等，入射波高與反射波高之比值稱爲反射係數R(Reflected coefficient)反射係數介於0於1之間，而與防堤材料及波速有關，防波堤消波效果愈佳，反射係數愈小。

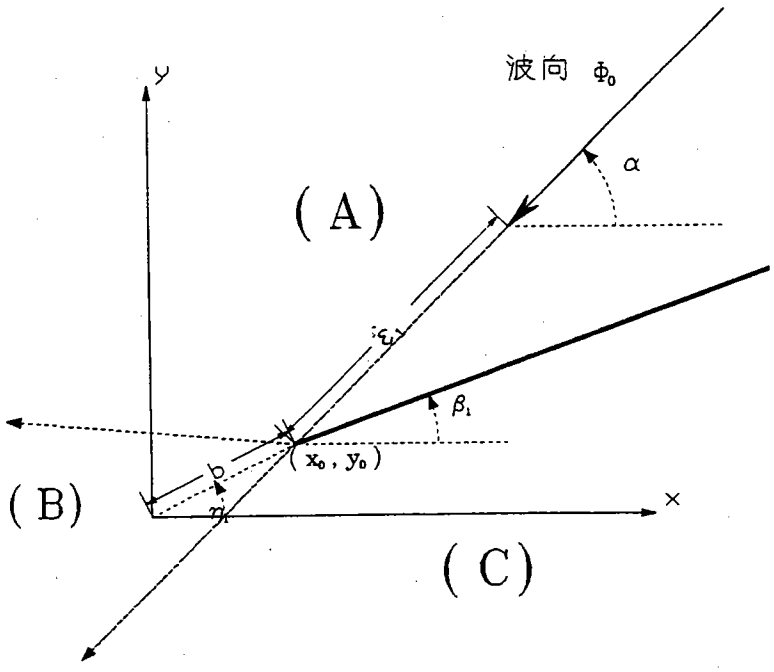

圖2-6-1波浪作用於半無限長堤之示意圖

考慮一透水性半無限長堤(semi-infinite cushion type Breakwater)，反射係數(reflection coeficent)爲$R_1(R_1 < 1)$，置放於xy-平面上(如圖2-6-1)，堤頭位置(x_0, y_0)，堤與正x-軸夾α度，堤頭至原點(0,0)與正x-軸夾β_1度。假設在入射波函數$\phi_0(x, y)$爲

$$\phi_0(x,y)=\phi_0(r,\theta)=a_0e^{-i(kx\cos\alpha+ky\sin\alpha+\varepsilon)}=a_0e^{-i[kr\cos(\theta-\alpha)+\varepsilon]} \tag{2.6.1}$$

之作用下，經繞射(diffration)、反射(reflection)及散射(scatter)等效應，全區之波函數可表示爲

$$\begin{aligned}\phi_1(x,y)=&\phi_1(r_1,\theta_1)=ae^{is}\\ =&\frac{a_0}{\sqrt{2}}exp\{-i[kr_1\cos(\theta_1-\alpha_1)+\frac{\pi}{4}+\varepsilon_1]\}\times\{[c(\delta_{11})+\frac{1}{2}]+i[s(\delta_{11})+\frac{1}{2}]\}\\ +&R_1\frac{a_0}{\sqrt{2}}exp\{-i[kr_1\cos(\theta_1-\alpha_1)+\frac{\pi}{4}+\varepsilon_1]\}\times\{[c(\delta_{12})+\frac{1}{2}]+i[s(\delta_{12})+\frac{1}{2}]\}\end{aligned} \tag{2.6.2}$$

式中

$$\alpha_1=\alpha-\beta_1 \tag{2.6.3}$$

$$\delta_{11}=\sqrt{\frac{4kr_1}{\pi}}\cos\frac{(\theta_1-\alpha_1)}{2} \tag{2.6.4}$$

$$\delta_{12}=\sqrt{\frac{4kr_1}{\pi}}\cos\frac{(\theta_1+\alpha_1)}{2} \tag{2.6.5}$$

$$c(\delta_{11})=\int_0^{\delta}\cos(\frac{\pi}{2}x^2)dx \tag{2.6.6}$$

$$s(\delta_{12})=\int_0^{\delta}\sin(\frac{\pi}{2}x^2)dx \tag{2.6.7}$$

$$\varepsilon_1=bk\cos(\gamma_1-\alpha) \tag{2.6.8}$$

一般可將全區分爲如圖2-1之A,B及C三個區域:

A區: $\alpha_1\le\theta_1\le\pi-\alpha_1$

B區: $\pi-\alpha_1<\theta_1\le\pi+\alpha_1$

C區: $\pi+\alpha_1<\theta_1<2\pi+\beta_1$

因三個區域成份波特性不同，將ϕ改寫爲

$$\begin{aligned}\phi_1(x,y)=&\phi_1(r_1,\theta_1)=ae^{is}\\ =&a_0exp\{-i[kr_1\cos(\theta_1-\alpha_1)+\varepsilon_1]\}\\ +&\frac{a_0}{\sqrt{2}}exp\{-i[kr_1\cos(\theta_1-\alpha_1)+\frac{\pi}{4}+\varepsilon_1]\}\times\{[c(\delta_{11})-\frac{1}{2}]+i[s(\delta_{11})-\frac{1}{2}]\}\\ +&R_1a_0exp\{-i[kr_1\cos(\theta_1-\alpha_1)+\varepsilon_1]\}\\ +&R_1\frac{a_0}{\sqrt{2}}exp\{-i[kr_1\cos(\theta_1-\alpha_1)+\frac{\pi}{4}+\varepsilon_1]\}\times\{[c(\delta_{12})-\frac{1}{2}]+i[s(\delta_{12})-\frac{1}{2}]\}\end{aligned} \tag{2.6.9}$$

定義ϕ各分量ϕ_0,ϕ_r,ϕ_d及ϕ_s分別如下

$$\phi_0 = a_0 exp\{-i[kr_1\cos(\theta_1-\alpha_1)+\varepsilon_1]\} \tag{2.6.10}$$

$$\phi_d = \frac{a_0}{\sqrt{2}} exp\{-i[kr_1\cos(\theta_1-\alpha_1)+\frac{\pi}{4}+\varepsilon_1]\}\times\{[c(\delta_{11})-\frac{1}{2}]+i[s(\delta_{11})-\frac{1}{2}]\} \tag{2.6.11}$$

$$\phi_r = R_1 a_0 exp\{-i[kr_1\cos(\theta_1-\alpha_1)+\varepsilon_1]\} \tag{2.6.12}$$

$$\phi_s = R_1\frac{a_0}{\sqrt{2}} exp\{-i[kr_1\cos(\theta_1-\alpha_1)+\frac{\pi}{4}+\varepsilon_1]\}\times\{[c(\delta_{12})-\frac{1}{2}]+i[s(\delta_{12})-\frac{1}{2}]\} \tag{2.6.13}$$

其中ϕ_0爲入射波，ϕ_r爲反射波，$\phi_0+\phi_d$爲入射波加入射波因堤而產生之繞射波，$\phi_r+\phi_s$爲反射波加反射波因堤而產生之散射波。

A,B及C三個區域之主要成份波分別表示如下:

區域A :ϕ_A＝入射波＋反射波＋反射波因堤而產生之散射波。

區域B :ϕ_B＝入射波＋入射波因堤而產生之繞射波。

區域C :ϕ_C＝入射波因堤而產生之繞射波。

若堤之透過係數(transsmision coefficient)爲T_1,則在區域C尙存在有透過波ϕ_t:

$$\phi_t = T_1 a_0 exp\{-i[kr_1\cos(\theta_1-\alpha_1)+\varepsilon_1]\} \tag{2.6.14}$$

即在區域C改爲ϕ_C＝入射波因堤而產生之繞射波＋透過波。

在區域內任一點之振幅a與入射波之振幅a_0比值$k_d=\frac{a}{a_0}$稱繞射係數。波浪做用於防波堤,若無能量損失,則$R_1^2+T_1^2=1$,若有部份能量損失,則$R_1^2+T_1^2<1$。

考慮兩個透水性半無限長堤(semi-infinite cushion type Breakwater),兩堤之反射係數(reflection coeficent)分別爲R_1及R_2,置放於xy-平面上如圖2-6-2,各個堤位置之座標及相關符號定義如同圖2-6-1。

在入射波函數$\phi_0(x,y)$爲

$$\phi_0(x,y) = a_0 e^{-i(kx\cos\alpha+ky\sin\alpha+\varepsilon)} = a_0 e^{-i[kr\cos(\theta-\alpha)+\varepsilon]} \tag{2.6.15}$$

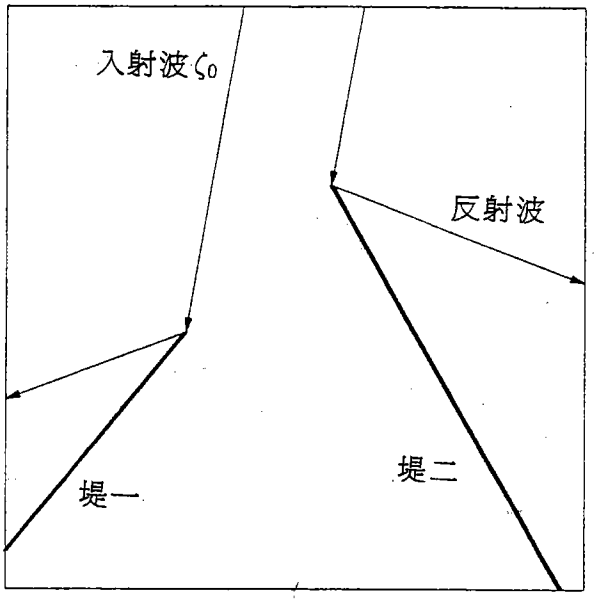

圖2-6-2波浪作用於雙半無限長堤之示意圖

之作用下，經繞射(diffration)、反射(reflection)及散射(scatter)等效應，全區之波函數可利用線性疊加原理求得。簡述如下:

若僅考慮堤一存在則對堤一之波函數表示爲:

$$\begin{aligned}\phi_1(r_1,\theta_1) =& a_1 e^{is_1} \\ =& \frac{a_0}{\sqrt{2}} exp\{-i[kr_1\cos(\theta_1-\alpha_1)+\frac{\pi}{4}+\varepsilon_1]\}\times\{[c(\delta_{11})+\frac{1}{2}]+i[s(\delta_{11})+\frac{1}{2}]\} \\ +R_1&\frac{a_0}{\sqrt{2}} exp\{-i[kr_1\cos(\theta_1-\alpha_1)+\frac{\pi}{4}+\varepsilon_1]\}\times\{[c(\delta_{12})+\frac{1}{2}]+i[s(\delta_{12})+\frac{1}{2}]\} \quad (2.6.16)\end{aligned}$$

式中

$$\alpha_1=\alpha-\beta_1, \qquad \varepsilon_1=b_1 k\cos(\alpha_1-\alpha) \quad (2.6.17)$$

若僅考慮堤二存在則對堤二之波函數表示爲:

$$\begin{aligned}\phi_2(r_2,\theta_2) =& a_2 e^{is_2} \\ =& \frac{a_0}{\sqrt{2}} exp\{-i[kr_2\cos(\theta_2-\alpha_2)+\frac{\pi}{4}+\varepsilon_2]\}\times\{[c(\delta_{21})+\frac{1}{2}]+i[s(\delta_{21})+\frac{1}{2}]\} \\ +R_2&\frac{a_0}{\sqrt{2}} exp\{-i[kr_2\cos(\theta_2-\alpha_2)+\frac{\pi}{4}+\varepsilon_2]\}\times\{[c(\delta_{22})+\frac{1}{2}]+i[s(\delta_{22})+\frac{1}{2}]\} \quad (2.6.18)\end{aligned}$$

式中

$$\alpha_2 = \alpha - \beta_2, \qquad \varepsilon_2 = b_2 k \cos(\alpha_2 - \alpha) \tag{2.6.19}$$

因波浪作用角度不同及雙堤之配置不同,此處僅提出一種方案:波浪完整做用於任一堤,堤與堤之間無遮蔽之情行。一堤之反射波不再通過或影響另一堤(如圖2-6-2)。此時全區之波函數利用線性疊加原理,並減去重覆之入射波可表示爲:

$$\phi = \phi_1 + \phi_2 - \phi_0 = ae^{is} \tag{2.6.20}$$

考慮有限長堤(finite-length cushion type Breakwater),之反射係數(reflection coeficent)爲R_1,置放於xy-平面上如圖2-6-3,堤頭位置之座標爲(x_1, y_1)、(x_2, y_2)及相關符號定義如同圖2-6-1。

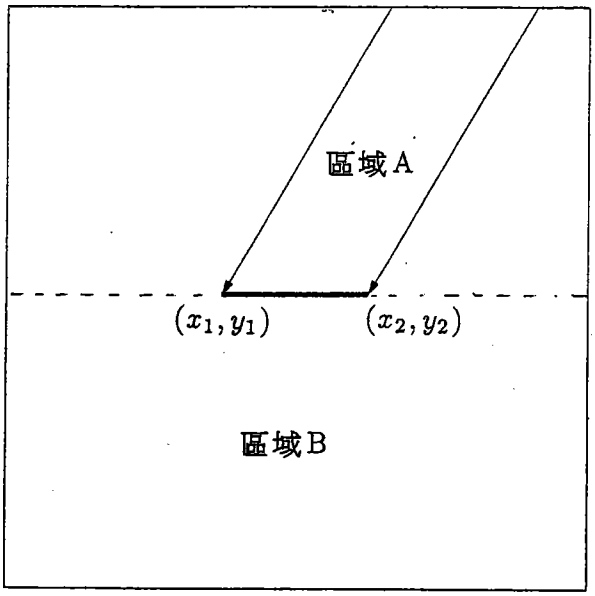

圖2-6-3波浪作用於有限長堤之繞射示意圖

有限長堤之波場計算可假設爲兩重疊之半無限長堤情行,其雙堤頭各爲兩半無限長堤之堤頭,有限長堤部份則爲二堤之重疊部份。因此波浪作用於堤全區之波函數利用線性疊加原理,並減去重覆之入射波可表示爲:

區域A:

$$\phi = \phi_1 + \phi_2 - \phi_0 - \phi_r \tag{2.6.21}$$

區域B:

$$\phi = \phi_1 + \phi_2 \tag{2.6.22}$$

圖2-6-4～圖2-6-6分別爲半無限長堤、兩半無限長堤及有限長堤之等繞射係數分佈圖。

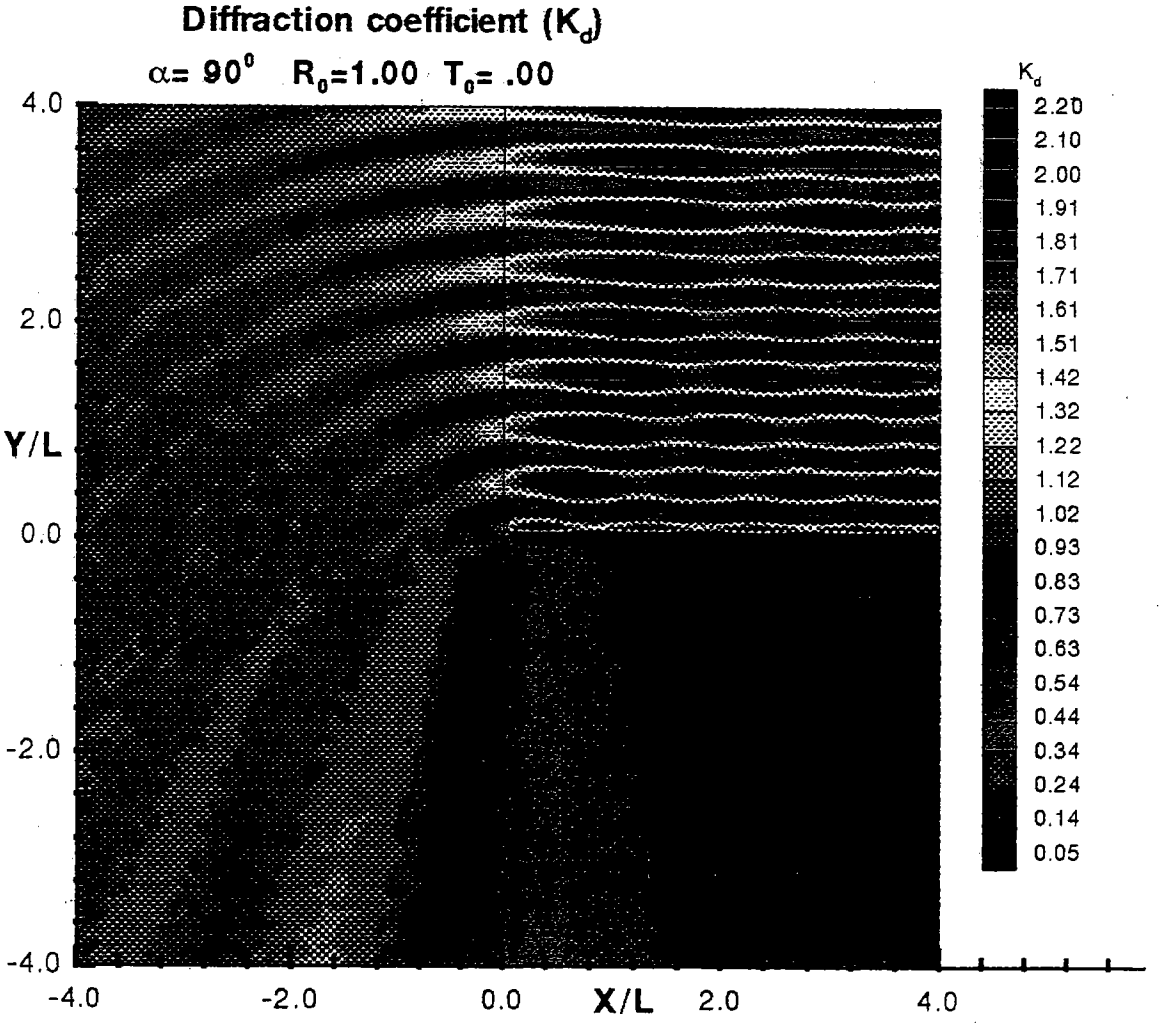

圖2-6-4波浪作用於半無限長堤之等繞射係數K_d分佈圖

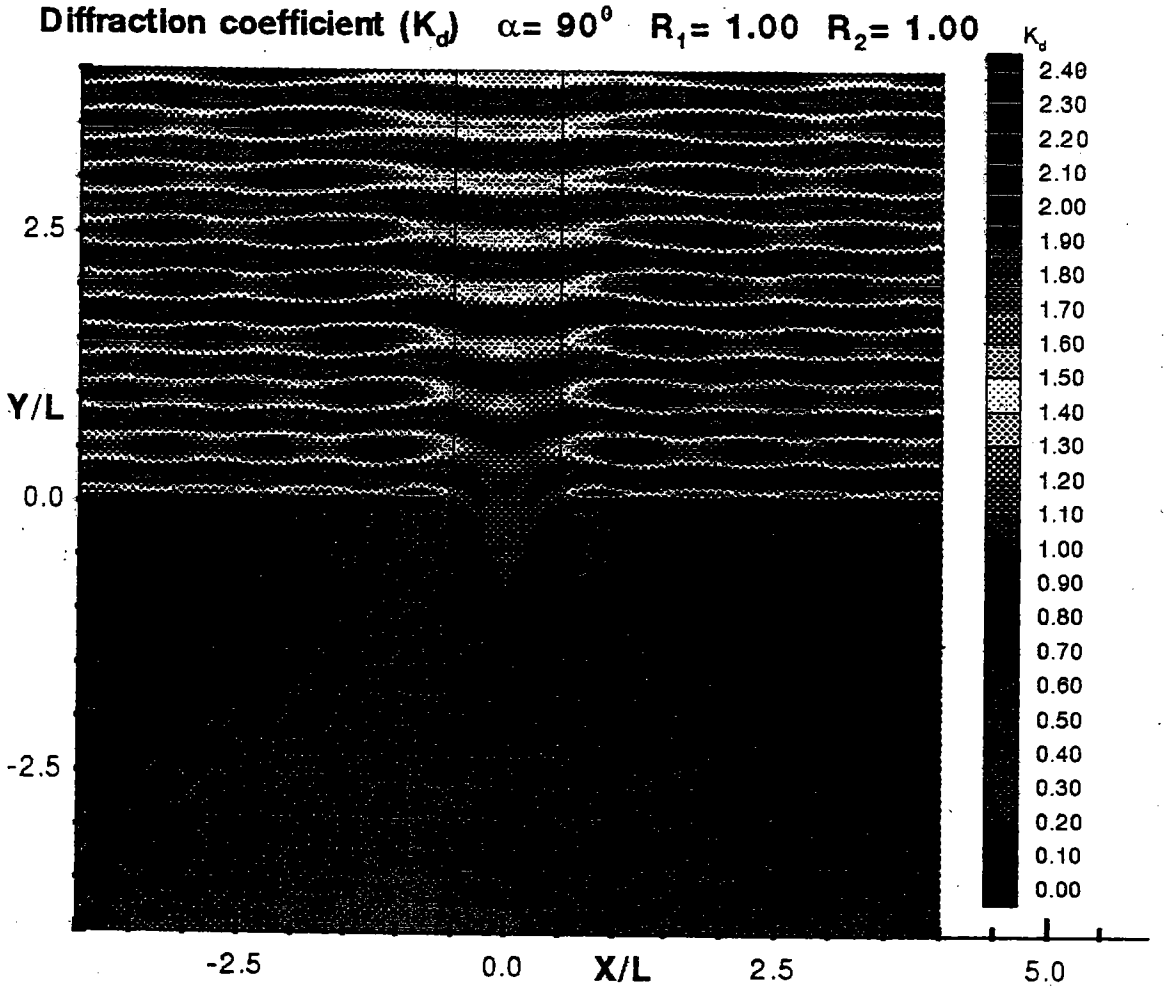

圖2-6-5波浪作用於兩半無限長堤之等繞射係數K_d分佈圖

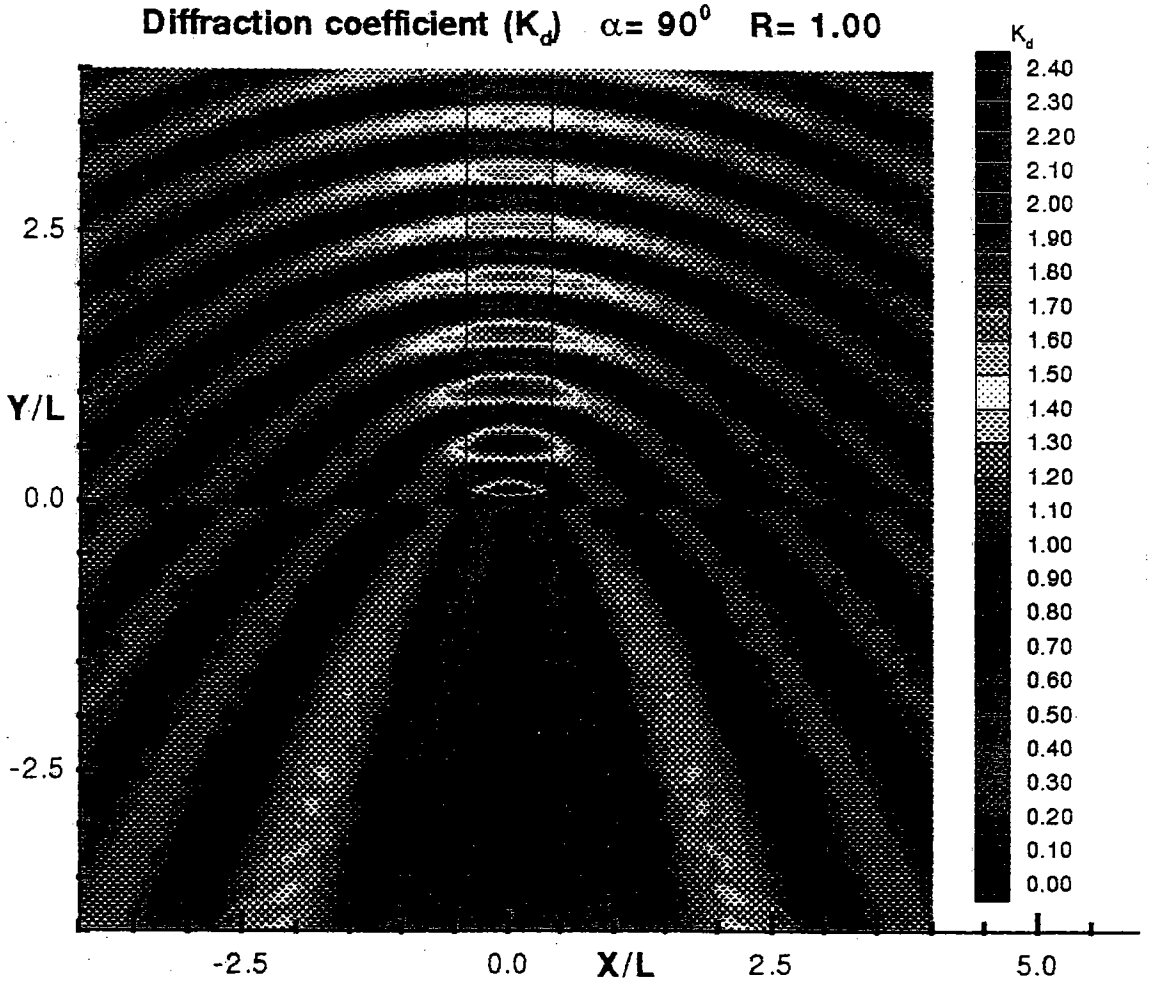

圖2-6-6波浪作用於有限長堤之等繞射係數K_d分佈圖

2.7 波浪引起之港池共振

考慮以不透水性岸壁設計之封閉矩型形狀港池，如附圖 2-7-1，y 軸向上爲正，原點在港池上邊界之左側點，z 軸向上爲正，港區假設爲等水深 h 。

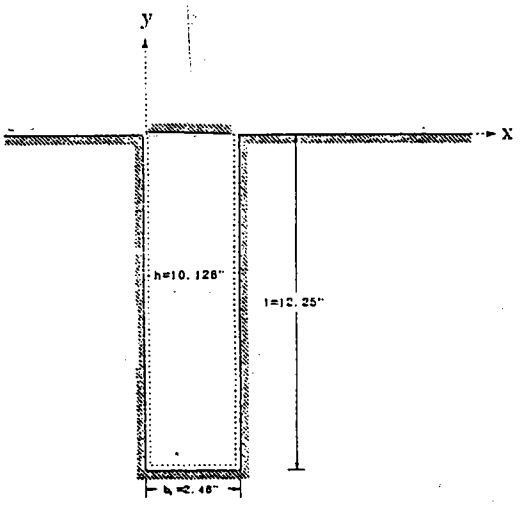

圖 2-7-1　封閉矩型港池計算區域示意圖

假設流體滿足不可壓縮、無黏性及非旋流之條件因此存在流速勢(velocity potential) $\Phi(x,y,z,t)$ 滿足三維拉普拉氏方程式(Laplace equation)

$$\frac{\partial^2\Phi}{\partial x^2}+\frac{\partial^2\Phi}{\partial y^2}+\frac{\partial^2\Phi}{\partial z^2}=0 \tag{2.7.1}$$

水域之流速勢 Φ 分別滿足線性自由表面動力邊界條件及運動邊界條件，即

$$\frac{\partial\zeta}{\partial t}-\frac{\partial\Phi}{\partial z}=0, \qquad ,z=0 \tag{2.7.2a}$$

$$\frac{\partial\Phi}{\partial t}+g\zeta=0, \qquad ,z=0 \tag{2.7.2b}$$

式中 $\zeta(x,y,t)$ 表示在水域之水位變化，g 爲重力加速度。

上二式可合併爲

$$\frac{\partial^2\Phi}{\partial t^2}+g\frac{\partial\Phi}{\partial z}=0, \qquad ,z=0 \tag{2.7.2c}$$

基於線性理論，我們假設水位變化 ζ 爲週期性函數，可表示爲

$$\zeta(x,y,t) = f(x,y)e^{-i\sigma t} \tag{2.7.3}$$

式中 f 爲波函數(wave function)。

在等水深區,假設海底不透水,則滿足

$$\frac{\partial \Phi}{\partial z} = 0, \qquad z = -h \tag{2.7.4}$$

根據控制方程式(2.7.1),海底不透水邊界條件(2.7.4)式及水位變化週期性條件(2.7.3)式,則流速勢 $\Phi(x,y,z,t)$ 可表示爲:

$$\Phi(x,y,z,t) = A_0 \cosh[k_0(h+z)]f(x,y)e^{i\sigma t} \tag{2.7.5}$$

其中 $i = \sqrt{-1}$, k_0 爲週波數(radian wave number), $k_0 = 2\pi/L_0$, L_0 爲波長(wave length), σ 爲週頻率(radian frequency), $\sigma = 2\pi/T$, T 爲波浪週期(wave period),常數 A_0 可表示爲

$$A_0 = \frac{iga_0}{\sigma \cosh(k_0 h)} \tag{2.7.6}$$

式中 a_0 爲波浪振幅(wave amplitude),波函數 f(x,y) 滿足下列荷姆茲方程式(Helmholtz eqution)

$$\frac{\partial^2 f}{\partial x^2} + \frac{\partial^2 f}{\partial y^2} + k_0^2 f = 0 \tag{2.7.7}$$

且波數 k_0 滿足分散關係式(dispersion relation)

$$\sigma^2 = g k_0 \ \tanh(k_0 h) \tag{2.7.8}$$

假設港池內壁爲直立不可穿透體,則其邊界上應滿足邊界條件

$$\frac{\partial f}{\partial x}(0,y) = \frac{\partial f}{\partial x}(b,y) = 0 \qquad for \quad -\ell < y < 0 \tag{2.7.9a}$$

$$\frac{\partial f}{\partial y}(x,0) = \frac{\partial f}{\partial y}(x,-\ell) = 0 \qquad for \quad 0 < x < b \tag{2.7.9b}$$

引用變數分離法(the method of separation of variables)原理,荷姆茲方程式(2.7.6)之解可表示爲

$$f(x,y) = X(x)Y(y) \tag{2.7.10}$$

由控制方程式(2.7.7)及，邊界條件(2.7.9)等式，港內之波函數f可表示爲：

$$f(x,y) = \sum_{m=0}^{\infty}\sum_{n=0}^{\infty} A_{mn}\cos(\frac{m\pi}{b}x)\cos(\frac{m\pi}{\ell}y) \tag{2.7.11a}$$

其中A_{mn}爲未定係數。各成份波可表示爲

$$f_{mn}(x,y) = A_{mn}\cos(\frac{m\pi}{b}x)\cos(\frac{m\pi}{\ell}y) \tag{2.7.11b}$$

將表示式(2.7.5)代入方程式(2.7.1)並引用(2.7.11)及分散關係式(2.7.8)在長波之假設條件下($\sigma^2 = gk_0^2h$)可求得產生共振週期T

$$T = \frac{2}{\sqrt{gh}}[(m/b)^2 + (n/\ell)^2]^{-1/2}, \quad m,n = 0,1,2... \tag{1.12}$$

式中ℓ爲港池長度，b爲港池寬度，g爲重力加速度，h爲水深。

對一維狹長之矩形港池(長度ℓ遠大於寬度b)之自然共振週期T，Merian's公式(Wilson, 1972)表示爲：

$$T = \frac{2\ell}{n\sqrt{gh}}, \quad n = 0,1,2... \tag{2.7.13}$$

如以無因次參數ℓ/L可表示爲：

$$\frac{\ell}{L} = \frac{n}{4} = \frac{1}{4},\frac{1}{2},\frac{3}{4},1,\frac{5}{4},\frac{3}{2},\frac{7}{4}.... \tag{2.7.14}$$

式中L爲波長。即產生共振之條件時，狹長之矩形港池端點兩側處爲駐波節點(水位爲零)或駐波奏點(水位變化最大)。可能發生之共振波長分別爲4ℓ或2ℓ或$4/3\ell$或ℓ或$4/5\ell$.....等倍數之港池長度。

同理對單開口一維不透水矩形港池(長度ℓ遠大於寬度b)之自然共振週期T，Merian's公式(Wilson, 1972)表示爲：

$$T = \frac{2\ell}{(2n+1)\sqrt{gh}}, \quad n = 0,1,2... \tag{2.7.15}$$

如以無因次參數ℓ/L可表示爲：

$$\frac{\ell}{L}=\frac{2n+1}{4}=\frac{1}{4},\frac{3}{4},\frac{5}{4},\frac{7}{4},\frac{9}{4},\frac{11}{4}\cdots\cdot \tag{2.7.16}$$

式中L爲波長。即產生共振之條件時，開口處爲駐波節點，即開口處水位爲零；港池底端爲駐波奏點，即底端處水位變化最大。可能發生之共振波長分別爲4ℓ或4/3ℓ或4/5ℓ或4/7ℓ.....等倍數之港池長度。

考慮以不透水性岸壁設計之矩型形狀港池,如附圖2-7-2,假設海岸線平直兩邊延x軸無限延伸,y軸向外海爲正,原點在港口最左側點,z軸向上爲正,外海海域及港區假設皆爲等水深h。同樣爲方便外海滿足輻射邊界條件,一般解析時常將計算區域分爲外海區(區域I)及港內區(區域II),此處並以港口$\overline{AB}$爲兩區之介面(如附圖2-7-2)。

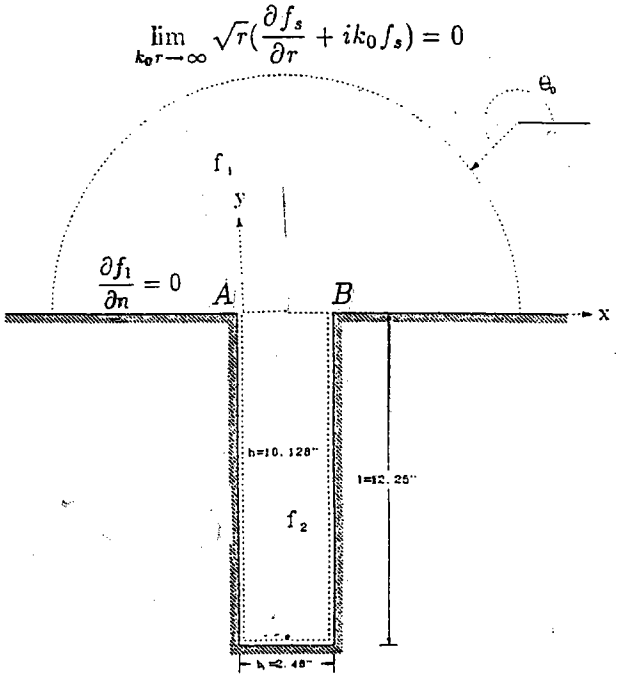

圖2-7-2　單開口矩形港池計算區域示意圖

假設流體滿足不可壓縮、無黏性及非旋流之條件因此存在流速勢(velocity potential) $\Phi_j(x,y,z,t)$, j=1,2分別滿足三維拉普拉氏方程式(Laplace equation)

$$\frac{\partial^2\Phi_j}{\partial x^2}+\frac{\partial^2\Phi_j}{\partial y^2}+\frac{\partial^2\Phi_j}{\partial z^2}=0, \qquad j=1,2 \tag{2.7.16}$$

Φ_1,Φ_2分別表示在區域Ⅰ及區域Ⅱ之流速勢。假設入射波ζ_0垂直作用於海岸線(x軸),如圖2-7-1,其複數表示式爲:

$$\zeta_0(x,y,t)=a_0e^{-i(k_0y-\sigma t)} \tag{2.7.17}$$

式中a_0爲波浪振幅(wave amplitude),$i=\sqrt{-1}$

k_0爲週波數(radian wave number), $k_0=2\pi/L_0$, L_0爲波長(wave length)

σ爲週頻率(radian frequency), $\sigma=2\pi/T$, T爲波浪週期(wave period)

區域Ⅰ及區域Ⅱ之流速勢Φ_1及Φ_2皆分別滿足線性自由表面動力邊界條件及運動邊界條件,即

$$\frac{\partial\zeta_j}{\partial t}-\frac{\partial\Phi_j}{\partial z}=0, \qquad j=1,2 \qquad ,z=0 \tag{2.7.18a}$$

$$\frac{\partial\Phi_j}{\partial t}+g\zeta_j=0, \qquad j=1,2 \qquad ,z=0 \tag{2.7.18b}$$

式中$\zeta_1(x,y,t),\zeta_2(x,y,t)$分別表示在區域Ⅰ及區域Ⅱ之水位變化，g爲重力加速度。

上二式可合併爲

$$\frac{\partial^2\Phi_j}{\partial t^2}+g\frac{\partial\Phi_j}{\partial z}=0, \qquad j=1,2 \qquad ,z=0 \tag{2.7.18c}$$

基於入射波條件及線性理論,我們可假設水位變化ζ_j爲週期性函數,可表示爲

$$\zeta_j(x,y,t)=f_j(x,y)e^{-i\sigma t}, \qquad j=1,2 \tag{2.7.19}$$

式中f_1,f_2分別稱爲區域Ⅰ及區域Ⅱ之波函數(wave function)。

在等水深區,假設海底不透水,則滿足

$$\frac{\partial\Phi_1}{\partial z}=0, \qquad z=-h \tag{2.7.20}$$

在外海區(區域Ⅰ),根據控制方程式(2.7.16),入射波條件(2.7.17)式,海底不透水邊界條件(2.7.20)式及水位變化週期性條件(2.7.19)式,則流速勢$\Phi_1(x,y,z,t)$可表示爲:

$$\Phi_1(x,y,z,t)=A_0\cosh[k_0(h+z)]f_1(x,y)e^{i\sigma t} \tag{2.7.21}$$

其中常數A_0定義爲

$$A_0 = \frac{iga_0}{\sigma \cosh(k_0 h)} \tag{2.7.22}$$

式中波函數f_1(x,y)滿足下列荷姆茲方程式(Helmholtz eqution)

$$\frac{\partial^2 f_1}{\partial x^2} + \frac{\partial^2 f_1}{\partial y^2} + k_0^2 f_1 = 0 \tag{2.7.23}$$

且波數k_0滿足分散關係式(dispersion relation)

$$\sigma^2 = g k_0 \ \tanh(k_0 h) \tag{2.7.24}$$

同樣以f_2表示港內區之波函數,則f_2滿足下列荷姆茲方程式(Helmholtz eqution)

$$\frac{\partial^2 f_2}{\partial x^2} + \frac{\partial^2 f_2}{\partial y^2} + k_0^2 f_2 = 0 \tag{2.7.25}$$

其中k_0爲入射波波數。

假設外海岸線爲平直向兩測無限延伸,其岸壁爲直立不可穿透,以∂C表示,則f_1在海岸線垂直分量滿足

$$\frac{\partial f_1}{\partial n} = 0, \qquad on \quad \overrightarrow{AC} \quad and \quad \overrightarrow{BD} \tag{2.7.26}$$

外海地區之波函數f_1,除包括入射波f_0,及受平直海岸線反射之反射波f_r,還包括港內由港口向外散射之散射波f_s,表示爲

$$f_1 = f_0 + f_r + f_s \tag{2.7.27}$$

其中散射波在無窮遠處,滿足輻射條件(Sommerfeld radiation condition)

$$\lim_{k_0 r \to \infty} \sqrt{r}\left(\frac{\partial f_s}{\partial r} + i k_0 f_s\right) = 0 \tag{2.7.28}$$

在區域 I 及區域 II 之界面處$\overline{AB}$,應分別滿足波函數及波函數之法線方向導數連續條件:

$$f_1 = f_2 \qquad on \quad \overline{AB} \tag{2.7.29a}$$

$$\frac{\partial f_1}{\partial n_1} = -\frac{\partial f_2}{\partial n_2} \qquad on \quad \overline{AB} \tag{2.7.29b}$$

式中 $\vec{n}_1$ 及 $\vec{n}_2$ 分別表示區域 I 及區域 II 在界面向外法線方向之單位向量，$\vec{n}_1 = -\vec{n}_2$ 。

假設港池內壁爲直立不可穿透體，則其邊界上（以 ∂B 表示）應滿足邊界條件

$$\frac{\partial f_2}{\partial x}(0,y) = \frac{\partial f_2}{\partial x}(b,y) = 0 \qquad for \quad -\ell < y < 0 \tag{2.7.30a}$$

$$\frac{\partial f_2}{\partial y}(x,-\ell) = 0 \qquad for \quad 0 < x < b \tag{2.7.30b}$$

對港池界面處 $\overline{AB}$，應滿足波函數之法線方向導數連續條件：

$$\frac{\partial f_2}{\partial y}(x,0) = \frac{\partial f_1}{\partial y}(x,0) = C(x) \qquad for \quad 0 < x < b \tag{2.7.30c}$$

港池放大係數R我們定義爲港內任意點 $\vec{x}$ 之振幅對港口外之入射波之振幅的比值，表示如下：

$$R = \frac{|\eta_2|}{|\eta_i + \eta_r|} = \frac{|f_2|}{|f_i + f_r|} = |f_2| \tag{2.7.31}$$

引用變數分離法（ the method of separation of variables）原理，荷姆茲方程式(2.7.22)之解可表示爲

$$f_2(x,y) = X(x)Y(y) \tag{2.7.32}$$

由控制方程式(2.7.25)及邊界條件(2.7.30)，港內之波函數 f_2 可表示爲：

$$f_2(x,y) = \sum_{n=0}^{\infty} A_n \cos\alpha_n x \cosh\beta_n(y+\ell) \tag{2.7.33}$$

其中 $\alpha_n = \frac{n\pi}{b}$ ，$\beta_n = \sqrt{(\frac{n\pi}{b})^2 - k_0^2}$ ，A_n 爲未定係數。

表示式(2.7.33)對y微分，可得

$$\frac{\partial f_2}{\partial y}(x,y) = \sum_{n=0}^{\infty} A_n\beta_n \cos\alpha_n x \sinh\beta_n(y+\ell) \tag{2.7.34}$$

令$y=0$,則(2.7.34)可得

$$\frac{\partial f_2}{\partial y}(x,0) = -A_0 k \sin k\ell + \sum_{n=1}^{\infty} A_n \beta_n \sinh \beta_n \ell \cos \alpha_n x \tag{2.7.35}$$

係數A_0及A_n,n=1,2,3...將引用正交序列$\cos \alpha_m x, m = 0,1,2,3...$在開口處$0 < x < b$,y=0之正交性，以求解。將表示式(2.7.35)每個項分別做積分運算$\int_0^b (\,)\cos \alpha_n x dx$,則可得

$$A_0 = \frac{-\int_0^b \frac{\partial f_2}{\partial y}(x,0)dx}{bk_0 \sin k_0 \ell} \tag{2.7.36a}$$

$$A_n = \frac{2\int_0^b \frac{\partial f_2}{\partial y}(x,0)\cos \alpha_n x dx}{b\beta_n \sinh \beta_n \ell}, \qquad n = 1,2,3..... \tag{2.7.36b}$$

由邊界條件(2.7.30c)知$\frac{\partial f_2}{\partial y}(x,0) = C(x)$,當$0 < x < b$,y=0,假如$C(x)$能求得則波函數$f_2$即可求得。此處將假設港池開口甚小,令$C(x)$爲一常數表示爲$C_0$,即$\frac{\partial f_2}{\partial y}(x,0) = C_0$,在$0 < x < b$,因此

$$A_0 = \frac{-C_0}{k_0 \sin k_0 \ell} \tag{2.7.37a}$$

$$A_n = \frac{2C_0 \sin \alpha_n b}{n\pi \beta_n \sinh \beta_n \ell}, \qquad n = 1,2,3..... \tag{2.7.37b}$$

將表示式(2.7.37a)及(2.7.37b)代入波函數(2.7.34)可得

$$f_2(x,y) = C_0 \cdot Q_2(x,y) \tag{2.7.38a}$$

式中Q_2定義爲

$$Q_2(x,y) = \frac{-\cos k_0(y+\ell)}{k_0 \sin k_0 \ell} + \sum_{n=1}^{\infty} \frac{2\sin \alpha_n b}{n\pi \beta_n \sinh \beta_n \ell} \cos \alpha_n x \cosh \beta_n (y+\ell), \tag{2.7.38b}$$

外海地區之波函數f_1,除包括入射波f_0,及受平直海岸線反射之反射波f_r,還包括港內由港口向外散射之散射波f_s,表示爲

$$f_1 = f_0 + f_r + f_s \tag{2.7.39}$$

因爲入射波 f_0 與海岸線反射之反射波滿足

$$f_r(x,y) = f_i(x,-y) \tag{2.7.40}$$

因此散射波在海岸線上滿足

$$\frac{\partial f_s}{\partial n} = 0 \qquad on \quad \overrightarrow{AC} \quad and \quad \overrightarrow{BD} \tag{2.7.41}$$

並在區域 I 及區域 II 之界面處 $\overline{AB}$, 由(2.7.29b)散射波應滿足波函數之法線方向導數連續條件:

$$\frac{\partial f_s}{\partial n} = -\frac{\partial f_2}{\partial n} \qquad on \quad \overline{AB} \tag{2.7.42}$$

而且散射波在無窮遠處,滿足輻射條件(Sommerfeld radiation condition)

$$\lim_{k_0 r \to \infty} \sqrt{r}(\frac{\partial f_s}{\partial r} + ik_0 f_s) = 0 \tag{2.7.43}$$

在滿足各項邊界條件之荷姆茲方程式(2.7.23)之 Weber 解在區域I散射波 f_s 可表示爲下列積分方程(Baker及Copson ,1950):

$$f_s(x,y) = b_0 \int_{\partial B_1} \left[f_s(x_0,0)\frac{\partial H_0^{(1))}(kr)}{\partial n} - H_0^{(1)}(kr)\frac{\partial f_s(x_0,0)}{\partial n} \right] ds \tag{2.7.44}$$

式中 ∂B_1 分別爲外海區之無限長海岸線, $b_0 = \frac{-i}{4}$,當 (x,y) 在區域I內部 $(y>0)$ 。 $b_0 = \frac{-i}{2}$,當 (x,y) 在x軸上(y=0) 。 $H_0^{(1)}(k_1 r)$ 爲第一類零階漢克函數(first kind the zeroth order Hankel function) 。 $r = \sqrt{(x-x_0)^2 + y^2}$, $(x_0,0)$ 爲邊界上之點, (x,y) 爲邊界上或區域內任一點。

若點(x,y)落在x軸上即y=0則

$$\frac{\partial}{\partial n}[H_0^{(1))}(kr)] = 0 \qquad on \quad y = 0 \tag{2.7.45}$$

因此

$$f_s(x,0) = -\frac{i}{2}\int_{\overline{AB}} H_0^{(1)}(kr)\frac{\partial f_2(x,0)}{\partial n}]ds \tag{2.7.46}$$

如上所示假設港池開口甚小,即 $\frac{\partial f_2}{\partial y}(x,0) = C_0$,在 $0 < x < b$, 因此

$$f_s(x,0) = -\frac{i}{2}C_0 \int_{\overline{AB}} H_0^{(1)}(kr)ds \tag{2.7.47}$$

因爲 $f_i + f_r$ 爲常數,不失一般性可令

$$f_i + f_r = 1 \qquad on \quad \overline{AB} \tag{2.7.48}$$

因此 $f_1(x,0)$ 可表示爲

$$f_1(x,0) = 1 - f_s(x,0) = 1 - C_0 \cdot Q_1 \tag{2.7.49a}$$

式中 Q_1 定義爲

$$Q_1 = \frac{i}{2b}[\int_0^x H_0^{(1)}(kr)dr + \int_0^{b-x} H_0^{(1)}(kr)dr] \tag{2.7.49b}$$

將波函數 f_1 表示式(2.7.38)及波函數 f_2 表示式(2.7.49)代入區域 I 及區域 II 之界面處 $\overline{AB}$,波函數連續條件(2.7.29a)可得

$$C_0 \cdot Q_2(x,0) = 1 - C_0 \cdot Q_1(x,0) \tag{2.7.50}$$

將表示式(2.7.50)每個項分別做積分運算 $\int_0^b (\ )dx$,則可得

$$C_0 \cdot \overline{Q}_2 = 1 - C_0 \cdot \overline{Q}_1 \tag{2.7.51}$$

式中

$$\overline{Q}_1 = \frac{i}{2b} \int_0^b [\int_0^x H_0^{(1)}(kr)dr + \int_0^{b-x} H_0^{(1)}(kr)dr]dx \tag{2.7.52a}$$

$$\overline{Q}_2 = \frac{-\cot k\ell}{k} + \sum_{n=1}^{\infty} \frac{2b\sin^2 \alpha_n b}{(n\pi)^2 \beta_n \tanh \beta_n \ell}, \tag{2.7.52b}$$

由(2.7.51)式可求得 C_0

$$C_0 = \frac{1}{\overline{Q}_1 + \overline{Q}_2} \tag{2.7.53}$$

引此波函數 f_2 表示式(2.7.38)可表爲

$$f_2(x,y)=\frac{1}{\overline{Q}_1+\overline{Q}_2}\cdot Q_2(x,y) \tag{2.7.54}$$

式中表示式$Q_2(x,y)$，係數$\overline{Q}_1$及$\overline{Q}_2$分別定義如(2.7.38b)、(2.7.52a)及(2.7.52b)。

考慮縱深ℓ=12.25英吋，寬b_1=2.48英吋，等水深h=10.128英吋全開口矩形港池，假設外海之海岸線及港池內壁爲不透水直立壁，向x軸兩側平直延伸。此處將探討從外海遠處垂直海岸線入射之不同週期波浪作用下，矩形港池底端中點之港池共振曲線變化，圖2-7-3爲矩形港池端點處無因次波浪參數$k_0\ell$與擴大率R之相關曲線圖，實線本文理論解之結果，虛線爲有限元素法模式(Model WE21)及邊界元素法模式(Model WH21)之結果，黑點則爲Lee (1969)之試驗結果，計算結果與試驗結果甚爲吻合。

對開口一維不透水矩形港池(長度遠大於寬度)之自然共振週期T，Merian's公式(Wilson, 1972)表示爲：

$$T=\frac{2\ell}{(2n+1)\sqrt{gh}},\quad n=0,1,2... \tag{2.7.55}$$

式中ℓ爲港池長度，g爲重力加速度，h爲水深。如以無因次參數ℓ/L可表示爲：

$$\frac{\ell}{L}=\frac{2n+1}{4}=\frac{1}{4},\frac{3}{4},1\frac{1}{4},1\frac{3}{4},2\frac{1}{4},2\frac{3}{4}.... \tag{2.7.56}$$

式中L爲波長。即產生共振之條件時，開口處爲駐波節點，即開口處水位爲零；港池底端爲駐波奏點，即底端處水位變化最大。可能發生之共振波長分別爲4ℓ或$4/3\ell$或$4/5\ell$或$4/7\ell$.....等倍數之港池長度。

根據數值模式推算上述不透水矩形港池(長與寬之比約爲5)因波浪引起之共振(開口處滿足水位連續及速度連續條件)，前兩個共振點分別發生在無因次參數$\ell/L=\frac{1}{4.8}$及$\ell/L=\frac{3}{4.5}$，相較Merian's公式估計值$\ell/L=\frac{1}{4}$及$\ell/L=\frac{3}{4}$甚爲接近，但略小。

根據數值模式推算一不透水矩形港池之第一共振點發生在長週期；其位於處港池底端之放大係數約爲8(如圖2-7-3)，即共振時底端之波高可爲原來8倍之多，但短週期之第二共振點處放大係數略小於3，相對較小。此顯示在不考慮能量消散之效應，一般長週期之共振也較短週期爲大。其次一般短週期之波浪，比較容易受如防波堤結構物之遮蔽，透水邊界能量消散及地形摩擦等效應之影響，而在進入港內後快速減衰，因此港外短週期成份波進入港內後迅速衰減，但長週期之波能相較則不易受遮蔽效應，或透水牆波能消散影響，且隨週期之增大，波長之增長影響之程度遞減，因此長週期波浪對港池共振之影響一般較短期波浪爲大，也較爲重要。

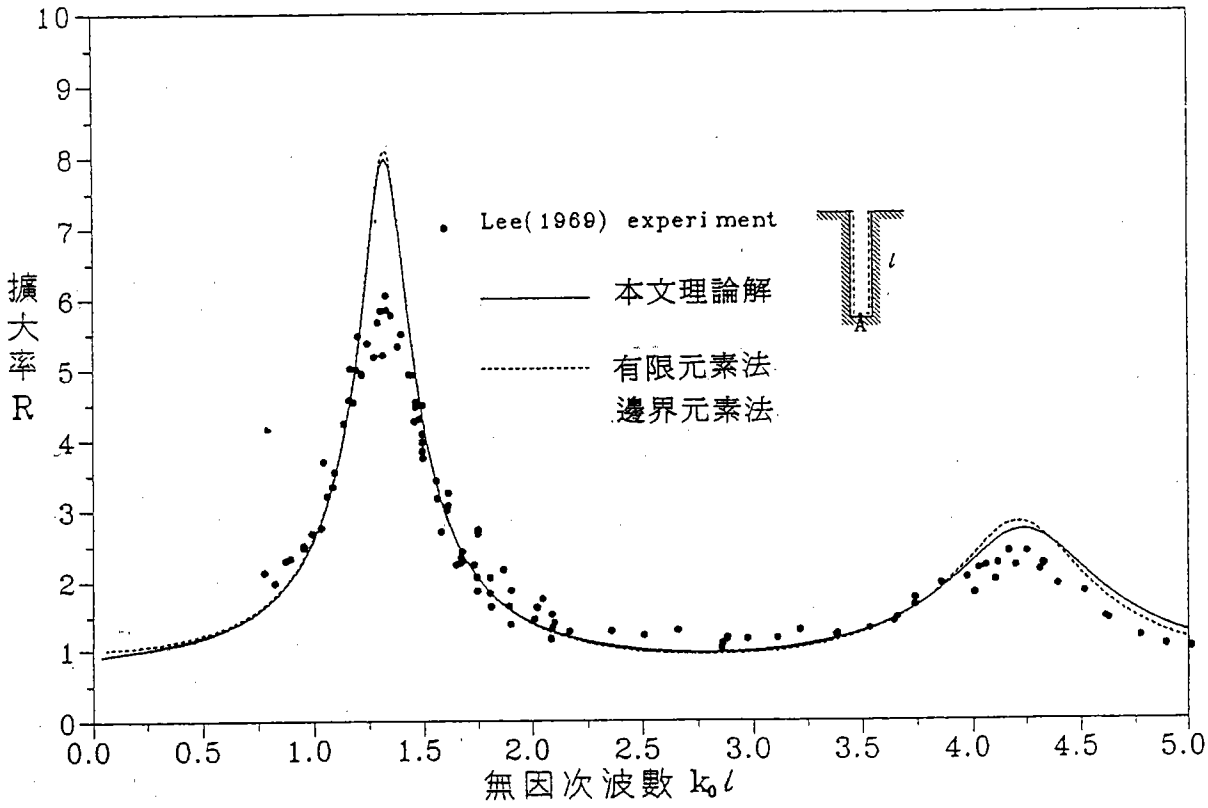

圖 2-7-3　矩形港池端點處無因次波浪參數 $k_0\ell$ 與擴大率 R 之相關曲線圖

—參、本所發展線性波場推算模式介紹—

有關線性波場推算數值模式,本所與台灣大學土木工程研究所合作研究之邊界元素法模式(Model WH21)、有限元素法模式(Model WE21)、有限差分法模式(Model WP21)等三種,分別介紹如后。

3-1邊界元素法模式-MODEL WH21

3-1-1理論解析

考慮以透水性岸壁設計之不規則形狀港池,如附圖3-1-1,假設海岸線平直兩邊延x軸無限延伸,y軸向外海爲正,原點在港口中心點,z軸向上爲正,外海海域及港區假設皆爲等水深h。同樣爲方便外海滿足輻射邊界條件,一般解析時常將計算區域分爲外海區(區域I)及港內區(區域II),此處並以港口$\overline{AB}$爲兩區之介面(如附圖3-1-1)。

$$\lim_{k_0 r\to\infty}\sqrt{r}\left(\frac{\partial f_s}{\partial r}+ik_0 f_s\right)=0$$

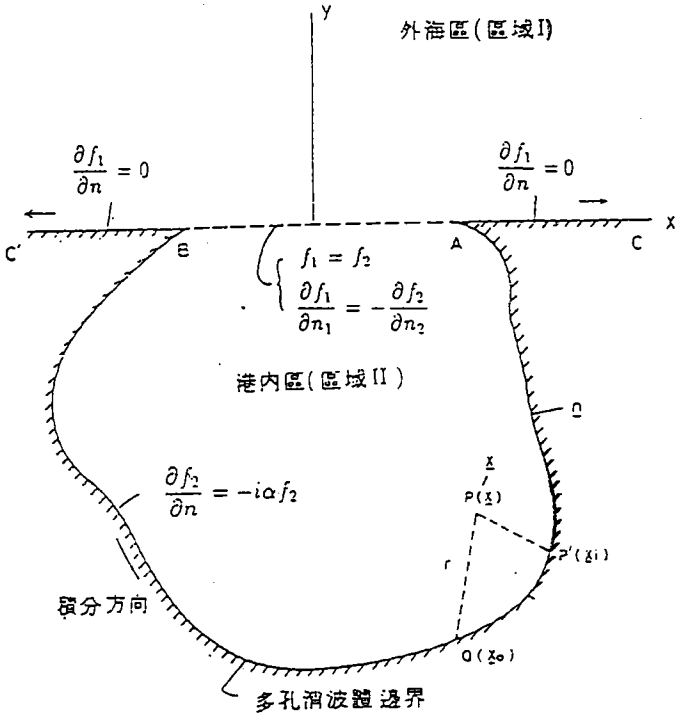

圖3-1-1 邊界元素法計算區域示意圖

假設流體滿足不可壓縮、無黏性及非旋流之條件因此存在流速勢(velocity potential) $\Phi_j(x,y,z,t)$, j=1,2分別滿足三維拉普拉氏方程式(Laplace equation)

$$\frac{\partial^2\Phi_j}{\partial x^2}+\frac{\partial^2\Phi_j}{\partial y^2}+\frac{\partial^2\Phi_j}{\partial z^2}=0,\qquad j=1,2 \tag{3.1.1.1}$$

Φ_1,Φ_2 分別表示在區域 I 及區域 II 之流速勢。假設入射波 ζ_0 波向線與正 x 軸成 θ_0 角度(如圖 3-1-1),其複數表示式爲:

$$\zeta_0(x,y,t)=a_0e^{-i[k_0(xcos\theta_0+ycos\theta_0)+i\sigma t]} \tag{3.1.1.2a}$$

或

$$\zeta_0(r,\theta,t)=a_0e^{-i[k_0r\cos(\theta-\theta_0)+i\sigma t]} \tag{3.1.1.2b}$$

式中 a_0 爲波浪振幅(wave amplitude), $x=r\cos\theta, y=r\sin\theta, i=\sqrt{-1}$

k_0 爲週波數(radian wave number), $k_0=2\pi/L_0$, L_0 爲波長(wave length)

σ 爲週頻率(radian frequency), $\sigma=2\pi/T$, T 爲波浪週期(wave period)

區域 I 及區域 II 之流速勢 Φ_1 及 Φ_2 皆分別滿足線性自由表面動力邊界條件及運動邊界條件,即

$$\frac{\partial\zeta_j}{\partial t}-\frac{\partial\Phi_j}{\partial z}=0,\qquad j=1,2\qquad ,z=0 \tag{3.1.1.3a}$$

$$\frac{\partial\Phi_j}{\partial t}+g\zeta_j=0,\qquad j=1,2\qquad ,z=0 \tag{3.1.1.3b}$$

式中 $\zeta_1(x,y,t),\zeta_2(x,y,t)$ 分別表示在區域 I 及區域 II 之水位變化，g 爲重力加速度。

上二式可合併爲

$$\frac{\partial^2\Phi_j}{\partial t^2}+g\frac{\partial\Phi_j}{\partial z}=0,\qquad j=1,2\qquad ,z=0 \tag{3.1.1.3c}$$

基於入射波條件及線性理論,我們可假設水位變化 ζ_j 爲週期性函數,可表示爲

$$\zeta_j(x,y,t)=f_j(x,y)e^{-i\sigma t},\qquad j=1,2 \tag{3.1.1.4}$$

式中 f_1,f_2 分別稱爲區域I及區域II之波函數(wave function)。

在等水深區,假設海底不透水,則滿足

$$\frac{\partial\Phi_1}{\partial z}=0,\qquad z=-h_1 \tag{3.1.1.5}$$

在外海區(區域I),根據控制方程式(3.1.1.1),入射波條件(3.1.1.2)式,海底不透水邊界條件(3.1.1.5)式及水位變化週期性條件(3.1.1.4)式,則流速勢 $\Phi_1(x,y,z,t)$ 可表示爲:

$$\Phi_1(x,y,z,t) = A_0 \cosh[k_0(h_1+z)] f_1(x,y) e^{i\sigma t} \tag{3.1.1.6}$$

其中常數A_0定義爲

$$A_0 = \frac{ig}{\sigma \cosh(k_0 h_1)} \tag{3.1.1.7}$$

式中波函數f_1(x,y)滿足下列荷姆茲方程式(Helmholtz eqution)

$$\frac{\partial^2 f_1}{\partial x^2} + \frac{\partial^2 f_1}{\partial y^2} + k_0^2 f_1 = 0 \tag{3.1.1.8}$$

且波數k_0滿足分散關係式(dispersion relation)

$$\sigma^2 = g k_0 \ \tanh(k_0 h_1) \tag{3.1.1.9}$$

在外海區(區域I)之波速爲$C_1 = L_0/T$,群波速(group velocity)爲$C_{1g} = \kappa_1 C_1$

式中κ_1定義爲

$$\kappa_1 = \frac{1}{2}\left[1 + \frac{2k_0 h_1}{\sinh 2k_0 h_1}\right] \tag{3.1.1.10}$$

同樣以f_2表示港內區之波函數,則f_2滿足下列荷姆茲方程式(Helmholtz eqution)

$$\frac{\partial^2 f_2}{\partial x^2} + \frac{\partial^2 f_2}{\partial y^2} + k_0^2 f_2 = 0 \tag{3.1.1.11}$$

其中k_0爲入射波波數。

我們引用Booij(1981)之海底能量消散效應,提出下列之修正荷姆茲方程式(modified Helmholtz eqution)

$$\frac{\partial^2 f_j}{\partial x^2} + \frac{\partial^2 f_j}{\partial y^2} + k_1^2 f_j = 0, \qquad j = 1,2 \tag{3.1.1.12a}$$

式中

$$k_1^2 = k_0^2 + \frac{i\sigma E_0}{gh} \tag{3.1.1.12b}$$

其中k_0爲入射波波數,σ爲週頻率(radian frequency), E_0爲每單位波能密度之能量消散。

假設外海岸線爲平直向兩測無限延伸,其岸壁爲直立不可穿透,以∂C表示,則f_1在海岸線垂直分量滿足

$$\frac{\partial f_1}{\partial n} = 0, \qquad on \quad \partial C \tag{3.1.1.13}$$

外海地區之波函數 f_1,除包括入射波 f_0,及受平直海岸線反射之反射波 f_r ,還包括港內由港口向外散射之散射波 f_s ,表示爲

$$f_1 = f_0 + f_r + f_s \tag{3.1.1.14}$$

其中散射波在無窮遠處,滿足輻射條件(Sommerfeld radiation condition)

$$\lim_{k_0 r \to \infty} \sqrt{r}\left(\frac{\partial f_s}{\partial r} + ik_0 f_s\right) = 0 \tag{3.1.1.15}$$

若假設外海岸線爲平直向兩測無限延伸,其爲完全消波海暗岸,則 f_1 在海岸線垂直分量滿足

$$\frac{\partial f_1}{\partial n} = -k_0 f_1, \qquad on \quad \partial C \tag{3.1.1.16}$$

因此外海地區之反射波 $f_r = 0$,方程式(3.1.1.15)改爲:

$$f_1 = f_0 + f_s \tag{3.1.1.16}$$

假設港池以多孔消波體設計爲內壁,則其邊界上(以 ∂B 表示)應滿足多孔邊界條件

$$\frac{\partial f_2}{\partial n} = -i\alpha f_2 \qquad on \quad \partial B \tag{3.1.1.17}$$

式中 α 爲阻尼係數(impedance coefficient)。

若港池岸壁爲部分反射體,根據蘇(1993)解析之結果,消波岸壁港池之消波特性主要由阻尼係數(impedence) α 決定其物理特性,阻尼係數 α 爲一複數，其實部之物理意義相當於電學之電阻(resistance) ,主要決定作用於消波岸壁後之反射波振幅大小；其虛部則相當於電學之電抗(reactance) ,主要決定入射波與反射波之相位差。若 α 爲實部及虛部皆不爲零之複數,蘇(1993)發現港池共振週期及其擴大率皆可能改變, α 之虛部主要影響共振週期之變化,其值爲負數時,將增長原有共振週期,其絕對值愈大改變愈大,反之其值爲正數時,將減短原有共振週期,其絕對值愈大改變也愈大;實部則影響振幅大小,其絕對值愈大能量消散也愈大。在假設無相位差及正向波作用之條件下,阻尼係數與反射係數 C_r 之關係式,根據蘇(1993)可表示爲

$$\alpha = -k_0 \frac{1 - C_r}{1 + C_r}, \qquad 0 \le C_r \le 1 \tag{3.1.1.18}$$

在區域 I 及區域 II 之界面處 $\overline{AB}$,應分別滿足波函數及波函數之法線方向導數連續條件:

$$f_1 = f_2 \qquad on \quad \overline{AB} \tag{3.1.1.19a}$$

$$\frac{\partial f_1}{\partial n_1} = -\frac{\partial f_2}{\partial n_2} \qquad on \quad \overline{AB} \tag{3.1.1.19b}$$

式中 $\vec{n}_1$ 及 $\vec{n}_2$ 分別表示區域 I 及區域 II 在界面向外法線方向之單位向量,$\vec{n}_1 = -\vec{n}_2$。

根據蘇(1993),在滿足各項邊界條件之荷姆茲方程式(3.1.1.8)之 Weber 解在區域 I 散射波 f_s 及區域 II 波函數 f_2 分別可表示爲下列積分方程(Baker 及 Copson ,1950):

$$f_s(\overline{x}) = b_0 \int_{\partial B_1} \left[f_s(\overline{x}_0) \frac{\partial H_0^{(1))}(k_1 r)}{\partial n_1} - H_0^{(1)}(k_1 r) \frac{\partial f_s(\overline{x}_0)}{\partial n_1} \right] ds \tag{3.1.1.20}$$

$$f_2(\overline{x}) = b_0 \int_{\partial b_2} \left[f_2(\overline{x}_0) \frac{\partial H_0^{(1))}(k_1 r)}{\partial n_2} - H_0^{(1)}(k_1 r) \frac{\partial f_2(\overline{x}_0)}{\partial n_2} \right] ds \tag{3.1.1.21}$$

式中 ∂B_1 及 ∂B_2 分別爲外海區之無限長海岸線 $(\partial B_1 = \partial C + \overline{AB})$ 及港內區之封閉邊界 $(\partial B_2 = \partial B + \overline{AB}\ )$。

$b_0 = \frac{-i}{4}$,當 $\overline{x}$ 在區域內部。

$b_0 = \frac{-i}{2}$,當 $\overline{x}$ 在平滑區域邊界上。

$b_0 = \frac{-i\pi}{2\beta}$,當 $\overline{x}$ 在內角爲 β 之邊界點上。

$H_0^{(1)}(k_1 r)$ 爲第一類零階漢克函數(first kind the zeroth order Hankel function)。

$r = |\overline{x}_0 - \overline{x}|$, $\overline{x}_0$ 爲邊界上之點, $\overline{x}$ 爲邊界上或區域內任一點。

積分方程式(3.1.1.20)及(3.1.1.21)式對不規則形狀之港池不易求得完整解析解,此處將利用邊界元素法求解波場。

3-1-2 邊界元素法

將港內區域 II 邊界 ∂B_2 ,切割爲 N 個線段, N 個中結點(mid-node)(附圖 3-1-2),每個線段代表一個元素,我們將引用常數元素,假設每一個線段上每個點之 f_2 及 $\frac{\partial f_2}{\partial n}$ 皆爲定值,而以線段中結點之值代表元素值,而元素上 $H_0^{(1)}$, $\frac{\partial H_0^{(1)}}{\partial n}$ 之值將引用高斯積分法,直接計算,而結點 i=1,2,3...N 編號一般以逆時鐘方向編排(如圖 3-1-2)。假設方程式(3.1.1.21)中之 $\overline{x}$ 點爲邊界上結點,則可化爲下列矩陣方程式

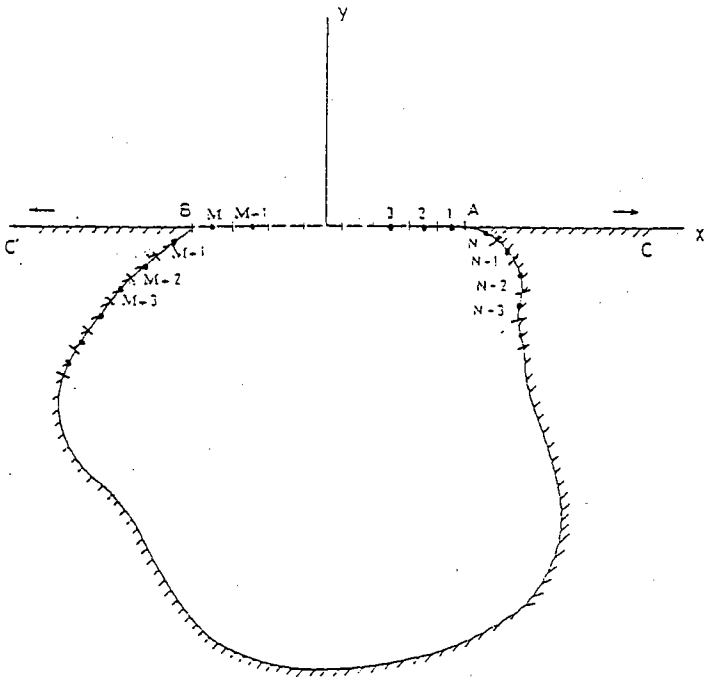

圖3-1-2　邊界元素分割示意圖

$$[H_2]\{F_2\} = [G_2]\{P_2\} \tag{3.1.2.1}$$

式中 $[H_2], [G_2]$ 皆爲 $N \times N$ 矩陣，其矩陣元素 $[H_2]_{ij}, [G_2]_{ij}$ 分別定義爲下列線積分 (line integral)表示式

$$[H_2]_{ij} = b_0 \int_{\Gamma_j} \frac{\partial H_0^{(1)}(k_1 r)}{\partial n_2} dS_j - \delta_{ij} \tag{3.1.2.2a}$$

$$[G_2]_{ij} = b_0 \int_{\Gamma_j} H_0^{(1)}(k_1 r) dS_j \tag{3.1.2.2b}$$

式中 Γ_j 爲邊界 ∂B_1 上第 j 個元素，$r = |\bar{x}_i - \bar{x}'_j|$，$\bar{x}_i$ 爲區域 II 邊界 ∂B_2 上元素之結點，i=1,2,3....N，$\bar{x}'_j$ 爲 Γ_j 元素上任一點，δ_{ij} 爲克郎克函數 (Knonecker delta function)，而 $\{F_2\}$ 及 $\{P_2\}$ 爲 $N \times 1$ 向量，其向量元素 $\{F_2\}_i, \{P_2\}_i$ 分別定義爲

$$\{F_2\}_i = f_2(\bar{x}_i) \tag{3.1.2.3}$$

$$\{P_2\}_i = \frac{\partial f_2(\overline{x}_i)}{\partial n_2} \tag{3.1.2.4}$$

對區域 I 之邊界 ∂B_1 而言，即X軸上之平直海岸線 ∂C 及港口 $\overline{AB}$，邊界上 $\vec{n}_1$ 之方向與正Y軸相同，當方程式(3.1.1.20)之 $\overline{x}$ 爲X軸上之點，則r方向與X軸平行，且與 $\vec{n}_1$(Y軸)垂直，因此滿足

$$\frac{\partial H_0^{(1)}(k_1 r)}{\partial n_1} = 0, \qquad on \quad \partial B_1 \tag{3.1.2.5}$$

式中 $r = |\overline{x}_i - \overline{x}'_j|$，$\overline{x}_i$ 爲X軸上任一結點，$\overline{x}'_j$ 爲 Γ_j 元素上任一點。

假設海岸線爲不透水直立壁因此滿足

$$\frac{\partial f_s(\overline{x})}{\partial n_1} = 0, \qquad on \quad \partial C \tag{3.1.2.6}$$

同理利用邊界元素分離化原理，將港口 $\overline{AB}$ 切割爲M個元素(附圖3-8)，並對應區域II相鄰邊界之結點，$i = 1, 2, ..M, M < N$。假設(3.1.1.20)式中 $\overline{x}$ 點爲邊界 $\overline{AB}$ 上任一結點，則積分方程(3.1.1.21)可化爲下列矩陣方程式

$$\{F_s\} = -[G_1]\{P_s\} \tag{3.1.2.7a}$$

式中 $[G_1]$ 皆爲 $M \times M$ 矩陣，其矩陣元素 $[G_1]_{ij}$ 定義同上爲

$$[G_1]_{ij} = b_0 \int_{\Gamma_j} H_0^{(1)}(k_1 r) dS_j \tag{3.1.2.7b}$$

式中 $r = |\overline{x}_i - \overline{x}'_j|$ ，$\overline{x}_i$ 爲 $\overline{AB}$ 上之結點i=1,2,3.....M, $\overline{x}'_j$ 爲 Γ_j 元素上任一點。$\{F_s\}$ 及 $\{P_s\}$ 爲 $M \times 1$ 向量，其向量元素 $\{F_s\}_i$,$\{P_s\}_i$ 分別定義爲

$$\{F_s\}_i = f_s(\overline{x}_i) \tag{3.1.2.8}$$

$$\{P_s\}_i = \frac{\partial f_s(\overline{x}_i)}{\partial n_1} \tag{3.1.2.9}$$

根據港內與外海二區界面連續條件(3.1.1.19a)及(3.1.1.19b)分別可表示爲矩陣表示式

$$\{F_2^x\} = \{F_i\} + \{F_s\} \tag{3.1.2.10a}$$

及

$$\{P_2^x\} = -\{P_s\} \tag{3.1.2.10b}$$

式中向量$\{F_t\}$爲入射波及反射波波函數之和，$\{F_2^x\}$及$\{P_2^x\}$上標爲x,表示由區域II邊界在港口介面處$\overline{AB}$之結點所形成$M\times 1$向量,又定義$[G_2^0],[H_2^0],\{F_2^0\}$及$\{P_2^0\}$上標爲0,表示在區域II邊界上除港口$\overline{AB}$處結點以外所形成$N\times(N-M)$矩陣或$(N-M)\times 1$向量,因此可定義：

$$[G_2]=[G_2^0 \quad G_2^x],\qquad [H_2]=[H_2^0 \quad H_2^x] \tag{3.1.2.11a}$$

$$\{P_2\}=\begin{Bmatrix}P_2^0\\P_2^x\end{Bmatrix},\qquad \{F_2\}=\begin{Bmatrix}F_2^0\\F_2^x\end{Bmatrix} \tag{3.1.2.11b}$$

假設港池以多孔消波體設計做爲港池內壁,則應滿足下列關係式

$$\{P_2^0\}=[A]\{F_2^0\} \tag{3.1.2.12a}$$

式中矩陣[A]之元素$[A]_{ij}$定義爲

$$[A]_{ij}=-i\alpha^j\delta_{ij},\qquad i,j=1,2...N-M \tag{3.1.2.12b}$$

α^j爲第j個元素上消波岸壁之阻尼係數。

由式(3.1.2.1) (3.1.2.7)及(3.1.2.10)可組合爲：

$$\begin{bmatrix}Q_2^0 & H_2^x & G_2^x\\ 0 & I & G_1\end{bmatrix}\begin{Bmatrix}F_2^0\\F_2^x\\-P_2^x\end{Bmatrix}=\begin{Bmatrix}0\\F_t\end{Bmatrix} \tag{3.1.2.13}$$

式中I爲單位矩陣,且$[Q_2^0]$定義爲

$$[Q_2^0]=[H_2^0]-[G_2^0][A] \tag{3.1.2.14}$$

矩陣方程式(3.1.2.13)計有N+M個方程式,港內邊界上波函數f_2有N個未知量及港口處$\frac{\partial f_2}{\partial n_2}$有M個未知量,可利用高斯消去法求解。而港內任一點之波函數$f_2(\bar{x})$可由表示式(3.1.1.21)求得,同理外海任一點之波函數$f_1(\bar{x})$可由表示式(3.1.1.20)先求得散射波$f_s(\bar{x})$。

考慮縱深ℓ=12.25英吋,寬b_1=2.48英吋,等水深h=10.128英吋全開口矩形港池,假設外海之海岸線及港池內壁爲不透水直立壁,向x軸兩側平直延伸。此處將探討從外海遠處垂直海岸線入射之不同週期波浪作用下,矩形港池底端中點之港池共振曲線變化,圖2-7-3爲矩形港池端點處無因次波浪參數$k_0\ell$與擴大率R之相關曲線圖,實線本文理論解之結果,虛線爲有限元素法模式(Model WE21)及邊界元素法模式(Model WH21)之結果,黑點則爲Lee (1969)之試驗結果,計算結果與試驗結果甚爲吻合。

3-2有限元素法模式-MODEL WE21

3-2-1理論解析

考慮包括任意不規則形狀港池及緩變地形變化之近岸海域,如圖3-2-1平面示意圖,x軸置於海岸線上,原點爲海岸線上適當點,正y軸向外海方向。有限港池區(包括港內區與港口處半徑R_a之半圓區)稱區域Ⅱ,水深$h_2(x,y)$爲緩慢變化之不等水深區;港外區(稱區域Ⅰ)爲外海無限範圍,爲等水深區(水深h_1),區域Ⅰ與區域Ⅱ之相連邊界爲半徑R_a之半圓(理論上不一定爲半圓),以∂A表示。假設滿足不可壓縮、無黏性及非旋流之條件因此存在流速勢(velocity potential)$\Phi_j(x,y,z,t), j=1,2$分別滿足三維拉普拉氏方程式(Laplace equation)

$$\frac{\partial^2\Phi_j}{\partial x^2}+\frac{\partial^2\Phi_j}{\partial y^2}+\frac{\partial^2\Phi_j}{\partial z^2}=0, \qquad j=1,2 \tag{3.2.1.1}$$

Φ_1,Φ_2分別表示在區域Ⅰ及區域Ⅱ之流速勢。假設入射波ζ_0波向線與正x軸成θ_0角度(如圖3-2-1),其複數表示式爲:

$$\zeta_0(x,y,t)=a_0e^{-i[k_0(x\cos\theta_0+y\cos\theta_0)-i\sigma t]} \tag{3.2.1.2a}$$

或

$$\zeta_0(r,\theta,t)=a_0e^{-i[k_0r\cos(\theta-\theta_0)-i\sigma t]} \tag{3.2.1.2b}$$

式中a_0爲波浪振幅(wave amplitude), $x=r\cos\theta, y=r\sin\theta, i=\sqrt{-1}$

k_0爲週波數(radian wave number), $k_0=2\pi/L_0$, L_0爲波長(wave length)

σ爲週頻率(radian frequency), $\sigma=2\pi/T$, T爲波浪週期(wave period)

區域Ⅰ及區域Ⅱ之流速勢Φ_1及Φ_2皆分別滿足線性自由表面動力邊界條件及運動邊界條件,即

$$\frac{\partial\zeta_j}{\partial t}-\frac{\partial\Phi_j}{\partial z}=0, \qquad j=1,2 \qquad ,z=0 \tag{3.2.1.3a}$$

$$\frac{\partial\Phi_j}{\partial t}+g\zeta_j=0, \qquad j=1,2 \qquad ,z=0 \tag{3.2.1.3b}$$

式中$\zeta_1(x,y,t),\zeta_2(x,y,t)$分別表示在區域Ⅰ及區域Ⅱ之水位變化,g爲重力加速度。

上二式可合併爲

$$\frac{\partial^2\Phi_j}{\partial t^2}+g\frac{\partial\Phi_j}{\partial z}=0, \qquad j=1,2 \qquad ,z=0 \tag{3.2.1.3c}$$

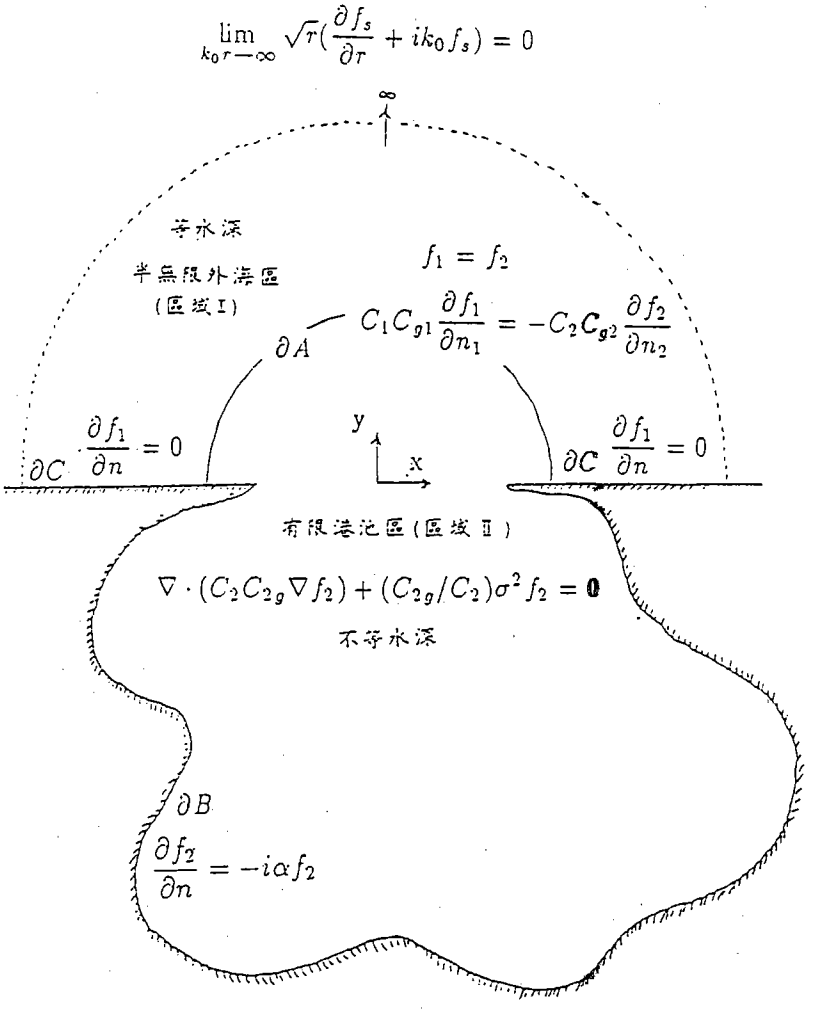

圖3-2-1 有限元素法計算區域示意圖

基於入射波條件及線性理論,我們可假設水位變化ζ_j爲週期性函數,可表示爲

$$\zeta_j(x,y,t) = f_j(x,y)e^{i\sigma t}, \qquad j = 1,2 \tag{3.2.1.4}$$

式中f_1, f_2分別稱爲區域I及區域II之波函數(wave function)。

在外海區(區域I)爲等水深區,假設海底不透水,則滿足

$$\frac{\partial \Phi_1}{\partial z} = 0, \qquad z = -h_1 \tag{3.2.1.5}$$

在有限港池區(區域II)爲不等深區,同理假設海底不透水,則滿足

$$\frac{\partial \Phi_2}{\partial z}+\frac{\partial \Phi_2}{\partial x}\frac{\partial h_2}{\partial x}+\frac{\partial \Phi_2}{\partial y}\frac{\partial h_2}{\partial y}=0, \qquad z=-h_2(x,y) \tag{3.2.1.6}$$

在外海區(區域I),根據控制方程式(3.2.1.1),入射波條件(3.2.1.2)式,邊界條件(3.2.1.5)式及水位變化週期性條件(3.2.1.4)式,則流速勢$\Phi_1(x,y,z,t)$可表示爲:

$$\Phi_1(x,y,z,t)=A_0\cosh[k_0(h_1+z)]f_1(x,y)e^{i\sigma t} \tag{3.2.1.7}$$

其中常數A_0定義爲

$$A_0=\frac{ig}{\sigma\cosh(k_0h_1)} \tag{3.2.1.8}$$

式中波函數f_1(x,y)滿足下列荷姆茲方程式(Helmholtz eqution)

$$\frac{\partial^2 f_1}{\partial x^2}+\frac{\partial^2 f_1}{\partial y^2}+k_0^2 f_1=0 \tag{3.2.1.9}$$

且波數k_0滿足分散關係式(dispersion relation)

$$\sigma^2=gk_0\ \tanh(k_0h_1) \tag{3.2.1.10}$$

在外海區(區域I)之波速爲$C_1=L_0/T$,群波速(group velocity)爲$C_{1g}=\kappa_1 C_1$

式中κ_1定義爲

$$\kappa_1=\frac{1}{2}\left[1+\frac{2k_0h_1}{\sinh 2k_0h_1}\right] \tag{3.2.1.11}$$

在有限港池區(區域II),假設深度爲緩慢變化,流速勢$\Phi_2(x,y,z,t)$表示爲:

$$\Phi_2(x,y,z,t)=A_0\phi_2(x,y,z)e^{i\sigma t} \tag{3.2.1.12}$$

式中ϕ_2爲波函數。

我們引用 Booij(1981)修正Berkhoff(1972)提出之一階修正緩坡方程式(modified mild slope equation):

$$\nabla\cdot(C_2C_{2g}\nabla f_2)+(C_{2g}/C_2+i\sigma E_0)\sigma^2 f_2=0 \tag{3.2.1.13a}$$

式中$f_2(x,y)\cosh[k(h_2+z)]$爲波函數$\phi_2(x,y,z)$之一階項,$f_2(x,y)$爲二維波函數,E_0爲每單位波能密度之能量消散。$\nabla=(\frac{\partial}{\partial x},\frac{\partial}{\partial y})$二維梯度運算子,$C_2=L_2/T$爲波速,$k_2=2\pi/L_2$爲波數,$C_{2g}=\kappa_2C_2$爲群波速(group velocity),$\kappa_2$定義爲

$$\kappa_2 = \frac{1}{2}\left[1 + \frac{2k_2h_2}{\sinh 2k_2h_2}\right] \tag{3.2.1.13b}$$

在淺水波(shallow water wave), $k_2h_2 \ll 1, C_2 = \sqrt{gh_2}, C_{2g} = C_2$,則方程式(3.2.1.13)可簡化爲

$$\nabla \cdot (h_2 \nabla f_2) + (\sigma^2/g + + i\sigma E_0/g) f_2 = 0 \tag{3.2.1.14}$$

在深水波(deep water wave),$k_2h_2 \gg 1, C_2 = g/\sigma, C_{2g} = 0.5C_2$,則方程式(3.2.1.13)可簡化爲修正荷姆茲方程式

$$\frac{\partial^2 f_2}{\partial x^2} + \frac{\partial^2 f_2}{\partial y^2} + (k_2^2 + \frac{i\sigma E_0}{gh_2}) f_2 = 0 \tag{3.2.1.15}$$

荷姆茲方程式(3.2.1.9)及修正緩坡方程式(3.2.1.13)分別爲港外區及有限港池區之主要控制方程式。

假設外海岸線爲平直向兩測無限延伸,其岸壁爲直立不可穿透,以∂C表示,則f_1在海岸線垂直分量滿足

$$\frac{\partial f_1}{\partial n} = 0, \qquad on \quad \partial C \tag{3.2.1.16}$$

外海地區之波函數f_1,除包括入射波f_0,及受平直海岸線反射之反射波f_r(假設港口爲封閉),還包括港內由港口向外散射之散射波f_s,表示爲

$$f_1 = f_0 + f_r + f_s \tag{3.2.1.17}$$

其中散射波在無窮遠處,滿足輻射條件(Sommerfeld radiation condition)

$$\lim_{k_0 r \to \infty} \sqrt{r}(\frac{\partial f_s}{\partial r} + ik_0 f_s) = 0 \tag{3.2.1.18}$$

假設港池以多孔消波體設計爲內壁,則其邊界上(以∂B表示)應滿足多孔邊界條件

$$\frac{\partial f_2}{\partial n} = -i\alpha f_2 \qquad on \quad \partial B \tag{3.2.1.19}$$

式中α爲阻尼係數(impedance coefficient)。

在區域 I 及區域 II 之界面處∂A,應分別滿足波函數及波函數之法線方向導數連續條件:

$$f_1 = f_2 \qquad on \quad \partial A \tag{3.2.1.20a}$$

$$C_1 C_{g1} \frac{\partial f_1}{\partial n_1} = -C_2 C_{g2} \frac{\partial f_2}{\partial n_2} \qquad on \quad \partial A \tag{3.2.1.20b}$$

式中 $\vec{n}_1$ 及 $\vec{n}_2$ 分別表示區域 I 及區域 II 在界面向外法線方向之單位向量，$\vec{n}_1 = -\vec{n}_2$ 。

3-2-2、有限元素法模式

本節將使用混合元素法(hybrid finite element method) (Chen及Mei ,1974) , (Tsay及Liu ,1983)以求解上述橢圓型態緩坡方程式之邊界值問題。在有限港池區域 II 爲有限範圍，切割爲有限個三角形元素，以求解元素結點上之未知波函數，圖 3-2-1 爲一10度開口圓形港池之元素切割及編號例子。外海區域 I 爲無

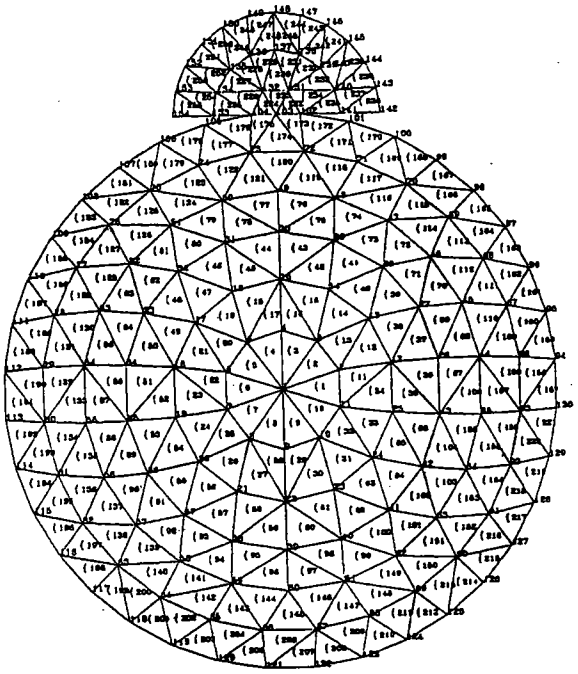

圖 3-2-1 10度開口圓形港池三角形元素分割示意圖

限範圍，我們則應用特徵函數(eigenfunctions)表示法(Tsay及Liu ,1983)，將波函數 f_1 之各成份波 f_0 、 f_r 、 f_s 分別表示如下：

$$f_0(x,y) = f_0(r,\theta) = A_0 e^{-ik_0 r\cos(\theta-\theta_0)}$$

$$= \sum_{n=0}^{\infty} \epsilon_n (-i)^n J_n^{(1)}(k_0 r) \cos[n(\theta - \theta_0)] \qquad (3.2.2.1a)$$

$$f_r(x,y) = f_r(r,\theta) = Ae^{-ik_0 r\cos(\theta+\theta_0)}$$
$$= \sum_{n=0}^{\infty} \epsilon_n (-i)^n J_n^{(1)}(k_0 r) \cos[n(\theta + \theta_0)] \qquad (3.2.2.1b)$$

$$f_s(x,y) = f_s(r,\theta) = \sum_{n=0}^{\infty} \mu_n H_n^{(1)}(k_0 r) \cos(n\theta) \qquad (3.2.2.1c)$$

式中常數A定義如式(2.8), $J_n^{(1)}(k_0 r)$為第一類n階貝索函數(first kind the n-th order Bessel fumction), $H_n^{(1)}(k_0 r)$為第一類第n階漢克函數(first kind the n-th order Hankel function)。μ_n為未知係數。係數ϵ_n定義為

$$\epsilon_n = \begin{cases} 2, & \text{n=0} \\ 1, & \text{n=1,2,3...} \end{cases} \qquad (3.2.2.1d)$$

入射波f_0表示式(3.2.2.1a)滿足入射波(2.2)之條件,反射波f_r表示式(3.2.2.1b)滿足平直海岸線不透水邊界條件,散射波f_s表示式(3.2.2.1c)滿足散射波邊界條件(2.18)式。上述無窮級式收斂甚快,實際計算可取有限項。

根據變分法(calculus of variation)之極小化原理,上述控制方程式,邊界條件及區域分割原理(包括邊界連續條件),可得下列定態泛函數(stationary functional) J_0^s:

$$\begin{aligned} J_0^s(f_2, f_s) = & \int\int_B \frac{1}{2}[C_2 C_{2g}(\nabla f_2)^2 - (C_{2g}/C_2 + i\sigma E_0) f_2^2] dA \\ & + \int_{\partial A} \frac{1}{2} C_2 C_{2g} f_s \frac{\partial f_s}{\partial n_2} d\ell \\ & + \int_{\partial A} C_2 C_{2g} f_2 \frac{\partial f_s}{\partial n_2} d\ell \\ & - \int_{\partial A} C_2 C_{2g} f_2 \frac{\partial f_0}{\partial n_2} d\ell \\ & + \int_{\partial A} C_2 C_{2g} f_0 \frac{\partial f_s}{\partial n_2} d\ell \\ & - \int_{\partial B} \frac{i}{2} \alpha C_2 C_{2g} f_2^2 d\ell \end{aligned} \qquad (3.2.2.2)$$

利用有限元素法原理,將港池區域II之值域分割爲N個三角形元素,每個元素之邊長以不超過1/10波長爲原則,並用一組線性形狀函數(shape function) Ψ_i^e,i=1,2,3表示元素e之波函數f_2^e,波速C_2^e及群波速C_{2g}^e如下:

$$f_2^e = \sum_{i=1}^{3} \Psi_i^e f_{2i}^e, \qquad e = 1,2,3...N \tag{3.2.2.3a}$$

$$C_2^e = \sum_{i=1}^{3} \Psi_i^e C_{2i}^e, \qquad e = 1,2,3...N \tag{3.2.2.3b}$$

$$C_{2g}^e = \sum_{i=1}^{3} \Psi_i^e C_{2gi}^e, \qquad e = 1,2,3...N \tag{3.2.2.3c}$$

式中C_{2i}^e及C_{2gi}^e爲元素e，結點i之已知波速及群波速值，f_{2i}^e爲元素e，結點i之未知波函數f_2值。將區域Ⅰ波函數f_0, f_r及f_s之表示式(3.2.2.1)及區域Ⅱ之每一局部元素波函數f_2^e,波速C_2^e及群波速C_{2g}^e值表示式(3.2.2.3),代入泛函數(3.2.2.2)式,整理可得下列全區域之矩陣方程式

$$\begin{aligned} J_0^s(f_2,\mu) = {} & \frac{1}{2}\{f_2\}_{1\times N}^t [K_1]_{N\times N}\{f_2\}_{N\times 1} \\ & + \frac{1}{2}\{\mu\}_{1\times q}^t [K_2]_{q\times q}\{\mu\}_{q\times 1} \\ & + \{f_2^*\}_{1\times p}^t [K_3]_{p\times q}\{\mu\}_{q\times 1} \\ & + \{K_4\}_{1\times p}^t \{f_2^*\}_{p\times 1} \\ & + \{K_5\}_{1\times q}^t \{f_2^*\}_{p\times 1} \\ & + \frac{1}{2}\{f_2^\#\}_{1\times M}^t [K_6]_{M\times M}\{f_2^\#\}_{M\times 1} \end{aligned} \tag{3.2.2.4}$$

式中第一項已知勁度矩陣$[K_1]$及未知波函數向量$\{f_2\}$,由有限港池區(區域Ⅱ)所有三角元素之區域性矩陣$[K_1^e]$及向量$\{f_2^e\}$,e=1,2....N所組成

$$\begin{aligned} I_1^e &= \frac{1}{2}\int\int_{B^e} [C_2^e C_{2g}^e (\nabla f_2^e)^2 - (C_{2g}^e / C_2^e) f_2^2] dA \\ &= \frac{1}{2}\{f_2^e\}_{1\times 3}^t [K_1^e]_{3\times 3}\{f_2^e\}_{3\times 1}, \qquad e = 1,2....N \end{aligned} \tag{3.2.2.5}$$

式中$\{f_2^e\}^t$爲$\{f_2^e\}$之轉置(transposal matrix)矩陣,而矩陣$[K_1^e]$之元素定義爲

$$[K_1^e]_{ms} = \frac{1}{4\Delta^e}\sum_{i=1}^{3}\sum_{j=1}^{3}\frac{1}{12-\delta_{ij}}\cdot C_{2i}^e C_{2gj}^e (b_m b_s + c_m c_s)$$

$$-\frac{\sigma^2\Delta^e}{60}\sum_{k=1}^{3} d_{2k}(2 + 4\delta_{ms}\delta_{mk}\delta_{sk} + \delta_{mk} + \delta_{sk}), \qquad m,s = 1,2,3 \tag{3.2.2.6}$$

其中Δ^e爲元素e之面積

δ_{ij}爲克朗乃克函數(Knonecker delta function), δ_{ij}定義爲

$$\delta_{ij} = \begin{cases} 1, & \text{i=j} \\ 0, & \text{i} \neq \text{j} \end{cases}$$

$d_{2i} = C_{2gi}/C_{2i} + i\sigma E_{0i}, i = 1,2,3$

$a_i, b_i, c_i, i = 1,2,3$爲e元素線性形狀函數ψ_i^e之係數,其定義爲

$$\psi_i^e(x,y) = (a_i + b_i x + c_i y)/2\Delta^e, \qquad i = 1,2,3 \tag{3.2.2.7}$$

若(x_i, y_i)爲元素e之第i結點,i=1,2,3 ,或以i,j,k表示逆時鐘方向之三結點則

$$a_i = x_j y_k - y_j x_k, \quad i = 1,2,3 \tag{3.2.2.8a}$$

$$b_i = y_j - y_k, \quad i = 1,2,3 \tag{3.2.2.8b}$$

$$c_i = x_k - x_j, \quad i = 1,2,3 \tag{3.2.2.8c}$$

式中第二項已知勁度矩陣$[K_2]$及未知散射波函數向量$\{\mu\}$,由下式定義

$$\begin{aligned} I_2 &= \int_{\partial A} \frac{1}{2} C_2 C_{2g} f_s \frac{\partial f_s}{\partial n_2} d\ell \\ &= \frac{1}{2} \{\mu\}^t_{1\times q} [K_2]_{q\times q} \{\mu\}_{q\times 1} \end{aligned} \tag{3.2.2.9}$$

其中q爲散射波漢克函數展開之項數, R_a爲界面∂A半圓之半徑, H_j'則爲$H_j^{(1)}$之微分函數, j=0,1,2....,q-1。

矩陣$[K_2]$之元素定義爲

$$[K_2]_{ms} = \pi R_a k_0 C_2 C_{2g} 0.5 H'_{m-1} H^{(1)}_{m-1} \epsilon_m \delta_{ms}, \quad m,s = 1,2...q \tag{3.2.2.10}$$

式中第三項已知勁度短矩$[K_3]$及邊界∂A上未知波函數向量$\{f_2^*\}$則由下列表示式定義

$$\begin{aligned} I_3 &= + \int_{\partial A} C_2 C_{2g} f_2 \frac{\partial f_s}{\partial n_2} d\ell \\ &= \{f_2^*\}^t_{1\times p} [K_3]_{p\times q} \{\mu\}_{q\times 1} \end{aligned} \tag{3.2.2.11a}$$

矩陣$[K_3]$之元素定義爲

$$
\begin{aligned}
&[K_3]_{ms} \\
&= -k_0 L_a C_2 C_{2g} H'_s [\cos(s-1)\theta'_{m-1} + \cos(s-1)\theta'_m], 2 \le m \le p-1, 2 \le s \le q \\
&= -k_0 L_a C_2 C_{2g} H'_0, \qquad 2 \le m \le p-1, \quad s = 1 \\
&= -0.5 k_0 L_a C_2 C_{2g} H'_s \cos(s-1)\theta'_1, \qquad m = 1 \quad 2 \le s \le q \\
&= -0.5 k_0 L_a C_2 C_{2g} H'_s \cos(s-1)\theta'_{p-1}, \qquad m = p \quad 2 \le s \le q \\
&= -0.5 k_0 L_a C_2 C_{2g} H'_0, \qquad m = 1, p \quad s = 1
\end{aligned} \tag{3.2.2.11b}
$$

其中

$L_a = \frac{\pi R_a}{p-1}$,爲界面$\partial A$半圓上每個線段之長，$\theta'_1, \theta'_2 ..... \theta'_{p-1}$爲界面$\partial A$半圓上p-1個線段至原點與x軸之角度。

式中第四項已知向量$\{K_4\}$則由下列表示式定義:

$$
\begin{aligned}
I_4 &= -\int_{\partial A} C_2 C_{2g} f_2 \frac{\partial f_s}{\partial n_2} d\ell \\
&= \{K_4\}^t_{1\times p} \{f_2^*\}_{p\times 1}
\end{aligned} \tag{3.2.2.12a}
$$

向量$\{K_4\}$之元素定義爲

$$
\begin{aligned}
\{K_4\}_m &= -0.5 k_0 L_a C_2 C_{2g} (u_{m-1} + u_m), \qquad 2 \le m \le p-1 \\
&= u_1, \qquad m = 1 \\
&= u_{p-1}, \qquad m = p
\end{aligned} \tag{3.2.2.13a}
$$

$$
u_m = i\cos(\theta_m - \theta_0) e^{ik_0 R_a \cos(\theta_m - \theta_0)} + i\cos(\theta_m + \theta_0) e^{ik_0 R_a \cos(\theta_m + \theta_0)}
$$

$$
m = 1, 2, 3 .... p-1 \tag{3.2.2.13b}
$$

式中第五項已知向量$\{K_5\}$則由下列表示式定義:

$$
\begin{aligned}
I_5 &= \int_{\partial A} C_2 C_{2g} f_0 \frac{\partial f_s}{\partial n_2} d\ell \\
&= \{K_5\}^t_{1\times q} \{\mu\}_{q\times 1}
\end{aligned} \tag{3.2.2.14a}
$$

向量$\{K_5\}$之元素定義爲

$$
\begin{aligned}
\{K_5\}_m &= 2\pi k_0 R_a C_2 C_{2g} i^{m-1} J_{m-1} H'_{m-1} \cos[(m-1)\theta_0], \qquad 2 \le m \le p \\
&= 2\pi k_0 R_a C_2 C_{2g} J_0 H'_0, \qquad m = 1
\end{aligned} \tag{3.2.2.14b}
$$

$$J_m = J_m^{(1)}(k_0 R_a), \qquad m = 1,2,3....p-1 \tag{3.2.2.14c}$$

式中最後項已知勁度矩陣$[K_6]$及邊界∂B上未知波函數向量$\{f_2^{\#}\}$,則由邊界∂B上之M個線性元素e=1,2,3...M區域性矩陣$[K_6^e]$及$\{f_2^{\#e}\}$所組成:

$$\begin{aligned} I_6^e &= -\int_{\partial B^e} \frac{i}{2}\alpha C_2 C_{2g} f_2^2 d\ell \\ &= \frac{1}{2}\{f_2^{\#e}\}^t_{1\times 2}[K_6^e]_{2\times 2}\{f_2^{\#e}\}_{2\times 1}, \quad e = 1,2...M \end{aligned} \tag{3.2.2.15}$$

矩陣$[K_6^e]$之元素定義爲

$$\begin{aligned} [K_6^e]_{11} &= i\alpha L_b^e(\frac{1}{5}C_{21}^e C_{2g1}^e + \frac{1}{20}C_{21}^e C_{2g2}^e + \frac{1}{20}C_{22}^e C_{2g1}^e + \frac{1}{30}C_{22}^e C_{2g2}^e) \\ [K_6^e]_{22} &= i\alpha L_b^e(\frac{1}{30}C_{21}^e C_{2g1}^e + \frac{1}{20}C_{21}^e C_{2g2}^e + \frac{1}{20}C_{22}^e C_{2g1}^e + \frac{1}{5}C_{22}^e C_{2g2}^e) \\ [K_6^e]_{12} &= i\alpha L_b^e(\frac{1}{20}C_{21}^e C_{2g1}^e + \frac{1}{30}C_{21}^e C_{2g2}^e + \frac{1}{30}C_{22}^e C_{2g1}^e + \frac{1}{20}C_{22}^e C_{2g2}^e) \\ [K_6^e]_{21} &= [K_6^e]_{12}, \quad e = 1,2,3....M \end{aligned} \tag{3.2.2.16}$$

其中L_b^e爲線性元素e=1,2..M之長度。

C_{2i}及$C_{2gi}, i = 1,2$分別爲線性元素e兩端結點之值,而線性元素e之形狀函數$\psi_i^e, i = 1,2$定義爲

$$\psi_1(x) = 1 - /L_b, \qquad 0 \le x \le L_b \tag{3.2.2.17a}$$

$$\psi_2(\overline{x}) = \overline{x}/L_b, \qquad 0 \le x \le L_b \tag{3.2.2.17b}$$

最後爲簡化矩陣方程式我們將未知向量$\{f_2\}^t_{1\times N}$與$\{\mu\}^t_{1\times q}$合併爲$\{x\}^t_{1\times n}$:

$$\{x\}^t_{1\times n} = [\{f_2\}^t_{1\times N}\{\mu\}^t_{1\times q}] \tag{3.2.2.18}$$

其中n=N+q。

將已知勁度矩陣$[K_1],[K_2],[K_3]$及$[K_6]$依結點位置合併爲大勁度矩陣$[K]$示意如下

$$[K]_{n\times n} = \begin{bmatrix} & & 0 \\ K_1(K_6) & & K_3 \\ 0 & K_3 & K_2 \end{bmatrix} \tag{3.2.2.19}$$

最後將已知向量$\{K_4\}^t$及$\{K_5\}^t$合併爲向量$\{b\}^t$

$$\{b\}^t_{1\times n}=[\{0\}^t_{1\times(N-p)}\{K_4\}^t_{1\times p}\{K_5\}^t_{1\times q}] \tag{3.2.2.20}$$

因此矩陣方程式(3.2.2.4)可簡化爲

$$J^s_0(x)=\frac{1}{2}\{x\}^t_{1\times n}[K]_{n\times n}\{x\}_{n\times 1}+\{b\}^t_{1\times n}\{x\}_{n\times 1}+constant \tag{3.2.2.21}$$

而定態泛函數J^s_0極小化產生於:

$$\frac{\partial J^s_0}{\partial x_i}=0,\qquad i=1,2,3...n \tag{3.2.2.22}$$

式中$x_i, i=1,2,3....n$爲向量$\{x\}$之第i個元素。

將(3.2.2.21)代入(3.2.2.22)可得

$$[K]_{n\times n}\{x\}_{n\times 1}=\{b\}_{n\times 1} \tag{3.2.2.23}$$

這是一個包括n個未知數x_i, n個方程式之矩陣方程式,可由高斯消去法(Gaussian elimination)求解。

港池擴大率R我們定義爲港內任意點$\vec{x}$之振幅對港口外之入射波與反射波和之振幅(假設港口爲封閉)的比值,表示如下:

$$R(\vec{x})=\left|\frac{f_2(\vec{x})}{f_0(\vec{x}_0)+f_r(\vec{x}_0)}\right| \tag{3.2.2.24}$$

式中$\vec{x}$港內任一點, $\vec{x}_0$爲港口外任一點。

同樣考慮縱深ℓ=12.25英吋,寬b_1=2.48英吋,等水深h=10.128英吋全開口矩形港池,假設外海之海岸線及港池內壁爲不透水直立壁,向x軸兩側平直延伸。此處將探討從外海遠處垂直海岸線入射之不同週期波浪作用下,矩形港池底端中點之港池共振曲線變化,圖2-7-3爲矩形港池端點處無因次波浪參數$k_0\ell$與擴大率R之相關曲線圖,實線本文理論解之結果,虛線爲有限元素法模式(Model WE21)及邊界元素法模式(Model WH21)之結果,黑點則爲Lee (1969)之試驗結果,計算結果與試驗結果甚爲吻合。

3-3有限差分法模式-MODEL WP21

3-3-1理論解析及有限差分法

考慮近岸海域(如示意圖3-3-1),海岸線可爲不規則形狀,海域水深h(x,y)爲緩慢變化(mild slope),我們將探討波浪從外海進入近岸海域時之波場變化。

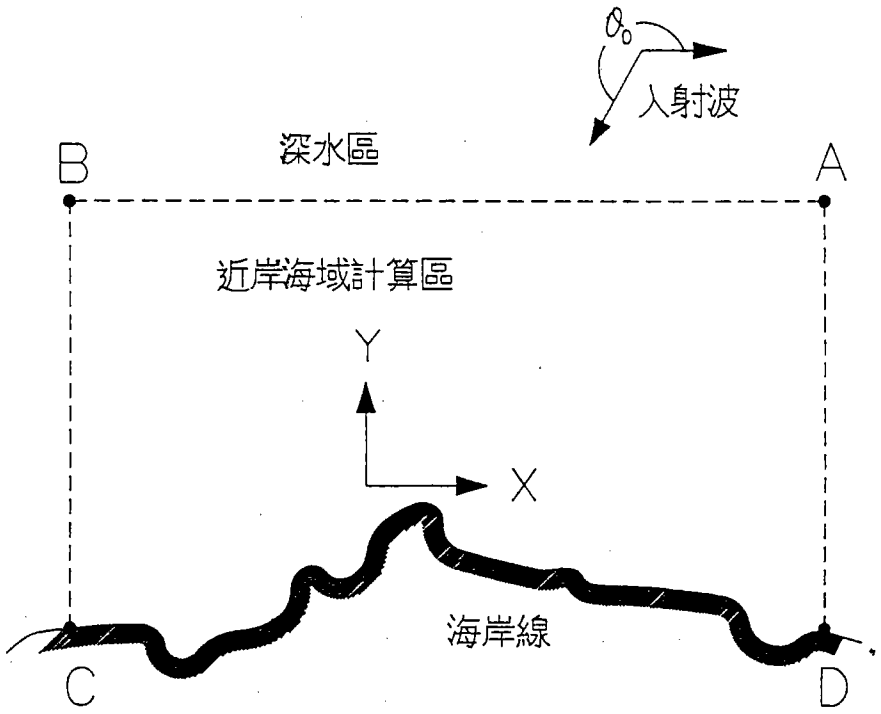

圖3-3-1 近岸海域示意圖

根據Tsay and Liu's(1982)之建議,在近岸緩變地形之區域水深h(x,y)可分爲$\overline{h}$及$\hat{h}$兩部分

$$h = \overline{h} + \hat{h} \tag{3.3.1}$$

式中$\overline{h}(x,y)$稱修正水深(modified depth)其選擇要件爲：在修正水深$\overline{h}$對應之各波場波向線不會相交。而一般選取$\overline{h}$之方法可參考Lozano and Liu(1980)之法則。$\hat{h}$則爲$\overline{h}$對應實際地形h(x,y)之微小修正量。

假設在近岸海域之波場波函數(wave function)$\phi(x,y,t)$可表示爲

$$\phi(x,y,t) = F(x,y)A(x,y)e^{i(S(x,y)+\sigma t)} \tag{3.3.2}$$

式中 $A(x,y)$ 及 $S(x,y)$ 分別爲對應修正水深 $\overline{h}$ 之振幅(amplitude)及相位(phase), σ 爲週頻率。$F(x,y)$ 稱繞射因子(diffraction factor)主要考慮實際水深與修正水深差,即 h_0 效應產生之影響效果。

根據波向線理論(the wave ray theory)振幅 A(x,y) 及相位 S(x,y) 分別滿足下列 eikonal equation 及 transport equation:

$$(\nabla S)^2 = \overline{k}^2 \tag{3.3.3}$$

$$\nabla \cdot (A^2 \overline{C}\overline{C}_g \nabla S) = 0 \tag{3.3.4}$$

其對應波數(wave number)$\overline{k}$ 滿足下列分散關係式(dispersion relation)

$$\sigma^2 = g\overline{k}\tanh\overline{k}\overline{h} \tag{3.3.5}$$

而其對應波速(phase velocity) $\overline{C} = \sigma/\overline{k}$ 及群速度(group velocity) $\overline{C}_g = d\sigma/d\overline{k}$, σ 爲週頻率(radian frequency)。

其中波數向量(wave number vedor)$\overline{K}$, 滿足非旋轉條件

$$\nabla \times \overline{K} = 0 \tag{3.3.6}$$

式中

$$\overline{K} = (\overline{k}_x, \overline{k}_y) = (\overline{k}\cos\theta, \overline{k}\sin\theta), \qquad \overline{k} = |\overline{K}| \tag{3.3.7}$$

將表示式(3.3.2)及利用關係式(3.3.3)及(3.3.4)代入修正緩坡方程式(2.13a),並取 $E_0 = 0$,則可化爲

$$2i\overline{K}\cdot\nabla F + \left(\frac{2\nabla A}{A} + \frac{\nabla G}{G}\right)\cdot\nabla F + \nabla^2 F + \hat{k}^2 F = 0 \tag{3.3.8}$$

式中 $\hat{k}^2$ 定義爲

$$\hat{k}^2 = k^2 - \overline{k}^2 + \frac{i\overline{G}}{G}\nabla\left(\frac{G}{\overline{G}}\right)\cdot\nabla S + \frac{\nabla G}{G}\cdot\frac{\nabla A}{A} + \frac{\nabla^2 A}{A} \tag{3.3.9}$$

其中

$$G = CC_g, \qquad \overline{G} = \overline{C}\overline{C}_g \tag{3.3.10a}$$

式中海域波速(phase velocity) $C = \sigma/k$ 及群速度(group velocity) $C_g = d\sigma/dk$, 波數(wave number)k 滿足下列分散關係式(dispersion relation)

$$\sigma^2 = gk\tanh kh \tag{3.3.10b}$$

若忽略式(3.3.8)二次以上之微分項可化簡爲

$$\hat{k}^2 = k^2 - \overline{k}^2 \tag{3.3.11}$$

假如取曲線座標系統(curvilinear co-ordinate system) (ξ,η)與原來直角座標系統(x,y)滿足下列轉關係

$$x = T_x(\xi,\eta) \tag{3.3.12}$$

$$y = T_y(\xi,\eta) \tag{3.3.12b}$$

則在(x,y)座標系統之橢圓方程式(ellitic equation)(2.13a)可化爲在(ξ,η)座標系統之拋物線方程式(parabolic equation)如下：

$$\left[\frac{2i}{J_4}\left(\frac{-\partial T_y}{\partial\xi}\overline{k}_x + \frac{\partial T_x}{\partial\xi}\overline{k}_y\right) + \frac{1}{GJ_4^2}\left(J_3\frac{\partial G}{\partial\eta} - J_2\frac{\partial G}{\partial\xi}\right) + \frac{2}{AJ_4^2}\left(J_3\frac{\partial A}{\partial\eta} - J_2\frac{\partial A}{\partial\xi}\right)\right]\frac{\partial F}{\partial\eta}$$

$$+\left[\frac{2i}{J_4}\left(\frac{\partial T_y}{\partial\eta}\overline{k}_x - \frac{\partial T_x}{\partial\eta}\overline{k}_y\right) + \frac{1}{GJ_4^2}\left(J_1\frac{\partial G}{\partial\xi} - J_2\frac{\partial G}{\partial\eta}\right) + \frac{2}{AJ_4^2}\left(J_1\frac{\partial A}{\partial\xi} - J_2\frac{\partial A}{\partial\eta}\right)\right]\frac{\partial F}{\partial\xi}$$

$$+\frac{1}{J_2}\left(J_3\frac{\partial^2 F}{\partial\eta^2} - 2J_2\frac{\partial^2 F}{\partial\eta\partial\xi} + J_1\frac{\partial^2 F}{\partial\xi^2}\right) + \hat{k}^2 F = 0 \tag{3.3.13}$$

式中

$$J_1 = \left(\frac{\partial T_x}{\partial\eta}\right)^2 + \left(\frac{\partial T_y}{\partial\eta}\right)^2 \tag{3.3.14a}$$

$$J_2 = \frac{\partial T_x}{\partial\xi}\frac{\partial T_x}{\partial\eta} + \frac{\partial T_y}{\partial\xi}\frac{\partial T_y}{\partial\eta} \tag{3.3.14b}$$

$$J_3 = \left(\frac{\partial T_x}{\partial\xi}\right)^2 + \left(\frac{\partial T_y}{\partial\xi}\right)^2 \tag{3.3.14c}$$

$$J_4 = \frac{\partial T_x}{\partial\xi}\frac{\partial T_y}{\partial\eta} - \frac{\partial T_x}{\partial\eta}\frac{\partial T_y}{\partial\xi} \tag{3.3.14d}$$

因爲在(ξ,η)平面上海岸線與η線平行，一般相位線(phase line)多少會與等水深線平行，所以式(3.3.13)中F對η之二次微分項可忽略，簡化爲

$$\left[\frac{2i}{J_4}\left(\frac{-\partial T_y}{\partial\xi}\overline{k}_x + \frac{\partial T_x}{\partial\xi}\overline{k}_y\right) + \frac{1}{GJ_4^2}\left(J_3\frac{\partial G}{\partial\eta} - J_2\frac{\partial G}{\partial\xi}\right) + \frac{2}{AJ_4^2}\left(J_3\frac{\partial A}{\partial\eta} - J_2\frac{\partial A}{\partial\xi}\right)\right]\frac{\partial F}{\partial\eta}$$

$$+\left[\frac{2i}{J_4}\left(\frac{\partial T_y}{\partial \eta}\overline{k}_x-\frac{\partial T_x}{\partial \eta}\overline{k}_y\right)+\frac{1}{GJ_4^2}\left(J_1\frac{\partial G}{\partial \xi}-J_2\frac{\partial G}{\partial \eta}\right)+\frac{2}{AJ_4^2}\left(J_1\frac{\partial A}{\partial \xi}-J_2\frac{\partial A}{\partial \eta}\right)\right]\frac{\partial F}{\partial \xi}$$

$$+\frac{1}{J_2}\left(-2J_2\frac{\partial^2 F}{\partial \eta \partial \xi}+J_1\frac{\partial^2 F}{\partial \xi^2}\right)+\hat{k}^2F=0 \qquad (3.3.15)$$

同樣波數方程式(3.3.6)在(ξ,η)座標系統可化爲

$$\frac{\partial T_y}{\partial \eta}\frac{\partial \overline{k}_y}{\partial \xi}+\frac{\partial T_x}{\partial \eta}\frac{\partial \overline{k}_x}{\partial \xi}-\frac{\partial T_y}{\partial \xi}\frac{\partial \overline{k}_y}{\partial \eta}-\frac{\partial T_x}{\partial \xi}\frac{\partial \overline{k}_x}{\partial \eta}=0 \qquad (3.3.16)$$

而transport equation(3.3.4)在(ξ,η)座標系統上可化爲

$$\frac{\partial T_y}{\partial \eta}\frac{\partial}{\partial \xi}(\overline{Gk}_xA^2)-\frac{\partial T_x}{\partial \eta}\frac{\partial}{\partial \xi}(\overline{Gk}_yA^2)-\frac{\partial T_y}{\partial \xi}\frac{\partial}{\partial \eta}(\overline{Gk}_xA^2)+\frac{\partial T_x}{\partial \xi}\frac{\partial}{\partial \eta}(\overline{Gk}_yA^2)=0 \qquad (3.3.17)$$

爲引用有限差分法解析邊界值問題,網格切割之規則形狀要求,一般解將直角座標系統(x,y)平面上不規則狀區域,經貼壁曲線座標系統(boundary fitted curvilinear co-ordinate system)轉換爲在(ξ,η)平面上之長方形區域,如示意圖3-3-2。(x,y)平面上海岸線$\widetilde{CD}$,及沿海岸線方向曲線$\widetilde{AB}$,經轉換爲(ξ,η)平面上之線段$\overline{CD}(\eta=0)$,及線段$\overline{AB}(\eta=\eta_0)$,(x,y)平面上向(離)岸之曲線$\widetilde{DA}$及$\widetilde{CB}$,經轉換爲$(\xi,\eta)$平面上之線段$\overline{DA}(\xi=0)$及線段$\overline{CB}(\xi=\xi_0)$。一般可先給定$\eta_0$值,$\eta_0$值大小即控制轉換後尺度大小,對應$\overline{BC}$及$\overline{DA}$,必轉換至$\xi=0$及$\xi=\xi_0$。如何求得座標轉換函數(3.3.9)式,並保持一些重要幾何特性,是轉換時一個重要考慮因素。

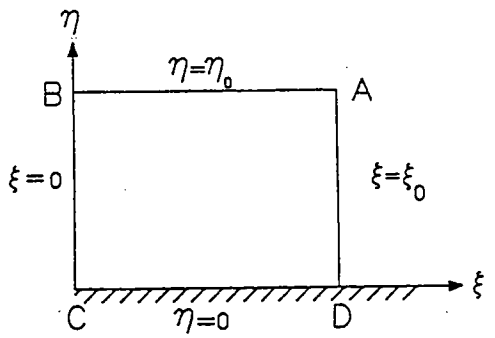

圖3-3-2 座標轉換示意圖

本文將在保角(conformal mapping)之條件下,求解轉換函數T_x及T_y,並假設其滿足拉普拉氏方程式(Laplace equation)

$$\frac{\partial^2 T_x}{\partial \xi^2}+\frac{\partial^2 T_x}{\partial \eta^2}=0 \tag{3.3.18a}$$

$$\frac{\partial^2 T_y}{\partial \xi^2}+\frac{\partial^2 T_y}{\partial \eta^2}=0 \tag{3.3.18b}$$

對應(ξ,η)之座標系統也滿足拉普拉氏方程式

$$\frac{\partial^2 \xi}{\partial x^2}+\frac{\partial^2 \xi}{\partial y^2}=0 \tag{3.3.19a}$$

$$\frac{\partial^2 \eta}{\partial x^2}+\frac{\partial^2 \eta}{\partial y^2}=0 \tag{3.3.19b}$$

而且滿足Cauahy-Riemann條件

$$\frac{\partial \xi}{\partial x}=\frac{\partial \eta}{\partial y},\qquad \frac{\partial \xi}{\partial y}=-\frac{\partial \eta}{\partial x} \tag{3.3.20a}$$

$$\frac{\partial x}{\partial \xi}=\frac{\partial y}{\partial \eta},\qquad \frac{\partial x}{\partial \eta}=-\frac{\partial y}{\partial \xi} \tag{3.3.20b}$$

引用 Cauchy-Riemann條件(3.3.20),則對應ξ之控制方程式(3.3.19a)邊界條件爲

$$\xi=\xi_0,\qquad on\quad \overline{DA} \tag{3.3.21a}$$

$$\xi=0,\qquad on\quad \overline{BC} \tag{3.3.21b}$$

$$\frac{\partial \xi}{\partial n}=0,\qquad on\quad \overline{AB} \tag{3.3.21c}$$

$$\frac{\partial \xi}{\partial n}=0,\qquad on\quad \overline{CD} \tag{3.3.21d}$$

式中$\frac{\partial}{\partial n}=\vec{n}\cdot\nabla$表示正向微分(nomal derivative),$\vec{n}$沿邊界向區域外之單位向量。

同樣對應η之控制方程式(3.3.16b)邊界條件爲

$$\eta=0,\qquad on\quad \overline{CD} \tag{3.3.22a}$$

$$\eta=\eta_0,\qquad on\quad \overline{AB} \tag{3.3.22b}$$

$$\frac{\partial \eta}{\partial n} = 0, \qquad on \quad \overline{BC} \tag{3.3.22c}$$

$$\frac{\partial \eta}{\partial n} = 0, \qquad on \quad \overline{DA} \tag{3.3.22d}$$

此處將引用邊界元素法原理，求解上述兩組邊界值問題(3.3.19a)、(3.3.21)及(3.3.19b)、(3.3.22)。

拉普拉氏方程式(3.3.19a)及(3.3.19b)之Weber解在區域內分別可表示爲下列積分方程(Baker及Copson ,1950):

$$\xi(\overline{x}) = b_0 \int_{\partial R} \{\xi \frac{\partial}{\partial n}[ln(r)] - [ln(r)]\frac{\partial \xi}{\partial n}\} d\ell \tag{3.3.23a}$$

$$\eta(\overline{x}) = b_0 \int_{\partial R} \{\eta \frac{\partial}{\partial n}[ln(r)] - [ln(r)]\frac{\partial \eta}{\partial n}\} d\ell \tag{3.3.23b}$$

式中∂R爲近海區域R之封閉邊界，$\partial R = \overline{AB} + \overline{BC} + \overline{CD} + \overline{DA}$。

$b_0 = \frac{-i}{4}$，當$\overline{x}$在區域內部。

$b_0 = \frac{-i}{2}$，當$\overline{x}$在平滑區域邊界上。

$b_0 = \frac{-i\pi}{2\beta}$，當$\overline{x}$在內角爲$\beta$之邊界點上。

$ln(r)$爲自然對數函數(natural logarithmic function)。

$r = |\overline{x}_0 - \overline{x}|$，$\overline{x}_0$爲邊界上之點，$\overline{x}$爲邊界上$\partial R$或區域R內任一點。

積分方程式(3.3.23a及(3.3.23b)式對不規則形狀之區域不易求得解析解，將利用邊界元素法求解波場。將(x,y)平面區域之邊界$\partial B = \widetilde{AB} + \widetilde{BC} + \widetilde{CD} + \widetilde{DA}$，分別切割爲N個線段，N個中結點(mid-node)，每個線段代表一個元素，並引用常數元素，假設每一個線段上每個點之η, ξ及$\frac{\partial \eta}{\partial n}$，$\frac{\partial \xi}{\partial n}$皆爲定值，而以線段中結點值代表元素值，元素上$ln(r)$，$\frac{\partial ln(r)}{\partial n}$之值將引用高斯積分法，直接計算，而N個結點編號一般以逆時鐘方向編排。

假設方程式(3.3.23a)中之$\overline{x}$點爲邊界上結點，則可化爲下列矩陣方程式

$$[G]\{P_1\} = [H]\{Q_1\} \tag{3.3.24}$$

式中$[H], [G]$皆爲$N \times N$矩陣，其矩陣元素$[H]_{jk}, [G]_{jk}$分別定義爲下列線積分(line integral)表示式

$$[H]_{jk} = b_0 \int_{\Gamma_k} \frac{\partial}{\partial n} ln(r) d\ell_k - \delta_{jk}, \qquad j,k = 1,2,3...N \tag{3.3.25a}$$

$$[G]_{jk} = b_0 \int_{\Gamma_k} ln(r) d\ell_k, \qquad j,k = 1,2,3...N \tag{3.3.25b}$$

式中Γ_k爲第k個元素，$r = |\overline{x}_j - \overline{x}|$，$\overline{x}_j$爲區域$R$之邊界$\partial R$上元素之結點，j=1,2,3....$N$，$\overline{x}$爲第k個元素$\Gamma_k$上任一點，$\delta_{jk}$爲克郎克函數(Knonecker delta function)，而$\{Q_1\}$及$\{P_1\}$爲$N \times 1$向量，其向量元素分別定義爲

$$\{Q_1\}_j = \eta(\overline{x}_j), \qquad j = 1,2...N \tag{3.3.26a}$$

$$\{P_1\}_j = \frac{\partial \eta(\overline{x}_j)}{\partial n}, \qquad j = 1,2...N \tag{3.3.26b}$$

同樣方程式(3.3.23b)中之$\overline{x}$點爲邊界上結點，則可化爲下列矩陣方程式

$$[G]\{P_2\} = [H]\{Q_2\} \tag{3.3.27}$$

$\{Q_2\}$及$\{P_2\}$爲$N \times 1$向量，其向量元素分別定義爲

$$\{Q_2\}_j = \xi(\overline{x}_j), \qquad j = 1,2...N \tag{3.3.28a}$$

$$\{P_2\}_j = \frac{\partial \xi(\overline{x}_j)}{\partial n}, \qquad j = 1,2...N \tag{3.3.28b}$$

分別利用矩陣方程式(3.3.24)之邊界條件(3.3.21)，以及短陣方程式(3.3.27)、邊界條件(3.3.22)，即可求得邊界上之$\xi, \frac{\partial \xi}{\partial n}, \eta, \frac{\partial \eta}{\partial n}$值。

當在整個邊界∂R上座標(x,y)對應之(ξ, η)值求得後，反言之座標(ξ, η)其對應之(x,y)亦可獲得，即

$$x = T_x(\xi, 0), \qquad y = T_y(\xi, 0), \quad on \quad \overline{CD} \tag{3.3.29a}$$

$$y = T_x(\xi, \eta), \qquad y = T_y(\xi, \eta_0), \quad on \quad \overline{AB} \tag{3.3.29b}$$

$$x = T_x(0, \eta), \qquad y = T_y(0, \eta), \quad on \quad \overline{DA} \tag{3.3.29c}$$

$$y = T_x(\xi_0, \eta), \qquad y = T_y(\xi_0, \eta), \quad on \quad \overline{BC} \tag{3.3.29d}$$

利用 Cauahy-Riemann Codition, $\frac{\partial T_x}{\partial n}$ 及 $\frac{\partial T_y}{\partial n}$ 在邊界上之值可由下式求得

$$\frac{\partial T_x}{\partial n}=\frac{\partial T_x}{\partial \eta}=-\frac{\partial T_y}{\partial \xi},\qquad \frac{\partial T_y}{\partial n}=\frac{\partial T_y}{\partial \eta}=\frac{\partial T_x}{\partial \xi},\quad on\quad \overline{AB} \tag{3.3.30a}$$

$$\frac{\partial T_x}{\partial n}=-\frac{\partial T_x}{\partial \eta}=-\frac{\partial T_y}{\partial \xi},\qquad \frac{\partial T_y}{\partial n}=-\frac{\partial T_y}{\partial \eta}=-\frac{\partial T_x}{\partial \xi},\quad on\quad \overline{CD} \tag{3.3.30b}$$

$$\frac{\partial T_x}{\partial n}=\frac{\partial T_x}{\partial \xi}=\frac{\partial T_y}{\partial \eta},\qquad \frac{\partial T_y}{\partial n}=\frac{\partial T_y}{\partial \eta}=-\frac{T_x}{\partial \eta},\quad on\quad \overline{BC} \tag{3.3.30c}$$

$$\frac{\partial T_x}{\partial n}=-\frac{\partial T_x}{\partial \xi}=-\frac{T_y}{\partial \eta},\qquad \frac{\partial T_y}{\partial n}=-\frac{\partial T_y}{\partial \xi}=-\frac{\partial T_x}{\partial \eta},\quad on\quad \overline{AD} \tag{3.3.30d}$$

假設(ξ,η)爲區域R內部之點則$\overline{T}=(T_x,T_y)$可由下式求得

$$\overline{T}(\xi,\eta)=b_0\int_{\partial R}\{\overline{T}\frac{\partial}{\partial n}[ln(r)]-\frac{\partial \overline{T}}{\partial n}[ln(r)]\}ds \tag{3.3.31}$$

式中∂R爲邊界$(\overline{AB}+\overline{BC}+\overline{CD}+\overline{DA})$積分。$r=\sqrt{(\xi'-\xi)^2+(\eta'-\eta)^2}$, (ξ',η')爲邊界上∂R之任一點。

當(x,y)平面之不規則形狀區域,經上節轉換爲貼壁曲線座標系統(ξ,η)平面上之矩形區域後,並切割爲$N_x\times N_y$個矩形,其每個矩形大小爲$\triangle\xi\times\triangle\eta$。本節將引用有限差分法利用三個控制方程式(3.3.15)、(3.3.16)及(3.3.17)求解海域之振幅A,繞射因子F,相位S或波向角(θ_0)等三個變數。

因爲修正水深$\overline{h}$沿著等η線幾乎與等深線相同,所以

$$\frac{\partial \overline{h}}{\partial \xi}=0,\qquad \frac{\partial \overline{k}}{\partial \xi},\quad on\quad \eta=const \tag{3.3.32}$$

將(3.3.7)代入(3.3.16)並引用(3.3.32)之關係式可化爲

$$\begin{aligned}&\Big(\frac{\partial T_y}{\partial \eta}\overline{k}\cos\theta-\frac{\partial T_x}{\partial \eta}\overline{k}\sin\theta\Big)+\Big(\frac{\partial T_x}{\partial \xi}\overline{k}\sin\theta-\frac{\partial T_y}{\partial \xi}\overline{k}\cos\theta\Big)\frac{\partial\theta}{\partial\eta}\\&=\frac{\partial T_y}{\partial \xi}\frac{\partial \overline{k}}{\partial \eta}\sin\theta+\frac{\partial T_x}{\partial \xi}\frac{\partial \overline{k}}{\partial \eta}\cos\theta-\frac{\partial T_y}{\partial \eta}\frac{\partial \overline{k}}{\partial \xi}\sin\theta-\frac{\partial T_y}{\partial \eta}\frac{\partial \overline{k}}{\partial \xi}\cos\theta\end{aligned} \tag{3.3.33}$$

定義波向角

$$\theta_i^j=\theta(\xi_i,\eta_j) \tag{3.3.34a}$$

式中

$$\xi_i = i\triangle\xi, \qquad \eta_j = j\triangle\eta \tag{3.3.34b}$$

微分量 $\frac{\partial\theta}{\partial\eta}$ 取前差法(formard-difference method)

$$\frac{\partial\theta}{\partial\eta} = \frac{\theta_i^{j+1} - \theta_i^j}{\triangle\eta} \tag{3.3.35a}$$

微分量 $\frac{\partial\theta}{\partial\xi}$ 取中差分(centeral-difference method)

$$\frac{\partial\theta}{\partial\xi} = \frac{\theta_{i+1}^{j+1} - \theta_{i-1}^{j+1} + \theta_{i+1}^j - \theta_{i-1}^j}{4\triangle\xi} \tag{3.3.35b}$$

將(3.3.35)代入(3.3.33)則可化爲下列差分方程式

$$-\theta_{i-1}^{j+1} + c_1\theta_i^{j+1} + \theta_{i+1}^{j+1} = c_2 + \theta_{i-1}^j + c_1\theta_i^j - \theta_{i+1}^j \tag{3.3.36}$$

其中係數 c_1, c_2 分別定義爲

$$c_1 = \frac{4\triangle\xi}{\triangle\eta}\left(\frac{\partial T_x}{\partial\xi}\overline{k}\sin\theta - \frac{\partial T_y}{\partial\xi}\overline{k}\cos\theta\right)\left(\frac{\partial T_y}{\partial\eta}\overline{k}\cos\theta - \frac{\partial T_x}{\partial\eta}\overline{k}\sin\theta\right)^{-1} \tag{3.3.37a}$$

$$c_2 = \frac{4\triangle\xi}{k}\frac{\partial\overline{k}}{\partial\eta}\left(\frac{\partial T_y}{\partial\xi}\overline{k}\sin\theta + \frac{\partial T_x}{\partial\xi}\overline{k}\cos\theta\right)\left(\frac{\partial T_y}{\partial\eta}\overline{k}\cos\theta - \frac{\partial T_x}{\partial\eta}\overline{k}\sin\theta\right)^{-1} \tag{3.3.37b}$$

方程式(3.3.33)對變數波向角 θ 而言含有非線性項,因此差分方程式(3.3.36)將使用疊代法(iterative numerical method)以求解 θ,係數 c_1, c_2 皆包括 θ 之隱函數,θ 之值以上一次之疊代結果代入。

同樣定義 $A_i^j = A(\xi_i, \eta_j), i = 1, 2, ...N_x, j = 1, 2...N_y$ 則方程式(3.3.17)可化爲差分方程式

$$-A_{i-1}^{j+1} + \left(\frac{c_4}{c_3}\frac{4\triangle\xi}{\triangle\eta} - \frac{2c_5}{c_3}\triangle\xi\right)A_i^{j+1} + A_{i+1}^{j+1} = A_{i-1}^j + \left(\frac{c_4}{c_3}\frac{4\triangle\xi}{\triangle\eta} + \frac{2c_5}{c_3}\triangle\xi\right)A_i^j - A_{i+1}^j \tag{3.3.38}$$

其中係數 c_3, c_4, c_5 分別定義爲

$$c_3 = 2\left(\frac{\partial T_y}{\partial\eta}\overline{k}\cos\theta - \frac{\partial T_x}{\partial\eta}\overline{k}\sin\theta\right) \tag{3.3.39a}$$

$$c_4 = 2\Big(\frac{\partial T_x}{\partial \xi}\overline{k}\sin\theta - \frac{\partial T_y}{\partial \xi}\overline{k}\cos\theta\Big) \tag{3.3.39b}$$

$$c_5 = \frac{1}{G}\Big[\frac{\partial T_x}{\partial \eta}\frac{\partial}{\partial \xi}(\overline{Gk}\sin\theta) + \frac{\partial T_y}{\partial \xi}\frac{\partial}{\partial \eta}(\overline{Gk}\cos\theta)$$
$$-\frac{\partial T_x}{\partial \xi}\frac{\partial}{\partial \eta}(\overline{Gk}\cos\theta) - \frac{\partial T_y}{\partial \eta}\frac{\partial}{\partial \xi}(\overline{Gk}\cos\theta)\Big] \tag{3.3.39c}$$

差分方程式(3.3.38)對振幅A而言爲一線性方程式,假設方程式(3.3.36)中之波向角θ求得,則係數c_3, c_4, c_5皆爲已知。

同樣繞射因子F之相關微分量分別定義如下

$$\frac{\partial F}{\partial \xi} = \frac{F_{i+1}^{j} - F_i^j}{\triangle \xi} \tag{3.3.40a}$$

$$\frac{\partial F}{\partial \eta} = \frac{F_i^{j+1} - F_i^j}{\triangle \eta} \tag{3.3.40b}$$

$$\frac{\partial^2 F}{\partial \xi \partial \eta} = \frac{1}{2\triangle\xi\triangle\eta}(F_{i+1}^{j+1} - F_i^{j+1} - F_{i+1}^{j-1} + F_i^{j-1}) \tag{3.3.40c}$$

$$\frac{\partial^2 F}{\partial \xi^2} = \frac{1}{2(\triangle\xi)^2}(F_{i+1}^{j+1} - F_i^{j+1} - 2F_{i+1}^{j} - 2F_i^{j} + F_{i+1}^{j-1} + F_i^{j-1}) \tag{3.3.40d}$$

因此式(3.3.15)可化爲下列差分式

$$\Big(-1 + \frac{c_7\triangle\xi}{2c_9} + \frac{c_8\triangle\xi}{c_9\triangle\eta}\Big)F_{i-1}^{j+1} + \Big[2 - \frac{2c_6(\triangle\xi)^2}{c_9\triangle\eta} - \frac{k_0^2(\triangle\xi)^2}{c_9}\Big]F_i^{j+1}$$
$$+\Big(-1 - \frac{c_7\triangle\xi}{2c_9} - \frac{c_8\triangle\xi}{c_9\triangle\eta}\Big)F_{i+1}^{j+1} = \quad \Big(1 - \frac{c_7\triangle\xi}{2c_9} + \frac{c_8\triangle\xi}{c_9\triangle\eta}\Big)F_{i-1}^{j}$$
$$-\Big[2 + \frac{2c_6(\triangle\xi)^2}{c_9\triangle\eta} - \frac{k_0^2(\triangle\xi)^2}{c_9}\Big]F_i^j + \Big(1 + \frac{\eta\triangle\xi}{2q} - \frac{p\triangle\xi}{q\triangle\eta}\Big)F_{i-1}^{j} \tag{3.3.41}$$

其中係數c_6, c_7, c_8, c_9分別定義爲

$$c_6 = \frac{2i}{J_4}\Big(-\frac{\partial T_y}{\partial \xi}\overline{k}\cos\theta + \frac{\partial T_x}{\partial \xi}\overline{k}\sin\theta\Big) + \frac{1}{GJ_4^2}\Big(J_3\frac{\partial G}{\partial \eta} - J_2\frac{\partial G}{\partial \xi}\Big) + \frac{2}{GJ_4^2}\Big(J_3\frac{\partial A}{\partial \eta} - J_2\frac{\partial A}{\partial \xi}\Big) \tag{3.3.42a}$$

$$c_7 = \frac{2i}{J_4}\left(\frac{\partial T_y}{\partial \eta}\overline{k}\cos\theta - \frac{\partial T_x}{\partial \eta}\overline{k}\sin\theta\right) + \frac{1}{GJ_4^2}\left(J_1\frac{\partial G}{\partial \xi} - J_2\frac{\partial G}{\partial \eta}\right) + \frac{2}{AJ_4^2}\left(J_1\frac{\partial A}{\partial \xi} - J_2\frac{\partial A}{\partial \eta}\right) \quad (3.3.42b)$$

$$c_8 = \frac{2J_2}{J_4^2} \quad (3.3.42c)$$

$$c_9 = \frac{J_1}{J_4^2} \quad (3.3.42d)$$

數值計算繞射因子F以海岸線$\eta = \eta_0$爲起始線，並假射在起始線上F爲常數，並且假設側邊界$\xi = 0$及$\xi = \xi_0$滿足

$$\frac{\partial F}{\partial \xi} = 0, \qquad \xi = 0 \quad and \quad \xi = \xi_0$$

當海域之振幅A，繞射因子F及波向角(θ_0)(或相位S)等變數求得，則由方程式(3.3.2)可求得波場水位變化。

3-3-2 例子說明

考慮一等斜率1/20之海岸地區，在海岸線中央處有一凸岬存在，其等深線分佈如圖3-3-3，計算區大小約爲$(0 < y < 1000m)$, $-400m < x < 400m)$，本例子將計算週期10秒之波浪，由外海以入射角20° 之方向進入海岸後產生之波場分佈。

區域在(x, y)平面原座標系統之網格分佈如圖3-3-4a，經貼壁座標轉換後區域在(ξ, η)平面之網格分佈如圖3-3-4b，在(ξ, η)平面之計算範圍爲$(0 < \eta < 1000m, 0 < \xi < 800m)$，網格大小分別爲$\triangle\xi = 9m, \triangle\eta = 10m$。圖3-3-5爲計算區之等波高(米)分佈曲線圖，圖3-3-6爲計算區之等波向角(度)分佈曲線圖。

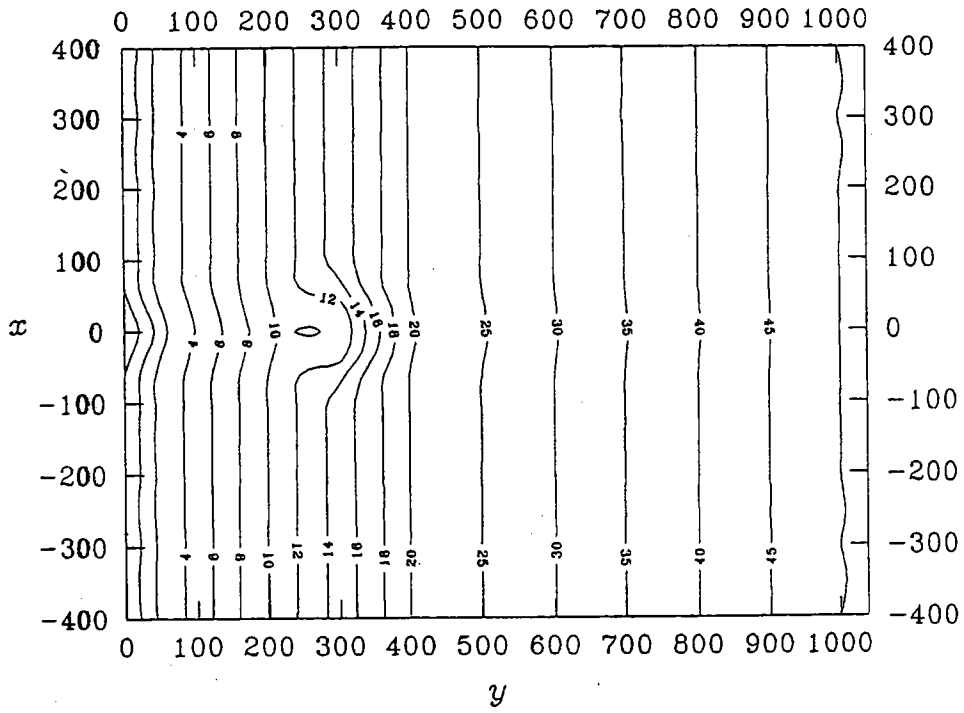

圖3-3-3 近岸區域等深線分佈圖

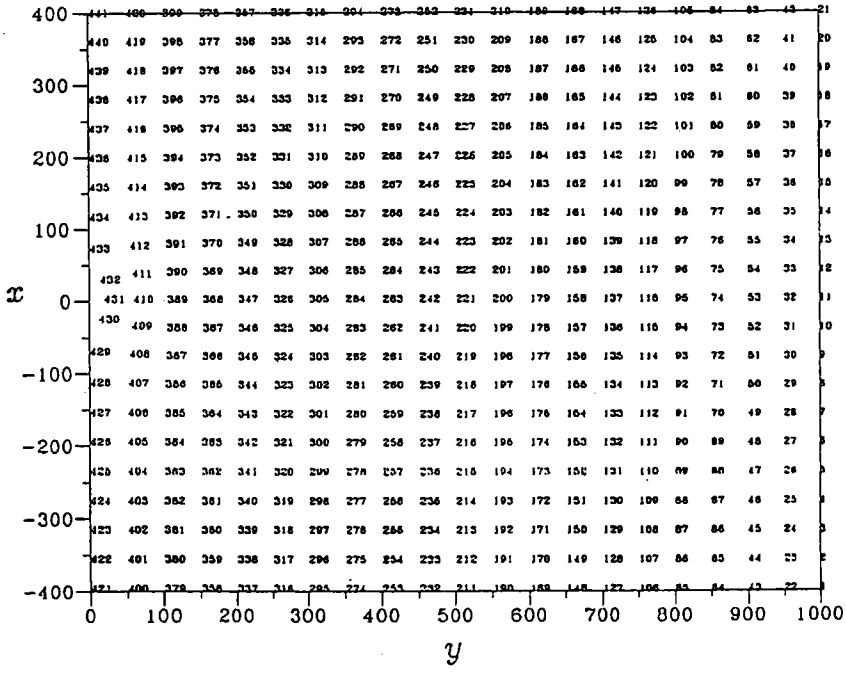

圖3-3-4a 近岸區域在(x,y)平面之網格分割示意圖

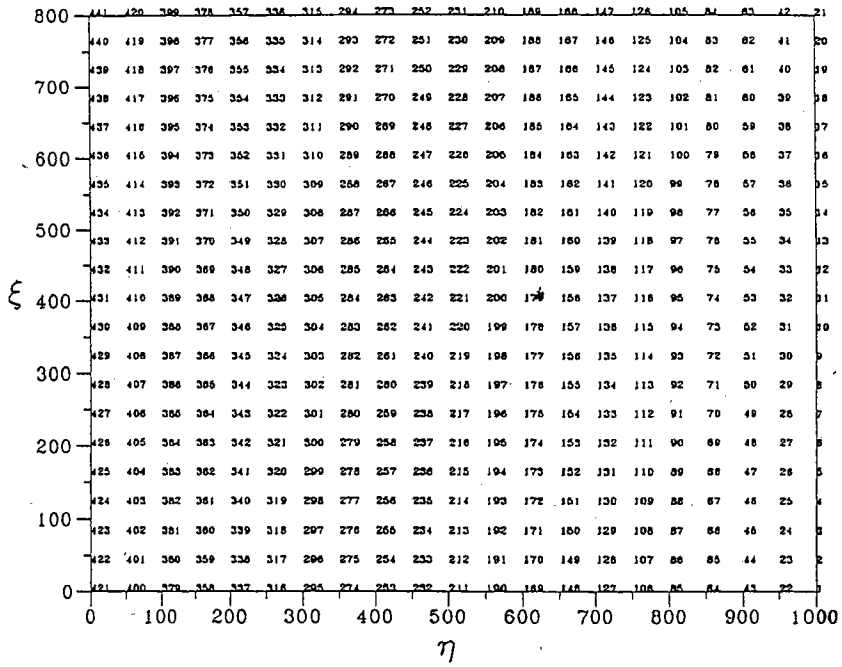

圖 3-3-4b 近岸區域在(ξ,η)平面之網格分割示意圖

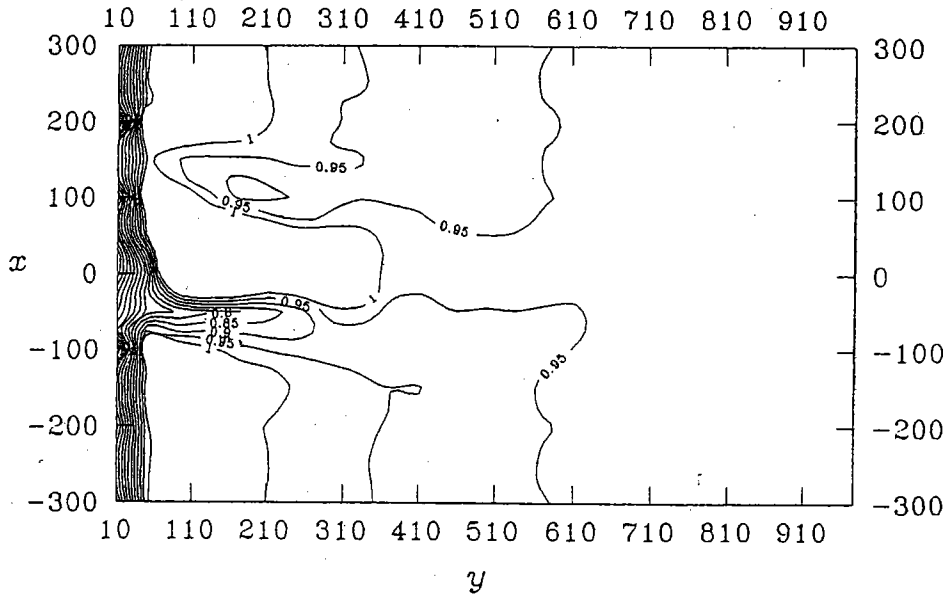

圖 3-3-5 近岸區域等波高(米)分佈曲線圖

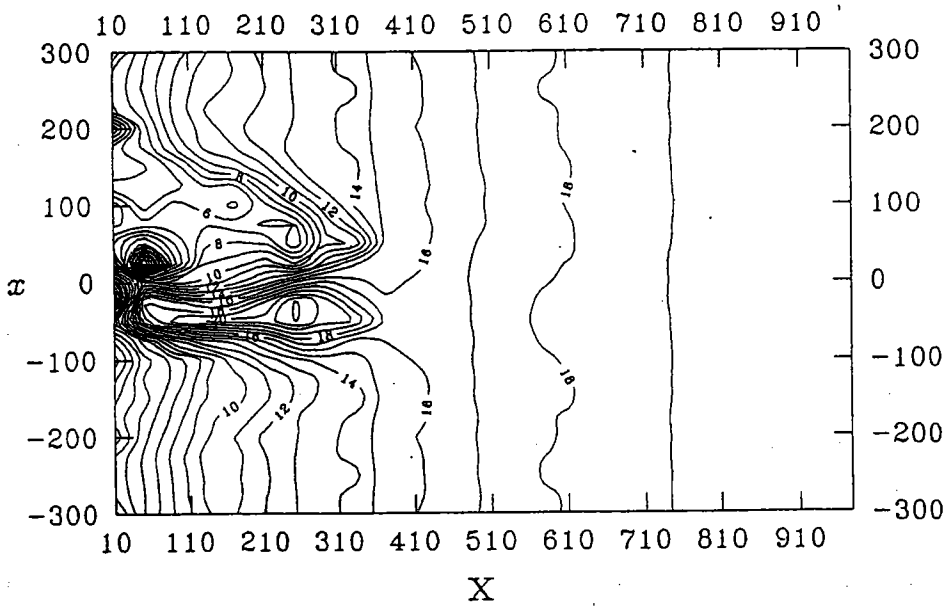

圖3-3-6 近岸區域等波向角(度)分佈曲線圖

—肆、Mike 21線性波浪推算模式介紹—

DHI MIKE 21 Wave Module爲丹麥水工研究所(Danish Hydraulic Institute)發展之波浪計算模式。其主要功能爲模擬計算外海、近岸海域或港區之波場變化。一般可應用於計算海洋、近岸、港口及湖泊等區域之波浪變化。MIKE 21 Linear Wave Module包括OSW、NSW、PMS及EMS等四組,今將主要方程式、數值方法及例子說明,將介紹如后:

4-1外海風浪推算模組-MIKE21 OSW

水面波浪主要因風的作用而產生,OSW模組主要應用於探討在外海深水地區之風浪之進行、成長及減衰等現象。OSW模組之功能包括波浪之產生(風力)、折射、淺化、不同頻率間波與波交互作用等,並以波譜型態完整的描述波浪特性,包括波向之擴展(方向波譜),不同頻率分量之擴展(能量波譜)等。因模式不包括波浪之繞射、反射、碎波及底床摩擦等效應,因此不適合應用於推算近岸淺水地區或港區之波場變化。

OSW模組主要外力爲風,因爲風力常隨時間變化,因此OSW模組爲一時間函數之模式。如果在每個時段能給定已知區域之風力(風速及風向),即可推算該時段、該地區之波浪特性,包括波高(波能)、週期及波向等物理量。

MIKE 21前處理模組提供將颱風(中心氣壓、最大風速、移動速度、最大風半徑等)轉換爲風場分佈(風速及風向),因此OSW模組基本上,具有颱風波浪推算之功能。

OSW模式基本方程組爲能量平衡方程式(The Energy balance equation)

$$\frac{\partial E}{\partial t}+\frac{\cos\theta}{C}\frac{\partial(ECC_g)}{\partial x}+\frac{\sin\theta}{C}\frac{\partial(ECC_g)}{\partial y}+\frac{C_g}{C}(\sin\theta\frac{\partial C}{\partial x}-\cos\theta\frac{\partial C}{\partial y})\frac{\partial E}{\partial\theta}=S \qquad (4.1.1)$$

式中E(x,y,f,θ, t)爲方向頻率波譜(directional-frequency wave energy spectrum),f爲頻率,θ爲波向角,t爲時間,C_g爲群速,C爲波速,S爲淨源項(net source term)。方程式左側項描述波浪之折射及淺化之變化,方程式右側淨源項S包括輸入之風能、波與波交互作用之能量轉換,及消散(disspation)之能量損失等。

OSW模組之數值方法使用Semi-Lagrangian Explicit Higher Order Method,詳細參考OSW模組使用手冊。

以下將計算一深水地區有限風揚(fetch-limited)之波浪成長以說明OSW之應用。考慮長500公里(東西向),寬125公里(南北向),水深爲1000m之開放海域,假設風速20m/s,由西向東(270°)持續吹襲海面,計算區網格大小爲25km × 25km,模擬時間約27小時,時間間格取1200秒(約82次)啓始時間設定爲1月1日12時整。

圖4-1-1爲24小時後(1月2日12時)之波向量分佈圖,因計算區域爲開放等水深區,故每個網格之波高及波向皆相同,若考慮西側邊界爲封閉邊界,則波向量分佈如附圖4-1-2,顯示因西側邊界效應之影響,近西邊之區域風揚(fetch)長度較小,產生之波高也較小。若取格點(5,3)爲觀測點,則圖4-1-3爲點(5,3)主要週期(T_p)隨時間之變化曲線,實線爲西邊取封閉邊界,虛線爲西邊取開放邊界。比較顯示在開放邊界之條件下,成熟之波浪週期較長。圖4-1-4爲點(5,3)平均波高(H_{mo})隨時間之變化曲線,同樣實線部份爲西邊取封閉邊界,虛線部份爲西邊取開放邊界。同週期變化一樣格點(5,3)上開放邊界之成長後平均波高較封閉邊界情形爲大。若西邊爲開放邊界,考慮風速分別爲20m/sec, 15m/sec, 10m/sec及5m/sec,則成熟波浪之平均波高H_{mo}分別爲8.9米, 5.1米, 2.4米及1.5米,主要週期T_p分別爲10.4秒, 8.4秒, 6.3秒及4.1秒。

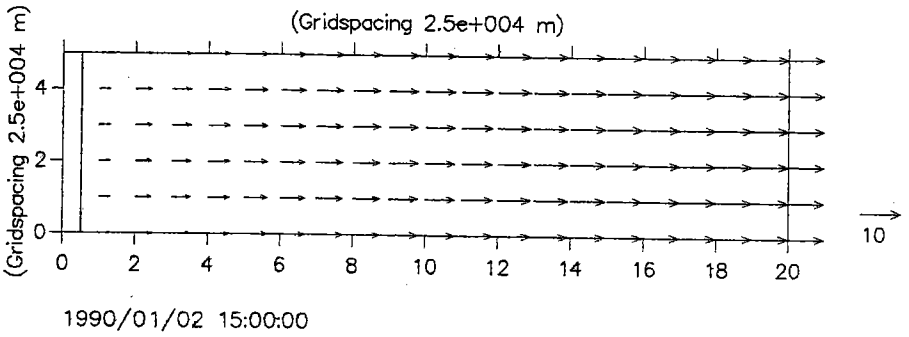

圖4-1-1 西側邊界爲開放邊界24小時後(1月2日12時)之波向量分佈圖

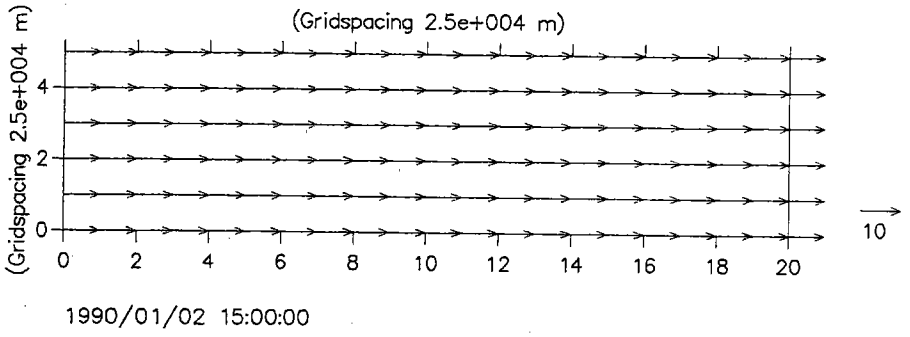

圖4-1-2 西側邊界爲封閉邊界24小時後(1月2日12時)之波向量分佈圖

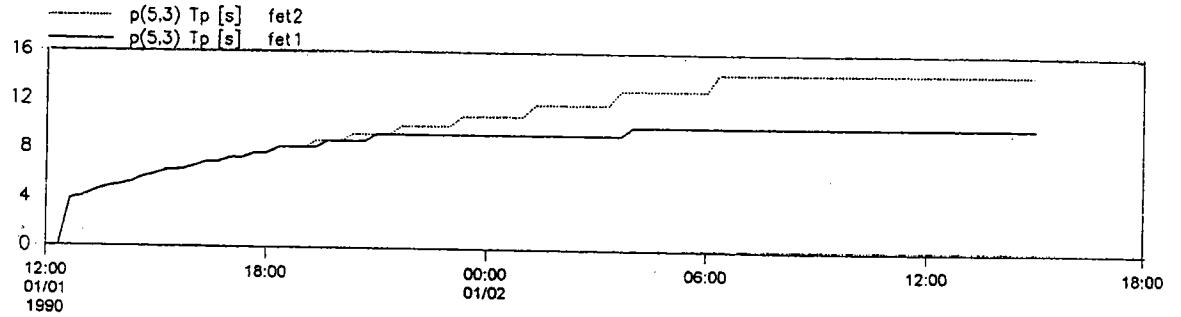

圖 4-1-3 點(5,3)主要週期(T_p)隨時間之變化曲線

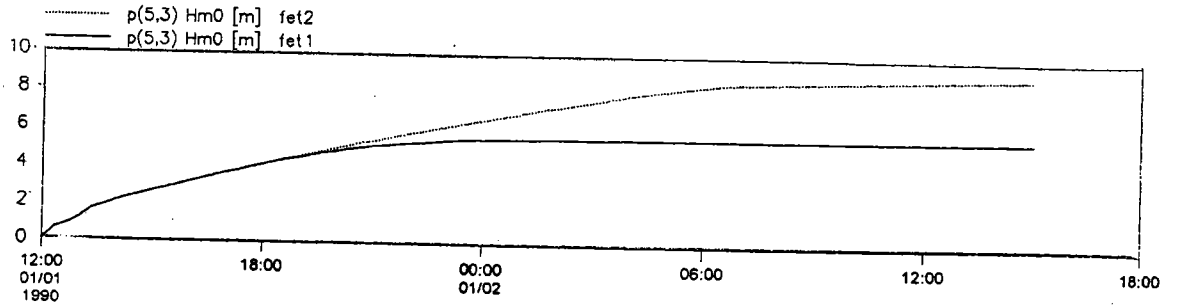

圖 4-1-4 點(5,3)平均波高(H_{mo})隨時間之變化曲線

4-2 近海風浪推算模組-*MIKE 21 NSW*

MIKE 21 NSW主要應用於探討近海地區之風浪進行、成長及減衰等現象，NSW模組之功能包括波浪之產生(風力)、折射、淺化、碎波、底床摩擦、波與流交互作用等，並以不規則波譜型態完整描述波向之擴展及不同頻率分量之擴展等現象。因考慮碎波及底床摩擦等效應甚重要之近岸地區，因此也可推算幅射應力(radiation stress)。但因模式不包括波浪之繞射、反射及波與波交互作用，因此不適合應用於結構物影響甚大之近岸地區及港區之遮蔽計算。NSW模組與OSW模組相同也可直接納入風力之計算。NSW模式基本方程式爲波運動密度能譜守恒方程式(the conservation equation for the spectral wave action density)

$$\frac{\partial(C_{gx}m_o)}{\partial x}+\frac{\partial(C_{gy}m_o)}{\partial y}+\frac{\partial(C_\theta m_o)}{\partial \theta}=T_o \qquad (4.2.1a)$$

$$\frac{\partial(C_{gx}m_1)}{\partial x}+\frac{\partial(C_{gy}m_1)}{\partial y}+\frac{\partial(C_\theta m_1)}{\partial \theta}=T_1 \qquad (4.2.1b)$$

式中$m_o(x,y,\theta)$及$m_1(x,y,\theta)$分別爲第0階能譜及第1階能譜，C_{gx}及C_{gy}分別爲群速度C_g在x及y方向之分量，C_θ則爲波速C在θ方向之分量，其中θ則爲波前進之方向角，T_o及T_1爲源項(Source term)。第n階能譜$m_n(x,y,\theta)$定義爲

$$m_n(x,y,\theta)=\int_o^\infty f^n A(x,y,f,\theta)df, \quad n=0,1,2 \qquad (4.2.2)$$

式中f爲絕對頻率(the absolute frequency)，A爲波運動密度能譜(the spectral wave action density)。

方程式(4.2.1)左項包括波浪之折射及淺化效應，右項T_o及T_1則包括風力、碎波與底床摩擦之能量損失及流之影響等效應。

NSW模組之數值方法主要引用Eulerian有限差分法技巧(finite difference technique)。差分方法可選用linear upwinded differencing, central differencing或quadratic upwinded differencing等之一種方法。

考慮一長2000米(南北向)及寬400米(東西向)之近海地區，西邊界爲海岸線，東邊界處水深爲20米，等深線平行海岸，東西向之地形坡度爲1/20，本例子將探討波浪由外海進入此近海區域之折射及淺化現象，外海入射波浪條件爲$H_{1/3}=1$米，T_s=5秒，波向爲240°N(來向)，計算網格大小取D_x=4米，D_y=200米。圖4-2-1爲波向量分佈圖，圖4-2-2爲點(0,5)至點(99,5)斷面之波向角變化圖，圖4-2-3則爲點(0,5)至點(99,5)斷面之角平均波高變化，圖4-2-4則爲幅射應力S_{xx}分量分佈圖。

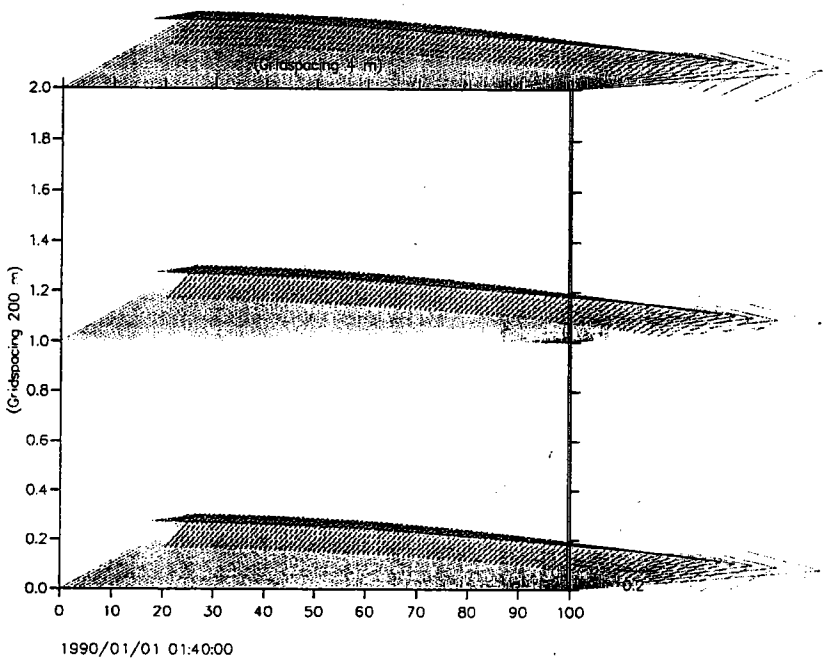

圖4-2-1 波向量分佈圖

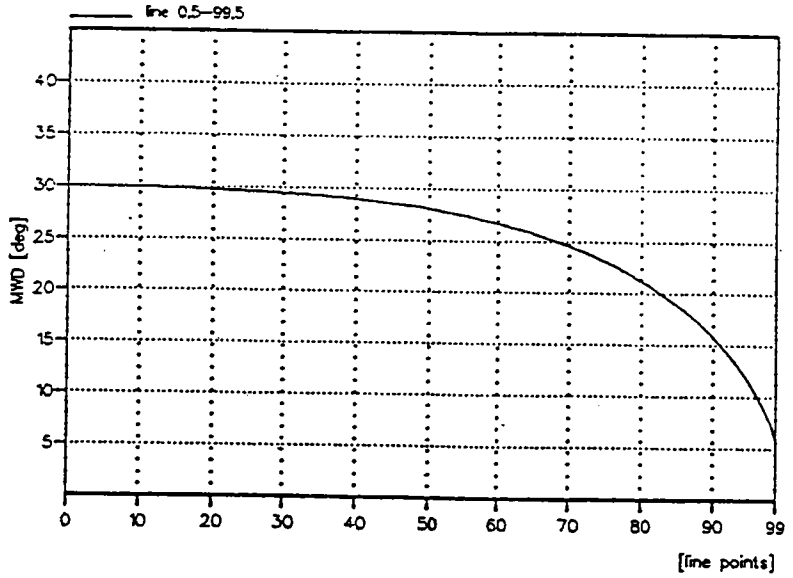

圖4-2-2 點(0,5)至點(99,5)斷面之波向角變化圖

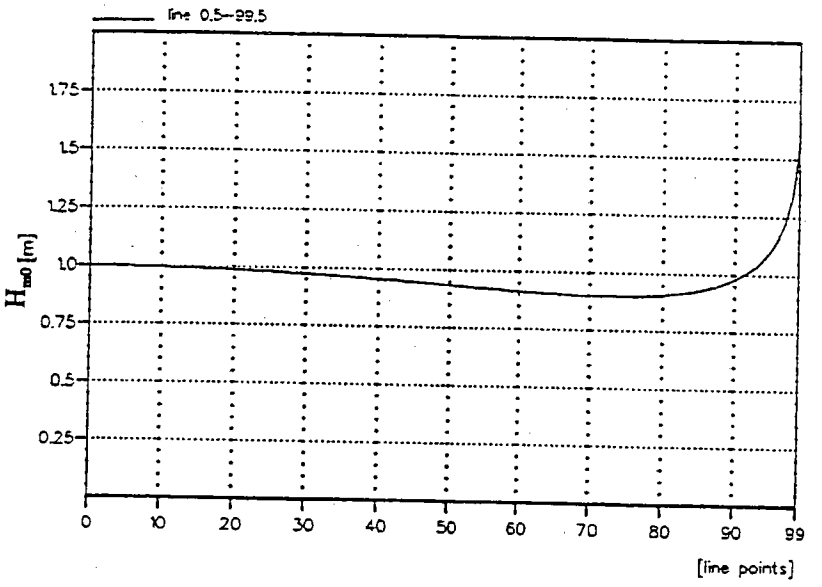

圖 4-2-3 點(0,5)至點(99,5)斷面之角平均波高變化圖

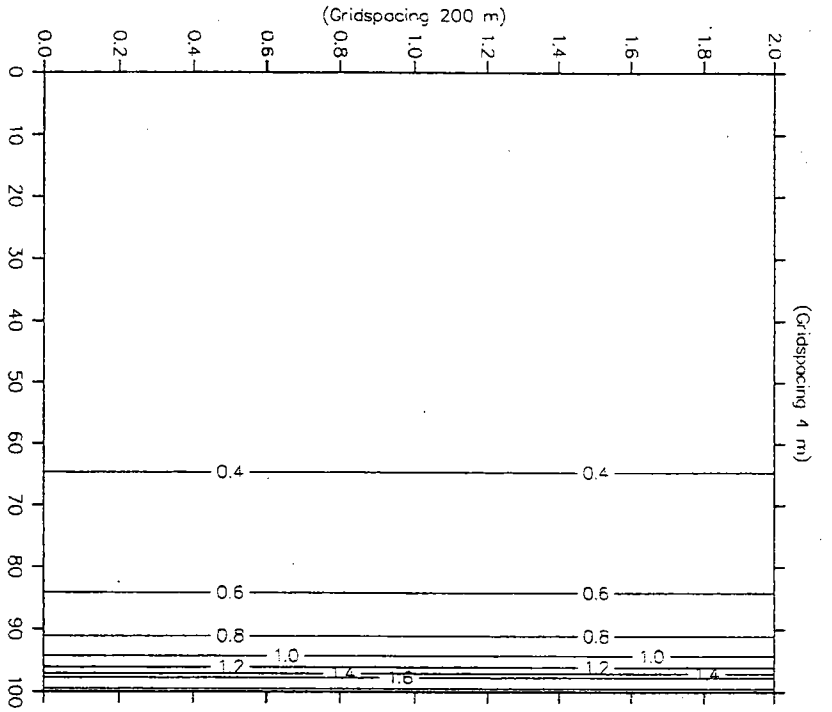

圖 4-2-4 幅射應力 S_{xx} 分量分佈圖

4-3近岸波浪推算模組-*MIKE21 PMS*

MIKE 21 PMS基本方程式爲拋物線型態之緩坡方程式(parabolic approximation to the mild slope equation)。緩坡方程式基本上可納入折射及繞射等效應,因此PMS模組主要應用於探討含有凸堤或離岸堤等結構物之近岸地區波場變化。

PMS模組之功能包括繞射、折射、淺化、碎波、底床摩等效應,並可考慮入射波爲不規則波。但因基本方程式爲拋物線型態因此不包括波浪反射,而且也不包括波與波交互作用,波與流交互作用及風力作用等項。

緩坡方程式(the elliptic rild-slope equation)爲

$$\nabla \cdot (CC_g \nabla \phi) + (k^2 CC_g + i\omega W)\phi = 0 \tag{4.3.1}$$

式中$\nabla = (\frac{\partial}{\partial x}, \frac{\partial}{\partial y})$, $C(x,y)$爲波速, $C_g(x,y)$爲群速, $\phi(x,y)$波函數, k爲波數, $k = 2\pi/L$, L爲波長, W爲能量消散項, ω爲角頻率,$\omega = 2\pi/T$, T爲週期。

波函數$\phi(x,y)$與流速勢$\Phi(x,y,z,t)$下列之關係存在

$$\Phi(x,y,z,t) = g/\omega \phi(x,y) \frac{\cosh k(z+h)}{\cosh kh} e^{-i\omega t} \tag{4.3.2}$$

式中g爲重力加速度, h爲水深。

水位變化$\eta(x,y,t)$與波函數$\phi(x,y)$有下列之關係

$$\eta(x,y,t) = \phi(x,y) e^{-i(\omega t + \pi/2)} \tag{4.3.3}$$

PMS模組之數值方法主要引用the Grank-Nicholson數值方法以求解拋物型態緩坡方程式,此處不再詳述。

以下將探討長20公里(南北向),寬1公里(東西向),並存在有三個凸堤之近岸地區,在受外海波浪作用下之波場分佈情形。地形及凸堤配置如附圖4-3-1,東邊界爲海岸線,西邊界爲開放水域(水深爲20米),等深與海岸線平行,坡度爲1/20,計算網格大小取5m × 5m,外海入射波之條件爲波高$H_{rms} = 2$米,主要週期$T_p = 9$秒,波向50°N(來向)。圖4-3-2爲波向量分佈圖,圖4-3-3則爲在瞬時之水位分佈圖。

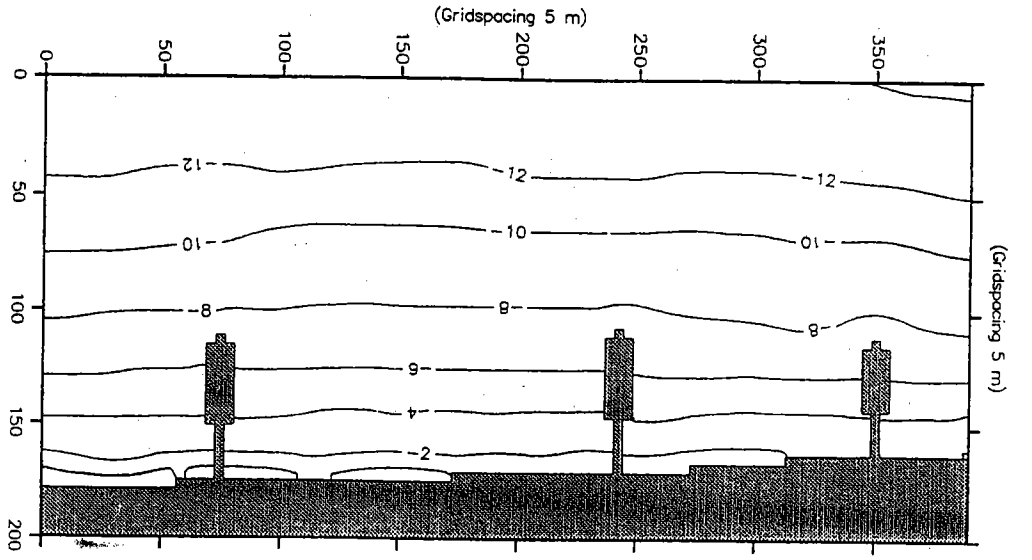

圖4-3-1 計算區地形及凸堤配置示意圖

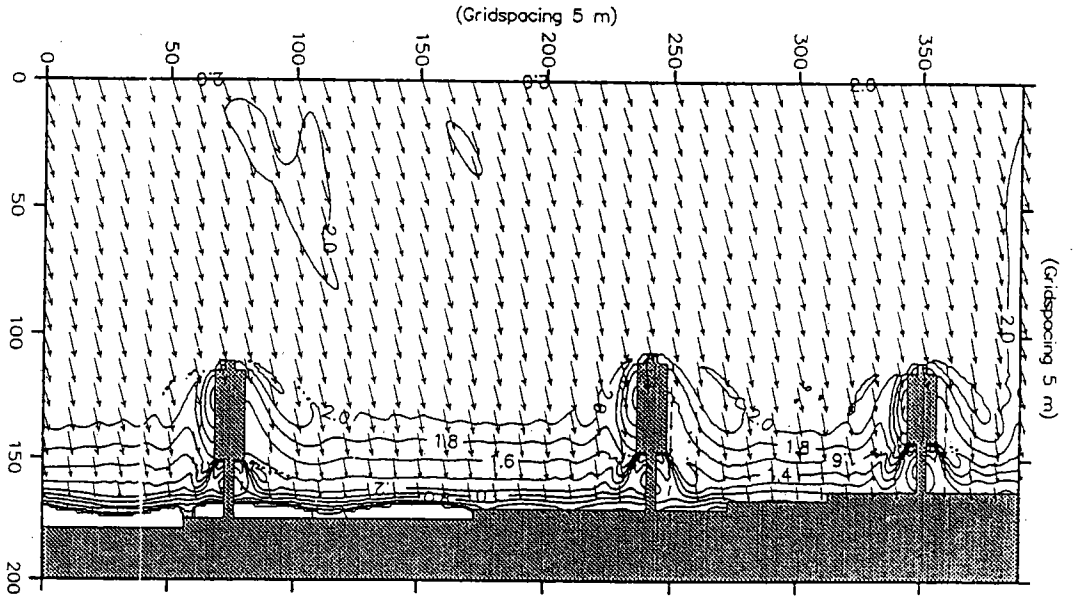

圖4-3-2 波向量分佈圖

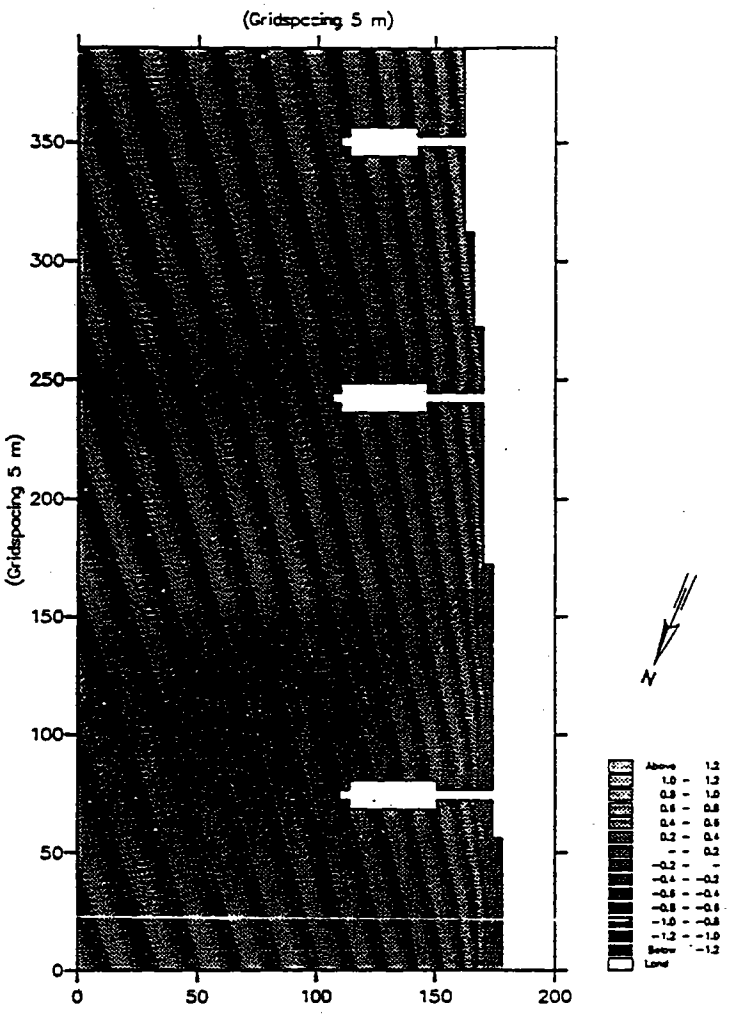

圖4-3-3 瞬時之水位分佈圖

4-4 港池波浪推算模組-*MIKE21 EMS*

MIKE 21 EMS基本方程式(4.3.1)爲橢圓型態緩坡方程式(the elliptic mild slope equation)橢圓型態緩坡方程基本上除已考慮繞射、折射(淺化)效應,若固體邊界考慮爲完全反射體或部份透過、部份反射,則可納入波浪反射、部分反射、部份透射之效應。因此EMS模組主要應用於探討結構物複雜波浪繞射,及多次反射現象明顯之港區。EMS模組之功能包括繞射、折射、淺化、反射、部份反射、部份透射、碎波、底床摩擦等項目,本模式甚爲適合推算港池共振現象。但本模組僅考慮規則波之計算,不包括不規則波推算,而波與波交互作用、波與流交互作用及風力作用等效應也未納入考慮。

引入x及y方向之流量P*及Q*,則緩坡方程式可以質量及動量守恒方程式形式表爲:

$$\frac{\partial P^*}{\partial t} + CC_g\frac{\partial \eta}{\partial x} = 0 \tag{4.4.1a}$$

$$\frac{\partial Q^*}{\partial t} + CC_g\frac{\partial \eta}{\partial y} = 0 \tag{4.4.1b}$$

$$\frac{C_g}{C}\frac{\partial \eta}{\partial t} + \frac{\partial P^*}{\partial t}\frac{\partial Q^*}{\partial y} = 0 \tag{4.4.1c}$$

假設時間變量爲簡諧(Harmonic)穩定解,則η、P^*及Q^*可分別以下式表示:

$$\eta = S(x,y,t)e^{i\omega t} \tag{4.4.2a}$$

$$P^* = P(x,y,t)e^{i\omega t} \tag{4.4.2b}$$

$$Q^* = Q(x,y,t)e^{i\omega t} \tag{4.4.2c}$$

式中S,P,Q之時間變量假設爲緩變特性,在考慮入射波、部分反射波、散射波、吸收邊界、底床摩擦及碎波效應,則控制方程式可化簡爲

$$\lambda_1\frac{\partial S}{\partial t} + \lambda_2 S + \frac{\partial P}{\partial x} + \frac{\partial Q}{\partial y} = SS \tag{4.4.3a}$$

$$\lambda_1\frac{\partial P}{\partial t} + \lambda_3 P + C_g^2\frac{\partial S}{\partial x} = 0 \tag{4.4.3b}$$

$$\lambda_1\frac{\partial Q}{\partial t} + \lambda_3 Q + C_g^2\frac{\partial S}{\partial y} = 0 \tag{4.4.3c}$$

式中λ_1、λ_2及λ_3分別定義爲

$$\lambda_1 = \frac{C_g}{C} \tag{4.4.4a}$$

$$\lambda_2 = \frac{C_g}{C} i\omega + f \tag{4.4.4b}$$

$$\lambda_3 = \frac{C_g}{C}\omega(i + f_p) + f_s + e_f + e_b \tag{4.4.4c}$$

式中ω爲波浪頻率，i爲複數虛部，SS爲單位水平面上之源流強度，f_p爲多孔體線性摩擦損失之能量，f_s爲吸收邊界之線性摩擦因子，e_f爲底床摩擦造成之能量消散，e_b爲因碎波引致之能量損失。

根據以上控制方程式之描述，在模式計算中只要設定適當之計算範圍，給定欲模擬計算之波浪波高與週期，再配合必要邊界條件及相關參數之設定，則港口遮蔽效應與港內靜穩度即可計算求得。

計算模式中由於流量P^*及Q^*爲時間變量，使得橢圓型態之緩坡方程式變形成爲拋物線型方程式，因此在使用有限差分法求解之過程中，網格之大小尺度必須滿足每一波長至少10至15個分割點。另對於流體計算穩定性相關之Courant Number (C_r)之限制亦必須滿足。C_r係用來描述一單位計算時距內，計算訊息傳播影響之格點數目，可表示爲：

$$C_r = C\frac{\Delta t}{\Delta x} \tag{4.4.5}$$

式中C表示計算訊息之傳遞速度，Δx及Δt分別爲計算格距及時距。C_r值在計算區域內必須小於1，數值計算方易趨於穩定，否則將導致發散。除以上計算格距及時距之限制外，計算範圍之人爲邊界尙必須離計算區域有效結構物邊界至少4至6倍波長之距離，藉以減小人爲邊界對計算結果之影響。數值模式計算結果之可靠性與準確性，除受計算模式解析方法及控制方程式建立之假設所限制外，相關邊界條件之設定及參數之使用亦有密切的關係，本究相關之參數及邊界條件設定如下：

(1)底床摩擦

底床摩擦爲促使波浪失去部分能量之致因，能量失去量之大小隨波浪行進距離、波高及波浪週期增加而增大，但隨水深之變深而遞減。對於單一簡諧波而言，其能量消散率可表爲

$$\frac{dE}{\Delta x} = \frac{-1}{6\pi}\frac{f_e}{2g}\left(\frac{\omega H}{\sinh kd}\right)^3 \tag{4.4.6}$$

式中f_e表能量消散係數，ω爲波浪週頻率，k爲波浪週波數，d爲水深，H爲波高。

對於波高具雷利(Rayleigh)分佈之波浪而言，其能量消散率可表爲

$$\frac{dE}{\Delta x} = \frac{-1}{8\sqrt{\pi}} \frac{f_e}{2g} \left(\frac{\omega H_{rms}}{\sinh kd} \right)^3 \tag{4.4.7}$$

式中H_{rms}爲波高之均方根值，f_s與尼古拉(Nikuradse)糙度係數K_N有關，其關係如下：

$$f_e = 0.24, \quad a_b/K_N < 2 \tag{4.4.8a}$$

$$f_e = exp(-5.977 + 5.213(a_b/K_N)^{-0.194}), \quad a_b/K_N \geq 2 \tag{4.4.8b}$$

式中a_b爲底床上波浪水粒子之運動振幅，一般設定$K_N = 0.002m$。

(2)碎波

碎波爲因波浪尖銳度增大而變得不穩定後所產生之能量消散效果，其能量消散量可依下式計算

$$E_{diss} = \frac{-1}{4T} Q_b H_{max}^2 \tag{4.4.9a}$$

式中H_{max}表某一水深下允許之最大波高,而

$$H_{max} = \gamma_1/k \tanh \gamma_2 kd/\gamma_1) \tag{4.4.9b}$$

表碎波量，可依下式估算

$$\frac{1 - Q_b}{\ell n Q_b} = -\left(\frac{H_{rms}}{H_{max}} \right)^2 \tag{4.4.9c}$$

上列式中，T爲波浪週期，k爲波浪週波數，d表水深，H_{rms}爲波高均方根值。γ_1及γ_2爲碎波控制指標，一般使用$\gamma_1 = 1$而$\gamma_2 = 0.8$。

(3)邊界設定

邊界之設定有三類：第一爲反射邊界，可依據結構物反射率之大小，透過線性摩擦係數之轉換而設定，依美國工程兵團海岸保護手冊之資料，對於不透水之光滑海岸，反射係數一般設爲0.8，對於粗糙之斜坡海灘及透水性之結構物，反射係數一般在0.3至0.6間。第二類邊界爲吸收邊界，可依據港池特性及模擬區域需要而設置，藉以減小不必要及人爲邊界導致之反射影響。第三類爲造波邊界，可依據計算範圍配合上述二類邊界之設定選定造波方向。

EMS模組之數值方法主要引用AD有限差分法(finite difference schence),此處不再詳述。

第一個例子考慮長400米,寬5米,水深4米之斷面水槽,寬5米之一透水性結構物置於水槽中央(如附圖4-4-1),透水結構物之線性摩係數爲4.0,水槽兩側則置放5米寬之消波層,而兩條造波線之位置分別爲(6,0)至(6,5)及(7,0)至(7,5)。造波線產生之波高爲1米,週期爲5秒,計算網格大小爲1m × 1m。圖4-4-2爲延者水槽之相對波高變化圖,透水結構物前波高因入射波與部份反射波合成,相對波高大於1米。

第二個例子爲探討波浪通過長700米,寬50米之離岸堤後之波場分佈情形。計算區長1500米(南北向),寬500米(東西向),東邊界爲海岸線,西邊界爲開放水域,等深線平行於海岸線,最西側水深11米,最東側水深2米,東側及西側邊界分別置放消波層,而南側及北側因未置消波層,爲完全反射邊界。離岸堤放之範圍爲點(0,80), (0,220), (10, 80), (10, 220)圍成之長方形區域,並假設離岸堤爲不透水反射體。兩條造波線之位置分別爲(6,0)至(6,300)及(7,0)至(7,300),入射波高爲1米,週期爲8秒。計算網格大小爲5米 × 5米。圖4-4-3爲不考慮碎波條件之等波高線圖,圖4-4-4爲考慮碎波效應之等波高線圖,圖4-4-5爲等幅射應力 S_{xy} 分量分佈圖。圖4-4-6爲由MIKE21 HD模組計算波浪引起之流場分佈圖。

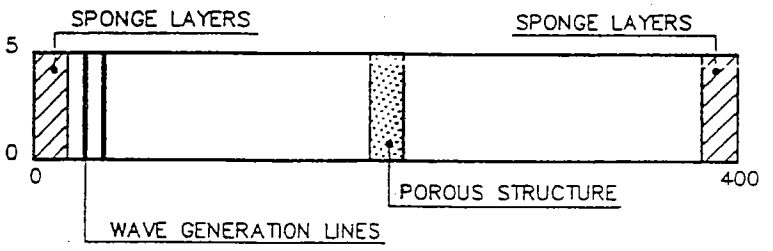

圖4-4-1 斷面水槽透水性結構受波浪作用示意圖

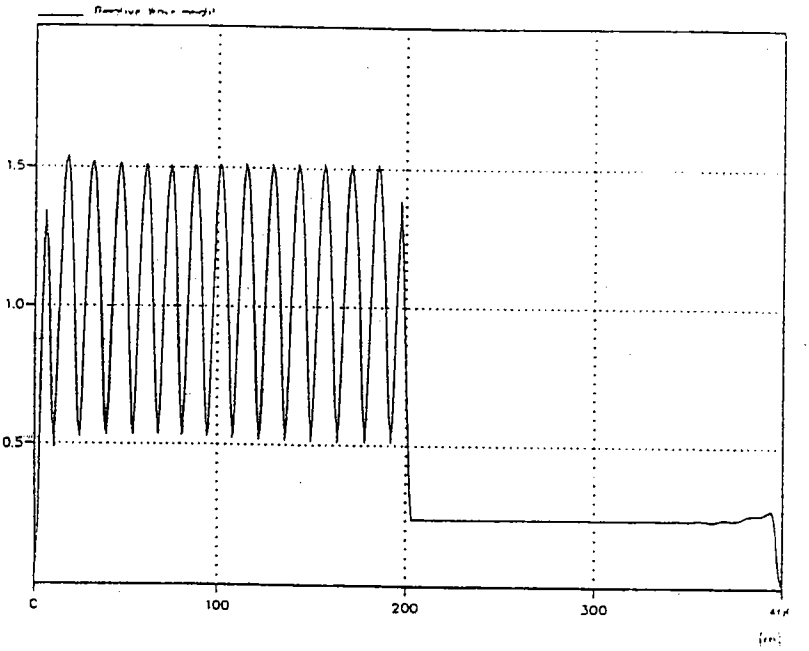

圖4-4-2 延者水槽之相對波高變化圖

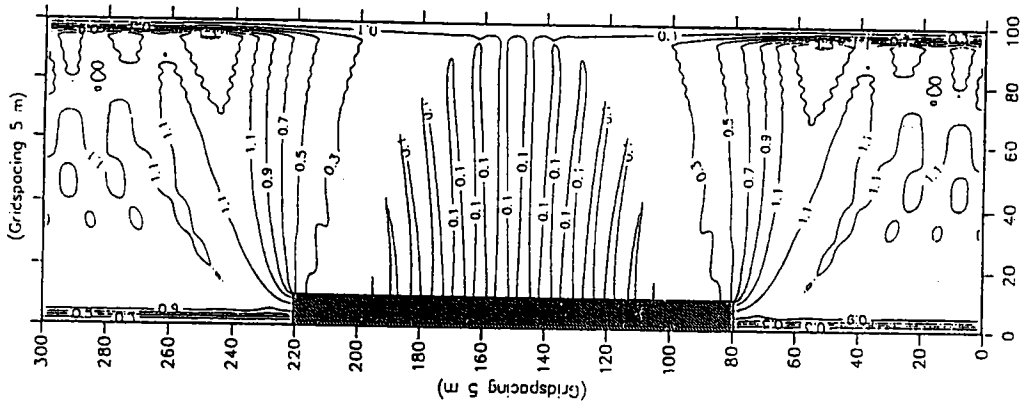

圖4-4-3 不考慮碎波條件之等波高線圖

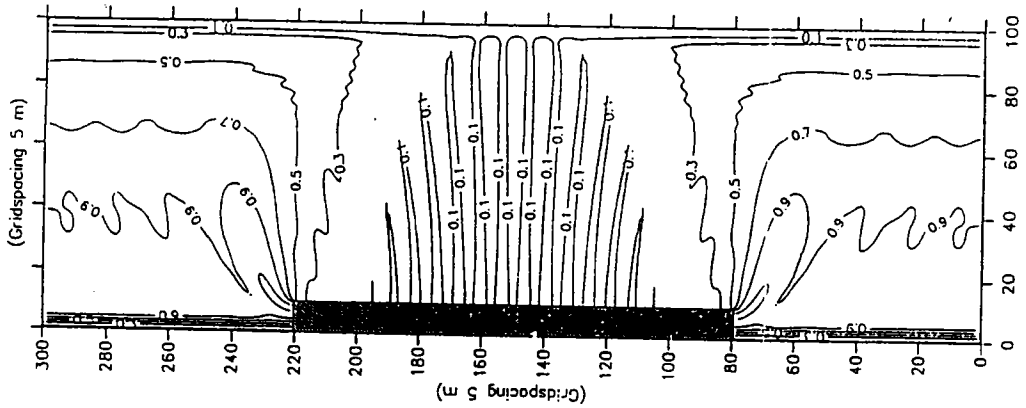

圖4-4-4 考慮碎波效應之等波高線圖

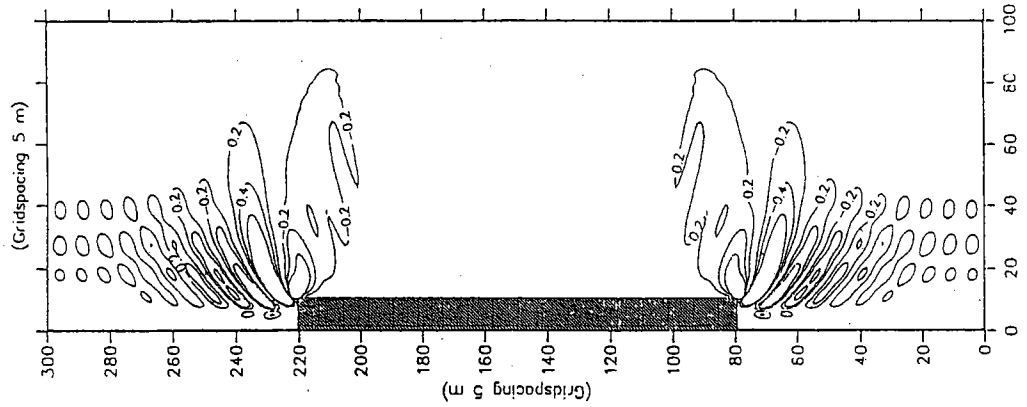

圖4-4-5 等幅射應力S_{xy}分量分佈圖

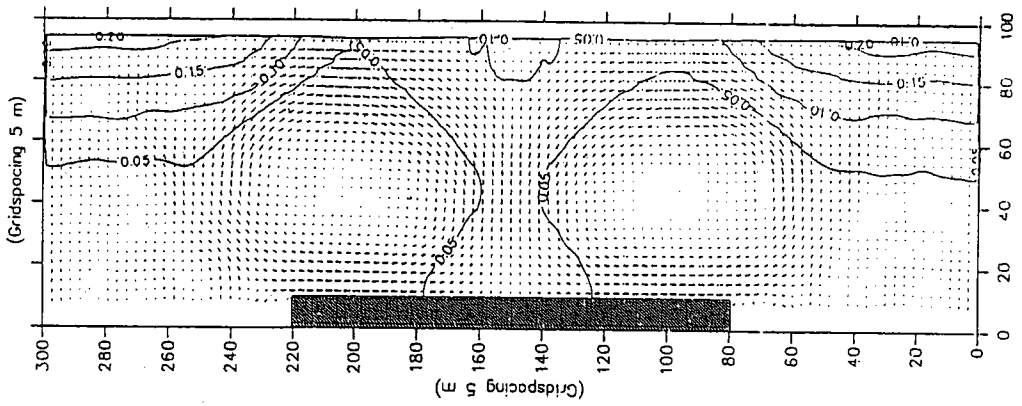

圖4-4-6 MIKE21 HD模組計算波浪引起之流場分佈圖

伍、討論及結論

一、 Model WP21主要應用於推算波浪從外海傳遞至近岸海域之波場分佈,如果海岸線爲平緩沙灘,反射波不明顯之情形,引用拋物線型態緩坡方程式建立之有限差分法模式甚爲適用。在應用貼壁座標轉換,其可取較大之網格點,將節省甚多之記憶體,遠較有限元素法模式爲佳。

二、 Model WH21主要應用於推算等水深或水深變化不明顯之不規則形狀港池之波場分佈或港池共振變化,因邊界元素法模式處理一維邊界之元素遠較有限元素法之二維之三角形元素方便。

二、 Model WE21主要應用於推算水深緩變化之不規則形狀港池之波場分佈或港池共振變化,在推算港池波場,則不宜使用有限差分法模式(拋物線型態方程式)。

三、 波場推算模式,乃可結合有限差分法模式及有限元素法模式二者之之優點。整個計算區可爲不等水深,外海區以有限差分法模式由外海深水區推算至適當港口處,由港口處至港池之區域再引用有限元素法模式計算波場分佈。此方法將可改進有限元素法模式,在港口外爲等水深及海岸線皆需爲平直之不實際假設條件。

四、 Mike 21 OSW模組主要應用於探討在外海深水地區之風浪之進行、成長及減衰等現象。OSW模組之功能包括波浪之產生(風力)、折射、淺化、不同頻率間波與波交互作用等,並以波譜型態完整的描述波浪特性,包括波向之擴展(方向波譜),不同頻率分量之擴展(能量波譜)等。因模式不包括波浪之繞射、反射、碎波及底床摩擦等效應,因此不適合應用於推算近岸淺水地區或港區之波場變化。MIKE 21前處理模組提供將颱風轉換爲風場分佈(風速及風向),因此OSW模組基本上,具有颱風波浪推算之功能。

五、 MIKE 21 NSW主要應用於探討近海地區之風浪進行、成長及減衰等現象,NSW模組之功能包括波浪之產生(風力)、折射、淺化、碎波、底床摩擦、波與流交互作用等,並以不規則波譜型態完整描述波向之擴展及不同頻率分量之擴展等現象。因考慮碎波及底床摩擦等效應甚重要之近岸地

區，因此也可推算幅射應力(radiation stress)。但因模式不包括波浪之繞射、反射及波與波交互作用，因此不適合應用於結構物影響甚大之近岸地區及港區之遮蔽計算。NSW模組與OSW模組相同也可直接納入風力之計算。

六、 MIKE 21 PMS基本方程式爲拋物線型態之緩坡方程式，可納入折射及繞射等效應，因此PMS模組主要應用於探討含有凸堤或離岸堤等結構物之近岸地區波場變化。PMS模組之功能包括繞射、折射、淺化、碎波、底床摩等效應，並可考慮入射波爲不規則波。但因基本方程式爲拋物線型態因此不包括波浪反射，而且也不包括波與波交互作用，波與流交互作用及風力作用等項。

七、 MIKE 21 EMS基本方程式爲橢圓型態緩坡方程式程，基本上除已考慮繞射、折射(淺化)效應，若固體邊界考慮爲完全反射體或部份透過、部份反射，則可納入波浪反射、部分反射、部份透射之效應。因此EMS模組主要應用於探討結構物複雜波浪繞射，及多次反射現象明顯之港區。EMS模組之功能包括繞射、折射、淺化、反射、部份反射、部份透射、碎波、底床摩擦等項目，本模式甚爲適合推算港池共振現象。但本模組僅考慮規則波之計算，不包括不規則波推算，而波與波交互作用、波與流交互作用及風力作用等效應也未納入考慮。

參考文獻

1. Baker, B. B. and E. T. Copson ,"The Mathematical Theory of Huygen's Principle",Oxford Universiyty Press, London (1950).

2. Berkhoff, J. C. W., "Computation of Combined Refraction Diffraction", Proc. 13th Coastal Engineering Conference, Vol. 1 (1972) .

3. Booij, N. ,"Gravit Waves on Water with Non-Uniform Depth and Current ", thesis present to the Technical University of Delft , The Netherlands, in partial fulfillment of the requirements for the degree of Doctor of Philosophy (1981).

4. Chen, H. S. and C. C. Mei ,"Oscillations and Wave Forces in an Offshore Harbor", Ralph M. Parsons Laboratory, Report No. 190, MIT, August(1974).

5. Chen, H. S. , " Effects of Bottom Friction and Boundary Absorption on Water Wave Scattering", Appl. Ocean Research, Vol. 8, pp.99 ~ 104(1986).

6. Chwang, A.T., S. H. Ou and C.H. Su , "Dissipation of Wave Energy by a Porous Wall ", CKHORT-89-005 ,Dept. of Hydraulics and Ocean Eng., National Cheng Kung Univ. ,Taiwan, R.O.C. (1989).

7. Chwang, A. T., S. H. Ou and C. H. Su , "Wave Oscillations inside Porous-Wall Harbors", Proc. of 5th Conf. on Hydr. Eng. , Taiwan, R.O.C. pp.853 ~ 868 (1990).

8. Dalrymple, R. A. , M. A. Losada and P. A. Martin ," Reflection and Transmission from Porous Structures under Oblique Wave Attack ", J. Fluid Mech., Vol.224, pp. 625 ~ 644 (1991).

9. Danish Hydraulic Institute, " MIKE 21 PP (Pre- and Post-processing) User Gide and Referencemanual " ,1997.

10. Danish Hydraulic Institute, " MIKE 21 OSW(Offshore Spectral Wind-Wave) Module User Gide and Referencemanual " ,1997.

11. Danish Hydraulic Institute, " MIKE 21 NSW(Nearshore Spectral Wind-Wave) Module User Gide and Referencemanual " ,1997.

12. Danish Hydraulic Institute, " MIKE 21 PMS(Parabolic Mild-Slope) Module User Gide and Referencemanual " ,1997.

13. Danish Hydraulic Institute, " MIKE 21 EMS(Elliptic Mild-Slope) Module User Gide and Referencemanual " ,1997.

14. Danish Hydraulic Institute, " MIKE 21 HD (Hydrodynamic) Module User Gide and Referencemanual " ,1997.

15. Ho, R. T. and H. Bomze , "Basin Oscillations in an Offshore Harbor," Paper No. OTC 2331, Proceedings of the Offshore Technology Conference, Vol., 11, Houston, Texas , pp.853 ~ 969 (1975).

16. Hwang , L.S. and E.O. Tuck ," On the Oscillation of Harbors of Arbitrary Shape ", J. Fluid. Mech. Vol. 42 , No. 3, pp. 447 ~ 464 (1970).

17. Ippen, A. T. and Y. Goda , "Wave Induced Oscilations in Harbors : The Solution for a Rectangular Harbor Connected to the Open-Sea" , Report No.59, Hydrodynamics Laboratory , M.I.T. (1963).

18. Lee, J.J., "Wave-Induced Oscillations in Harbours of Arbitrary Shape ", Report KH-R-20, W. M. Keek laboratory of Hydraulics and Water Resources, California, Institute of Technology, Berkeley, Calif. (1969).

19. Lee, J. J., "Wave-induced Oscillations in Harbours of Arbitrary Geometry", J. Fluid Mec. , Vol. 45, pp. 375 ~ 394 (1971).

20. Lee, J. J. and F. Raichlen " Oscillations in Harbors with Connected Basins ", Report KH-R-26, W. Keek Laboratory of Hydraulics and Water Resources, California Institute of Technology (1971).

21. Lee, J. J. and F. Raichlen , "Oscillations in Harbors with Connected Basins," J. Waterw. , Har. and Coastal Eng. Div. , Vol. 98, No. WW3, pp.311 ~ 332 (1972).

22. Liu, P.L.-F. , "Parabolic Wave Equation in Surface Water Waves", Miscellaneous Report CERC 86. U.S. Army, Corps of Engineers, Coastal Engineering Research Center, Vicksburg, MS (1986).

23. Liu, P.L.-F. , "Wave Transformation " ,in B. LeMehaute and D.M. Hanes (eds.), The Sea Vol. 9: Ocean Engineering Science, Wiley, New York (1989).

24. Liu, P.L.-F. and T., -K. Tsay, "Numerical Prediction of Wave Transformation", J. Waterway Port Coastal Ocean Eng. ASCE, Vol. 114, pp.237 ~ 247 (1988).

25. Lozano C. and T. K. Tsay ,"Refraction-Diffration Model for Linear Surface water Waves", J. Fluid Mech. Vol. 101 , pp.705 ~ 720 (1980).

26. Madsen, O.S. ," Wave Transmission through Porous Structures ", J. Waterw., Port, Coastal and Ocean Eng., ASCE Vol. 100, pp. 169 ~ 188(1974).

27. Madsen ,O.S. and S.M. White," Wave Transmission through Trapezoidal Breakwaters " , Proc. 15th Conf. on Coastal Eng., ASCE, Honolulu, Hawaii, pp.2662 ~ 2676 (1976).

28. Madsen, P.A.," Wave Reflection from a Vertical Permeable Wave Absorber", Coastal Eng. ,Vol.7,pp. 381 ~ 396 (1983).

29. Mattioli , F. and S. Tinit , "Discretization of Harbor Resonance Problem", J. Waterw. Port , Coastal and Ocean Division ,ASCE, Vol. WW4 ,pp. 464 ~ 469 (1979).

30. McNown, J. S. ,"Waves and Seiche in Idealized Ports", Gravity Wave Symposium , National Bureau of Standrds Circular 521.

31. Miles, J. and W., Munk , "Harbor pardors", J. Water.and Harbors Divi., ASCE, WW 3, pp.111- 130 (1961).

32. Morse, P.M. and K.U. Ingard, *Theoretical Acoustics*, Princeton Univ. Press, U.S.A. (1968).

33. Richey E.P. and C.K. Sollitt, "Wave Attenuation by Porous Walled Breakerwater " , J. Water. Har. and Coast. Eng. Div., ASCE, Vol. 96, pp. 643 ~ 663 (1970).

34. Sollitt, C.K. and R.H. Cross, "Wave Transmission through Permeable Breakwaters" ,Proc. 13th Conf. on Coastal Eng. ASCE, Vancouver, Canada, pp.1827 ~ 1846 (1972).

35. Radder, A. C. ,"On the Parabolic Equation Method for Water-Wave Propagation ", J. Fluid Mech. Vol. 95 , pp.159 ~ 176 (1979).

36. Segerlind L. J. , *Applied Finite Element Analysis*, Pentech Press London (1974).

37. Tsay, T. K. and P. L- F. Liu ,"Numerical Solution of Water Wave Refraction and Diffraction Problems in the Parabolic Approximation " , J. geophys. Res. , Vol. 87 pp. 7932 ~ 7940(1982).

38. Tsay, T. K. and P. L- F. Liu ,"A Finite Element Model for Wave Refraction and Diffration " , Appl. Ocean Research ,Vol. 5, pp.30 ~ 37 (1983).

39. Tsay, T., K. , W. Zhu and P. L-F. Liu ,"A Finite Element Model for Wave Refraction , Diffraction ,Reflection and Dissipation", Applied Ocean Research , Vol. 11, No1. pp.33 ~ 38 (1989).

40. Tsay, T., B. A. Ebersole and P. L-F. Liu ,"Numerical Modelling of Wave Propagation Using Parabolic Approximation with a Boundary-Fitted Coordinate System ",Inter. J. for Num. Methods in Eng. , Vol. 27, pp.37 ~ 55 (1989).

41. 林銘崇、謝宗誠，「波浪折射-繞射之有限-邊界元素解析」，中華造船工程學刊，第四期，第131 ~ 137頁(1985).

42. 林銘崇、許永誠，「波浪折射-繞射與海流共同效應之有限-邊界元素解析」，國立台灣大學造船工程學研究所，Rept. No. 227 (1985).

43. 周宗仁、林炤圭，「應用邊界元素法解析任意地形及水深之港池水面波

動問題」，第八屆海洋工程研討會，第111～129頁(1986)。

44. 周宗仁、林炤圭，「任意反射率防波堤或岸壁的港池水面振動數值分析」，第十一屆海洋工程研討會，第365～381頁(1989)。

45. 周宗仁、韓文育，張景程，「任意形狀、水深及反射率港池的水面振動實例」，第十四屆海洋工程研討會，第423～443頁(1992a)。

46. 周宗仁、韓文育、朱忠一，「消波式碼頭對港內水面振動之影響」，第六屆水利工程研討會，第668～679頁(1992b)。

47. 陳柏旭、蔡丁貴「局部輻射邊界條件在水波數值模式上應用」，中華民國第十二屆海洋工程研討會論文集，第1～18頁(1990)。

48. 歐善惠、林西川、林火旺、蘇青和，「不等水深多孔岸壁港池之共振模式」，中華民國第十二屆海洋工程研討會論文集，台中，第74～94頁(1990)。

49. 蘇青和、歐善惠、章梓雄，「多孔岸壁港池之波能消散現象」，港灣技術，第七期，第1～24頁(1992)。

50. 蘇青和、蔡丁貴、歐善惠，「數值方法及輻射邊界在港池共振應用之探討」，中華民國第十三屆海洋工程研討會論文集，第23～37頁(1991).

非線性波浪引起港池振盪之研究

劉立方
教授
土木及環境工程研究所
美國康乃爾大學

蔡丁貴
教授
土木工程研究所
國立台灣大學

蘇青和
研究員
數學模式組
港灣技術研究所

Harbor Oscillations Induced by Nonliner Transient Waves

Philip L.-F. Liu

School of Civil and Environmental Engineering

Hollister Hall

Cornell University

Ithaca ,New York ,U.S.A.

Ting-Kuei Tsay

Department of Civil Engineering

National Taiwan University

Taipei, Taiwan

Ching-Ho Su

Mathematical Modelling Devision

Institute of Harbor & Marine Technology

Wuchi, Taichung District, Taiwan

摘 要

本文首先介紹有關港池共振相關之研究論文,並說明本研究計畫之內容與目的,其次介紹現有幾種有關港池共振之數值模式。本計畫主要建立新的非線性港池振盪有限元素法模式,新的模式包括二維連續方程式及運動方程式之垂直積分理論建立，而描述弱非線性與弱分散波也爲本模式之基礎。本年度主要探討一維之問題,時間積分方面比較隱性及顯性兩種不同積分結果,而數值計算之穩定及正確爲比較重點。空間積分方面探討Galerkin與Petrov-Galerkin兩種不同方法之優劣結果,邊界條件則包括有Dirichlet邊界條件及Neumann邊界條件兩種。最後本文並計算七個應用例子,以探討模式可能之應用範圍及驗證模式之正確性。

Summary

In this report a brief literature review is given first to summarize the background and research approaches in studying harbor oscillations. Several existing numerical models for calculating wave oscillations in a harbor are then reviewed. The need for developing a finite element model for computing harbor oscillations induced by nonlinear transient waves is firmly established. Vertically integrated two-dimensional continuity and momentum equations, describing weakly nonlinear and weakly dispersive waves, are the basis of the new numerical model. In this report attention is focused on one-dimensional problems. Two numerical time-integration schemes, an explicit Taylor-Galerkin finite element scheme and an implicit (predictor-corrector) Galerkin finite element scheme, are employed. Numerical instability and accuracy of different algorithms are discussed. For spatial-integration the weighted residual method is used. Both Galerkin and Petrov-Galerkin methods, using different combinations of linear and cubic-spline functions as weighting function and basis function, are tested. Both Dirichlet boundary condition (for incident waves) and Neumann boundary condition (for a reflecting wall) are implemented. Several examples are included in the report to demonstrate the range of applicability and the accuracy of the model.

Harbor Oscillations Induced by Nonlinear Transient Waves (I)

Contents

List of Figures

1 Introduction

Harbor resonance is the phenomenon of trapping and amplification of wave energy inside a semi-enclosed water body, such as a harbor or a bay. If flow motions inside a harbor are forced at one or more of natural frequencies of the harbor, which can be determined from the harbor configuration, the amplitudes of harbor oscillations will become rather large. These large amplitude oscillations could create unacceptable vessel movements and excessive mooring forces leading to the breaking of mooring lines. In designing a new harbor or modifying an existing harbor, it is essential to have a good understanding of the natural frequencies of the harbor and the possible sources of forcing for harbor resonance. Moreover, a model, either numerical or physical model, should be used to examine the temporal and spatial variations of wave amplitudes inside the proposed harbor under the design wave conditions.

Typical resonant periods for a reasonable sized harbor or a moored vessel are of the order of magnitude of several minutes. Therefore, harbor resonance at this frequency range is not caused directly by wind waves since wind wave periods are of the order of magnitude of several seconds. Other possible sources of resonance forcing include tsunamis, atmospheric pressure disturbances, locally generated infragravity waves, and free infragravity waves generated at and radiated from distant shores. Tsunamis and atmospheric pressure disturbances have been shown convincingly in previous studies as causes for harbor resonance (e.g., Carrier et al. 1971). However, they alone cannot account for the resonance problems existing in many harbors around the world. Munk (1949) was the first one who observed the infragravity waves associated with wind waves. Later, Longuet-Higgins and Stewart (1962) gave physical and mathematical explanations for the generation of the free and bound infragravity waves through nonlinearity. Recent field observations in three small harbors (two in Hawaii and one in California) have shown that harbor resonance can be forced primarily by the free infragravity waves originated in the offshore region (Okihiro et al 1993, Okihiro and Guza 1996). However, many researchers have also shown theoretically and experimentally that the bound infragravity waves (associated with groups of wind waves impinging at a harbor mouth) can cause harbor resonance (e.g., Bowers 1977, Mei and Agnon 1989, Wu and Liu 1990). Moreover, free infragravity waves can also be generated locally (inside or in the vicinity of a harbor) through interactions of bound infragravity waves and harbor boundaries.

For a simple harbor geometry and depth variations the natural frequencies and the corresponding free surface oscillations can be predicted analytically. However, for more complex harbor geometry, for transient excitations, and for cases where nonlinear effects are important, the harbor response can be determined only from experiments conducted in a hydraulic model or with a numerical model. Although the usefulness of conducting a hydraulic model study should never be underestimated, there are several limitations. It is costly to construct and modify the

hydraulic model to collect data for a long duration with a fine spatial resolution. The scaling of the hydraulic model is also a difficult issue when both short waves and infragravity waves are of interest. Therefore, research efforts focused on the development of numerical models for calculating the harbor oscillations induced by nonlinear transient waves are essential.

There are several existing numerical models that could be used to calculate the harbor oscillations with or without any modification. In this section only the models which have been designed specifically for studying the harbor oscillation problems and have been applied to field problems are briefly discussed. This brief review should also provide justifications for proposing a new numerical model.

1.1 Finite element model based on the mild-slope equation

Using the linear mild-slope equation, several research groups have developed various finite element models for harbor resonance (e.g., Chen, 1984, 1986, Tsay and Liu 1983, Kostense et al. 1986, Xu, et al. 1996). These models calculate linear monochromatic wave oscillations in harbors of arbitrary configuration and variable bathymetry. The effects of bottom friction and boundary absorption (reflection) are usually included. These models use a hybrid element solution method that involves the combination of analytical (in offshore area) and finite element numerical (near and inside the harbor) solutions to determine the harbor response to a small amplitude wave with a single wave frequency. These models are the extension of the original model developed by Chen and Mei (1974), which was based on the linear shallow water equations.

Because of their simplicity these models have been used for assessing the design or modifications of existing harbors (e.g., Lillycrop et. al. 1993). However, the most serious drawback of the model is the limitation of the linear theory. These models can not be used to investigate harbor oscillations induced by nonlinear transient waves.

1.2 Finite element model based on Boussinesq-type equations

Lepelletier (1980) developed a finite element model for solving the weakly nonlinear-dispersive-dissipative equations of motion for variable depth (also see Lepelletier and Raichlen 1987). Several dissipative effects such as bottom friction and entrance losses, were included in the model. A time varying radiation condition at a finite distance from the harbor entrance is used to simulate the open sea conditions.

Since the Boussinesq approximation was employed in the model, the weakly nonlinear effects were included. However, the water depth must remain small relative to the wavelength throughout the entire domain of interest, including the offshore region. Therefore, this model is not suitable for studying the problems

where the incident waves consist of short wave components. For example, in the Haw-lien harbor situation, the dominating wave outside of the harbor has a wavelength such that $kh \approx 1$ and cannot be considered as a shallow water wave. As discussed in the previous section, these short wave components are responsible for generating bound and free infragravity waves near and inside the harbor, which might be resonated in the harbor.

1.3 Finite differences models based on Boussinesq-type equations

During the last twenty-five years scientists and engineers at the Danish Hydraulic Institute (DHI) have developed a series of finite differences models based on either the nonlinear shallow water equations or Boussinesq-type equations (e.g., Abbott 1979, Abbott, et al. 1978, Madsen, et al. 1991). These harbor models are components of a much larger system called MIKE 21 for studying the flow phenomena in estuaries and coastal waters. The disadvantages of these finite differences models are primarily due to the inflexibility of finite-difference methods in modeling the irregular boundaries as well as the complex bathymetry. Furthermore, the MIKE 21 is a commercial package. It is impossible to obtain the source program for any further investigation and improvement.

From the brief review given above, it is clear that either the linear wave theory (mild-slope equation) or the shallow water depth assumption (Boussinesq-type equations) restricts the existing numerical models. It is the objective of this research project to develop a finite element model, using the fully nonlinear and weakly dispersive wave equations, to investigate the nonlinear transient harbor oscillations.

2 Basic Equations for the Numerical Model

The objective of the research project is to develop a finite element model for computing transient, nonlinear harbor oscillations. The theoretical foundation of the proposed new model is based on the fully nonlinear and weakly dispersive wave equations that can be applied in both intermediate and shallow water (e.g., Liu 1994, Wei et al. 1995). A brief review of the historical development of these governing equations is given as follows.

Boussinesq-type equations provide a means for studying water wave propagation over a gradual varying bathymetry. The core of the Boussinesq-type equations is made of the shallow water equations for linear nondispersive wave propagation. This basic foundation is expanded by adding terms that represent effects of nonlinearity and frequency dispersion.

Assuming that both the nonlinearity and the frequency dispersion are weak and are in the same order of magnitude, Peregrine (1967) derived the standard Boussinesq equations for variable depth with the depth-averaged velocity as a dependable variable. Peregrine's Boussinesq equations can be recast into similar equations in terms of either the velocity on the bottom or the velocity on the free surface. While the dispersion relationship and the wave celerity associated with these equations differ slightly, the order of magnitude of accuracy of these equations remains the same. Numerical results based on the standard Boussinesq equations or the equivalent formulations have been shown to give predictions that compared quite well with field data (Elgar and Guza 1985) and laboratory data (Goring 1978, Liu et al. 1985).

The applications of the standard Boussinesq equations are limited to the shallow water depth because of the assumption of the weak frequency dispersion effects. The standard Boussinesq equations written in terms of the depth-averaged velocity break down when the depth is greater than one-fifth of the equivalent deep-water wavelength. For many engineering applications including storm surge computations, where the incident wave energy spectrum consists of many frequency components, a lesser depth restriction is desirable. Furthermore, when the Boussinesq equations are solved numerically, high frequency oscillations with wavelengths related to the grid size could cause instability. To extend the applications to shorter waves many modified forms of Boussinesq-type equations have been introduced (e.g. Madsen et al. 1991, Nwogu 1993, Chen and Liu, 1995). Although the methods of derivation are different, the resulting dispersion relations of the linear components of these modified Boussinesq equations are similar, and may be viewed as a slight modification of the (2,2) Pade approximation of the full dispersion relation for linear water wave (Witting 1984). It has been demonstrated that the modified Boussinesq equations are able to simulate wave propagation from deep water to shallow water including the wave-current interaction (Chen et al. 1998).

Despite of the success of the modified Boussinesq equations in intermediate and

deep water, these equations are still restricted to weakly nonlinear interactions. As waves approach shore, wave height increases due to shoaling and wave breaks on most gentle natural beaches. The wave-height to water depth ratios associated with this physical process become too high for the Boussinesq approximation. Of course this restriction can be readily removed by eliminating the weak nonlinearity assumption (e.g., Wei et al. 1995). Strictly speaking, these fully nonlinear equations can no longer be called Boussinesq-type equations since the nonlinearity is no longer in balance with the frequency dispersion, which is the spirit of the original Boussinesq assumption.

To be able to use the depth-integrated equations to simulate the surf zone dynamics, energy dissipation due to wave breaking needs to be parameterized. For the Boussinesq-type equations the simple eddy viscosity model has been used as the turbulence closure model (Zelt 1991). Madsen et al. (1997) has also employed the "roller model" with empirical coefficients.

Denoting η as the dimensionless free surface displacement and $\vec{u}_\alpha$ as the dimensionless horizontal velocity components evaluated at $z = z_\alpha$, the governing equations in the dimensionless form can be expressed as (Liu 1994; Wei et al. 1995)

$$\frac{\partial \eta}{\partial t} + \nabla \cdot \vec{M} = 0 \tag{1}$$

$$\frac{\partial \vec{u}_\alpha}{\partial t} + \varepsilon \left(\vec{u}_\alpha \cdot \nabla\right) \vec{u}_\alpha + \nabla \eta + \mu^2 \vec{V}_1 + \varepsilon \mu^2 \vec{V}_2 = 0\left(\mu^4\right) \tag{2}$$

in which

$$\vec{M} = \vec{M}_1 + \vec{M}_2 \tag{3}$$

$$\vec{M}_1 = (h + \varepsilon\eta)\, \vec{u}_\alpha \tag{4}$$

$$\begin{aligned} \vec{M}_2 = \mu^2 (h + \varepsilon\eta) \Big\{ \Big[\frac{1}{2} z_\alpha^2 - \frac{1}{6} \left(h^2 - \varepsilon\eta h + (\varepsilon\eta)^2\right) \Big] \nabla \left(\nabla \cdot \vec{u}_\alpha\right) \\ + \Big[z_\alpha + \frac{1}{2}(h - \varepsilon\eta) \Big] \nabla \left(\nabla \cdot (h\vec{u}_\alpha)\right) \Big\} + 0\left(\mu^4\right) \end{aligned} \tag{5}$$

$$\begin{aligned} \vec{V}_1 = \frac{1}{2} z_\alpha^2 \nabla \left(\nabla \cdot \frac{\partial \vec{u}_\alpha}{\partial t}\right) + z_\alpha \nabla \left(\nabla \cdot \left(h \frac{\partial \vec{u}_\alpha}{\partial t}\right)\right) \\ - \nabla \left[\frac{1}{2} (\varepsilon\eta)^2 \nabla \cdot \left(\frac{\partial \vec{u}_\alpha}{\partial t}\right) + \varepsilon\eta \nabla \cdot \left(h \frac{\partial \vec{u}_\alpha}{\partial t}\right) \right] \end{aligned} \tag{6}$$

$$\vec{V}_2 = \nabla \Big[(z_\alpha - \varepsilon\eta) \left(\vec{u}_\alpha \cdot \nabla\right) \left(\nabla \cdot h\vec{u}_\alpha\right) + \frac{1}{2} \left(z_\alpha^2 - (\varepsilon\eta)^2\right) \left(\vec{u}_\alpha \cdot \nabla\right) \left(\nabla \cdot \vec{u}_\alpha\right)$$

$$+\frac{1}{2}\left(\nabla\cdot(h\vec{u}_\alpha)+\varepsilon\eta\,\nabla\cdot\vec{u}_\alpha\right)^2\Big] \tag{7}$$

In these non-dimensional equations two parameters have been defined

$$\varepsilon=\frac{a}{h_0} \tag{8}$$

$$\mu^2=(k_0h_0)^2 \tag{9}$$

where a is the characteristic scale of wave amplitude, h_0 the water depth and k_0 a reference wave number. The continuity equation (1) and the momentum equations (2) are obtained by assuming that $\varepsilon = 0(1)$ and $\mu^2 << 0(1)$. Therefore, these equations are suitable for modeling finite amplitude waves with weakly dispersive effects. By improving the linear dispersion characteristics of these equations with an appropriate choice of z_α value, these equations can be used in the intermediate depth (e.g., Nwogu 1993, Chen and Liu 1995). For instance, Chen and Liu (1995) suggested that the best value for z_α should be approximately -0.52 h (See figure 1 for the comparisons).

If the assumption that $0(\varepsilon)\simeq 0(\mu^2) << 1$ has been applied in (1) - (7), the governing equations reduce to the Boussinesq-type equations. We should point out that by including the higher order frequency dispersive effects and the nonlinear effects the third order spatial derivatives are introduced in the conservation of mass, $\nabla\cdot\vec{M}_2$, and the momentum equation, $\varepsilon\mu^2\vec{V}_2$, respectively. Special attention needs to be focused on the treatment of these third derivative terms in the development of numerical algorithms.

Once the horizontal velocity vector $\vec{u}_\alpha$ is obtained, the vertical profiles of velocity components can be expressed as

$$\vec{u}=\vec{u}_\alpha+\mu^2\left\{(\nabla z_\alpha-1)\,\nabla\cdot(h\vec{u}_\alpha)+(z_\alpha\nabla z_\alpha-z_\alpha)\,\nabla\cdot\vec{u}_\alpha\right.$$

$$\left.+(z_\alpha-z)\,\nabla\left[\nabla\cdot(h\vec{u}_\alpha)\right]+\frac{1}{2}\left(z_\alpha^2-z^2\right)\nabla\left(\nabla\cdot\vec{u}_\alpha\right)\right\}+0(\mu^4) \tag{10}$$

$$w=-\mu^2\left[\nabla\cdot(h\vec{u}_\alpha)+z\nabla\cdot\vec{u}_\alpha\right]+0(\mu^4) \tag{11}$$

in which w is the vertical velocity component.

2.1 One-dimensional Governing Equations

In this report, only the one-dimensional problem will be discussed in detail. The governing equations, (1) - (7), can be simplified for one-dimensional problems as:

$$\frac{\partial\eta}{\partial t}+\frac{\partial M}{\partial x}=0 \tag{12}$$

$$\frac{\partial u_\alpha}{\partial t} + \varepsilon u_\alpha \frac{\partial u_\alpha}{\partial x} + \frac{\partial \eta}{\partial x} + \mu^2 V_1 + \varepsilon \mu^2 V_2 = 0\left(\mu^4\right) \tag{13}$$

in which

$$M = M_1 + M_2 \tag{14}$$

$$M_1 = (h + \varepsilon\eta)\, u_\alpha \tag{15}$$

$$M_2 = \mu^2 (h + \varepsilon\eta) \left\{ \left[\frac{1}{2} z_\alpha^2 - \frac{1}{6}\left(h^2 - \varepsilon\eta h + (\varepsilon\eta)^2\right) \right] \frac{\partial^2 u_\alpha}{\partial x^2} + \left[z_\alpha + \frac{1}{2}(h - \varepsilon\eta) \right] \frac{\partial^2 h u_\alpha}{\partial x^2} \right\} + 0\left(\mu^4\right) \tag{16}$$

$$V_1 = \frac{1}{2} z_\alpha^2 \frac{\partial^3 u_\alpha}{\partial t \partial x^2} + z_\alpha \frac{\partial^2}{\partial x^2}\left(h \frac{\partial u_\alpha}{\partial t}\right) - \frac{\partial}{\partial x}\left[\frac{1}{2} (\varepsilon\eta)^2 \frac{\partial^2 u_\alpha}{\partial t \partial x} + \varepsilon\eta \frac{\partial}{\partial x}\left(h \frac{\partial u_\alpha}{\partial t}\right) \right] \tag{17}$$

$$V_2 = \frac{\partial}{\partial x}\left[(z_\alpha - \varepsilon\eta)\, u_\alpha \frac{\partial^2 h u_\alpha}{\partial x^2} + \frac{1}{2}\left(z_\alpha^2 - (\varepsilon\eta)^2\right) u_\alpha \frac{\partial^2 u_\alpha}{\partial x^2} + \frac{1}{2}\left(\frac{\partial h u_\alpha}{\partial x} + \varepsilon\eta \frac{\partial u_\alpha}{\partial x} \right)^2 \right] \tag{18}$$

We reiterate here that in the above equations $0(\varepsilon)$ has been treated as an order one quantity. Note that the third order x-derivative terms appear in both governing equations. If the assumption of $0(\varepsilon) \simeq 0(\mu^2) << 1$ is applied in (12) - (18), the governing equations are reduced to the modified Boussinesq equations as follows:

$$\frac{\partial \eta}{\partial t} + \frac{\partial M}{\partial x} = 0 \tag{19}$$

$$\frac{\partial u_\alpha}{\partial t} + \varepsilon u_\alpha \frac{\partial u_\alpha}{\partial x} + \frac{\partial \eta}{\partial x} + \mu^2 V_1 = 0\left(\mu^4\right) \tag{20}$$

in which

$$M = M_1 + M_2 \tag{21}$$

$$M_1 = (h + \varepsilon\eta)\, u_\alpha \tag{22}$$

$$M_2 = \mu^2 h \left\{ \left[\frac{1}{2} z_\alpha^2 - \frac{1}{6} h^2 \right] \frac{\partial^2 u_\alpha}{\partial x^2} + \left[z_\alpha + \frac{1}{2} h \right] \frac{\partial^2 h u_\alpha}{\partial x^2} \right\} + 0\left(\mu^4\right) \tag{23}$$

$$V_1 = \frac{1}{2} z_\alpha^2 \frac{\partial^3 u_\alpha}{\partial t \partial x^2} + z_\alpha \frac{\partial^2}{\partial x^2} \left(h \frac{\partial u_\alpha}{\partial t} \right) \tag{24}$$

Note that the third order x-derivative terms appear in the continuity equation, but not in the momentum equations. The conventional Boussinesq equations appear in several different forms. They can be expressed in terms of the velocity on the free surface, $z_\alpha = 0$, the velocity along the bottom, $z_\alpha = -h$, or the depth-averaged velocity, $\mathbf{u}$. Using the following substitutions:

$$u_\alpha = \mathbf{u}, \quad M_2 = 0 \tag{25}$$

$$V_1 = \frac{h^2}{6} \frac{\partial^3 \mathbf{u}}{\partial t \partial x^2} - \frac{h}{2} \frac{\partial^2}{\partial x^2} \left(h \frac{\partial \mathbf{u}}{\partial t} \right) \tag{26}$$

the corresponding continuity equation and momentum equation can be expressed by (19) and (20) in terms of the depth-averaged velocity. Note that the third order x-derivative terms disappear in the governing equation.

3 Numerical Schemes

The major effort of the proposed research is to develop an efficient and accurate finite element model to solve the governing equations (1) and (2) with a variable depth and an arbitrary harbor configuration. We shall discuss several possible numerical schemes for one-dimensional problems. Appropriate boundary conditions will be discussed in a later section.

The proper reasoning for the choice of time integration scheme and spatial approximation scheme will be investigated carefully and will be the main focus of attention for the present research.

3.1 Spatial Approximation Schemes

Two spatial discretization methods are examined. Although both methods are finite element schemes, they use different weighting functions and basis functions.

3.1.1 Bubnov-Galerkin finite element method

We shall present first the Bubnov-Galerkin method, which is commonly referred to as the Galerkin method (we shall adopt it henceforth). The Galerkin method uses the same family of functions as the basis functions and the weight functions. For simplicity, we discuss the method based on the case of constant depth. The governing equations reduce to (in dimensional form):

$$\frac{\partial \eta}{\partial t} + \frac{\partial}{\partial x}\left[(h+\eta)\, u_\alpha\right] + \kappa \frac{\partial^3 u_\alpha}{\partial x^3} = 0 \tag{27}$$

$$\frac{\partial u_\alpha}{\partial t} + g\frac{\partial \eta}{\partial x} + u_\alpha \frac{\partial u_\alpha}{\partial x} + \beta h^2 \frac{\partial^3 u_\alpha}{\partial t \partial x^2} = 0 \tag{28}$$

where

$$\beta = \frac{1}{2}\left(\frac{z_\alpha}{h}\right)^2 + \frac{z_\alpha}{h} \tag{29}$$

$$\kappa = \left(\beta + \frac{1}{3}\right) h^3 \tag{30}$$

$$0 \le x \le L \tag{31}$$

The weak forms of the above equations are

$$\int_0^L w\dot{\eta}\ dx \quad = \int_0^L \frac{\partial w}{\partial x}\left[(h+\eta)\, u_\alpha + \kappa \frac{\partial^2 u_\alpha}{\partial x^2}\right] dx - w\left[(h+\eta)\, u_\alpha + \kappa \frac{\partial^2 u_\alpha}{\partial x^2}\right]\Bigg|_0^L \tag{32}$$

$$\int_0^L \left(w + \beta h^2 \frac{\partial w}{\partial x} \frac{\partial^2}{\partial x^2} \right) \dot{u_\alpha} \, dx = \int_0^L \frac{\partial w}{\partial x} \left[g\eta + \frac{1}{2}(u_\alpha)^2 \right] \, dx - w \left[g\eta + \frac{1}{2}(u_\alpha)^2 \right] \Big|_0^L \tag{33}$$

For spatial approximation, the computational domain is subdivided into J elements of length $\Delta x_j = x_j - x_{j-1}$, $j = 1, 2, ..., J$. The unknown quantities are expressed in terms of the basis functions $(\phi_j(x))$ and the corresponding nodal values $\left(\{\eta\}_j^n, \{u_\alpha\}_j^n \right)$ as follows:

$$\eta(x, n\Delta t) \cong \sum_{j=0}^{J} \phi_j(x) \{\eta\}_j^n \tag{34}$$

$$u_\alpha(x, n\Delta t) \cong \sum_{j=0}^{J} \phi_j(x) \{u_\alpha\}_j^n \tag{35}$$

Since the Galerkin's method has the same basis function and weighting function, the substitutions of (34) and (35) and the weighting functions $(\phi_j(x), \quad j = 0, 1, ...J)$ into the weak formulations, (32) and (33), lead to the following matrix equations:

$$[M^\eta]_{ij} \{\dot{\eta}\}_j^n = \{f^\eta\}_j^n + \{q^\eta\}_j^n \qquad i = 0, 1, ..., J \tag{36}$$

$$[M^u]_{ij} \{\dot{u_\alpha}\}_j^n = \{f^u\}_j^n + \{q^u\}_j^n \qquad i = 0, 1, ..., J \tag{37}$$

$$[M^\eta]_{ij} = \sum_{j=0}^{J} \int_{\Delta x_j} \phi_i \, \phi_j \, dx \tag{38}$$

$$[M^u]_{ij} = \sum_{j=0}^{J} \int_{\Delta x_j} \left[\phi_i \, \phi_j + \beta h^2 \phi_i \left(\frac{d^2 \phi}{dx^2} \right)_j \right] \, dx \tag{39}$$

$$\{f^\eta\}_j^n = \sum_{j=0}^{J} \int_{\Delta x_j} \left(\frac{d\phi}{dx} \right)_i \left[h \phi_j \{u_\alpha\}_j^n + \sum_{k=0}^{J} \phi_j \, \phi_k \{\eta\}_j^n \{u_\alpha\}_k^n + \kappa \left(\frac{d^2 \phi}{dx^2} \right)_j \{u_\alpha\}_j^n \right] \, dx \tag{40}$$

$$\{f^u\}_j^n = \sum_{j=0}^{J} \int_{\Delta x_j} \left(\frac{d\phi}{dx} \right)_i \left[g \phi_j \{\eta\}_j^n + \frac{1}{2} \left(\phi_j \{u_\alpha\}_j^n \right)^2 \right] \, dx \tag{41}$$

$$\{q^\eta\}_j^n = - \sum_{j=0}^{J} \phi_i \left[h \, \phi_j \{u_\alpha\}_j^n + \sum_{k=0}^{J} \phi_j \, \phi_k \{\eta\}_j^n \{u_\alpha\}_k^n + \kappa \left(\frac{d^2 \phi}{dx^2} \right)_j \{u_\alpha\}_j^n \right] \Big|_{x_j}^{x_{j+1}} \tag{42}$$

$$\{q^u\}_j^n = -\sum_{j=0}^{J} \phi_i \left[g\,\phi_j \{\eta\}_j^n + \frac{1}{2}\left(\phi_j \{u_\alpha\}_j^n\right)^2 \right] \Big|_{x_j}^{x_{j+1}} \tag{43}$$

In the above equations the superscript n represents the time level based on a specified time increment, i.e., $t^n = n\Delta t$ and $t^{n+1} = (n+1)\Delta t$. For the interior elements the boundary terms $\{q^\eta\}_j^n$, $\{q^u\}_j^n$ are canceled out from the contributions from two adjacent elements. Only at the boundary points $j = 0$ and $j = J$ nonzero values exist for these boundary terms. The proper treatment of the boundary conditions will be discussed in a later section.

In the above matrix equations, the integrands of ($[M^u]_{ij}$ and $\{f^\eta\}_j^n$) contain second-order spatial derivatives. The usual linear or C^0-type element cannot be used. The basis functions should be continuous up to the first derivative throughout the computational domain (i.e., C^1-type element). Therefore, we have chosen the cubic B-splines as basis and weighting functions in this approach.

In our computational domain, $0 = x_0 < x_1 < x_2 \cdots < x_J = J$, the set of splines $\{\phi_0, \phi_1, ..., \phi_J\}$ form the basis functions and the weight functions. As shown in Figure 2, each cubic B-splines spans four elements; consequently each element $[x_{j-1}, x_j]$ is also covered by segments of four splines $\{\phi_{j-2}, \phi_{j-1}, \phi_j, \phi_{j+1}\}$ that are given in terms of a local coordinate system ξ by

$$\phi_{j-2} = \frac{1}{6\Delta x_j^3}(\Delta x_j - \xi)^3$$

$$\phi_{j-1} = \frac{1}{6\Delta x_j^3}\left\{\Delta x_j^3 + 3\Delta x_j^2(\Delta x_j - \xi) + 3\Delta x_j(\Delta x_j - \xi)^2 - 3(\Delta x_j - \xi)^3\right\}$$

$$\phi_j = \frac{1}{6\Delta x_j^3}\left\{\Delta x_j^3 + 3\Delta x_j^2\xi + 3\Delta x_j\xi^2 - 3\xi^3\right\}$$

$$\phi_{j+1} = \frac{1}{6\Delta x_j^3}\left\{\xi^3\right\} \tag{44}$$

where $\xi_j = x - x_{j-1}$ and $0 \le \xi_j \le \Delta x_j$.

3.1.2 Petrov-Galerkin finite element method

The Petrov-Galerkin method is another class of approximation methods in which the set of weighting functions is different from that of basis functions. The advantages of this method are that the computational effort is relatively less and that the treatment of the boundary conditions is more straightforward. To apply the Petrov-Galerkin method to the governing equations, we need to modify the weak forms as presented in (32) and (33). The modified weak forms can be expressed as:

$$\int_0^L w\dot{\eta}\ dx = \int_0^L \left[\frac{\partial w}{\partial x}\left\{(h+\eta)\,u_\alpha\right\} - \kappa\frac{\partial^2 w}{\partial x^2}\frac{\partial u_\alpha}{\partial x}\right] dx$$

$$-w\left[(h+\eta)\,u_\alpha + \kappa\frac{\partial^2 u_\alpha}{\partial x^2}\right]\Bigg|_0^L + \kappa\frac{\partial w}{\partial x}\left[\frac{\partial u_\alpha}{\partial x}\right]\Bigg|_0^L \tag{45}$$

$$\int_0^L \left(w - \beta h^2\frac{\partial w}{\partial x}\frac{\partial}{\partial x}\right)\dot{u_\alpha}\,dx = \int_0^L \frac{\partial w}{\partial x}\left[g\eta + \frac{1}{2}(u_\alpha)^2\right] dx$$

$$-w\left[g\eta + \frac{1}{2}(u_\alpha)^2 + \beta h^2\frac{\partial \dot{u_\alpha}}{\partial x}\right]\Bigg|_0^L \tag{46}$$

Noted that in (45) and (46), by trading second spatial derivatives to the weighting function, the dependent variables are now required to be differentiable only once. In other words, we can now choose the basis function for the dependent variable as piecewise linear with C^0 continuity and the weighting function as piecewise cubic with C^1 continuity.

Now the dependent variables are approximated in the form of a linear combination of the basis functions $(\psi_j(x))$, which is now different from the weighting functions $(\phi_j(x))$ and the corresponding nodal values $\left(\{\eta\}_j^n, \{u_\alpha\}_j^n\right)$ as follows:

$$\eta(x, n\Delta t) \cong \sum_{j=0}^{J} \psi_j(x)\{\eta\}_j^n \tag{47}$$

$$u_\alpha(x, n\Delta t) \cong \sum_{j=0}^{J} \psi_j(x)\{u_\alpha\}_j^n \tag{48}$$

By substituting these approximations and the weighting functions, (44), into the modified weak form, (45) and (46), we obtain the following matrix equations:

$$[M^\eta]_{ij}\,\{\dot{\eta}\}_j^n = \{f^\eta\}_j^n + \{q^\eta\}_j^n \qquad i = 0, 1, ..., J \tag{49}$$

$$[M^u]_{ij}\,\{\dot{u_\alpha}\}_j^n = \{f^u\}_j^n + \{q^u\}_j^n \qquad i = 0, 1, ..., J \tag{50}$$

where

$$[M^\eta]_{ij} = \sum_{j=0}^{J} \int_{\Delta x_j} \phi_i\,\psi_j\,dx \tag{51}$$

$$[M^u]_{ij} = \sum_{j=0}^{J} \int_{\Delta x_j} \left[\phi_i\,\psi_j - \beta h^2\left(\frac{d\phi}{dx}\right)_i\left(\frac{d\psi}{dx}\right)_j\right] dx \tag{52}$$

$$\{f^{\eta}\}_j^n = \sum_{j=0}^{J} \int_{\Delta x_j} \left[\left(\frac{d\phi}{dx}\right)_i \left(h\psi_j \{u_\alpha\}_j^n + \sum_{k=0}^{J} \psi_j \, \psi_k \{\eta\}_j^n \{u_\alpha\}_k^n \right) \right.$$
$$\left. -\kappa \left(\frac{d^2\phi}{dx^2}\right)_i \left(\frac{d\psi}{dx}\right)_j \{u_\alpha\}_j^n \right] dx \qquad (53)$$

$$\{f^{u}\}_j^n = \sum_{j=0}^{J} \int_{\Delta x_j} \left(\frac{d\phi}{dx}\right)_i \left[g\psi_j \{\eta\}_j^n + \frac{1}{2} \left(\psi_j \{u_\alpha\}_j^n\right)^2 \right] dx \qquad (54)$$

$$\{q^{\eta}\}_j^n = -\sum_{j=0}^{J} \left[\phi_i \left(h\,\psi_j \{u_\alpha\}_j^n + \sum_{k=0}^{J} \psi_j \, \psi_k \{\eta\}_j^n \{u_\alpha\}_k^n \right) \right.$$
$$\left. -\kappa \left(\frac{d\phi}{dx}\right)_i \left(\frac{d\psi}{dx}\right)_j \{u_\alpha\}_j^n \right] \Bigg|_{x_j}^{x_{j+1}} \qquad (55)$$

$$\{q^{u}\}_j^n = -\sum_{j=0}^{J} \phi_i \left[g\,\psi_j \{\eta\}_j^n + \frac{1}{2} \left(\psi_j \{u_\alpha\}_j^n\right)^2 + \beta\, h^2 \left(\frac{d\psi}{dx}\right)_j \{\dot{u_\alpha}\}_j^n \right] \Bigg|_{x_j}^{x_{j+1}} \qquad (56)$$

Once again, we reiterate that the second derivatives are only required for the weighting functions. In the following discussions, we have chosen the typical linear C^0-type basis function and the cubic B-spline C^1-type weighting functions. There are two immediate advantages by using this combination of basis and weighting functions. The first one is that we can reduce the computaional cost since the bandwidth of $[M^{\eta}]$ and $[M^{u}]$ is reduced. Although the bandwidth reduction is rather small for the one-dimensional problem (from 7, in the case of Galerkin method to 5), the similar reduction in bandwidth for two-dimensional problems will be significant. The second advantage for using the Petrov-Galerkin method is the ease in implementing the boundary conditions, since the nodal values are calculated directly.

3.2 Time Integration Scheme

3.2.1 An explicit Taylor-Galerkin finite element scheme

Katopodes and Wu (1987) developed an explicit scheme for solving conventional Boussinesq-type equations. The concept behind their scheme is to update the free surface displacement, η, and the velocity vector, u_α, by applying the Taylor's expansion over a small time step, Δt. Thus, in our previous one-dimensional case,

$$\{\eta\}_j^{n+1} = \{\eta\}_j^n + \Delta t \{\dot{\eta}\}_j^n + \frac{1}{2} (\Delta t)^2 \{\ddot{\eta}\}_j^n + 0(\Delta t)^3 \qquad (57)$$

$$\{u_\alpha\}_j^{n+1} = \{u_\alpha\}_j^n + \Delta t\{\dot{u}_\alpha\}_j^n + \frac{1}{2}(\Delta t)^2\{\ddot{u}_\alpha\}_j^n + 0(\Delta t)^3 \tag{58}$$

The first time derivatives, $\{\dot{\eta}\}_j^n$ and $\{\dot{u}_\alpha\}_j^n$ can be found from (36) and (37). The second time derivatives can be obtained by differentiating (27) and (28) with respect to time, i.e.

$$\frac{\partial^2\eta}{\partial t^2} = \frac{\partial}{\partial x}\left[h\dot{u}_\alpha + \dot{\eta}u_\alpha + \eta\dot{u}_\alpha\right] + \kappa\frac{\partial^3\dot{u}_\alpha}{\partial x^3} \tag{59}$$

$$\left(1 + \beta h^2\frac{\partial^2}{\partial x^2}\right)\frac{\partial^2 u_\alpha}{\partial t^2} = g\frac{\partial\dot{\eta}}{\partial x} + \frac{1}{2}\left(\frac{\partial\dot{u}_\alpha}{\partial x}\right)^2 \tag{60}$$

After applying the same Galerkin finite element formulation to this system of equations, we obtain

$$[M^\eta]_{ij}\{\ddot{\eta}\}_j^n = \{f^{\dot{\eta}}\}_j^n + \{\dot{q}^\eta\}_j^n \qquad i = 0, 1, ..., J \tag{61}$$

$$[M^u]_{ij}\{\ddot{u}_\alpha\}_j^n = \{f^{\dot{u}}\}_j^n + \{\dot{q}^u\}_j^n \qquad i = 0, 1, ..., J \tag{62}$$

where

$$\{f^{\dot{\eta}}\}_j^n = \sum_{j=0}^{J}\int_{\Delta x_j}\left(\frac{d\phi}{dx}\right)_i\left[h\phi_j\{\dot{u}_\alpha\}_j^n + \sum_{k=0}^{J}\phi_j\phi_k\{\dot{\eta}\}_j^n\{u_\alpha\}_k^n + \sum_{k=0}^{J}\phi_j\phi_k\{\eta\}_j^n\{\dot{u}_\alpha\}_k^n + \kappa\left(\frac{d^2\phi}{dx^2}\right)_j\{\dot{u}_\alpha\}_j^n\right]dx \tag{63}$$

$$\{f^{\dot{u}}\}_j^n = \sum_{j=1}^{J}\int_{\Delta x_j}\left(\frac{d\phi}{dx}\right)_i\left[g\phi_j\{\dot{\eta}\}_j^n + \frac{1}{2}\left(\phi_j\{\dot{u}_\alpha\}_j^n\right)^2\right]dx \tag{64}$$

Therefore we have four matrix equations (36), (37), (61), and (62) for four unknown vectors $\{\dot{\eta}\}_j^n, \{\ddot{\eta}\}_j^n, \{\dot{u}_\alpha\}_j^n$, and $\{\ddot{u}_\alpha\}_j^n$. Notice that mass matrices for equation (36) and (37) are the same as those of (61) and (62), respectively. After solving (36) and (37) for $\{\dot{\eta}\}_j^n$ and $\{\dot{u}_\alpha\}_j^n$, we can calculate $\{\ddot{\eta}\}_j^n, \{\ddot{u}_\alpha\}_j^n$ from equations (61) and (62) since the right hand side vectors are functions of known quantities $\{\dot{\eta}\}_j^n$ and $\{\dot{u}_\alpha\}_j^n$. From equation (57) and (58), solutions are marched to the next time level.

For the Boussinesq-type equations, $0(\varepsilon) = 0(\mu^2) << 1$, Katopodes and Wu (1987) have shown that the explicit scheme is conditionally stable, but its stability region is substantially larger than the typical discretization required for convergent solutions by most of implicit methods. By calculating two-dimensional solitary waves in a L-shaped channel with a constant depth, Katopodes and Wu stated that the explicit scheme is approximately four times faster than the implicit scheme of similar accuracy and requires only 50% of the real memory allocation.

3.2.2 An implicit Galerkin finite element scheme

In this section, we will describe an iterative time integration procedure, which is similar to the one developed by Lepelleteir (1980) (also, Lepelletier and Raichlen 1987). From equations (36) and (37), we can express the first order time derivative term by using the forward time difference:

$$[M^u]_{ij}\{\dot{u}_\alpha\}_j^n = [M^u]_{ij}\left(\frac{\{u_\alpha\}_{j(1)}^{n+1} - \{u_\alpha\}_j^n}{\Delta t}\right) = \{f^u(\eta^n, u^n)\}_j \tag{65}$$

where the value in the parenthesis in $\{u_\alpha\}_{j(1)}^{n+1}$ indicates that this is the first predictor value. The notation on the right hand side of the equation has been altered slightly, i.e., from $\{f^\eta\}_j^n$ to $\{f^u(\eta^n, u^n)\}_j$. The solution for $\{u_\alpha\}_{j(1)}^{n+1}$, can be written as:

$$\{u_\alpha\}_{j(1)}^{n+1} = \{u_\alpha\}_j^n + \Delta t\,[M^u]_{ij}^{-1}\{f^u(\eta^n, u^n)\}_j \tag{66}$$

A weighted solution between $\{u_\alpha\}_{j(1)}^{n+1}$ and $\{u_\alpha\}_j^n$ according to the weighting factor β_* can be expressed as:

$$\{u_\alpha\}_{j(1)}^{n+\beta_*} = \beta_*\{u_\alpha\}_{j(1)}^{n+1} + (1-\beta_*)\{u_\alpha\}_j^n \tag{67}$$

If 0.5 is used for β_*, it is called the Mid-point rule.

The solution for $\{\eta\}_{j(1)}^{n+1}$ can be obtained from equation (36)

$$[M^\eta]_{ij}\{\dot{\eta}\}_j^n = [M^\eta]_{ij}\left(\frac{\{\eta\}_{j(1)}^{n+1} - \{\eta\}_j^n}{\Delta t}\right) = \{f^\eta(\eta^n, \{u_\alpha\}_{j(1)}^{n+\beta_*})\}_j \tag{68}$$

Noted that $\{u_\alpha\}_{j(1)}^{n+\beta_*}$ has been used in the place of $\{u_\alpha\}_j^n$.

In the second and subsequent corrector step (k=2,3,...), the following procedures are followed until the error between two successive results reaches a required limit.

$$\{\eta\}_{j(k)}^{n+\beta_*} = \beta_*\{\eta\}_{j(k)}^{n+1} + (1-\beta_*)\{\eta\}_j^n \tag{69}$$

$$[M^u]_{ij}\left(\frac{\{u_\alpha\}_{j(k+1)}^{n+1} - \{u_\alpha\}_j^n}{\Delta t}\right) = \{f^u(\{\eta\}_{j(k)}^{n+\beta_*}, \{u_\alpha\}_{j(k)}^{n+\beta_*})\}_j \tag{70}$$

$$\{u_\alpha\}_{j(k+1)}^{n+\beta_*} = \beta_*\{u_\alpha\}_{j(k+1)}^{n+1} + (1-\beta_*)\{u_\alpha\}_j^n \tag{71}$$

$$[M^\eta]_{ij}\left(\frac{\{\eta\}_{j(k+1)}^{n+1} - \{\eta\}_j^n}{\Delta t}\right) = \{f^\eta(\{\eta\}_{j(k)}^{n+\beta_*}, \{u_\alpha\}_{j(k+1)}^{n+\beta_*})\}_j \tag{72}$$

for $k = 2, 3, 4....$ If the convergence requirement is satisfied, the solutions for the next time step are updated, i.e.,

$$\{\eta\}_j^{n+1} \Leftarrow \{\eta\}_{j(k+1)}^{n+1}$$

$$\{u_\alpha\}_j^{n+1} \Leftarrow \{u_\alpha\}_{j(k+1)}^{n+1} \tag{73}$$

3.3 Boundary Conditions

Appropriate boundary conditions are needed to obtain proper numerical solutions for wave propagation in a finite computational domain. Here, we shall discuss two kinds of boundary conditions, *i.e.*, an incident wave boundary condition and the perfect reflection boundary condition.

3.3.1 Incident wave boundary condition

At the incident wave boundary the time series of η and u are known. Since the nodal value at the boundary is known, it is regarded as an essential boundary condition. The following procedure is used to implement the boundary condition in the Petrov-Galerkin method with the implicit time integration scheme.

Suppose that the nodal values of η and u at node number m are given throughout the entire time history. As shown in the previous section, equation (65) is solved for $\{u_\alpha\}_{j(1)}^{n+1}$. Since $\{u_\alpha\}_{m(1)}^{n+1}$ is known, the matrices $[M^u]_{ij}$, and vector $\{f^u(\eta^n, u^n)\}_j$ should be modified. Specifically, the m-th row of $[M^u]$ are set to zero, except for the element $[M^u]_{mm}$ that is set equal to unity. The m-th row of the vector $\{f^u(\eta^n, u^n)\}_{j=m}$ is also replaced by the following known information:

$$\{f^u(\eta^n, u^n)\}_m = \left(\frac{\{u_\alpha\}_m^{n+1*} - \{u_\alpha\}_m^n}{\Delta t}\right) \tag{74}$$

where $\{u_\alpha\}_m^{n+1*}$ is the known value at next time step. The m-th row of the matrix equation, equation(65), becomes,

$$[0\ 0\ \cdots 1 \cdots 0\ 0]\left(\frac{\{u_\alpha\}_{m(1)}^{n+1} - \{u_\alpha\}_m^n}{\Delta t}\right) = \left(\frac{\{u_\alpha\}_m^{n+1*} - \{u_\alpha\}_m^n}{\Delta t}\right) \tag{75}$$

in which the '1' locates at m-th column. Consequently, the boundary condition for $\{u_\alpha\}_m$ has been applied. The same approach is applied to the equations for η and the subsequent iterative procedure.

Since the B-cubic spline function is used as weighting function that is distributed over four elements (5 node) (See figure 2), the j-th node solution depends on ϕ_{j-2} and ϕ_{j-1}. Therefore if the incident wave boundary is located at the left-hand side of the computational domain ($j = 0$), nodal values at points $j = 0$, 1 are both needed.

3.3.2 Reflective wall boundary

The horizontal velocity normal to a vertical, perfect reflecting wall is always zero. The normal gradient of surface elevations is also zero up to the leading order of the Boussinesq approximation. These conditions can be implemented by the method of image.

Suppose that the node at $j = J - 2$ is the wall boundary. Therefore, the following is true

$$\{u_\alpha\}_{J-2} = 0. \tag{76}$$

$$\{u_\alpha\}_{J-1} = -\{u_\alpha\}_{J-3} \tag{77}$$

$$\{u_\alpha\}_{J} = -\{u_\alpha\}_{J-4} \tag{78}$$

$$\{\eta\}_{J-1} = \{\eta\}_{J-3} \tag{79}$$

$$\{\eta\}_{J} = \{\eta\}_{J-4} \tag{80}$$

We can apply the essential boundary condition for $\{u_\alpha\}_{J-2}$, and the natural boundary condition for $\{\eta\}_{J-2}$. To satisfy the natural boundary condition for $\{\eta\}_{J-2}$, we treat two additional nodes $j = J - 1, J$ as essential boundary condition. We can solve for $\{\eta\}_{J-2}$.

The general procedure for dealing with the essential boundary condition is similar to the incident wave boundary condition discussed in the previous section except the fact that now the nodal value where the essential boundary is applied is not known *a priori*. They should be solved together with the prescribed condition.

If we apply the iterative (implicit) time integration scheme, the boundary conditions indicated above can be dealt with in such a way that (after modifying the matrix for the corresponding row)

$$\begin{aligned}[M^u]_{J-2\ j}\left(\frac{\{u_\alpha\}^{n+1}_{J-2(k+1)} - \{u_\alpha\}^n_{J-2}}{\Delta t}\right) &= \{f^u(\eta^n, u^n)\}_{J-2} \\ &= \left(\frac{0 - \{u_\alpha\}^n_{J-2}}{\Delta t}\right)\end{aligned} \tag{81}$$

$$\begin{aligned}[M^u]_{J-1\ j}\left(\frac{\{u_\alpha\}^{n+1}_{J-1(k+1)} - \{u_\alpha\}^n_{J-1}}{\Delta t}\right) &= \{f^u(\eta^n, u^n)\}_{J-1} \\ &= \left(\frac{-\{u_\alpha\}^{n+1}_{J-3(k)} - \{u_\alpha\}^n_{J-1}}{\Delta t}\right)\end{aligned} \tag{82}$$

$$[M^u]_{J\ j}\left(\frac{\{u_\alpha\}^{n+1}_{J(k+1)}-\{u_\alpha\}^n_J}{\Delta t}\right) = \{f^u(\eta^n,u^n)\}_J$$
$$= \left(\frac{-\{u_\alpha\}^{n+1}_{J-4(k)}-\{u_\alpha\}^n_J}{\Delta t}\right) \qquad (83)$$

$$[M^\eta]_{J-1\ j}\left(\frac{\{\eta\}^{n+1}_{J-1(k+1)}-\{\eta\}^n_{J-1}}{\Delta t}\right) = \{f^\eta(\eta^n,u^n)\}_{J-1}$$
$$= \left(\frac{\{\eta\}^{n+1}_{J-3(k)}-\{\eta\}^n_{J-1}}{\Delta t}\right) \qquad (84)$$

$$[M^\eta]_{J\ j}\left(\frac{\{\eta\}^{n+1}_{J(k+1)}-\{\eta\}^n_J}{\Delta t}\right) = \{f^\eta(\eta^n,u^n)\}_J$$
$$= \left(\frac{\{\eta\}^{n+1}_{J-4(k)}-\{\eta\}^n_J}{\Delta t}\right) \qquad (85)$$

where equations from (81) to (85) represent the conditions described in equations from (76) to (80), respectively.

4 Numerical Results

4.1 Solitary wave propagation over constant depth

The solitary wave propagation in a constant depth over a long distance was tested to examine the stability and conservative property of the numerical schemes. To focus on the stability characteristics of different time integration scheme, the Galerkin method with linear elements for the conventional Boussinesq equations was used for this portion of the investigation. Furthermore, to avoid the potential complication caused by the boundary conditions, the surface profile and the velocity field for solitary wave are used as the initial conditions. The computational domain is large enough so that both the free surface profile and the velocity vanish at the boundary vanish. Figure 3 shows the snap shots of a solitary wave with amplitude 0.1 m over constant depth of 1 m. The wavelength (λ) is estimated as 13.5 m and the corresponding wave period (T) is 4.3 sec. $\Delta x = 0.15$ m, $\Delta t = 0.02$ sec are used so that $\lambda/\Delta x = 90$ and $T/\Delta t = 215$. Because Δx and Δt are small, the numerical results from different time integration scheme are almost identical to the exact solution, which is also plotted in figure 3. By changing the number of grids per wavelength and the number of time steps per wave period, the stability and accuracy of different time integration scheme is also investigated The numerical stability area in which the convergent solution can be obtained is shown in figure 4. The stability area of the explicit time integration scheme is smaller than that of the iterative time integration scheme, indicating that the explicit scheme is more sensitive than implicit (iterative scheme) especially when the T/dt is less than 50. During the soliton fission process in which the original soliton is split into several smaller solitons (we will discuss in section 4.3 in more detail), the calculated maximum wave height from the explicit time integration scheme shows continuous growth as shown in figure 5. Therefore, the iterative implicit time integration scheme is employed for the rest of the study.

If the initial wave amplitude of the solitary wave is increased to 0.7 m ($\epsilon = 0.7$), a small oscillatory tail develops behind the main wave and the wave height decreases by 10 % at the beginning of the computation (figure 6). The numerical results were obtained by using the extended Boussinesq equation model with $T/dt = 50$ and $\lambda/\Delta x = 40$. The oscillatory tails appears because the analytical solution for solitary wave is no longer valid for such a large wave. The numerical model adjusts the mismatch between the initial conditions and the model and finally produces a numerical permanent-form solitary wave solution after propagating a long distance. This numerical solitary wave solution is compared with that of different numerical models with different governing equations (Figure 7). These models include the boundary element method (BEM) of fully nonlinear potential flow by Grilli *et al.* (1994), the finite difference method (FDM) of extended Boussinesq equations by Nwogu (1993), and the finite difference method of fully nonlinear Boussinesq

equations by Wei et al. (1995). The numerical results of the Galerkin finite element model (FEM) and Petrov-Galerkin FEM are also plotted. The calculated results from other numerical models are obtained by digitizing the plots presented in Wei's et al. paper. The results shows current finite element solutions are very close to those of other numerical models.

4.2 Solitary wave shoaling on slopes

Numerical results for the shoaling of a non-breaking solitary wave are also obtained using both Galerkin and Petrov-Galerkin methods. The wave height, ϵ, of the initial solitary wave is 0.2 and the beach slope is 1:35 (water depth at $x/ho = 10$ is 0.71 m and at $x/ho = 28$ is 0.2 m). In numerical computations, $T/dt = 100$ and $\lambda/\Delta x = 80$ are used. As shown in Figure 8, the present numerical solutions agree well with those of other models in terms of wave asymmetry and the shoaling factor. The snapshots of wave profiles at different time are plotted in Figure 9, 10 and 11, respectively. The dimensionless time has been scaled by $(gh_o)^{1/2}$. The numerical results of Galkerin and Petrov-Galerkin method are almost the same, even when the wave is near the theoretical breaking point (Figure 11). The Galerkin and Petrov-Galerkin results are lower than those of Nwogu's FDM, but higher than those predicted by the fully nonlinear models (Griili *et al.*'s BEM, Wei, et al.'s FDM)

4.3 Fission of solitary wave

It has been found theoretically and experimentally that a solitary wave traveling from one constant depth to another smaller constant depth disintegrates into several solitary waves of varying sizes, which is called fission. Figure 12 shows the evolution of a solitary wave propagating over a slope onto a smaller depth. The numerical results are calculated from the extended Boussinesq equations model using $T/dt = 50$ and $\lambda/\Delta x = 50$. The ϵ of the incoming wave at $x/h = 0$ is 0.12 and the varying depth exists from $x/h = 10$ to $x/h = 15$ with the slope of $1 : 20$. The fission process is well demonstrated. In Figure 13, the numerical results of the current models (Galerkin and Petrov-Galerkin) are compared to those of Navier-stokes equations model (Lin and Liu 1998). The agreement among the numerical results is excellent. The numerical solutions of the Galerkin and Petrov-Galerkin method are almost identical, indicating that the accuracy of the Petrov-Galerkin method is similar to that of the Galerkin method.

4.4 Propagation of deep water wave

A numerical experiment is performed to evaluate the ability of the current model to simulate the propagation of regular waves in deep water. The wavelength of 3 m

and the constant water depth of 1 m are used in the experiment so that $\mu^2 = 4.3$. For this simulation, $T/dt = 80$ and $\lambda/\Delta x = 50$ are chosen. First, the conventional Boussinesq equation model is tested (Figure 14). The vertical dotted line indicates the location of a wave crest at different time according to the exact phase speed calculated from the linear dispersion relationship. The numerically generated wave propagates slower than the theoretical one. On the other hand, the phase speed of extended Boussinesq equation model agrees very well the exact phase speed as shown in Figure 15.

4.5 Wave-wave interaction

By simulating two solitary waves propagating in the opposite directions, the capability of the numerical model in dealing with nonlinear wave-wave interactions can be tested. Two identical solitary waves with $\epsilon = 0.6$ are introduced in a constant water depth (see Figure 16). In the computations, $T/dt = 100$ and $\lambda/\Delta x = 70$ are used. Due to the inadequacy of the analytic solutions to describe the large solitary wave, small oscillatory tails are generated initially. After these tails are separated from the numerically generated solitary wave, the process of collision of two solitary waves is well represented in Figure 16.

The time history of free surface elevation and velocity at the middle of the wave tank is presented in Figure 17(a) and (b). The maximum elevation over depth at the center is more than 1.2, which is the linear superposition of two colliding solitary waves. In Figure 17(c), the total mass, kinetic energy, potential energy and total energy are shown. All these values are normalized by their own value at $t = 0$. When two solitary waves collide together the kinetic energy in the system is zero, while the potential energy reaches its maximum value (When the maximum elevation occurs.). The total energy that is the sum of the kinetic and potential energy should be unchanged. This property and the conservation of mass over the whole computational time are well presented.

4.6 Applications of the incident wave boundary condition

The incident wave boundary is applied to the left-hand side and the perfect reflecting wall boundary condition is set to the right-hand side of the computational domain. First, a solitary wave of amplitude 0.1 m over the constant water depth of 1 m is generated through the boundary. In the computations $T/dt = 100$ and $\lambda/\Delta x = 70$ are used (Figure 18). The numerical results show that the incident wave boundary and reflective wall boundary works well for solitary wave of $\epsilon = 0.1$. To test the suitability of the incident wave boundary for waves in intermediate water depth, the sinusoidal wave of $kh = 1.25, ka = 0.01$ is generated (Figure 19). The conventional Boussinesq equation model cannot properly simulate this type of waves. The modified Boussinesq equation model predicts the general features of

incident and reflected waves reasonably well. However, small element-size oscillations are generated near the incident wave boundary. These oscillations persist in the whole computation period.

In Figure 20, with the intermediate water wave of $kh = 1.25$ a steeper wave slope than the previous case ($ka = 0.1$) is used for the incident wave boundary. The element-size wiggles also appear in this case.

4.7 Simulations of reflective wall boundary

To check further the accuracy of the reflected wall boundary condition, a solitary wave is set free to propagate between two perfectly reflecting walls. Since the reflection of solitary wave of $\epsilon = 0.1$ has been shown in Figure 18, the reflection of a solitary wave of $\epsilon = 0.6$ is shown in this section (Figure 21). The general characteristics of this large amplitude solitary wave reflected from both ends wall are calculated reasonably well.

If the numerical algorithm and the reflective wall boundary condition has been perfect, the wave shape, the mass and total energy should be conserved. To verify these properties, the time history of the free surface elevation and velocity at the center of the tank ($x = 0$), the total mass and the total energy of the computational domain are plotted in Figure 22. The computations were performed up to 40 wave periods, during which time the wave has moved forward and backward seven times. The computational domain is shown in Figure 21 and $\lambda/\Delta x = 70$, $T/dt = 100$ are used here. As shown in Figure 22(a) and (b), the maximum amplitude and velocity at different period remain almost constant over the whole computational period. Small fluctuations are generated from the initial condition for a large solitary wave. Figure 22(c) shows the conservation property of mass and energy. Once again all properties are normalized by their own initial values. The total mass is conserved over whole period. However the total energy is not conserved perfectly when the wave hits the wall. One possible contributing factor to the inaccuracy is that the reflective boundary condition is accurate up to the leading order of Boussinesq approximation.

Figure 23(a) and (b) shows the results of the case where the initial solitary wave has a smaller amplitude, $\epsilon = 0.1$. The maximum amplitude and velocity at different period show no fluctuations. However, similar pattern of the inaccuracy in the total energy as the wave is reflected from the wall is also shown in Figure 23(c).

5 Concluding Remarks

In this report we have reviewed the state-of-arts numerical models for calculating harbor oscillation. It is recommended that in order to investigate the nonlinear, transient wave motions in a harbor, a new set of governing equations should be used. These equations can describe wave propagation in both intermediate and shallow water. The nonlinearity can also be added, if it is necessary. In anticipation of encountering complex geometry in modeling a realistic harbor, the finite element approach is suggested.

To investigate various time integration and spatial integration schemes, one-dimensional problems are examined in this report. Using several well-known physical examples as benchmark cases, the following conclusions can be made:

1. The implicit iterative scheme should be used since its range of stability is much larger than that of the explicit scheme. 2. Although the Galerkin scheme and the Petrov-Galerkin scheme give similarly accurate solutions, the Petrov-Galerkin method is recommended for the future development for two-dimensional problem, since the Petrov-Galerkin scheme is more economical and is also easier to treat the boundary condition. 3. Only the incident wave boundary condition and the reflection boundary condition have been implemented at this point. Future study will extend these conditions to include the dissipative effects.

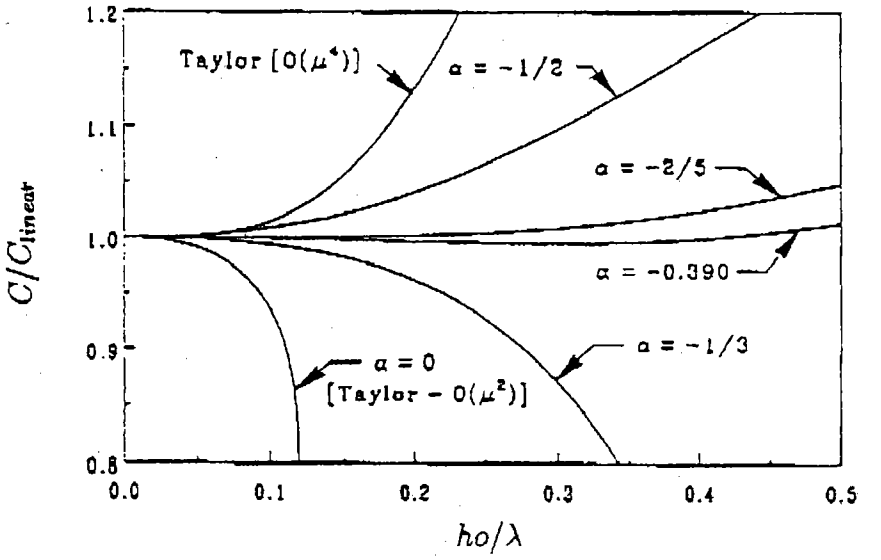

(a) Phase speeds

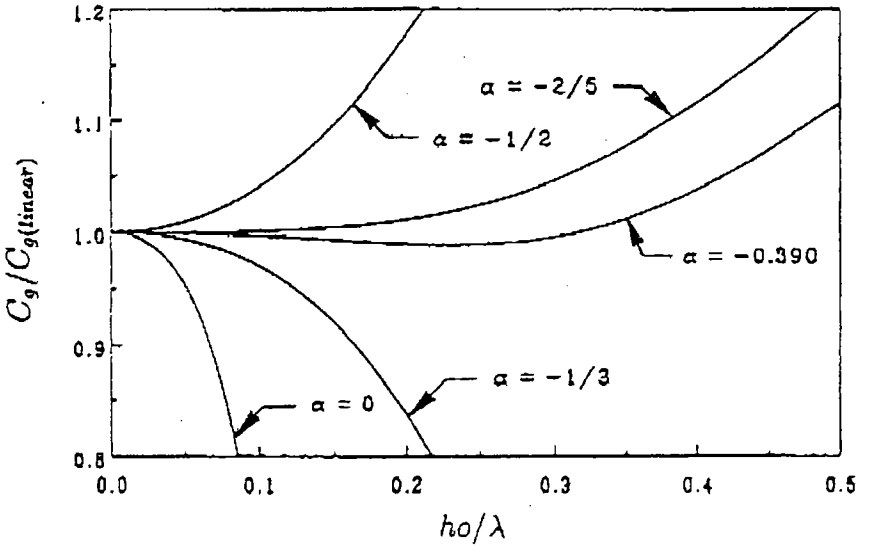

(b) Group velocities

Figure 1: Comparison of normalized phase speeds and group velocities for different values of α

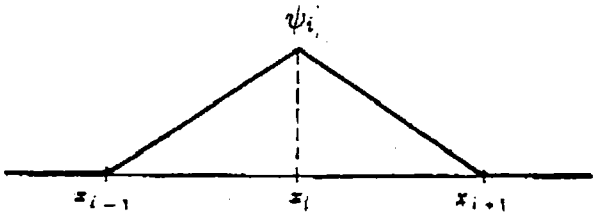

(a) Linear basis function for node i

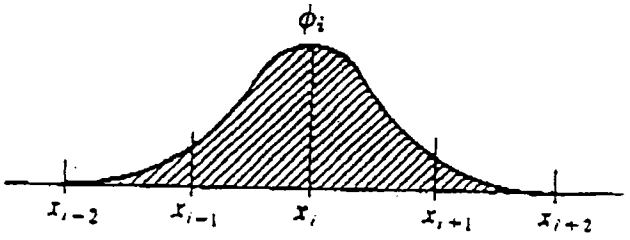

(b) B-cubic spline weighting function for node i

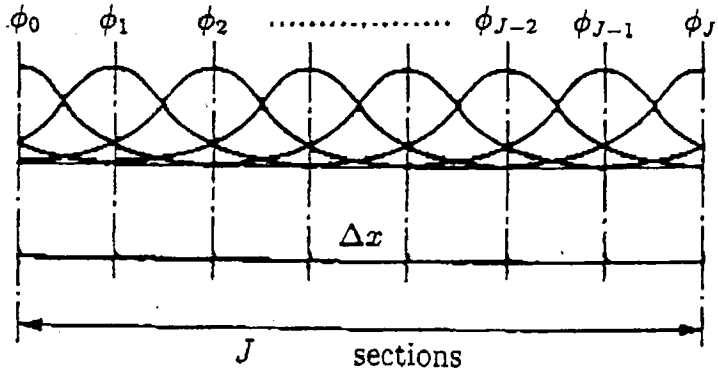

(c) Global expression for B-cubic spline weighting function

Figure 2: Linear basis function and B-cubic spline weight function.

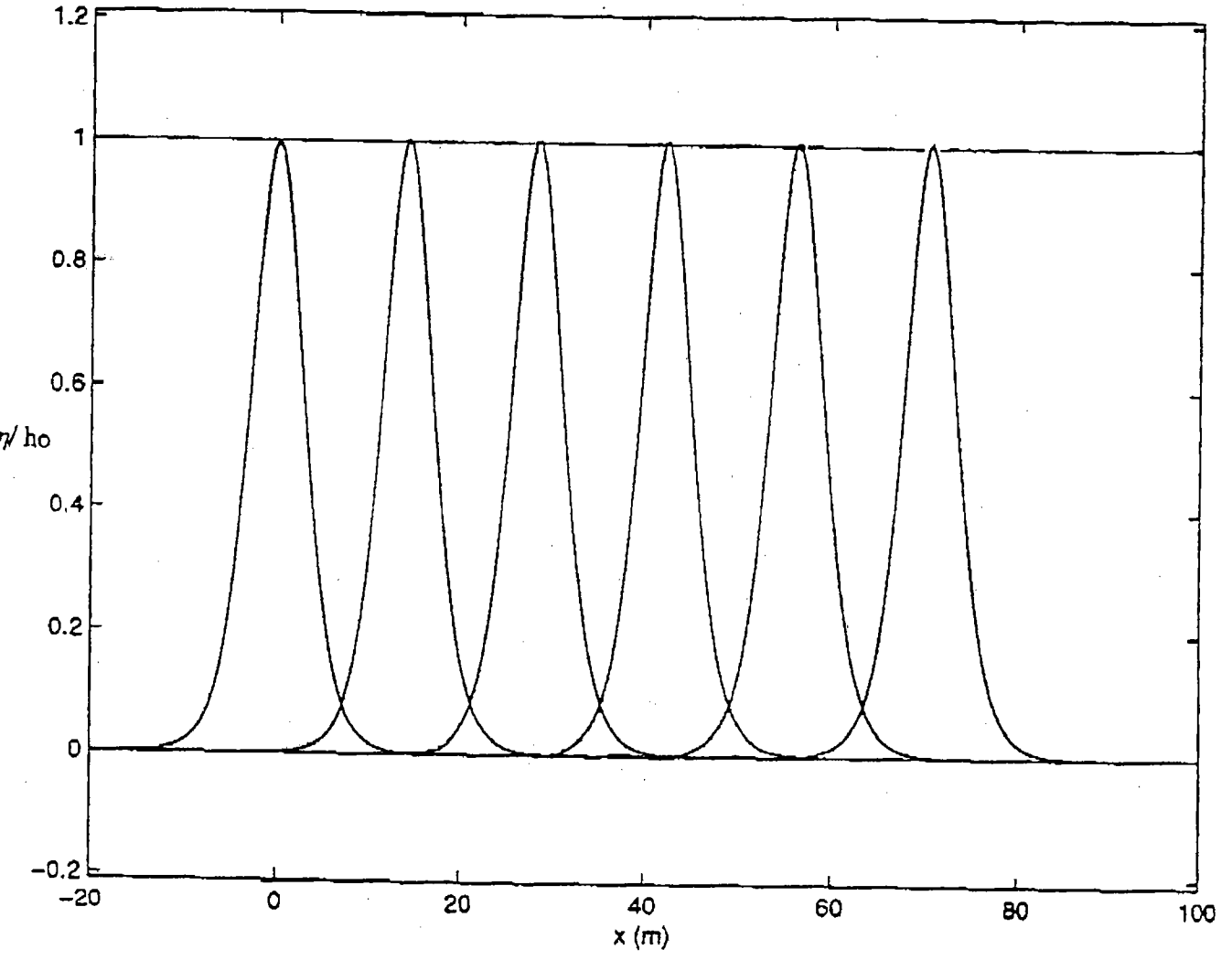

Figure 3: Solitary wave propagation over constant depth ($\epsilon = 0.1$)

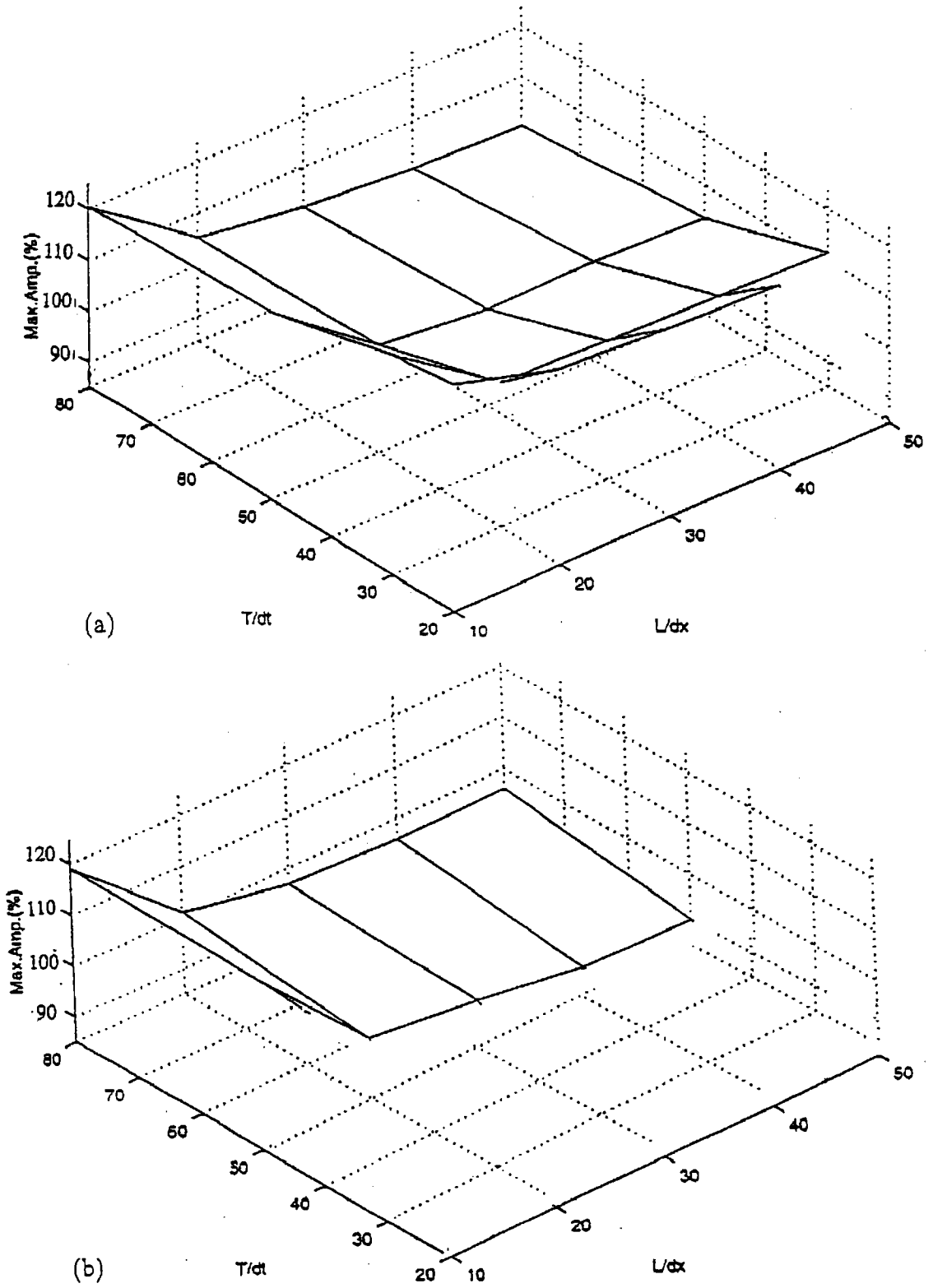

Figure 4: The area of stability of different time integration scheme. (a)Iterative, (b)Explicit

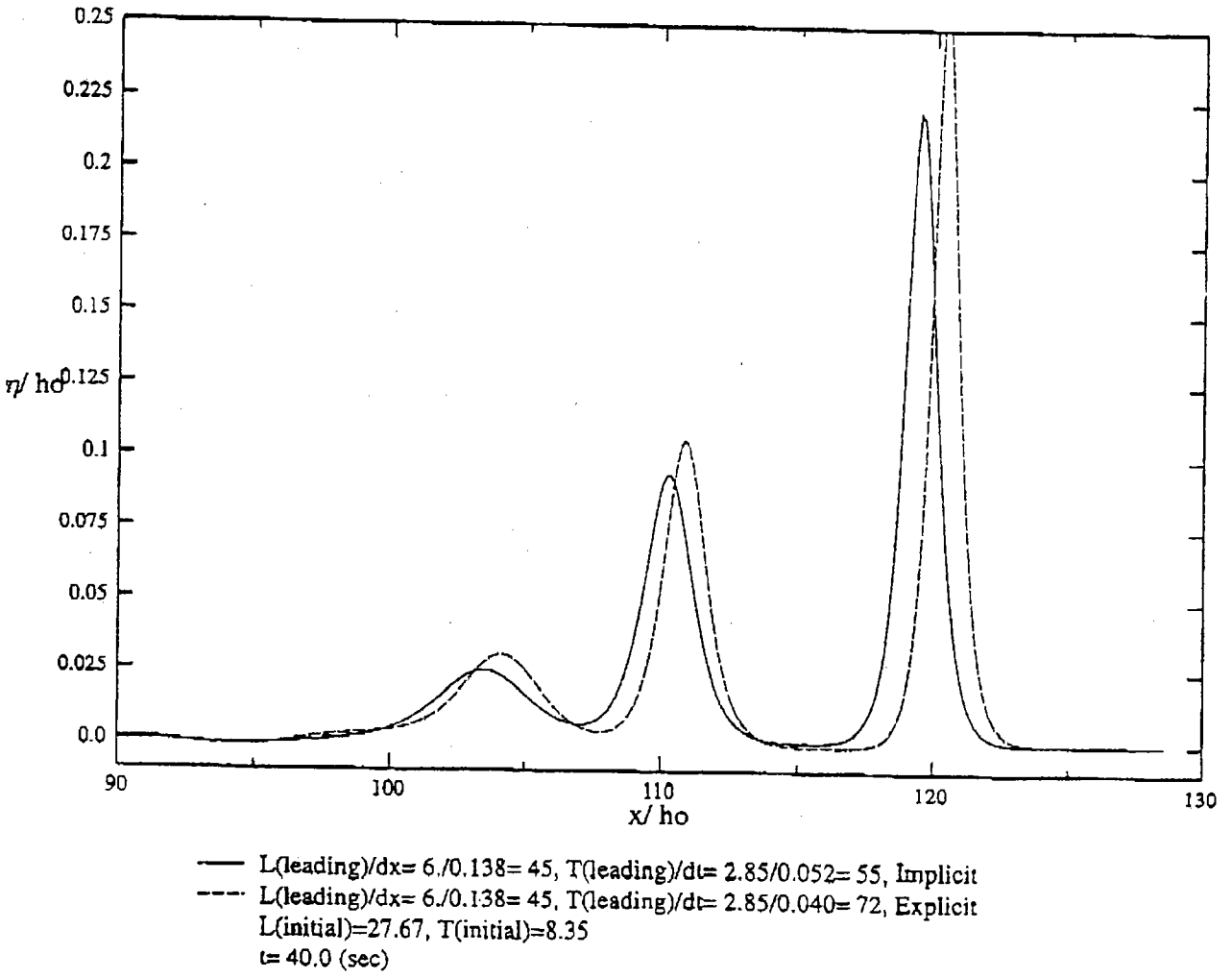

Figure 5: Snapshot of numerical free surface elevation using different time integration scheme. ————(a)Iterative, - - - - -(b)Explicit

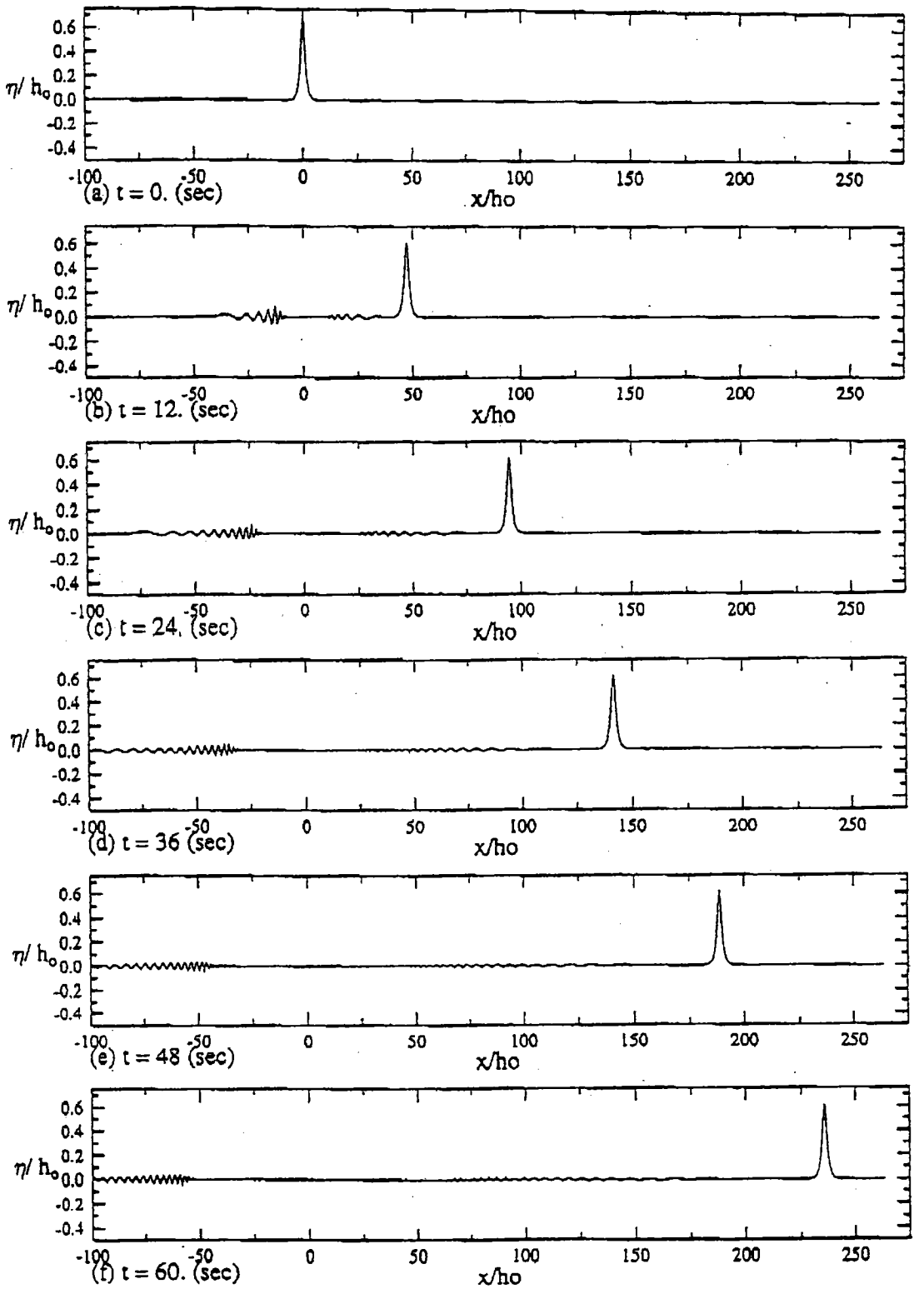

Figure 6: Solitary wave propagation over constant depth ($\epsilon = 0.7$)

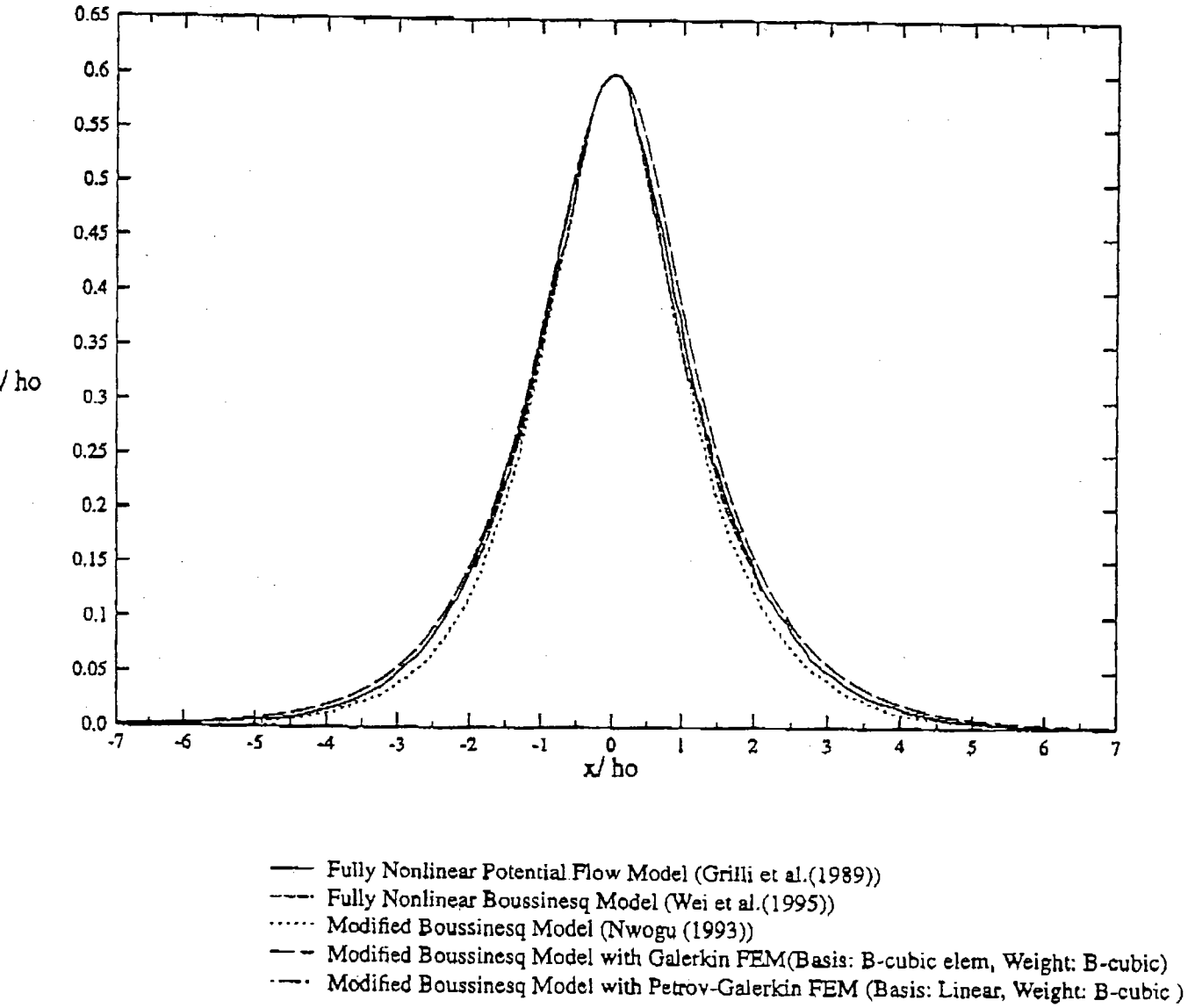

Figure 7: Comparison of different numerical solution for solitary wave shape for $\epsilon = 0.7$

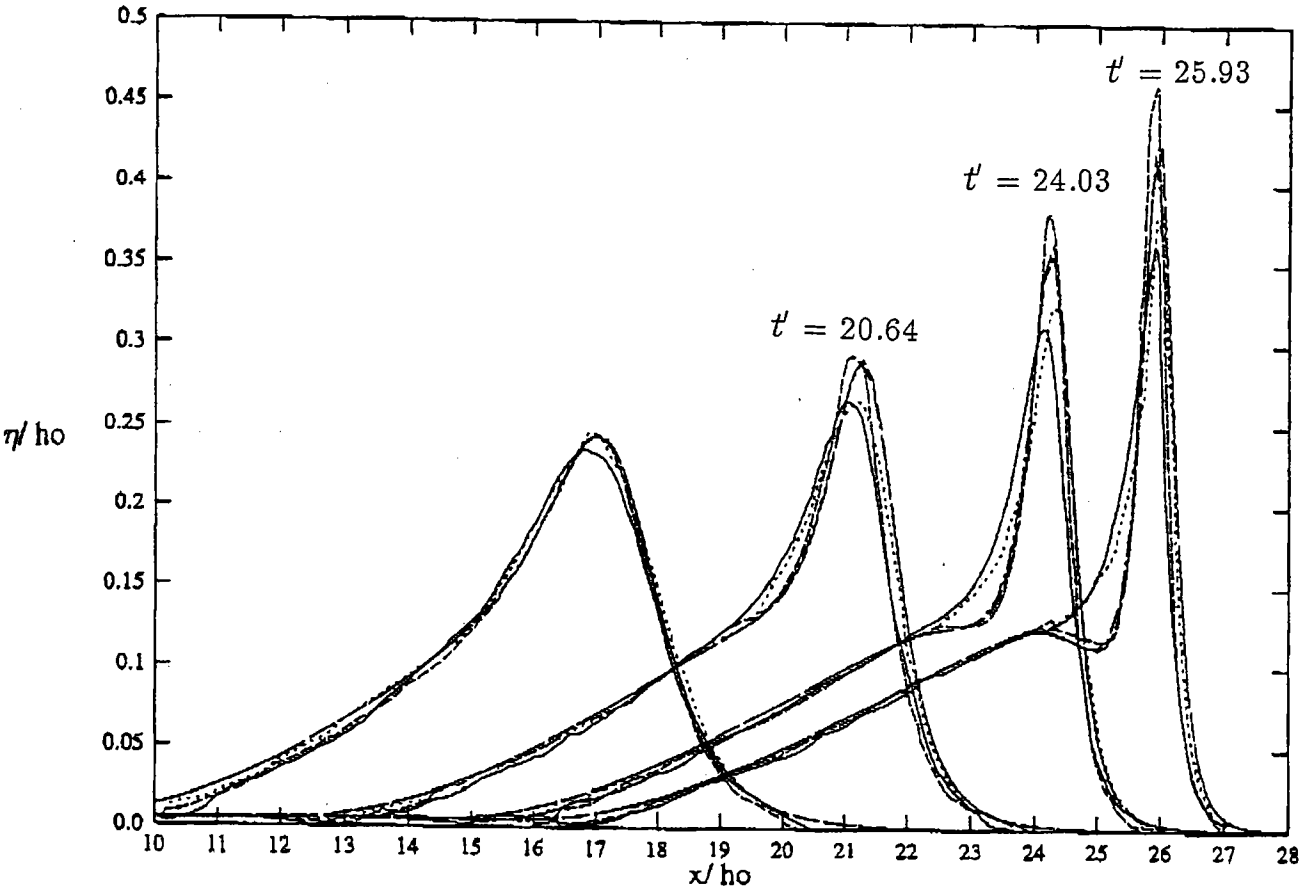

Figure 8: Comparison of spatial profile of solitary wave shoaling on slope 1:35 with $\epsilon = 0.2$ at different time step.

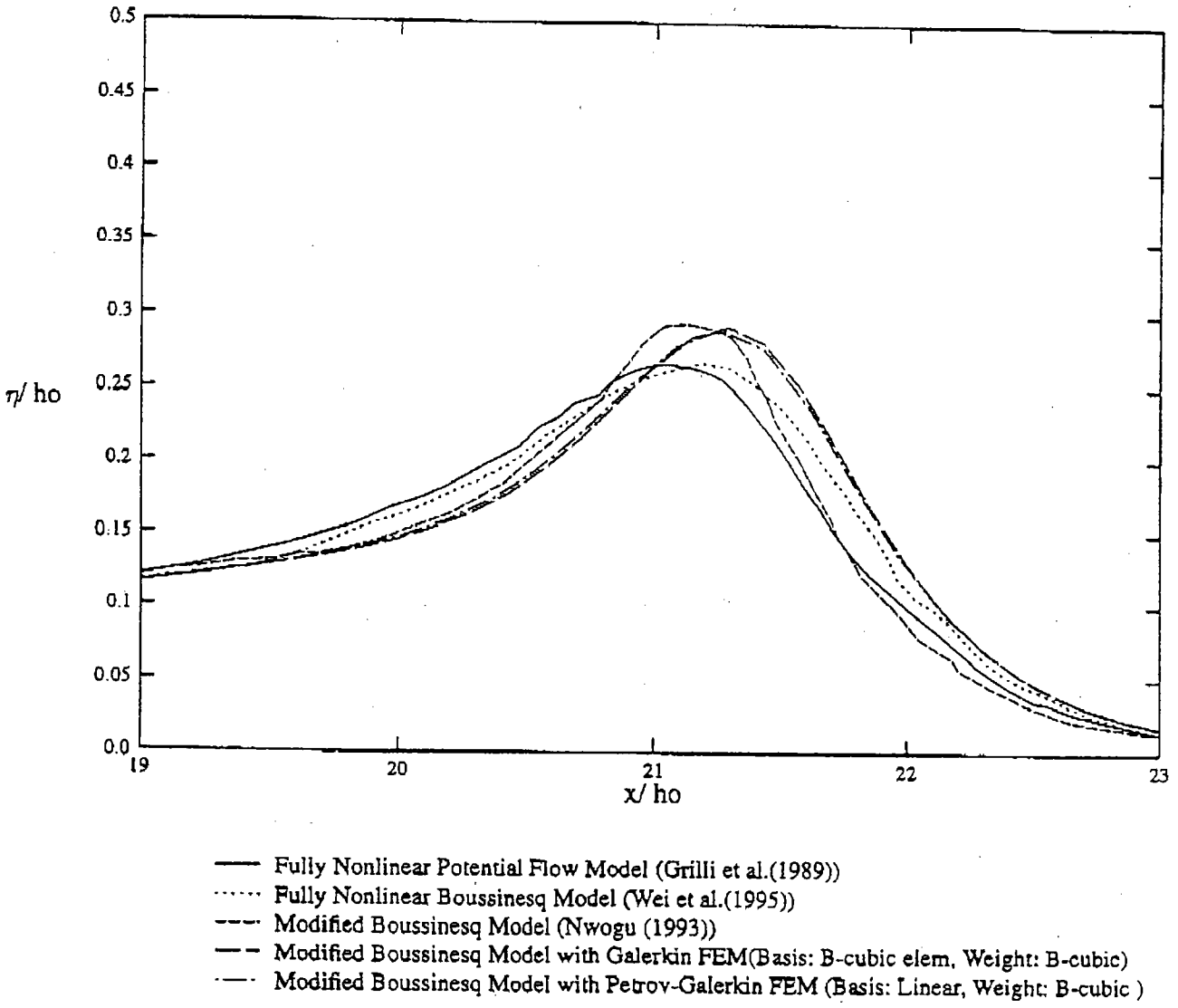

Figure 9: Comparison of spatial profile of solitary wave shoaling on slope 1:35 with $\epsilon = 0.2$ at $t' = 20.64$.

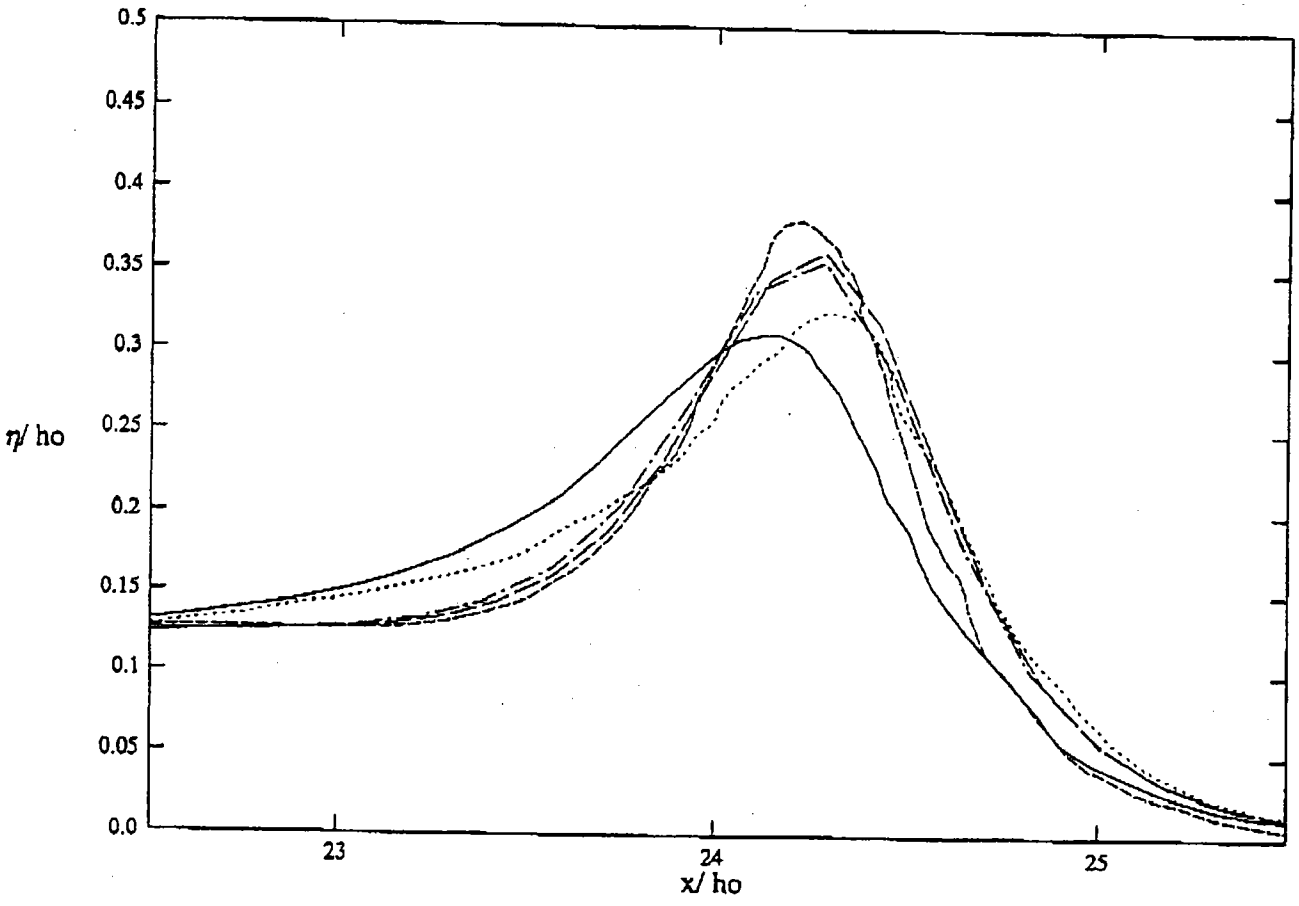

Figure 10: Comparison of spatial profile of solitary wave shoaling on slope 1:35 with $\epsilon = 0.2$ at $t' = 24.03$.

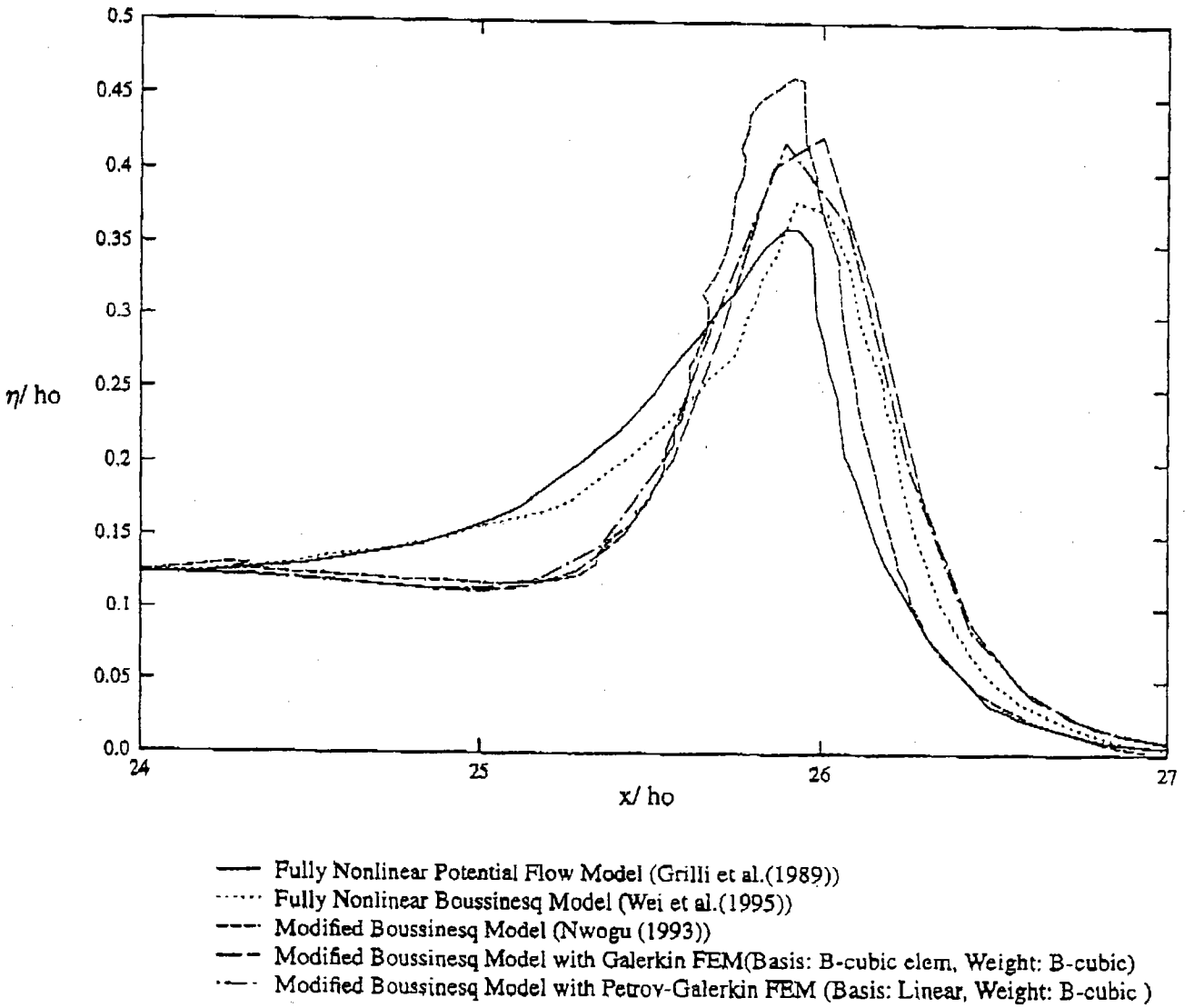

Figure 11: Comparison of spatial profile of solitary wave shoaling on slope 1:35 with $\epsilon = 0.2$ at $t' = 25.93$.

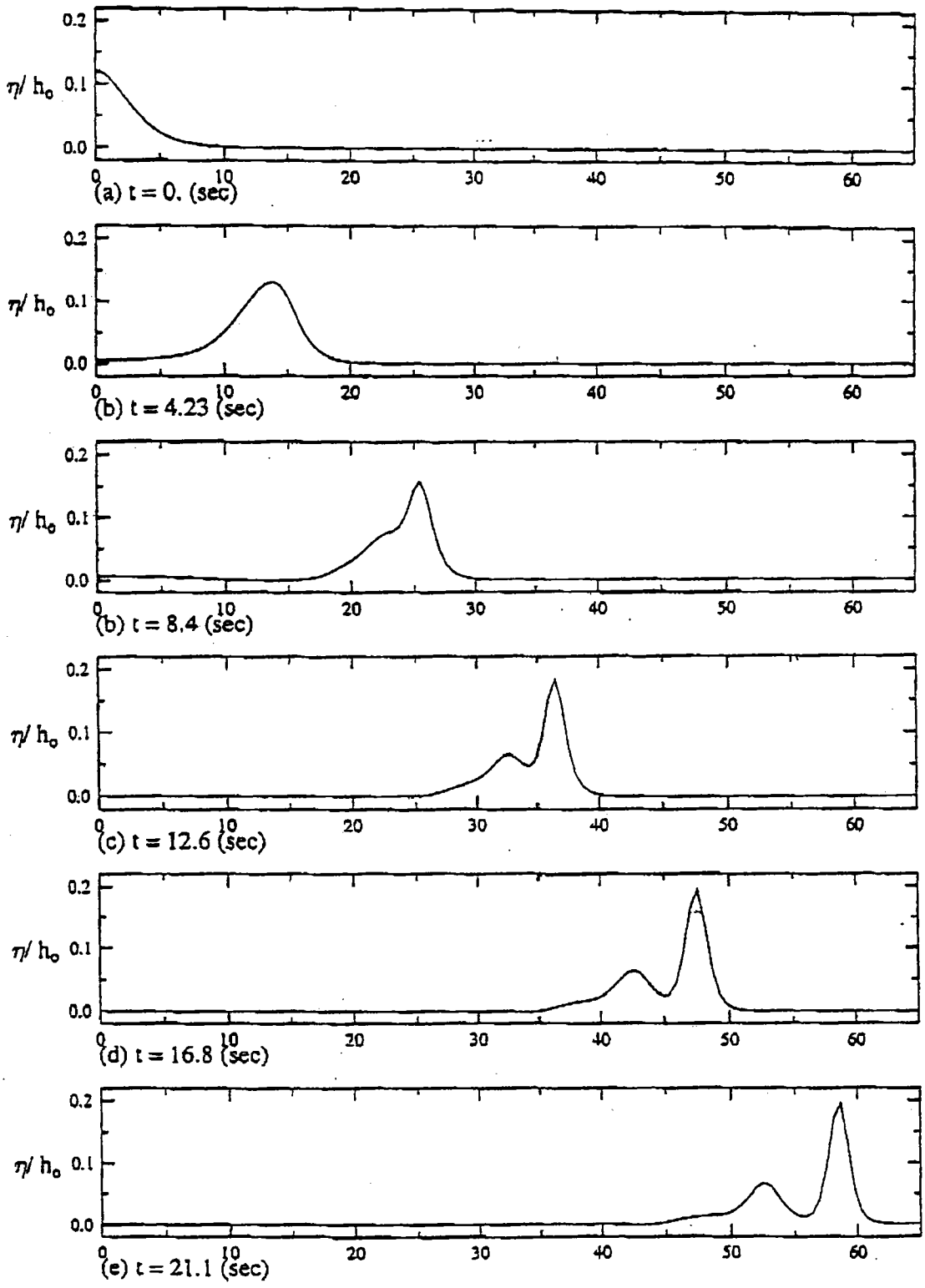

Figure 12: Fission of a solitary wave propagating over a slope 1:20 onto a smaller depth.

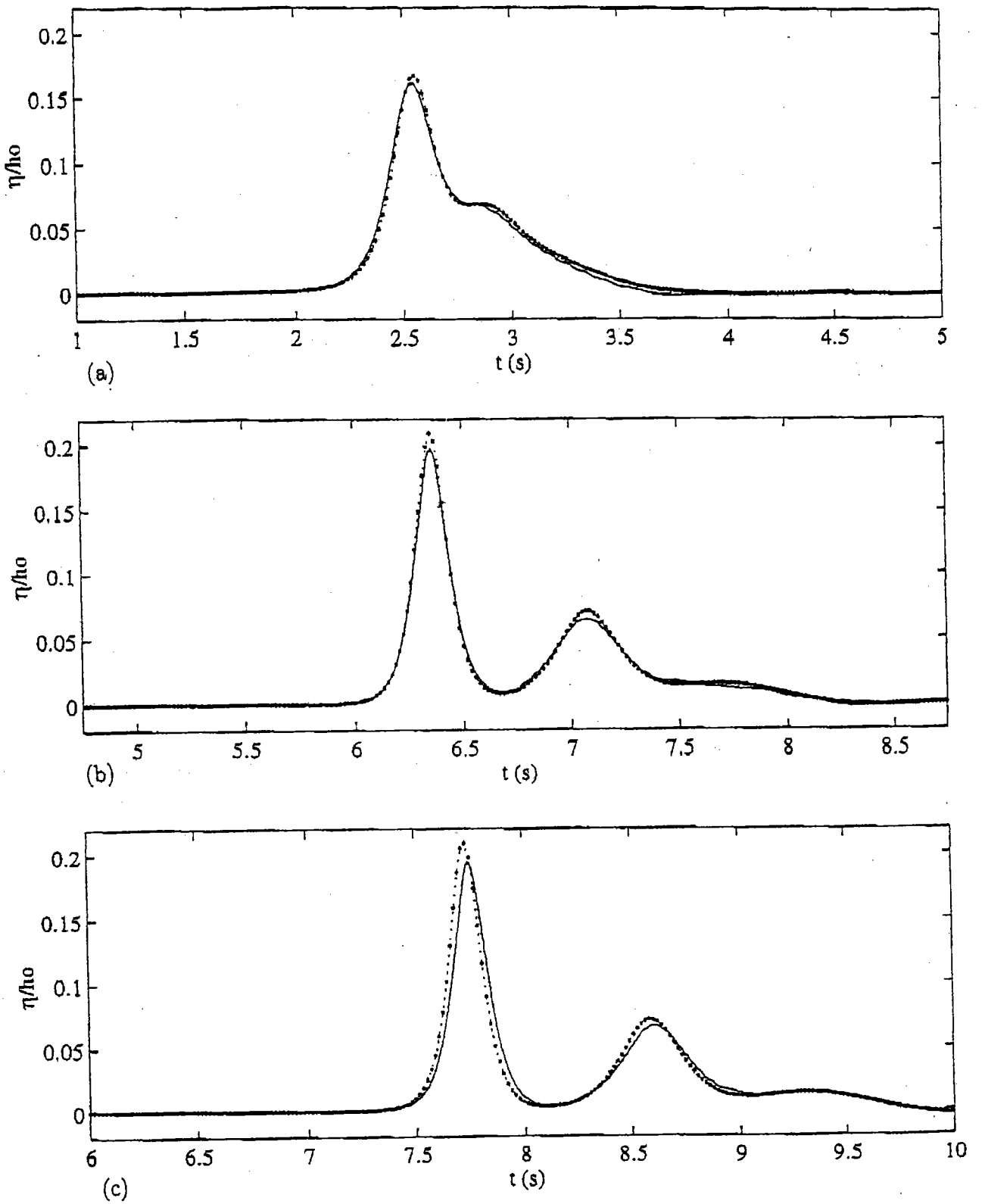

Figure 13: Comparison of time history of free surface at $x/h = 27, 57$ and 70. - - - - - Petrov-Galerkin, ... Galerkin, —— Lin and Liu (1998)

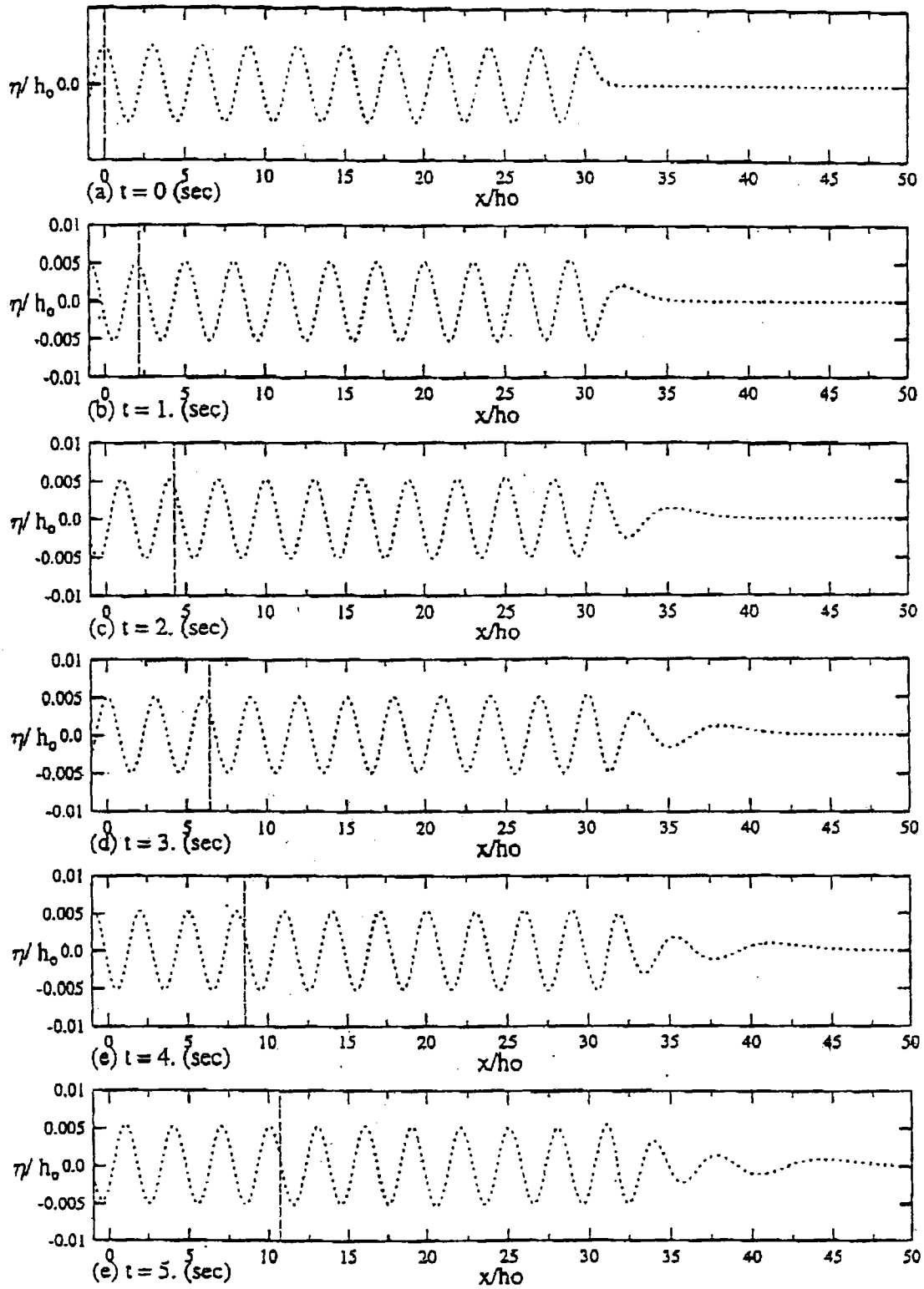

Figure 14: Numerical solution of the conventional Boussinesq equations model for the propagation of deep water wave.

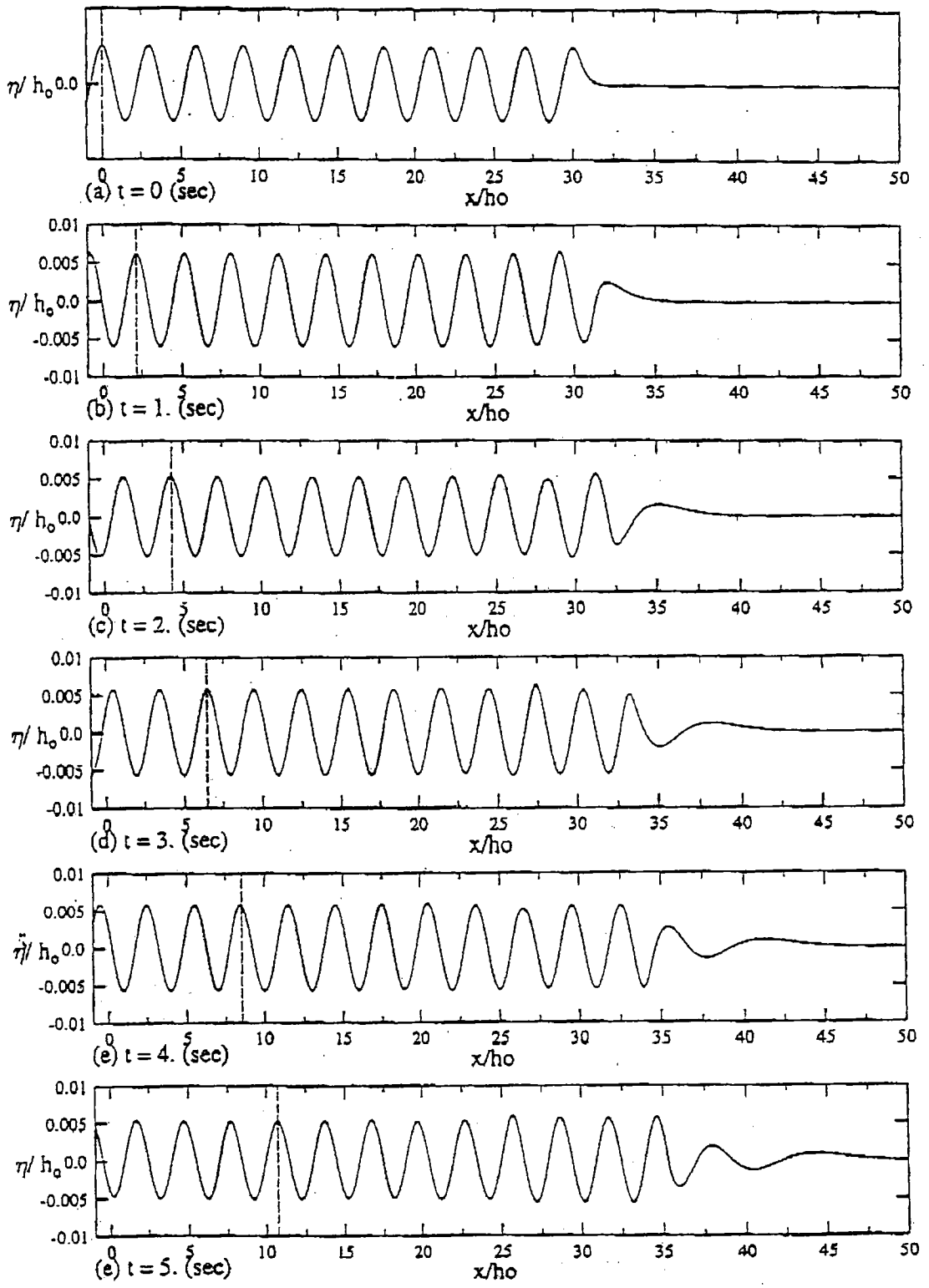

Figure 15: Numerical solution of the extended Boussinesq equations model for the propagation of deep water wave.

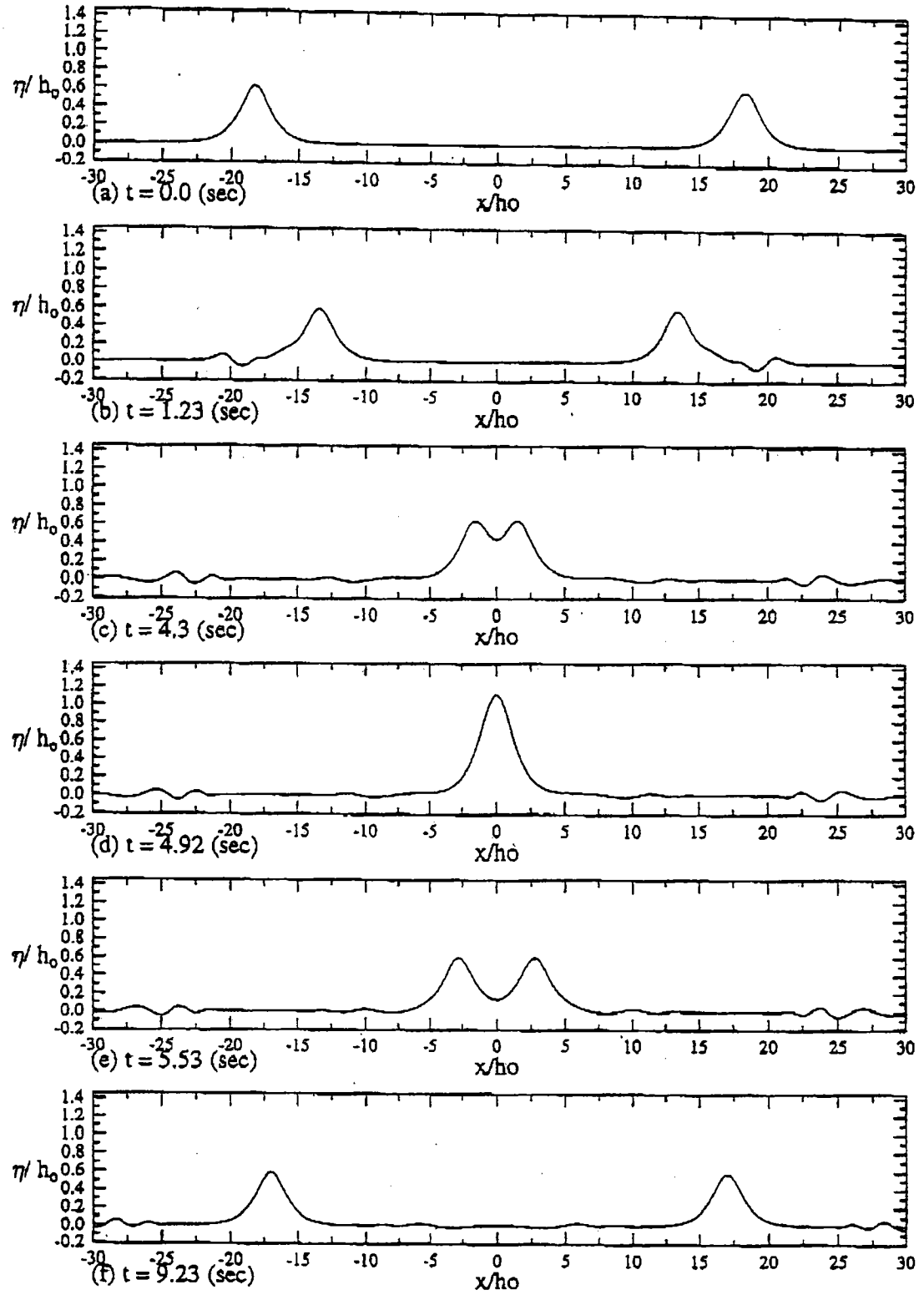

Figure 16: Interaction of solitary waves propagating in opposite direction

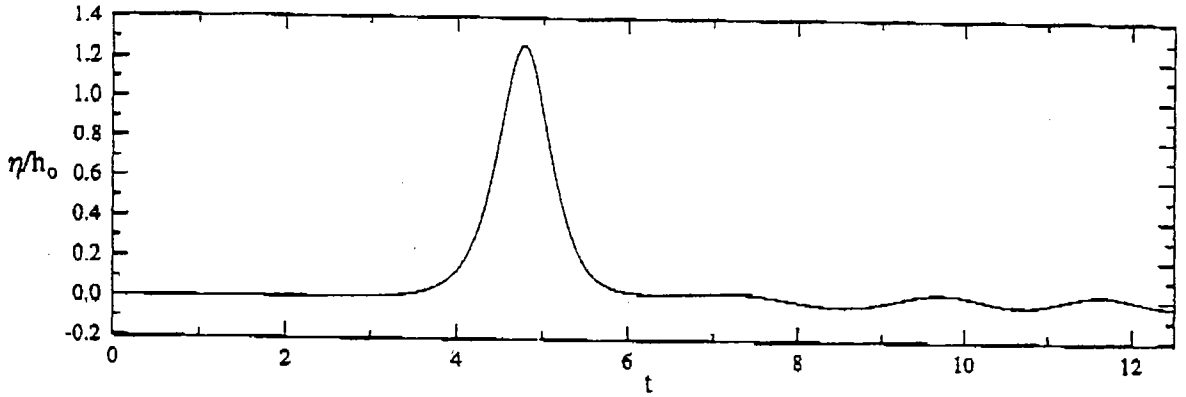

(a) Time history of free surface elevation at x = 0

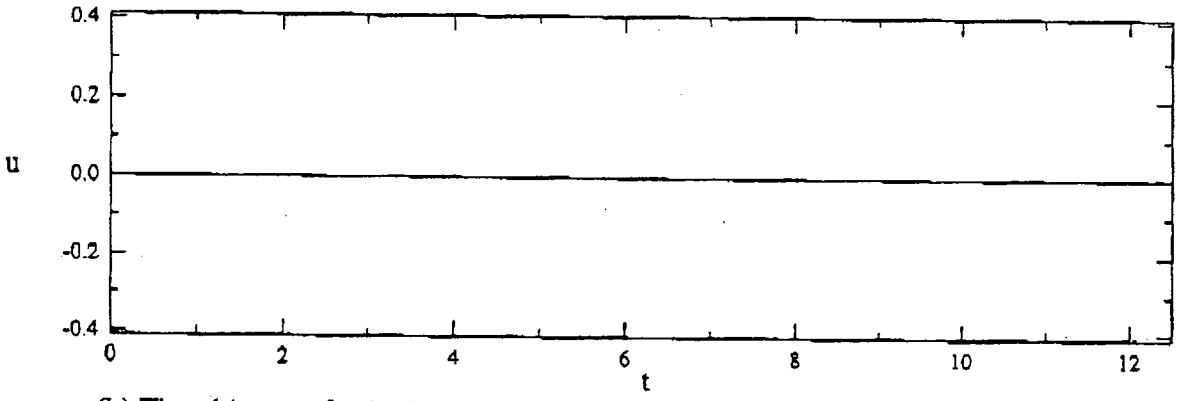

(b) Time history of velocity at x = 0

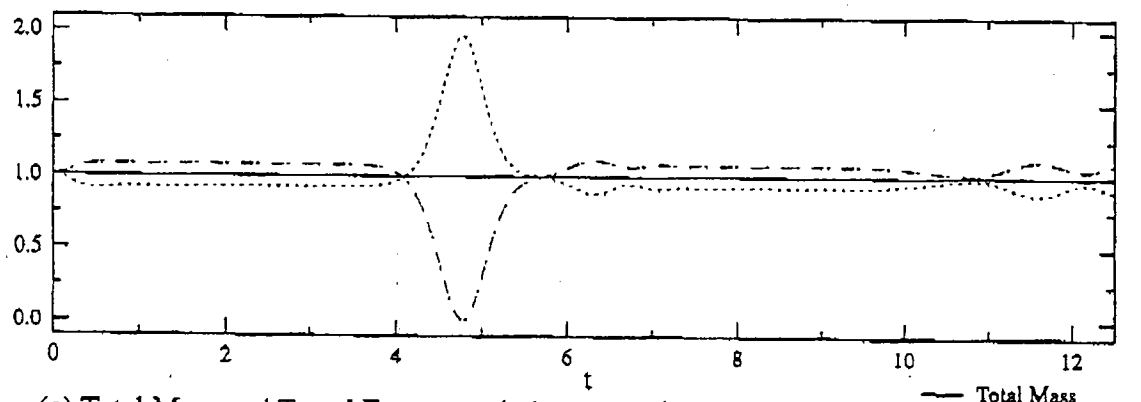

(c) Total Mass and Toatal Energy variations over time

Figure 17: Variation of free surface, velocity, total mass and total energy over time for the solitary waves propagting in opposite direction

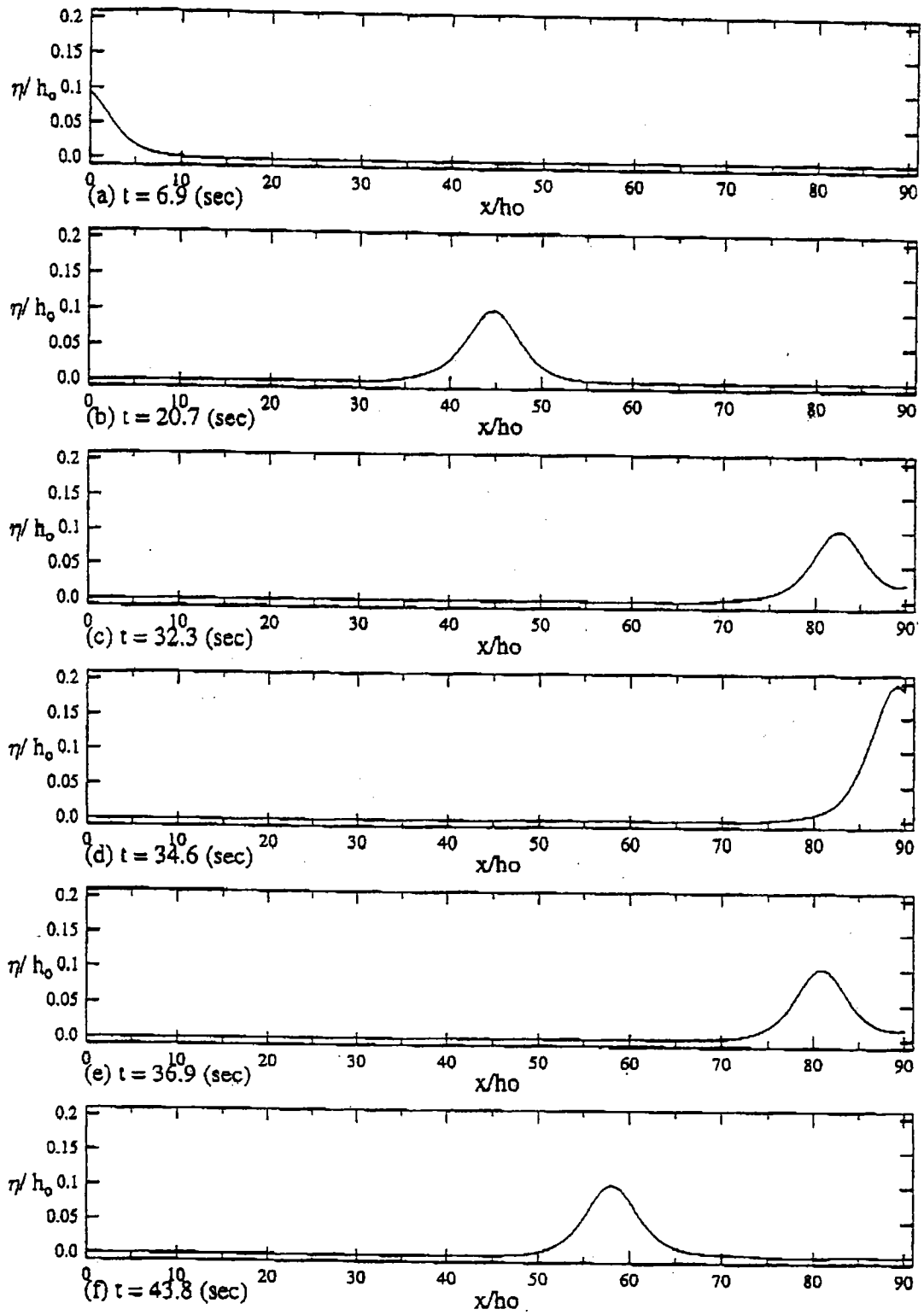

Figure 18: Numerical simulation of solitary wave propagation with incident and reflective boundary conditions (ϵ=0.1)

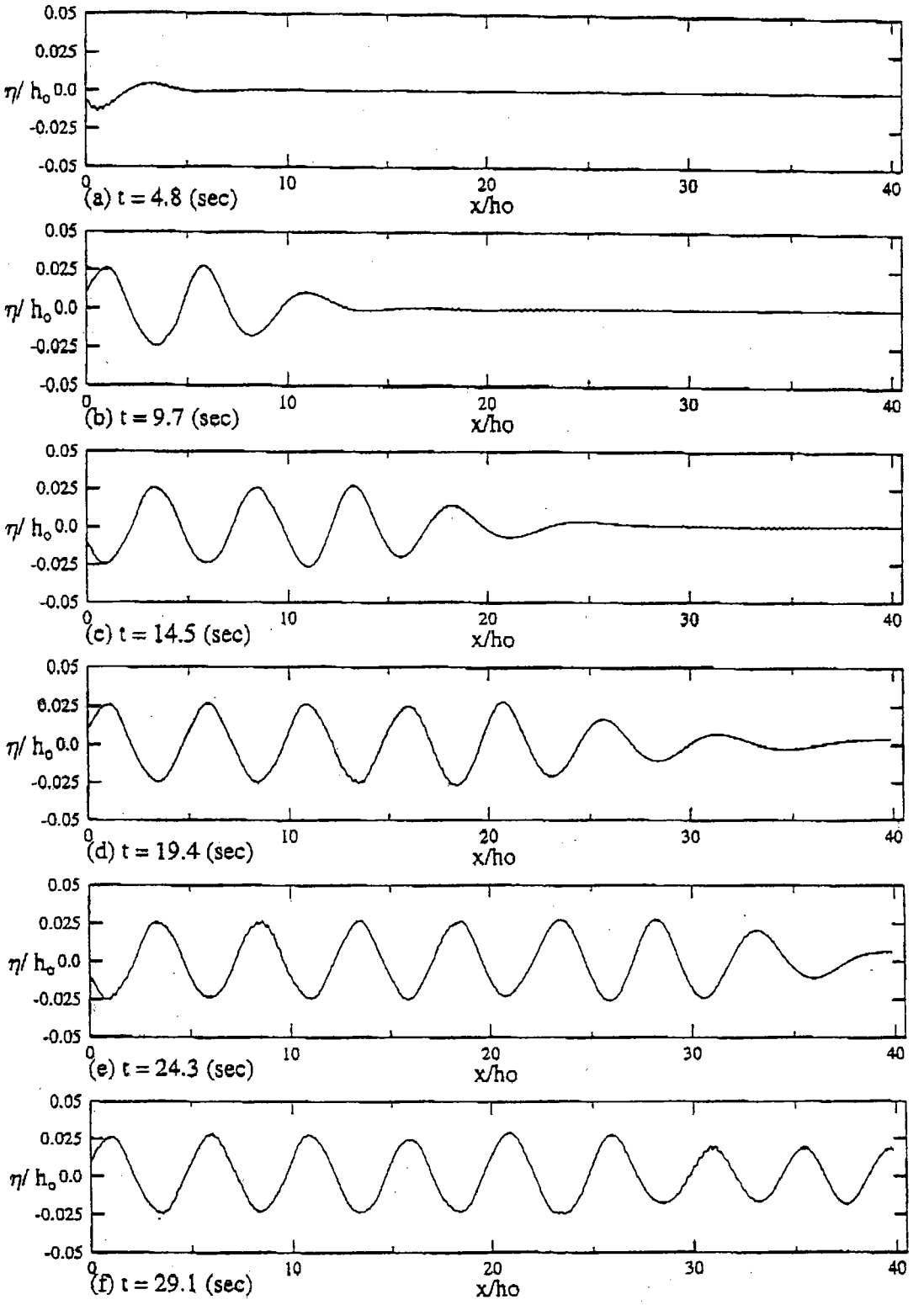

Figure 19: Sinusoidal intermediate water wave propagation through incident wave boundary condition (kh=1.25, ka=0.01)

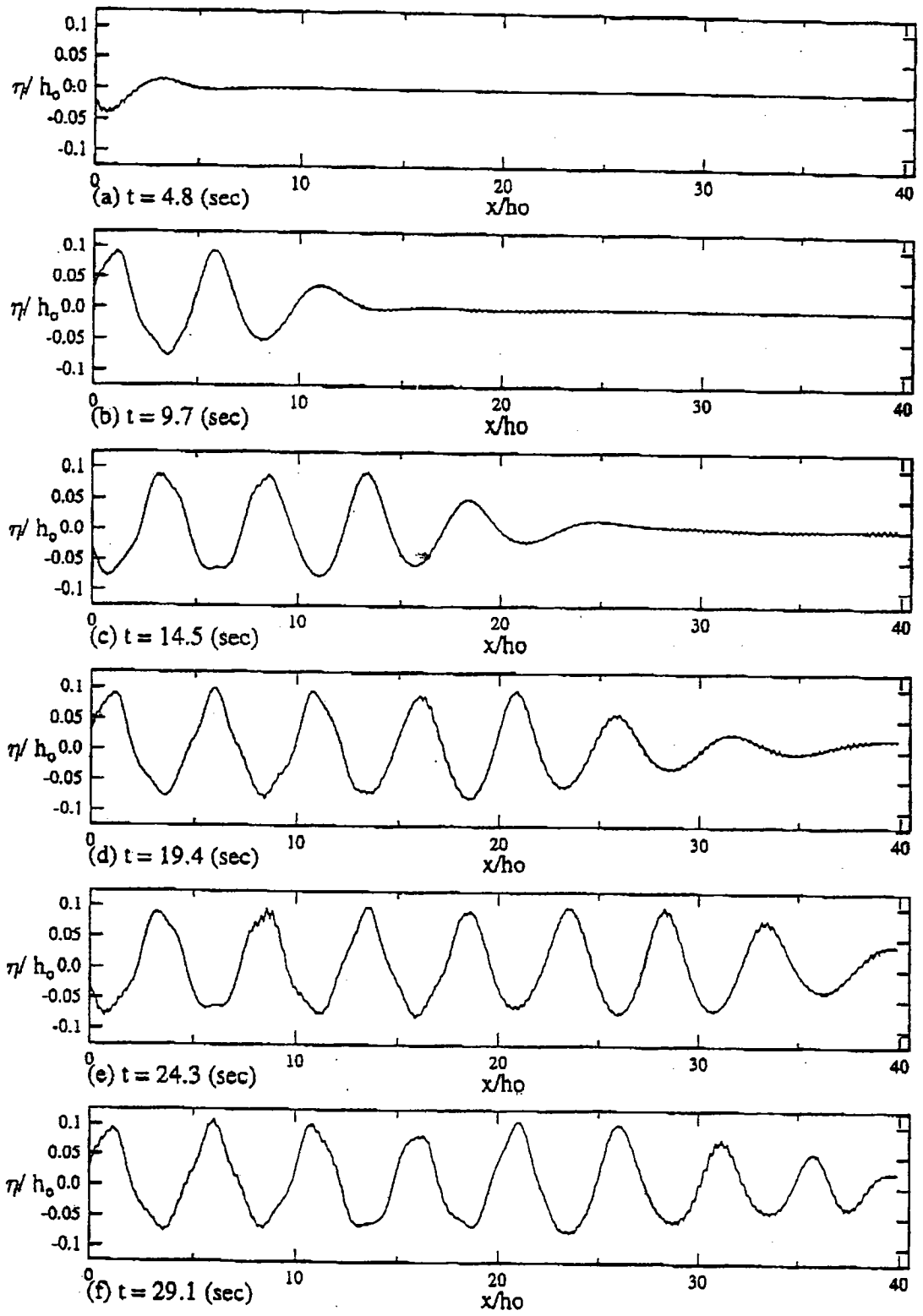

Figure 20: Sinusoidal intermediate water wave propagation through incident wave boundary condition (kh=1.25, ka=0.1)

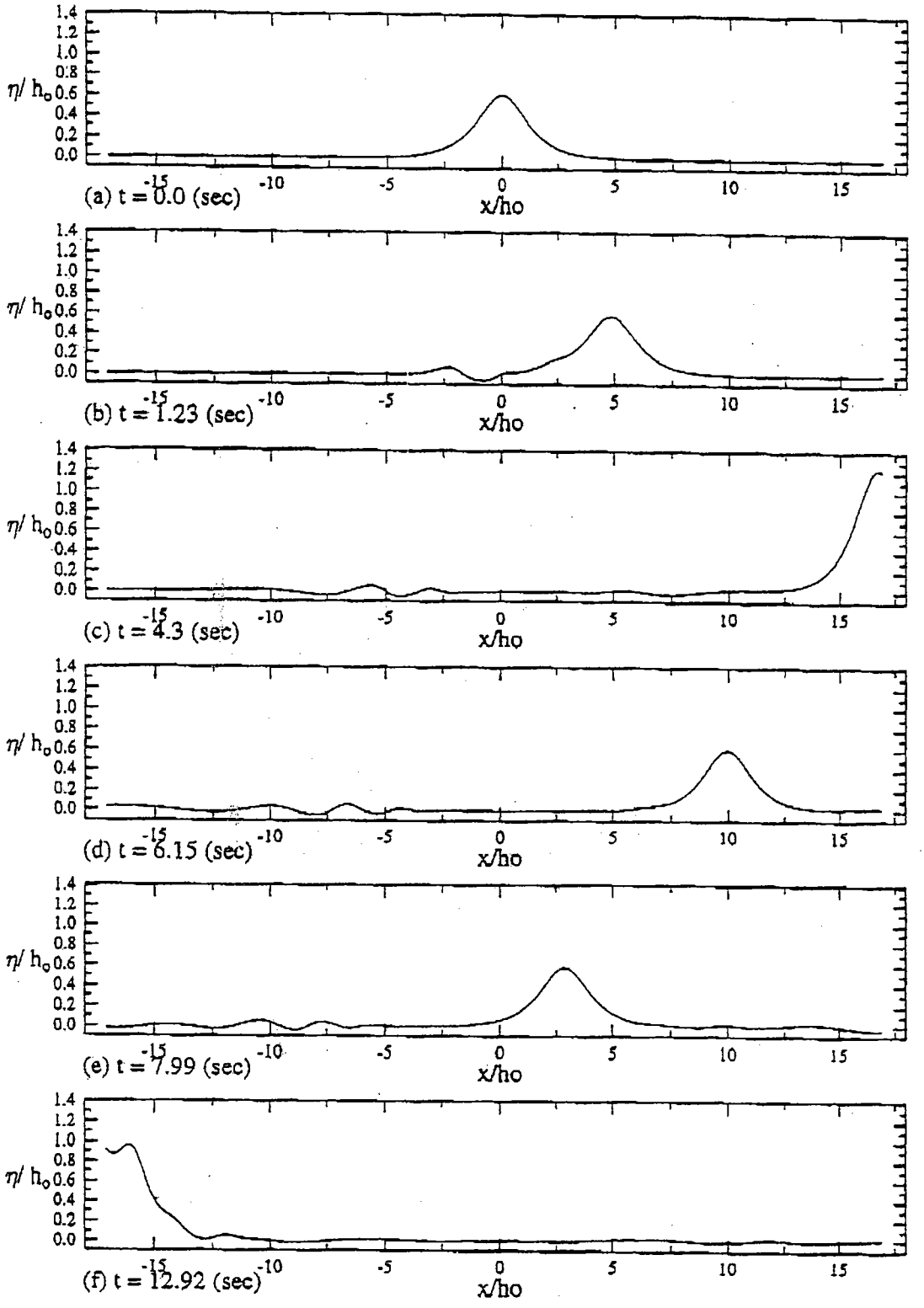

Figure 21: Numerical simulation of solitary wave interaction with two reflective wall boundary conditions (ϵ=0.6)

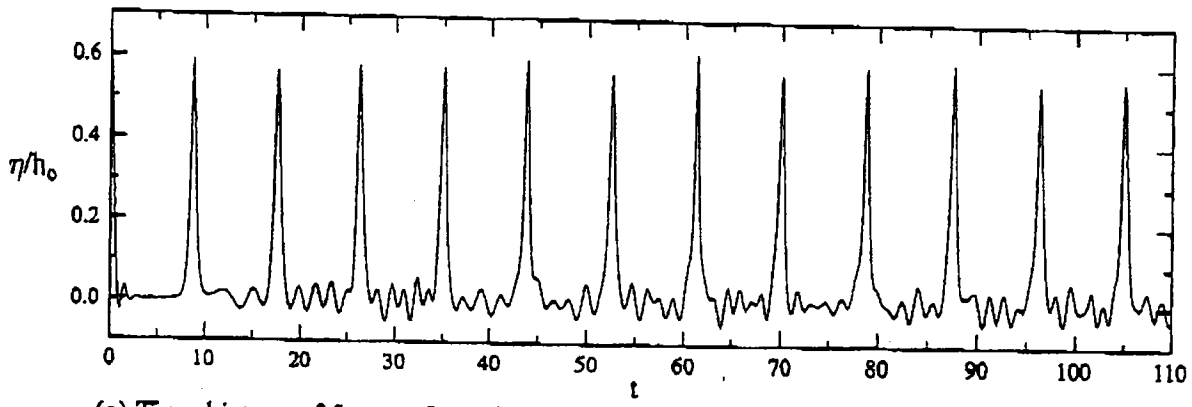

(a) Time history of free surface elevation at x = 0

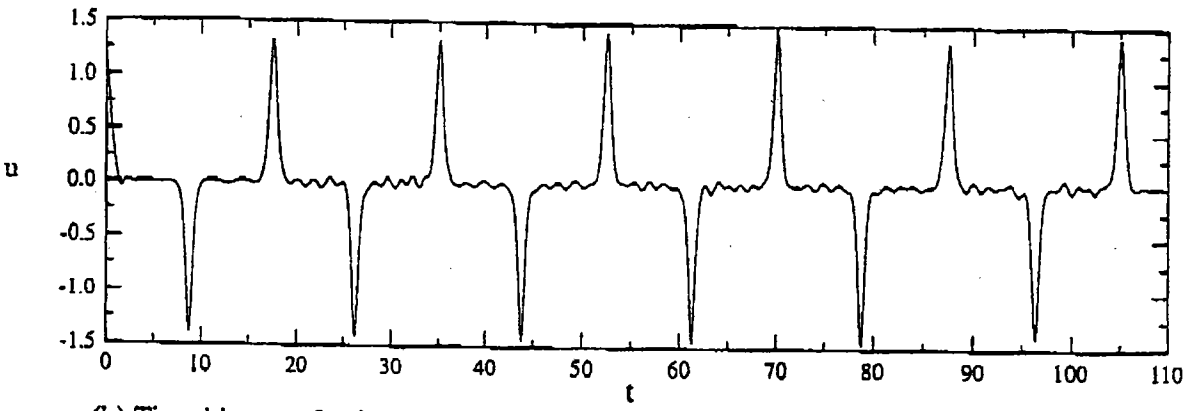

(b) Time history of velocity at x = 0

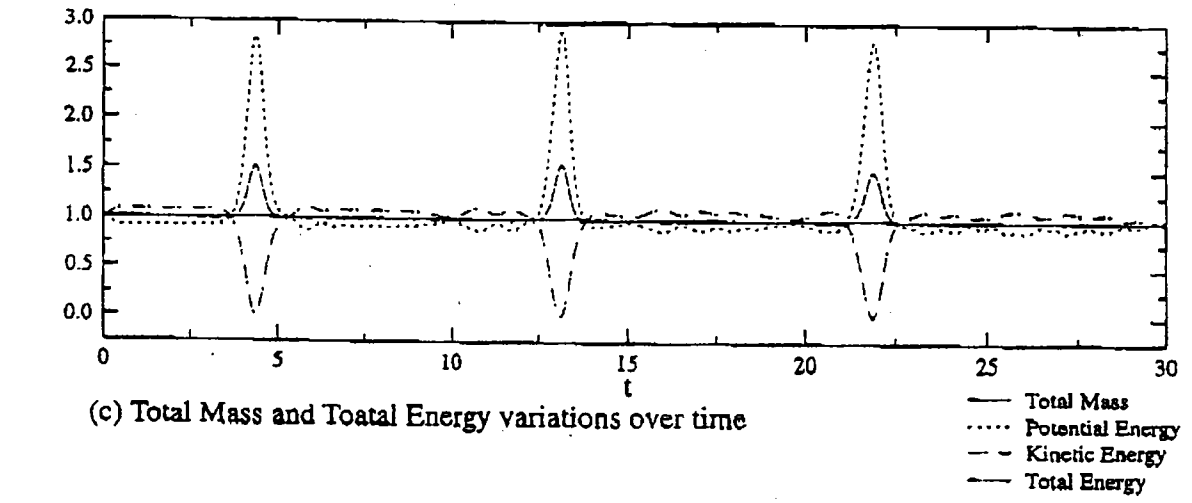

(c) Total Mass and Toatal Energy variations over time

Figure 22: Variations of free surface, velocity, total mass and total energy over time for the solitary wave simulations with two reflective wall boundary condition (ϵ=0.6)

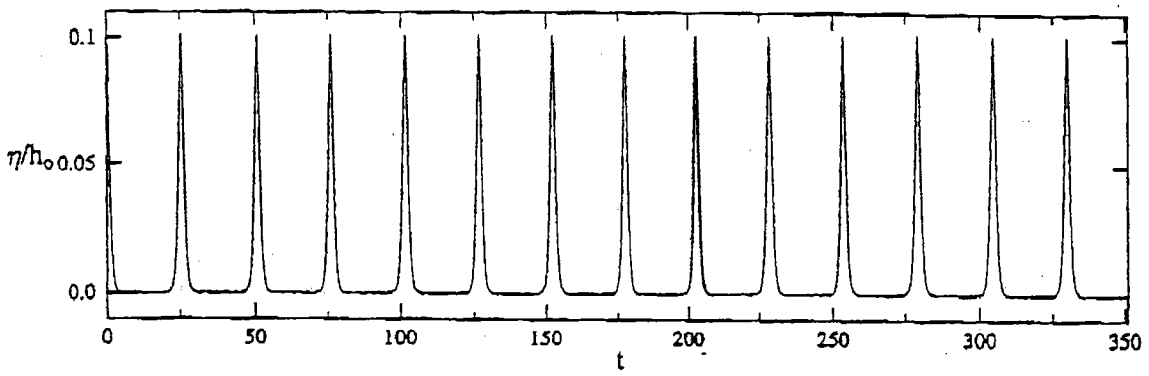

(a) Time history of free surface elevation at x = 0

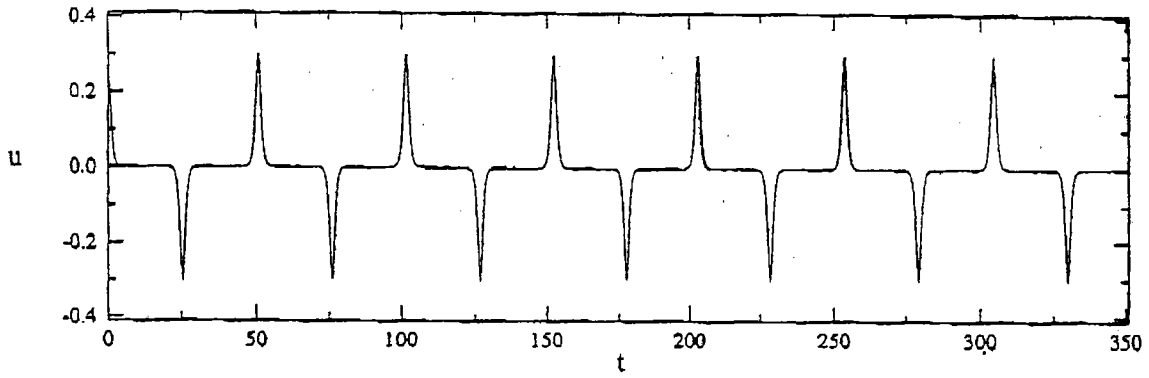

(b) Time history of velocity at x = 0

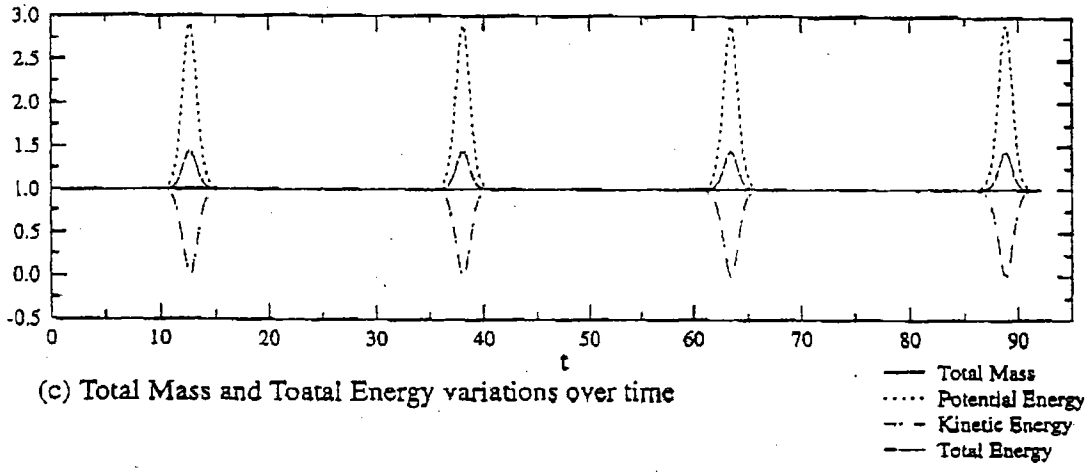

(c) Total Mass and Toatal Energy variations over time

Figure 23: Variations of free surface, velocity, total mass and total energy over time for the solitary wave simulations with two reflective boundary condition (ϵ=0.1)

References

[1] Abbott, M. B. 1979 "Computational Hydraulics: elements of the theory of free-surface flows," Pitman, London.

[2] Abbott, M. B., Petersen, H. M . and Skovgaard, O. 1978 "Numerical modelling of short waves in shallow water," *J. Hydraulic Res*, 3, pp. 173-203.

[3] Bowers, E. C. 1977 "Harbor resonance due to set-down beneath wave groups," *J. Fluid Mech.*, 79, pp. 71-92.

[4] Carrier, G. F., Shaw, R. P. and Miyata, M. 1971 "The response of narrow mouthed harbors in a straight coastline to periodic incident waves," *J. Appl. Mech.*, 38E-2, pp. 335-344.

[5] Chen, H. S. 1984 "Hybrid element modeling of harbor resonance," *Proceedings, 4th International Conference on Applied Numerical Modeling*, pp. 312-316.

[6] Chen, H. S. 1986 "Effects of bottom friction and boundary absorption on water wave scattering," *Applied Ocean Research*, 8, pp. 99-104.

[7] Chen, H. S. and Mei, C. C. 1974 "Oscillations and wave forces in an offshore harbor," *Report No. 190*, Department of Civil Engineering, MIT, Cambridge, MA.

[8] Chen, Y. and Liu, P. L.-F. 1995 "Modified Boussinesq equations and associated parabolic models for water wave propagation," *J. Fluid Mech.*, 288, pp. 351-381.

[9] Chen, Q., Madsen, P. A., Schaffer, H. A. and Basco, D. R., 1998 Wave-current interaction based on an enhanced Boussinesq approach", *Coastal Engng.*, 33, 11-39.

[10] Eldeberky, Y. and Battjes, J. A. 1996 "Spectral modeling of wave breaking: Application to Boussinesq equations," *J. Gophys. Res.*, 101, pp. 1253-1264.

[11] Elgar, S. and Guza, R. T. 1985 "Shoaling gravity waves: comparisons between field observations, linear theory and a nonlinear model", *J. Fluid Mech.*, 158, 47-70.

[12] Freilich, M. H. and Guza, R. T. 1984 "Nonlinear effects on shoaling surface gravity waves," *Philosophic Trans. Royal Soc. London*, A311, 1-41

[13] Goring, D. G. 1978 "Tsunamis - the propagation of long waves onto a shelf", Ph.D. dissertation, California Institute of Technology, Pasadena, CA.

[14] Grilli, S. T., Subramanya, R., Svendsen, I. A. and Veeramony, J. 1994 "Shoaling of solitary waves on plane beaches",*J. Waterway, Port, Coastal and Ocean Engineering*, ASCE, 120, pp. 609-628.

[15] Kaihatu, J. M. and Kirby, J. T. 1996 "Two-dimensional parabolic modeling of extended Boussinesq equations,"

[16] Katopodes, N. D. and Wu, C.-T. 1987 "Computation of finite-amplitude dispersive waves," *J. Waterway, Port, Coastal and Ocean Engineering*, ASCE, 113, pp. 327-346.

[17] Kostense, J. K., Meijer, K. L., Dingeman, M. W., Mynett, A. E. and van den Bosch, P. 1986 "Wave energy dissipation in arbitrarily shaped harbors of variable depth," *Proc. 20th Int. Conf. Coastal Engrg.*, pp. 2002-2016.

[18] Lee, J. J. 1971 "Wave-induced oscillations in harbors of arbitrary geometry," *J. Fluid Mech.*, 45, pp. 375-394.

[19] Lepelletier, T. G. 1980 "Tsunamis - Harbor oscillations induced by nonlinear transient long waves," *W. M. Keck Lab. Rep. No. KH-R-41*, California Institute of Technology.

[20] Lepelletier, T. G. and Raichlen, F. 1987 "Harbor oscillations induced by nonlinear transient long waves," *J. Waterway, Port, Coastal and Ocean Engineering*, Vol. 113, No. 4, pp. 381-400.

[21] Lillycrop, L. S., Briggs, M. J., Harkins, G. S., Boc, S. J. and Okihiro, M. S. 1993 "Barbers Point Harbor, Oahu, Hawaii, monitoring study," *Tech. Report CERC-93-18*, U.S. Army Corps of Engineers, Waterway Experiment Station.

[22] Lin, P. and Liu, P. L.-F., 1998 "A numerical study of breaking waves in the surf zone" *J. Fluid Mech.*, 359, 239-264.

[23] Liu, P. L.-F., 1986 "Effects of depth discontinuity on harbor oscillations" *Coastal Engineering*, 10, pp. 395-404.

[24] Liu, P. L.-F. 1990 "Wave transformation", in the Sea, v. 9, 27-63.

[25] Liu, P. L.-F., 1994 "Model equations for wave propagations from deep to shallow water," in *Advances in Coastal and Ocean Engineering*, (ed. by P. L.-F. Liu), Vol. 1, pp. 125-157.

[26] Liu, P. L.-F., Yoon, S. B. and Kirby, J. T. 1985 "Nonlinear refraction-diffraction of waves in shallow water," *J. Fluid Mech.*, 163, 185-201.

[27] Longuet-Higgins, M. S. and Stewart, R. W. 1962 "Radiation stress and mass transport in gravity waves, with applications to surf beats," *J. Fluid Mech.*, 79, pp. 71-92.

[28] Madsen, P. A., Murray, R. and Sorensen, O. R. 1991 "A new form of the Boussinesq equations with improved linear dispersion characteristics," *Coastal Engineering*, 15, pp. 371-388.

[29] Madsen, P. A., Sorensen, O. R. and Schaffer, H. A. 1997 "Surf zone dynamics simulated by a Boussinesq-type model. Part II. Surf beat and swash oscillation for wave groups and irregular waves", *Coastal Engng*, 32, 189-319.

[30] Mei, C. C. and Liu, P. L.-F. 1993 "Surface waves and coastal dynamics", *Annu. Rev. Fluid Mech.*, 25, 215-240.

[31] Mei, C. C. and Agnon, Y. 1989 "Long-period oscillations in a harbour induced by incident short waves," *J. Fluid Mech.*, 208, pp. 595-608.

[32] Munk, W. H. 1949 "Surf beats," *Eos Trans. American Geophysical Union*, 30(6), pp. 849-54.

[33] Nwogu, O. 1993 "An alternative form of the Boussinesq equations for nearshore wave propagation," *J. Waterway, Port, Coastal and Ocean Engrg.*, 119(6), pp. 618-638.

[34] Okihiro, M. and Guza, R. T. 1996 "Observation of seiche forcing and amplification in three small harbors," *J. Waterways, Port, Coastal and Ocean Engineering*, 122, No. 5, pp. 233-238.

[35] Okihiro, M., Guza, R. T. and Seymour, R. 1993 "Excitation of seiche observed in a small harbor," *J. Geophys. Res.*, 98 (C10), pp. 18201-18211.

[36] Peregrine, D. H. 1967 "Long waves on a beach" *J. Fluid Mech.*, 27, 815-882.

[37] Rogers, S. R. and Mei, C. C. 1978 "Nonlinear resonant excitation of a long and narrow bay," *J. Fluid Mech.*, 88, pp. 161-180.

[38] Schäffer, H. A., Madsen, P. A. and Deigaard, R. 1993 "A Boussinesq model for waves breaking in shallow water," *Coastal Engineering*, 20, pp. 185-202.

[39] Thompson, E. F., Chen, H. S., and Hadley, L. L. 1996 "Validation of numerical model for wind wave sand swell in harbors," *J. Waterways, Port, Coastal and Ocean Engrg.*, 122(5), pp. 245-257.

[40] Toba, Y., 1995 "The 3/2-power law for ocean wind waves and its applications", in Advances in coastal and Ocean Engineering, (ed. Philip L.-F. Liu), 3, 32-65.

[41] Tsay, T. K. and Liu, P. L.-F. 1983 "A finite element model for wave refraction and reflection," *Appl. Ocean Res.*, 5(1), pp. 30-37.

[42] Wei, G., Kirby, J. T., Grilli, S. T., and Subramanya, R. 1995 "A fully nonlinear Boussinesq model for surface waves. Part 1. Highly nonlinear unsteady waves," *J. Fluid Mech.*, 294, pp. 71-92.

[43] Witting, J. M. 1984 "A unified model for the evolution of nonlinear water waves", *J. Comp. Phys.*, 56, 203-236.

[44] Wu, J.-K. and Liu, P. L.-F. 1990 "Harbor excitations by incident wave groups," *J. Fluid Mech.*, 217, pp. 595-613.

[45] Xu, B., Panchang, V. and Demirbilek, Z. 1996 "Exterior reflections in elliptic harbor wave models," *J. Waterway, Port, Coastal and Ocean Engineering*, 112, (3), pp. 118-126.

[46] Zelt, J. L. 1991 "The run-up of nonbreaking and breaking solitary waves",

海洋波浪的弱非線性演化方程

陳冠宇

助理研究員

數學模式組

港灣技術研究所

The Weakly Nonlinear Evolution Equations for Waves in the Ocean

Guan-Yu Chen

Mathematical Modelling Devision

Institute of Harbor & Marine Technology

Wuchi, Taichung District, Taiwan

摘　　要

本研究針對海洋中四種常見的波，即深水 Stokes 波，赤道 Kelvin 波，海岸 Kelvin 波，與邊緣波(Edge Wave)的弱非線性演化方程進行探討。根據不同的尺度假設，這四種波可以分別以 Korteweg-de Vries(KdV)方程、Kadomtsev-Petviashvili(KP)方程，或非線性 Schroedinger(NLS)方程其中的一種或兩種來表示，因此本研究首先回顧這三個方程的推導及其特性。其次再就四種波的物理性質分別討論。

非線性演化方程之推得，固然是由基本的流體力學方程藉由尺度假設逐步演算的結果，但是也可以直接由頻散關係式及其他物理特性求得。這樣的方式較爲簡捷，其物理特性也比較容易明白。而且由於頻散關係式與演化方程的對應，吾人可以進一步由已知之演化方程倒推其頻散關係。其缺點則是結果不能涵蓋其他的波動，因此只適用在同一種波的交互作用。此外，頻散關係式通常也不容易求得。

最後，本研究介紹幾種數值模式，並進行初步的數值實驗。這些數值實驗的結果可以與理論計算的結果互相印證。本研究部份公式之導得，並利用符號運算軟體 Maple，以利爾後驗證與推廣。

The Weakly Nonlinear Evolution Equations for Waves in the Ocean

ABSTRACT

Chapter 1

Introduction to Weakly Nonlinear Ocean Waves

Since G. G. Stokes studied nonlinear water waves over one hundred years ago, the inclusion of nonlinearity in ocean waves had been viewed as a minor modification of the linear theory. However, the study of nonlinear wave theory in the last three decades has demonstrated that the accumulation of nonlinearity may change wave behavior dramatically. For example, the Stokes wave is subject to the so-called "sideband instability" due to the existence of nonlinearity. Another phenomenon which does not occur in linear wave theory is the existence of solitary waves.

To understand the effect of nonlinearity on ocean waves, it is helpful to begin by using weakly nonlinear theories in which the wave amplitude is small. Weak nonlinearity can be treated by the perturbation method, while there is no general method for strong nonlinearity. Just as the linear theory is the first step to the understanding of general wave problems, weakly nonlinear theory is the first step to the understanding of nonlinear waves.

In this chapter, we will explain some methods which are useful in the analysis of weakly nonlinear waves. In Chapter Two, the various forms of weakly nonlinear evolution equations are discussed. From Chapter Three to Chapter Six, four weakly nonlinear waves in the ocean are discussed respectively. These four waves are the Stokes wave in deep water, the edge wave, the equatorial Kelvin wave, and the coastal Kelvin wave. These four waves can be divided into two groups. The first two waves are not affected by the rotation of

the earth while for the last two waves are important only when we consider large scale wave motions. To coastal and ocean engineers, the Stokes wave is most familiar. In this review report, we try to relate some features of Stokes wave to edge waves. Similarly, the coastal Kelvin wave will be compared to the equatorial Kelvin wave which has been analyzed exhaustively in the dissertation of Chen. After the discussion in Chapter Seven, the eighth chapter will introduce some available numerical nonlinear ocean wave models which can be applied as tools for numerical experiments.

1.1 Analytic Method Applied in Weakly Nonlinear Ocean Waves

As mentioned previously, weakly nonlinear problems can be solved by the perturbation method, either regular or singular. In the following, a brief introduction to the perturbation method is cited. More details of perturbation methods and their application can be found in the dissertation of Chen and its references.

1.1.1 Regular and Singular Perturbation

If the wave amplitude is small that the nonlinear term is small and can be treated by a perturbation method with respect to a small perturbation parameter.

The parameter perturbations gives a solution valid for the whole domain when the perturbation parameter, say ϵ, is small.

Ordering

The mathematical tool used in the perturbation method is asymptotic expansion. To understand the asymptotic expansion, some ordering concept is necessary. Here the conventional order symbols o and O are used to define the order of magnitude of some quantity $f(\epsilon)$ compared to a gauge function $\Omega(\epsilon)$.

The small o is defined as

$$f(\epsilon) = o(\Omega(\epsilon)) \tag{1.1}$$

if

$$\lim_{\epsilon \to 0} \frac{f(\epsilon)}{\Omega(\epsilon)} = 0. \tag{1.2}$$

The large O is applied in

$$f(\epsilon) = O(\Omega(\epsilon)) \tag{1.3}$$

if there exists a constant k such that

$$\lim_{\epsilon \to 0} f(\epsilon) \leq k \lim_{\epsilon \to 0} \Omega(\epsilon). \tag{1.4}$$

Asymptotic Sequences and Expansions

As gauges for the perturbation, an asymptotic sequence $\Omega_n(\epsilon)$ satisfies

$$\Omega_n(\epsilon) = o(\Omega_{n-1}(\epsilon)), \qquad \epsilon \to 0. \tag{1.5}$$

Poincaré power sequence is one of the simplest asymptotic sequences. In it we have

$$\Omega_n(\epsilon) = \epsilon^n. \tag{1.6}$$

An asymptotic expansion of a function f is the expression

$$f(\epsilon) \sim \sum_{n=0}^{\infty} a_n \Omega_n(\epsilon) \qquad \epsilon \to 0 \tag{1.7}$$

where a_n does not relate to ϵ and can be computed as

$$a_0 = \lim_{\epsilon \to 0} \frac{f(\epsilon)}{\Omega_0(\epsilon)}, \tag{1.8}$$

$$a_n = \lim_{\epsilon \to 0} \frac{f(\epsilon) - \sum_{m=0}^{n-1} a_m \Omega_m(\epsilon)}{\Omega_n(\epsilon)}, \qquad n \geq 1. \tag{1.9}$$

There exists an infinite number of asymptotic sequences. However, the asymptotic expansion for a given asymptotic sequence $\Omega_n(\epsilon)$ is unique. That is, as an asymptotic expansion, the perturbation solution is unique, see Nayfeh [1973], and BenderOrszag [1978].

Uniformity and Singular Perturbation

Besides uniqueness, we also want to know if the asymptotic expansion obtained by perturbation method is uniformly valid.

Denote the residue for an asymptotic expansion of order $(N-1)$ as R_N. That is,

$$f(\epsilon) = \sum_{n=0}^{N-1} a_n \epsilon^n + R_N \,. \tag{1.10}$$

This asymptotic expansion is uniformly valid if

$$R_N = O(\epsilon^N) \tag{1.11}$$

throughout the whole domain. Otherwise, the expansion is nonuniform or singular.

A perturbation series that is uniformly valid is called a regular perturbation expansion. If nonuniformity occurs, the series is a singular perturbation expansion.

To obtain a uniformly valid solution, we need to find out the origin of nonuniformity and fix it. Several sources of nonuniformity are frequently seen. For example, a small parameter multiplying the highest derivative produces a boundary layer and the nonuniformity manifests itself by failing to satisfy all the boundary conditions.

In some cases the physics itself comprises more than one space scale or time scale. The straightforward perturbation will have secular terms whose error will grow with time. We can use the method of multiple scales to include all scales of interest and apply the solvability condition to eliminate secular terms. This method is frequently applied in the study of nonlinear wave packets and the derivation of NLS.

1.2 Symbolic Calculation Language

Perturbation methods have been developed for decades. However, they are not easy to apply because the computation for higher-order perturbation will become progressively more complicated and hence is difficult to carry out by hand. For example, in the study of Kelvin wave packets, we have to calculate more than 200 terms at the sixth-order. Therefore, a symbolic language like *MAPLE* or *MATHEMATICA* is very helpful to the study of weakly nonlinear waves.

Another advantage of a symbolic language is its accuracy. It can avoid most errors because some complicated operations can be done by just a few lines. The answer obtained can be easily checked, too, by substituting into the original equation.

In reading a scientific paper, symbolic languages can also be utilized to "repeat" the derivation so that any assumptions which are implicitly imposed on the solution can be found out.

As an example, the derivation of Stokes wave in Appendix A is prepared by *Maple*.

1.3 Numerical Method Applied in Weakly Nonlinear Waves

The perturbation method gives a solution that is correct to a specific order of the perturbation parameter. These analytic solutions are very useful in understanding the property of a solution. However, we still have to employ numerical computation in this study of weakly nonlinear waves for the following reasons.

(a) For the perturbation method to be consistent, we have to make some scale assumptions to make the perturbation parameter small. Therefore, the analytic solution is restricted to some parameter range. To find out the applicable parameter range, we need to compare the analytic solution to an "exact" solution. The most convenient "exact" solution is from the numerical method.

(b) When we obtain a solution to some physical problem, we do not know if it is stable. For example, the Stokes wave is unstable; but this is not well-known before the classic experiment of Benjamin and Feir is done. Numerical experiments provide a cheap way to check the stability of the solution.

(c) Since the numerical model simulates the whole system, all possible modes will be included. On the other hand, usually only a few modes are considered in the theoretical study.

For the above reasons, lots of numerical calculation is conducted even in the theoretical study of weakly nonlinear waves. These numerical results are used as a check and extension of the theory, not a substitute to the theoretical calculation.

Some commercial packages are right now available at the IHMT. These packages have been exhaustively verified and referred. Among them the Mike21 model developed by the DHI is broadly applied in engineering problems and the results are widely accepted. There-

fore, it is a natural choice to apply the Mike21 model as long as the problem under research is applicable.

One obvious advantage of these commercial packages is that they can treat almost every possible bathymetries which have to be considered case by case in theoretical studies.

Chapter 2

Nonlinear Evolution Equations

As has been mentioned in the previous chapter, one phenomenon which does not occur in linear wave theory is the existence of solitary waves. In this chapter, three nonlinear evolution equations, viz., the Korteweg-de Vries (KdV) equation, Kadomtsev-Petviashvili (KP) equation, and the Nonlinear Schrödinger Equation (NLS). All these three equations allow solitary wave solutions. Besides, they are all integrable and hence can be solved by the so-called inverse-scattering method.

The basic mechanism for solitary wave formation is the balance between nonlinear steepening and (linear) dispersion. The Korteweg-de Vries (KdV) equation is the simplest equation which includes both nonlinearity and dispersion. Therefore, we will discuss KdV equation first.

Two generalizations of the solitary wave theory are also briefly discussed. Each of them has a different relationship between dispersion and nonlinear steepening. The first generalization is the envelope solitary wave. It occurs in a wave packet which has a narrow banded spectrum in the frequency domain and hence minimized dispersion. If the wave is strongly dispersive, the dispersion of a wave packet can still balance the nonlinear steepening and form a permanent envelope shape. Its behavior is governed by a nonlinear Schrödinger Equation (NLS).

The second generalization is the two-dimensional solitary wave whose evolution is the Kadomtsev-Petviashvili (KP) equation, a

natural two-dimensional extension of the KdV equation. In the field with depth variations, nonuniform currents, and variable wind, a two-spatial-dimensional model is more realistic.

2.1 The Generality of the Korteweg-de Vries (KdV) Equation

The simplest solitary wave model which includes both dispersion and nonlinear advection is the Korteweg-de Vries (KdV) Equation. By the inverse scattering method, any disturbance in a system governed by the KdV equation will evolve into one or more solitary waves and a dispersing ripple, see Gardner [1967], Boyd [1980].

For systems which (a) are quadratically nonlinear and (b) are weakly dispersive in the limit of long waves so that the linear dispersion relation is approximately

$$\omega = c_0\, k + c_2\, k^3 + O(k^5), \qquad k \ll 0 \tag{2.1}$$

where c_p is the phase speed, ω is the wave frequency, and k is the wavenumber, the KdV equation is a generic model.

To see this, we can introduce the substitution

$$\omega \rightarrow -i\partial_t \tag{2.2}$$

$$k \rightarrow i\partial_x \tag{2.3}$$

into equation (2.1) and cancel out the c_0 term by introducing a moving coordinate $x - c_0\, t$, we obtain

$$u_t + c_2\, u_{xxx} = 0 \tag{2.4}$$

In this linearized KdV equation, the nonlinear advective term is neglected; it can be computed separately for a weakly nonlinear wave. In fluid motion, the advective term $u\, u_x$ is the only nonlinear term in the momentum equation. Therefore, the resulting evolution equation will be of KdV type:

$$u_t + \mu\, u\, u_x + c_2\, u_{xxx} = 0. \tag{2.5}$$

2.2 The Generality of the Kadomtsev-Petviashvili (KP) Equation

Just like the derivation of the KdV equation, the KP equation starts from the dispersion relation, too.

First, we can rewrite the dispersion relation (2.1) as

$$\omega^2 = c_0^2\, k^2 + 2\, c_2\, k^4. \tag{2.6}$$

As was shown in Grimshaw et al. [1997, p 6], the later expression is more general and can be applied to a wide variety of waves in the ocean.

Then, following Infeld and Rowland [1990, p8], we write k^2 as the sum of k_x^2 and k_y^2 and assume that

$$k_x \gg k_y. \tag{2.7}$$

Consequently, by Taylor's expansion, we have

$$\omega = c_0\, k_x + c_2\, k_x^3 + \frac{1}{2}\frac{k_y^2}{k_x}. \tag{2.8}$$

After introducing the substitution

$$\omega \to -i\partial_t \tag{2.9}$$

$$k_x \to i\partial_x \tag{2.10}$$

$$k_y \to i\partial_y \tag{2.11}$$

and canceling out the c_0 term by introducing a moving coordinate $x - c_0\, t$, we obtain

$$u_{xt} + \mu\, u_x\, u_{xx} + c_2\, u_{xxxx} + \frac{1}{2}\, u_{yy} = 0 \tag{2.12}$$

2.3 The Generality of the NLS

To study envelope solutions, we need to understand the nonlinear Schrödinger equation (NLS) which governs the evolution of a general wave packet . For a linear wave packet, the envelope amplitude A can be expressed as a Fourier integral in the frequency domain and

the steepest descent method can be applied to evaluate the integral. The result is a linear Schrödinger equation

$$iA_\tau + \frac{1}{2}\omega''(k)\, A_{\zeta\zeta} = 0 \tag{2.13}$$

whose dispersive coefficient is $\frac{1}{2}\omega''(k)$. This computation can be found in solving the so-called Cauchy-Poisson problem, see ,e.g., Mei [1984].

For weakly nonlinear problems, the dispersion and nonlinearity enter the governing equation independently; hence, the dispersion coefficient is unchanged. After including the neglected weak nonlinearity, the governing equation becomes

$$iA_\tau + \frac{1}{2}\omega''(k)\, A_{\zeta\zeta} + \nu|A|^2 A = 0, \tag{2.14}$$

where the nonlinear coefficient ν is the so-called Landau constant.

This nonlinear Schrödinger Equation (NLS) equation describes the wave behavior best for some amplitude range in which the dispersive term $\left(\frac{1}{2}\omega''(k)\, A_{\zeta\zeta}\right)$ and the nonlinear term $(\nu|A|^2 A)$ are of the same order of magnitude. Under this magnitude assumption, the behavior of the wave packet can be analyzed from the solution of the NLS equation.

If $\left(\omega''(k)\nu\right) > 0$, solitary wave solution is possible. This solitary wave solution is an envelope solitary wave because the variable A is the amplitude of the envelope. However, a threshold exists: to form a solitary wave for NLS, the amplitude must be larger than some critical value. Some phenomena like the sideband instability and the Fermi-Pasta-Ulam (FPU) recurrence can occur only for $\left(\omega''(k)\nu\right) > 0$.

If $\left(\omega''(k)\nu\right) < 0$, solitary wave is impossible and the wave packet will disperse.

The generality of the NLS can be further shown by assuming the following nonlinear dispersion relation for a periodic wave of amplitude a:

$$\omega = \Omega(k, a^2). \tag{2.15}$$

The dependence on a^2 instead of a emphasizes that the wave velocity depends on the absolute value of the amplitude. For a sinusoidal wave train, the wavenumber is very close to some fixed value k_0 and

hence can be expanded as

$$\omega = \Omega(k_0, 0) + \left(\frac{\partial \Omega}{\partial k}\right)_0 (k - k_0) + \frac{1}{2}\left(\frac{\partial^2 \Omega}{\partial k^2}\right)_0 (k - k_0)^2 + + \left(\frac{\partial \Omega}{\partial a^2}\right)_0 \tag{2.16}$$

or

$$\delta\omega = \left(\frac{\partial \Omega}{\partial k}\right)_0 \delta k + \frac{1}{2}\left(\frac{\partial^2 \Omega}{\partial k^2}\right)_0 \delta k^2 + + \left(\frac{\partial \Omega}{\partial a^2}\right)_0 \tag{2.17}$$

If we apply the correspondence

$$\delta\omega \to -i\partial_T \tag{2.18}$$

$$\delta k \to i\partial_X \tag{2.19}$$

$$a \to |A|, \tag{2.20}$$

an NLS can be obtained. This derivation shows an NLS is very general for the evolution of various wave packets.

Chapter 3

The Evolution of Finite Amplitude Deep Water Waves (Stokes Waves)

For water waves propagation over an infinite sea, we can assume potential flow and hence the two-dimensional Laplace equation

$$(\frac{\partial^2}{\partial x^2}\phi(x,\,z,\,t)) + (\frac{\partial^2}{\partial z^2}\phi(x,\,z,\,t)) = 0 \tag{3.1}$$

has to be satisfied. Besides, the following exact boundary conditions are used:

$$g\,\zeta(x,\,t) + (\frac{\partial}{\partial t}\phi(x,\,z,\,t)) + \frac{1}{2}(\frac{\partial}{\partial x}\phi(x,\,z,\,t))^2 + \frac{1}{2}(\frac{\partial}{\partial z}\phi(x,\,z,\,t))^2 \tag{3.2}$$

$$(\frac{\partial^2}{\partial t^2}\phi(x,\,z,\,t)) + g\,(\frac{\partial}{\partial z}\phi(x,\,z,\,t)) + (\frac{\partial}{\partial t}\mathrm{u}^2(x,\,z,\,t)) + \frac{1}{2}(\frac{\partial}{\partial x}\phi(x,\,z,\,t))\,(\frac{\partial}{\partial x}\mathrm{u}^2(x,\,z,\,t)) + \frac{1}{2}(\frac{\partial}{\partial z}\phi(x,\,z,\,t))\,(\frac{\partial}{\partial z}\mathrm{u}^2(x,\,z,\,t)) = 0. \tag{3.3}$$

The first condition is the dynamic free surface boundary condition or the Bernoulli equation. The free surface elevation ζ can be obtained from this equation once the velocity potential ϕ is solved. The second condition is the combination of kinematic and dynamic equations such that ϕ is the only unknown. The detailed derivation of this condition can be found in Dingermans [1997].

The boundary condition at the sea bottom is that ϕ approaches zero as z approaches $-\infty$. Besides these three conditions, we also assume the wave is periodic. That is, the lowest order solution is a linear sinusoidal wave.

3.1 Dispersion Relation

The perturbation method applied in deriving Stokes wave solutions adopt the wave amplitude as the perturbation parameter. Therefore, the first step is to expand the boundary conditions with respect to the mean water level $z = 0$. After introducing the series

$$\phi = \varepsilon\,\phi 1(x,\, z,\, t)+\varepsilon^2\,\phi 2(x,\, z,\, t)+\varepsilon^3\,\phi 3(x,\, z,\, t)+\varepsilon^4\,\phi 4(x,\, z,\, t) \quad (3.4)$$

and

$$\zeta = \varepsilon\,\zeta 1(x,\, t) + \varepsilon^2\,\zeta 2(x,\, t) + \varepsilon^3\,\zeta 3(x,\, t) + \varepsilon^4\,\zeta 4(x,\, t), \quad (3.5)$$

we can solve this problem order by order.

After compute the wave to the third order, the dispersion relation can be obtained as

$$\omega = \sqrt{g\,k}(1 + \frac{1}{2}a^2k^2) \quad (3.6)$$

The detailed derivation is given in Appendix A.

3.2 Nonlinear Schrödinger Equation (NLS) and Sideband Instability

After we obtain the nonlinear dispersion relation, the method introduced in section 2.3 can be directly applied to derive the NLS. We can rewrite the dispersion relation as

$$\omega = \Omega(k, a^2), \quad (3.7)$$

where

$$\Omega(k, a^2) == \omega_0(1 + \frac{1}{2}a^2k^2) \quad (3.8)$$

where

$$\omega_0 = \sqrt{g\,k}. \quad (3.9)$$

Therefore, we have

$$\frac{1}{2}\left(\frac{\partial^2\Omega}{\partial k^2}\right)_0 = \frac{1}{2}\omega'' = -\frac{1}{8}\frac{\omega_0}{k^2} \tag{3.10}$$

$$\left(\frac{\partial\Omega}{\partial a^2}\right)_0 = \nu = -\frac{1}{2}\omega_0 k^2. \tag{3.11}$$

Consequently, after scaling out the A_X term, the NLS governing a Stokes wave packet in infinitely deep ocean is

$$iA_T - \frac{1}{8}\frac{\omega_0}{k^2}A_{XX} - \frac{1}{2}\omega_0 k^2|A|^2 A = 0. \tag{3.12}$$

As has been mention in section 2.3, if $\left(\omega''(k)\nu\right) > 0$, envelope solitary wave solution is possible. However, a threshold exists: to form a solitary wave for NLS, the amplitude must be larger than some critical value. Some phenomena like the sideband instability and the Fermi-Pasta-Ulam (FPU) recurrence can occur. These phenomena had been studied in a series of papers by Yuen, Lake, and their colleagues.

The conclusion that Stokes wave can be unstable is the most striking. This phenomena is first found in the classic experiment of Benjamin and Feir and hence is called the Benjamin-Feir sideband instability.

Chapter 4

The Evolution of Nonlinear Edge Waves

The theory of edge wave has a long history since Stokes first derive a linear edge wave solution in 1846. Accompanying the increase of our knowledge to it, more application of this special trapped wave to the coast is discovered. The importance of edge waves in rip current and coast formulation has long been recognized. From the theory of Longuet-Higgens and the investigation of Ishii and Abe, it was shown that tsunamis could be trapped by an island in the form of edge waves. Besides, edge wave is found in Hwa-Lian, Taiwan, to play an essential role in long-wave generation which are then responsible for the harbor resonance.

4.1 Introduction to Edge Wave Theories

For most coastal engineers, edge wave is a brand new concept. The basic mechanism of the trapping of edge waves, however, is simple. As was given graphically in the book of LeBlond and Mysak, a wave reflected by the shore will be refracted toward the shore again because the wave speed in the shallower region is slower than that in the region away from the shore. The condition for the existence of edge waves, therefore, is that the depth near the shore must be somewhere less than the depth far from the shore. The mathematical explanation to this condition can be found in Sabatier [1991].

According to the governing equation utilized, the development of the edge wave theory can be divided into two branches: the shallow

water model and the full Laplace equation model. Most papers devoted to this topic is established on the shallow water equation model which is much simpler to handle. The first complete linear edge wave theory of Eckhaus, based on the shallow water equations, gives the n-th eigenmode of a linear harmonic edge wave as

$$\zeta = e^{-k\,y} L_n(2\,k\,y) e^{i(k\,x-\omega t)}. \tag{4.1}$$

Here the coordinate y is perpendicular to the shoreline, x is along the shoreline, L_n is the n-th order Laguerre polynomial, ω is the frequency of the wave, and k is the wavenumber in the x direction. They are related by the dispersion relation

$$k = \frac{\omega^2}{(2\,n+1)\,s\,g}. \tag{4.2}$$

The slope s is assumed to be a constant.

Eckhaus's solution sheded light on the structure of edge waves. However, his assumption that the slope is uniform is not appropriate for the governing shallow water equation. The water depth is no longer shallow as the distance away from the shore, y, becomes large. Therefore, another theory which deals with the Laplace equation is developed by Ursell. The resulting dispersion relation is similar to that of Eckhaus's theory except the slope of the beach $s = tan(\alpha)$ is replace by $sin(\alpha)$. Here α is the angle between the beach and horizon. That is,

$$\omega^2 = (2\,n+1)\,g\,k\,sin(\alpha). \tag{4.3}$$

The comparison of these two theories can be found in Yeh [1987] and Mok [1995].

However, the full theory is so complicated that it is rarely applied except for the lowest mode, the so-called Stokes edge wave. This mode of edge wave on an infinite beach of constant slope can be represented by an ordinary water wave of infinitely deep water. This is because a velocity potential

$$\phi \sim e^{-k\,x+i\,k\,y} \tag{4.4}$$

automatically satisfies the Laplace equation

$$\Delta\phi = 0. \tag{4.5}$$

The linear edge wave theory is illuminating. However, since the surface elevation and the velocity amplitude of an edge wave are maximized at the shore where water depth is minimized, the nonlinear effect should not be neglected. Besides, Whitham [1976] had proved that first mode edge waves do not radiate and hence do not decay. This implies, at least for the first mode, the nonlinearity will accumulate and cannot be ignored.

4.2 Dispersion Relation

The dispersion relation of linear edge wave can be summarized as

$$\omega^2 = (2\,n + 1)\,g\,k\,s, \tag{4.6}$$

where $s = sin(\alpha)$ or $tan(\alpha)$ if the full theory or the shallow water theory is utilized.

Whitham [1976] applied Stokes expansion, or the Poincaré-Lindstedt technique, to nonlinear Stokes-mode edge waves. That is, the solution is assumed to be periodic and, besides the unknown ϕ and ζ, the wave velocity should also be expanded in terms of the wave amplitude. For more detail of this method, please refer to Appendix A.

The lowest-order solution is a sinusoidal edge wave of amplitude a and wavenumber k. The higher-order problems are inhomogeneous and the wave velocity perturbation is chosen to cancel any forcing of wavenumber k in the right hand side.

For both the full equation and the shallow water equation model, the nonlinear dispersion relation for Stokes edge wave is derived by Whitham as

$$\omega^2 = g\,k\,s(1 + \frac{1}{2}a^2k^2), \tag{4.7}$$

where $s = sin(\alpha)$ or $tan(\alpha)$ depending on which theory is utilized.

The above dispersion relation includes nonlinearity. However, the assumption that the beach has a uniform slope seriously restricts the applicability of the theory. It is desirable to derive a theory for arbitrary water depth variation. This theory can be established only on the shallow water equation because the full theory is too complicated even for the simplest geometry. Since the long edge waves are of more interest to coastal engineers, adopting the shallow water assumption is also reasonable.

Based on a perturbation theory with the alongshore wavenumber serves as the perturbation parameter, Grimshaw [1974] derived the dispersion relation of linear edge wave for arbitrary bathymetries as

$$\omega^2 = k^2\, g\, h_0[1 - (\mathcal{A}^2 + \frac{1}{3})k^2 h_0^2] \tag{4.8}$$

or

$$\omega = k\sqrt{g\, h_0}[1 - \frac{1}{2}(\mathcal{A}^2 + \frac{1}{3})k^2 h_0^2]. \tag{4.9}$$

Here h_0 is the water depth at infinity and $\mathcal{A}$ is defined by

$$\mathcal{A} = \frac{1}{h_0^2}\int_0^\infty [h_0 - h(x)]dx. \tag{4.10}$$

Note that the integral part is just the area between the sea bottom and the line $z = -h_0$.

4.3 Kadomtsev-Petviashvili (KP) Equation

Mathew and Akylas [1990] had derived a Kadomtsev-Petviashvili (KP) equation for a wide channel as

$$\eta_{tx} + \frac{3}{4}\left(\eta^2\right)_{xx} + \frac{1}{6}\eta_{xxxx} + \frac{1}{2}\eta_{yy}. \tag{4.11}$$

This KP equation is directly applicable to the study of edge waves.

The linear dispersion relation can be derived by assuming

$$\eta = e^{-k^2 \mathcal{A} y} e^{i(k\,x - \omega t)}, \tag{4.12}$$

where

$$\mathcal{A} = \frac{1}{h_0^2}\int_0^\infty [h_0 - h(x)]dx \tag{4.13}$$

where h_0 is the depth at $y \to \infty$. Substituting into the KP equation (4.15), we obtain the dispersion relation which is exactly the same as Grimshaw's result in nondimensionalized form:

$$\omega = -\frac{1}{2}\left(\mathcal{A}^2 + \frac{1}{3}\right)k^3. \tag{4.14}$$

In the one-dimensional approximation, the change in the y-direction can be neglected and the KP equation 4.11 becomes the KdV equation

$$\eta_t + \frac{3}{2}\eta\eta_x + \frac{1}{6}\eta_{xxx}. \tag{4.15}$$

The corresponding linear dispersion relation is

$$\omega = -\frac{1}{2}\left(\frac{1}{3}\right)k^3. \tag{4.16}$$

The difference between equation (4.14) and (4.16) is just $-\frac{1}{2}(\mathcal{A}^2)\,k^3$ which corresponds to the y-derivative term of the KP equation. That is, the two-dimensional effect of the edge wave is represented by the parameter $\mathcal{A}$ in the dispersion relation .

4.4 NLS of Edge Waves

Based on the nonlinear dispersion relation derived by Whitham

$$\omega = \sqrt{g\,k\,sin(\alpha)}(1 + \frac{1}{2}a^2k^2), \tag{4.17}$$

the nonlinear Schrödinger Equation (NLS) can be directly derived by Yeh [1985] via the method of section 3.2. The result is

$$iA_T - \frac{1}{8}\frac{\omega_0}{k^2}A_{XX} - \frac{1}{4}\omega_0 k^2|A|^2A = 0\,. \tag{4.18}$$

Note that the nonlinear coefficient is just half of that of the Stokes wave. This is not surprising because, as has been shown by Yih, the Stokes mode edge wave and the usual deep-water wave can be related by a simple coordinate transformation. In the direction perpendicular to the wave direction, a Stokes wave has uniform amplitude distribution while an edge wave has exponential decay. This implies the nonlinear self-interaction of edge waves is less then that in the Stokes wave and hence the nonlinear cofficient is smaller. The existence and sideband instability pf edge wave is the same as the Stokes waves.

Chapter 5

The Evolution of Nonlinear Equatorial Kelvin Waves

5.1 Introduction to Equatorial Waves

There are four species of equatorial waves: Kelvin waves, Rossby waves, gravity waves, and mixed Rossby-gravity waves. They are all trapped near the equator and can be treated as one-dimensional waves propagating zonally only. These waves have quite different latitudinal structures and dispersion relations.

When the governing equations of equatorial waves are linearized about a motionless ocean, the Kelvin wave is nondispersive and has nondimensional speed one toward the east , see Boyd [1980]. The Rossby wave propagates toward the west and its velocity depends on the latitudinal mode n as well as the wavenumber k. Gravity waves can propagate either to the east or to the west. Their velocities also depend on n and k. The mixed Rossby-gravity wave behaves like a Rossby wave for a small wavenumber and like a gravity wave for a large wavenumber.

These equatorial waves propagate in the equatorial ocean which is very complicated, and a model is very helpful to understand its physics. The physical model commonly used to describe the equatorial wave is the "one-and-a-half-layer" model on the equatorial β-plane. After nondimensionalizing, this model is represented by the following nondimensionalized shallow water equations (see Boyd [1983] and Moore and Philander [1977]).

$$u_t + uu_x + vu_y - yv + \phi_x = 0 \tag{5.1}$$

$$v_t + uv_x + vv_y + yu + \phi_y = 0 \tag{5.2}$$
$$\phi_t + u_x + (u\phi)_x + v_y + (v\phi)_y = 0 \tag{5.3}$$

where subscripts denote partial derivatives. Unknowns u and v are the eastward and northward currents. The undisturbed mixed layer thickness is one while the height field ϕ is its thickness variation. Positive ϕ corresponds to down-welling internal waves. Note that the nondimensional Coriolis parameter is just y in the equatorial β-plane.

The dynamics of the Kelvin wave are unique among equatorially trapped internal waves because it is nondispersive. This means that even weak nonlinearity will accumulate and without a spreading mechanism the wave will inevitably break. However, latitudinally sheared zonal flow interacts with the wave and makes it dispersive.

Equatorial Kelvin and Rossby waves are frequently observed in El Niño and Southern Oscillation (ENSO), which is a global climate change. In normal years, the trade wind piles up a huge amount of warm surface water in the west of the Pacific Ocean. In El Niño years, the trade wind relaxes; hence, the warm surface water is released and moves to the east in the form of Kelvin waves.

5.2 Dispersion Relation

The linear dispersion relation of Kelvin wave for arbitrary zonal mean flow $U(y)$ and its corresponding height field $\Phi(y)$ is derived in the dissertation of Chen as

$$\omega = \left\{1 + \tilde{\Omega}_1\delta + \tilde{\Omega}_2\delta^2\right\} k + \tilde{\omega}_2\delta^2 k^3, \tag{5.4}$$

where the perturbation parameter δ represents the amplitude of the flow The constants $\tilde{\Omega}_1$, $\tilde{\Omega}_2$, and $\tilde{\omega}_2$ all depend on U and Φ. The last term ($\tilde{\omega}_2\delta^2 k^3$) is the only dispersive term. Its coefficient is

$$\tilde{\omega}_2 = \frac{1}{\sqrt{\pi}}\int_{-\infty}^{\infty} e^{-y^2}\left\{\frac{1}{2}\Phi(y) + U(y) - \tilde{\Omega}_1\right\}\tilde{f}_S(y)\,dy \tag{5.5}$$

where

$$\tilde{f}_S(y) = -2\int_{-\infty}^{y} f_v(\tilde{y})\,d\tilde{y} \tag{5.6}$$

where

$$f_v(y) = e^{y^2}\int_{-\infty}^{y}\left\{\tilde{\Omega}_1 - U(\tilde{y}) - \frac{1}{2}\Phi(\tilde{y})\right\} e^{-\tilde{y}^2}\,d\tilde{y}. \tag{5.7}$$

5.3 Korteweg-de Vries (KdV) Equation

From the dispersion relation, the linear evolution equation is

$$\eta_t = -c_0\eta_x + \tilde{\omega}_2\delta^2\eta_{xxx} \tag{5.8}$$

where η is the wave induced zonal velocity at the equator. Dispersion of the Korteweg-de Vries (KdV) equation is exact up to $O(\delta^2)$. That is, the Kelvin wave is described by a KdV equation for arbitrary wavenumber k.

For a weakly nonlinear Kelvin wave, the nonlinear term is computed separately from the nondispersive case by Boyd as $\sqrt{\frac{3}{2}}\ \eta\ \eta_x$. For a weakly nonlinear wave, the dispersion and nonlinearity appear independently. Therefore, the governing KdV equation is

$$\eta_t + c_0\ \eta_x + \sqrt{\frac{3}{2}}\ \eta\ \eta_x - \tilde{\omega}_2\delta^2\eta_{xxx} = 0 \qquad (4.5) \qquad (5.9)$$

Using a new variable $A = 2\ \eta$, the KdV equation becomes

$$A_t + c_0\ A_x + \sqrt{\frac{3}{8}}\ A\ A_x - \tilde{\omega}_2\delta^2 A_{xxx} = 0. \tag{5.10}$$

5.4 Nonlinear Schrödinger Equation (NLS) and Envelope Solitons

The Korteweg-de Vries (KdV) equation of the Kelvin wave derived in the previous section is weakly dispersive, $O(\delta^2)$. It is not restricted to long waves because the dispersion is quadratic:

$$\omega = \left\{1 + \tilde{\Omega}_1\delta + \tilde{\Omega}_2\delta^2\right\} k + \tilde{\omega}_2\delta^2 k^3. \tag{5.11}$$

Therefore, the "slow" zonal variable does not appear in the equation.

It has been pointed out by R. S. Johnson [1976] that the long wave limit of NLS theory should be derived from KdV equation. Johnson also demonstrate that the NLS equation derived from the KdV is the long wave limit of the general NLS equation.

Because there is no long wave restriction in Kelvin-KdV theory, at least when the dispersion is small and can be computed by the perturbation of the flow shear, it follows we can always get the NLS equation of Kelvin wave from the Kelvin-KdV. The reason is

the resonance, which implies the lowest-order second harmonic and long wave are dominated by Kelvin modes. This resonance drastically simplifies the wave envelope problem to just Kelvin–Kelvin interaction which is the object of Kelvin-KdV theory. Therefore, Kelvin-KdV and Kelvin-NLS should be closely related to each other.

The method of Johnson, which is explained in more detail by Boyd [1983], is to apply the method of multiple scales to the KdV equation instead of the more complicated shallow water equations. This approach is much simpler than the standard derivation of NLS because there is just one dimension, the zonal coordinate, to deal with. The detailed derivation will be given in Appendix B and the resulting NLS is

$$i(A)_\tau + \frac{1}{2}\omega''(k)\,(A)_{\zeta\zeta} + \nu|A|^2 A = 0, \tag{5.12}$$

where

$$\nu \equiv -\frac{1}{6}\frac{\beta^2}{\gamma k}, \tag{5.13}$$

and

$$\frac{1}{2}\omega''(k) = -\frac{\beta^2}{2\nu} = -\frac{0.1875}{\nu}. \tag{5.14}$$

This NLS has exactly the same coefficients as the NLS derived from the shallow water equations, which takes perturbation to the seventh order in the dissertation of Chen.

Note that the coefficients $\left(\frac{1}{2}\omega''(k)\right)$ and ν are of different signs. This means in any case the envelope solitary wave does not exist.

Chapter 6

The Evolution of Nonlinear Coastal Kelvin Waves

6.1 Introduction to Coastal Kelvin Waves

A geophysical wave solution which propagate along the coast and has trivial velocity in the off-shore direction is first derive by Lord Kelvin. This is how coastal Kelvin wave gets its name. Like the Kelvin wave at the equator, the wave amplitude is an exponential function in the offshore direction due to geostrophic balance. This wave profile cannot exist unless a plane of symmetry exists. For the equatorial case, the equator as a plane makes the wave profile smooth ; in the coastal case, the coast plays the role of the symmetric plane.

Most features of the coastal Kelvin wave is similar to the equatorial one. One minor difference is that instead of the β-plane approximation adopted in the equatorial wave, the coastal Kelvin wave is usually analyzed via the f-plane approximation. That is, the Coriolis parameter is assume to be a constant, which is correct when the horizontal scale is not very large.

There are two other possible explanations for this difference. First, the orientation of the coast varies from place to place. It is not possible for a general theory to include all possible cases. Second, the f-plane approximation cannot be used in the equator If this approximation is applied, the Kelvin wave cannot exist for the lack of rotational effect.

Understanding of the coastal Kelvin waves is important to our

knowledge of the coastal physics. Tidal waves occur as the form of Kelvin wave because of the energy transfer when an incident Poincare wave interacts with the coast. This has been verified by the field data analysis and various mechanisms have been proposed by Crease, Pinsent, Howe and Mysak, and other authors.

6.2 Dispersion Relation and Nonlinear Evolution Equations

Just like its equatorial counterpart, a coastal Kelvin wave is nondispersive. The paper of Bennett, the first paper which discuss the nonlinearity of coastal Kelvin wave, concluded with a one-dimensional advection equation with forcing terms. Since the nonlinearity will accumulate, this equation predicts that a coastal Kelvin wave will inevitably break.

However, this is true only when the bathymetry is not considered. If the wave length is very long, the dispersion relation can be derived by perturbation method with the wavenumber k serving as the parameter. This has been performed by R. Smith on 1972 and the result is quite similar to the paper of Grimshaw [1974] on the study of edge waves. That is, the dispersion for the wave velocity is quadratic in k with a parameter similar to $\mathcal{A}$ of Grimshaw's paper.

The fact that the dispersion of both long coastal Kelvin wave and long edge wave is exactly the same as that of KdV equation is not surprising. As has been pointed out by R. S. Johnson [1976], the long wave limit of NLS theory should be derived from KdV equation. Therefore, the KdV equation is a good model for very long waves. Since the nonlinear term of the one-dimensional advection equation is also the same as that of the KdV, we conclude that the long coastal Kelvin wave is governed by a KdV equation.

However, the envelope evolution equation, possibly an NLS, for a coastal Kelvin wave or an edge wave, cannot be derived directly from the KdV because the quadratic dispersion relation is not generally valid for all wavenumber k, as the case of equatorial wave does. A more recent study on the topic of nonlinear coastal Kelvin wave can be found in Fedorov and Melville [1995].

Chapter 7

Discussion

7.1 Shallow Water Equation and the Korteweg-de Vries (KdV) Equation

As has been mentioned above, the long wave limit of various waves can be represented by the Korteweg-de Vries (KdV) equation. Since our mathematical model , the shallow water equation , is valid only when the wave length is much longer than the depth, one may ask if the KdV (or KP) equation can be directly applied for any wave on the shallow water equation?

The answer is not. Take equatorial wave as an example. We do have shown that KdV is a good model for Kelvin waves. However, other equatorial waves based on the same shallow water equation, i.e. Rossby waves, gravity waves, and mixed Rossby-gravity waves, can be represented by the KdV equation only for very long period. The NLS of their wave packet evolution cannot be derived from their KdV equation.

7.2 Simplified Method in Determining the Nonlinear Coefficient of the Korteweg-de Vries (KdV) Equation

The formal method of deriving the nonlinear coefficient in an evolution equation is by perturbation, either the multiple-scale method or the strained coordinates method. However, a simplified method of determining the nonlinear coefficient for Kelvin-KdV has been

proposed by Ripa [1982]:

The increase of celerity due to a finite amplitude wave is $\eta/2$ which is just $U/2$ for Kelvin waves where the surface elevation η equals the fluid velocity U. Besides, the Kelvin wave advects itself and hence the total increase of the celerity is $\frac{3}{2}U$. This implies if the evolution equation (KdV) is obtained from the dispersion relation , the nonlinear coefficient will be $\frac{3}{2}$. However, since the KdV equation is one-dimensional while the physics is two-dimensional, we have to average the variation along the wave front. This averaging gives the nonlinear coefficient $\sqrt{\frac{3}{2}}$ for equatorial Kelvin waves and the nonlinear coefficient 1 for coastal Kelvin waves. This is consistent with the results of previous chapters.

7.3 Simplifies Method in Deriving the NLS from the Dispersion Relation

The method discussed in section 3.2 shows how to derive the nonlinear from the dispersion relation in a simple and clear way. In fact, we can derive the nonlinear dispersion relation for a periodic wave from this method. For example, the Kelvin-NLS derived in the thesis of Chen :

$$i(A)_\tau - \frac{1}{16\,\tilde{\omega}_2\,k}|A|^2A + 3\,\tilde{\omega}_2\,k\,(A)_{\zeta\zeta} = 0, \tag{7.1}$$

implies

$$\left(\frac{\partial\Omega}{\partial a^2}\right)_0 = -\frac{1}{16\,\tilde{\omega}_2\,k} \tag{7.2}$$

and

$$\frac{1}{2}\left(\frac{\partial^2\Omega}{\partial k^2}\right)_0 = 3\,\tilde{\omega}_2\,k. \tag{7.3}$$

Consequently, the nonlinear dispersion relation for equatorial Kelvin can be obtained as

$$\omega = \tilde{\omega}_2\,k^3 - \frac{1}{16\,\tilde{\omega}_2\,k}\,a^2. \tag{7.4}$$

However, this method cannot be applied to all nonlinear wave problems. The first problem is, the derivation of the nonlinear dispersion relation usually is as tedious as the derivation of the

NLS. The second reason is that this method consider only the self-interaction of the wave mode we discuss. Sometimes the nonlinear interaction with other modes is comparable with the self-interaction and hence we have to include all possible modes in the nonlinear term computation. This does happen in the derivation of the equatorial Rossby, Yani, and gravity waves. Therefore, this method should be used with care.

7.4 Notes on the Nonlinear Coefficients due to Change of Variables

The dispersive term of the nonlinear evolution equation is obtained from the linear dispersion relation and can be universally applied. However, some care has to be taken when we deal with the nonlinear coefficient, as has been stated in the previous section.

If fact, in the actual nonlinear coefficient computation, there is something else to be noted. Since the nonlinear term of the KdV and KP equations is quadratic and that in the NLS is cubic comparing to other terms, these coefficient is subject to change when the unknown variable changes.

For example, in the equatorial Kelvin-KdV equation, the nonlinear coefficient is halved when we change the variable from u to $u+\phi$. In the NLS of edge waves, the same situation occurs: Akylas, Yeh, and Sabatier all derived an NLS for the Stokes mode edge waves. However, they use different variables. Therefore, these three NLS's have the same dispersive term, but the nonlinear terms are different.

Chapter 8

Numerical Experiments

In these four waves discussed above, the Stokes wave had been thoroughly investigated and a lot of experiments have been done, say, by Benjamin and Feir, Yuen and Lake, and others. Therefore, the verification of the theory seems to be of little problem.

Some edge wave experiments can be found in papers by, say, Ursell, Guza and his colleagues, and Yeh and his group. But the experiment on the bathymetric variation is still unavailable. For equatorial and coastal Kelvin waves, controlled physical experiment is difficult or even impossible. Therefore, it is desirable to have some numerical experiments to compare with the theory. In the following, three models are introduced for the last three waves.

8.1 Mike21 HD Model

The Mike21 is a collective of two-dimensional models developed by the DHI. Among these the Mike21 HD model and the Mike21 BW model can deal with nonlinear problems. The Mike21 HD model is a two-dimensional hydrodynamic model based on the primary governing equations. This model also includes Coriolis force and hence are perfect to simulate the coastal Kelvin wave.

8.2 Mike21 BW Model

The BW model is an extention to the conventional Boussinesq equation. Therefore, it can be applied not only in the shallow water, but also in the deeper water. For waves in deeper water, a deep water

term (DWT) has to be included. The detail of the theory can be found in a series of papers by Madsen and his colleagues.

The feature of an edge wave is that its amplitude is not uniform along the wave front. Therefore, some skills have to be applied to provide appropriate boundary conditions that the desired edge wave can be generated. In the following, we will discuss how to generate edge waves in the Mike21 BW model.

Generating Edge Waves through the Internal Generation Lines

The internal generation line provided by the BW model does allow the wave amplitude to be nonuniform along the line. However, this function has to be applied only with some specific wave spectrum, like Pierson-Moskowitz or Jonswap spectra. Therefore, we cannot arbitrarily change the amplitude of wave.

However, since this model allows at most eight generation lines, we can make a wave that has different amplitude for the eight section of the wave front and hence looks like an edge wave.

Generating Edge Waves through the Flux Boundary Condition

This approach is possible only when the deep water term (DWT) is not included. The DWT has a higher spatial derivative and hence need more boundary conditions.

Note that the BW model is intended to be applied not only in the shallow water, but also in the deeper water. When

$$0.22 \leq \frac{D_{min}}{L_{min}} \leq 0.5,$$

the deep-water term (DWT) has to be added to the model. When

$$\frac{D_{min}}{L_{min}} \leq 0.22,$$

this term is not necessary. Therefore, the minimum depth D_{min} in our numerical experiment should be as small as possible.

Since BW is a two-dimensional model, the flux boundary condition instead of the Neuman boundary condition (normal derivative of the surface elevation) has to be given. That is, for the incident

wave, we have to multiply the velocity of Eckhaus's theory by the local water depth to obtain the desired flux. For other open boundaries, the sponge layer is applied which is a convenient substitute for the radiation boundary condition.

8.3 Spectral Method Model to Simulate Equatorial Kelvin Waves

Commercial packages utilize either the finite element or the finite difference method that they can easily deal with irregular geometries. For equatorial waves, however, we do not have to worry about depth variation if the "one-and-a-half" model is adopted. Besides, except at both ends of the ocean which is far from the place of interest, the wave is not affected by the boundary. Therefore, the boundary treatment is quite easy.

There do exist some islands near the equator. But their sizes are very small compared with the typical wave length and hence their existence can be neglected.

The spectral method is appropriate to the study of wave properties when complicated computational space geometry is not required. Some benefits of the spectral method are that it is:

1. more accurate and efficient,
2. easy to treat higher-order derivatives,
3. easy for physical interpretation, and
4. easy to handle periodic boundary conditions, or any boundary condition that is satisfied by the basis functions.

If face, for the problem of wave evolution at an infinitely wide ocean, it is a good policy to replace the infinite boundary by the periodic boundary condition. Therefore, the spectral method is a reasonable choice to simulate equatorial Kelvin waves.

8.3.1 Model Set-up

Based on the equatorial shallow water equations with the β-plane approximation, a spectral model can be set up. There are two assumptions:

1. The model is symmetric with respect to equator for zonal velocity. Therefore, the computational domain can be halved.

2. The model is periodic in the zonal direction; thus, the boundary condition is automatically satisfied by the basis functions.

Besides, hyperviscosity is applied every five hundred timesteps to stabilize the model.

8.3.2 Numerical Experiments

The first numerical experiment performed is a Kelvin wave propagating without shear background flow. The wave will break in 40 days even when the wave amplitude is just one-tenth of the thermocline depth.

Then we add shear background flow to the same problem. The wave will not break. Instead, two solitary waves are generated. These two solitons may collide without changing forms.

The third experiment is to give a Kelvin wave packet as the initial condition. After some initial adjustment, this wave packet propagates steadily with its amplitude decays slowly. These experiments show that our theory gives a good description to the equatorial Kelvin waves.

Appendix A

Detailed Derivation of Stokes Waves

For water waves propagation over an infinite sea, the two-dimensional Laplace equation

$$(\frac{\partial^2}{\partial x^2}\phi(x,\,z,\,t)) + (\frac{\partial^2}{\partial z^2}\phi(x,\,z,\,t)) = 0 \tag{A.1}$$

and both the dynamic and the combined free surface boundary conditions:

$$g\,\zeta(x,\,t) + (\frac{\partial}{\partial t}\phi(x,\,z,\,t)) + \frac{1}{2}(\frac{\partial}{\partial x}\phi(x,\,z,\,t))^2 + \frac{1}{2}(\frac{\partial}{\partial z}\phi(x,\,z,\,t))^2 \tag{A.2}$$

$$\begin{aligned}(\frac{\partial^2}{\partial t^2}\phi(x,\,z,\,t)) + g\,(\frac{\partial}{\partial z}\phi(x,\,z,\,t)) + (\frac{\partial}{\partial t}\mathrm{u}^2(x,\,z,\,t)) \\ +\frac{1}{2}(\frac{\partial}{\partial x}\phi(x,\,z,\,t))(\frac{\partial}{\partial x}\mathrm{u}^2(x,\,z,\,t)) \\ +\frac{1}{2}(\frac{\partial}{\partial z}\phi(x,\,z,\,t))(\frac{\partial}{\partial z}\mathrm{u}^2(x,\,z,\,t)) = 0\end{aligned} \tag{A.3}$$

has to be satisfied.

The boundary condition at the sea bottom is that ϕ approaches zero as z approaches $-\infty$. Besides these three condition, we also assume the wave is periodic. That is, the lowest order solution is a linear sinusoidal wave.

This problem has been exhaustively investigated and the solution can be found in most textbooks on water waves. However, we decide

to redo this problem because the procedure can be applied to the nonlinear edge wave problem. Besides, since this is the simplest nonlinear wave problem, it is a good exercise and is very helpful for the understand of nonlinear phenomena.

As the first step, we perturb the solution as

$$\phi = \varepsilon\,\phi 1(x,\,z,\,t) + \varepsilon^2\,\phi 2(x,\,z,\,t) + \varepsilon^3\,\phi 3(x,\,z,\,t) + \varepsilon^4\,\phi 4(x,\,z,\,t) \tag{A.4}$$

$$\zeta = \varepsilon\,\zeta 1(x,\,t) + \varepsilon^2\,\zeta 2(x,\,t) + \varepsilon^3\,\zeta 3(x,\,t) + \varepsilon^4\,\zeta 4(x,\,t), \tag{A.5}$$

where ε is much smaller than one. Then after perturbing the free surface boundary conditions, we can solve this problem order by order.

First Order Solution

The perturbative governing equation and boundary conditions are

$$(\frac{\partial^2}{\partial x^2}\,\phi 1(x,\,z,\,t)) + (\frac{\partial^2}{\partial z^2}\,\phi 1(x,\,z,\,t)) = 0 \tag{A.6}$$

$$(\frac{\partial^2}{\partial t^2}\,\phi 1(x,\,z,\,t)) + g\,(\frac{\partial}{\partial z}\,\phi 1(x,\,z,\,t)) = 0 \tag{A.7}$$

$$g\,\zeta 1(x,\,t) + (\frac{\partial}{\partial t}\,\phi 1(x,\,z,\,t)) = 0. \tag{A.8}$$

The formal procedure for solving this boundary value problem is to solve the Laplace equation by separation of variables. By assuming a periodic wave form

$$\zeta 1(x,\,t) = a\cos(k\,x - \omega\,t) \tag{A.9}$$

the lowest order velocity potential can be derived via the dynamic boundary condition as

$$\phi 1(x,\,z,\,t) = \frac{a\,g\,e^{(k\,z)}\sin(k\,x - \omega\,t)}{\omega}. \tag{A.10}$$

The dispersion relation then is obtained via the combined boundary condition and the result is

$$\omega = \omega_0 = \sqrt{g\,k}. \tag{A.11}$$

However, for a nonlinear wave, this solution cannot be extended to higher orders. It had been observed by G. G. Stokes that the

velocity of a nonlinear wave is a function of the wave amplitude. Therefore, we have to include this amplitude dependence and assume a dispersion relation as

$$\omega = \omega_0 (1 + a^2 \varepsilon^2 \lambda), \tag{A.12}$$

where λ is an unknown constant. This is to avoid secularity in the higher orders. That is, we must choose perturbation of wave velocity to cancel any forcing of wavenumber k in the right hand side of higher order equations.

After applying this new ω, we have

$$\zeta 1(x, t) = a \cos(k x - \omega_0 (1 + a^2 \varepsilon^2 \lambda) t), \tag{A.13}$$

$$\phi 1(x, z, t) = \frac{a g e^{(k z)} \sin(k x - \omega (1 + a^2 \varepsilon^2 \lambda) t)}{\omega_0 (1 + a^2 \varepsilon^2 \lambda)}. \tag{A.14}$$

Second Order Solution

The perturbative governing equation and boundary conditions are

$$(\frac{\partial^2}{\partial x^2} \phi 2(x, z, t)) + (\frac{\partial^2}{\partial z^2} \phi 2(x, z, t)) = 0 \tag{A.15}$$

$$g \zeta 2(x, t) + (\frac{\partial}{\partial t} \phi 2(x, z, t)) + \frac{1}{2} (\frac{\partial}{\partial x} \phi 1(x, z, t))^2$$
$$+ (\frac{\partial^2}{\partial z \partial t} \phi 1(x, z, t)) \zeta 1(x, t) + \frac{1}{2} (\frac{\partial}{\partial z} \phi 1(x, z, t))^2 = 0 \tag{A.16}$$

$$g (\frac{\partial}{\partial z} \phi 2(x, z, t)) + ((\frac{\partial^3}{\partial z \partial t^2} \phi 1(x, z, t)) + g (\frac{\partial^2}{\partial z^2} \phi 1(x, z, t))) \zeta 1(x, t)$$
$$+ 2 (\frac{\partial}{\partial z} \phi 1(x, z, t)) (\frac{\partial^2}{\partial z \partial t} \phi 1(x, z, t)) + (\frac{\partial^2}{\partial t^2} \phi 2(x, z, t)) = 0 \tag{A.17}$$

The solutions can be easily verified as

$$\zeta 2(x, t) = \frac{1}{2} k a^2 \cos(2 k x - 2 \omega_0 (1 + a^2 \varepsilon^2 \lambda) t), \tag{A.18}$$

$$\phi 2(x, z, t) = 0. \tag{A.19}$$

Third Order Solution

The perturbative governing equation and dynamic boundary condition are

$$(\frac{\partial^2}{\partial x^2}\,\phi 3(x,\,z,\,t)) + (\frac{\partial^2}{\partial z^2}\,\phi 3(x,\,z,\,t)) = 0 \qquad \text{(A.20)}$$

$$(\frac{\partial}{\partial t}\,\phi 3(x,\,z,\,t)) + (\frac{\partial}{\partial z}\,\phi 1(x,\,z,\,t))\,(\frac{\partial}{\partial z}\,\phi 2(x,\,z,\,t))$$

$$+(\frac{\partial}{\partial x}\,\phi 1(x,\,z,\,t))\,(\frac{\partial}{\partial x}\,\phi 2(x,\,z,\,t)) + \frac{1}{2}\,(\frac{\partial^3}{\partial z^2\,\partial t}\,\phi 1(x,\,z,\,t))\,\zeta 1(x,\,t)^2$$

$$+(\frac{\partial^2}{\partial z\,\partial t}\,\phi 1(x,\,z,\,t))\,\zeta 2(x,\,t) + ((\frac{\partial}{\partial z}\,\phi 1(x,\,z,\,t))\,(\frac{\partial^2}{\partial z^2}\,\phi 1(x,\,z,\,t))$$

$$+(\frac{\partial}{\partial x}\,\phi 1(x,\,z,\,t))\,(\frac{\partial^2}{\partial z\,\partial x}\,\phi 1(x,\,z,\,t))$$

$$+(\frac{\partial^2}{\partial z\,\partial t}\,\phi 2(x,\,z,\,t)))\zeta 1(x,\,t) + g\,\zeta 3(x,\,t) = 0 \qquad \text{(A.21)}$$

Obviously, the Laplace equation is satisfied by the solution

$$\phi 3 = 0. \qquad \text{(A.22)}$$

Substituting $\phi 3$ and the lower order solutions into the dynamic boundary condition, we have

$$\zeta 3 = \frac{3}{8}\,a^3\,k^2\cos(3\,k\,x - 3\,\omega\,t) - \frac{3}{8}\,a^3\,k^2\cos(k\,x - \omega\,t). \qquad \text{(A.23)}$$

The combined boundary condition after expanding the free surface with respect to $z = 0$ is

$$2\,(\frac{\partial}{\partial x}\,\phi 1(x,\,z,\,t))\,(\frac{\partial}{\partial z}\,\phi 1(x,\,z,\,t))\,(\frac{\partial^2}{\partial z\,\partial x}\,\phi 1(x,\,z,\,t))$$

$$+g\,(\frac{\partial}{\partial z}\,\phi 3(x,\,z,\,t)) + (\frac{\partial}{\partial x}\,\phi 1(x,\,z,\,t))^2\,(\frac{\partial^2}{\partial x^2}\,\phi 1(x,\,z,\,t))$$

$$+((\frac{\partial^3}{\partial z\,\partial t^2}\,\phi 1(x,\,z,\,t)) + g\,(\frac{\partial^2}{\partial z^2}\,\phi 1(x,\,z,\,t)))\,\zeta 2(x,\,t)$$

$$+((\frac{\partial^3}{\partial z\,\partial t^2}\,\phi 2(x,\,z,\,t)) + 2\,(\frac{\partial^2}{\partial z\,\partial x}\,\phi 1(x,\,z,\,t))\,(\frac{\partial^2}{\partial x\,\partial t}\,\phi 1(x,\,z,\,t))$$

$$+g\,(\frac{\partial^2}{\partial z^2}\,\phi 2(x,\,z,\,t)) + 2\,(\frac{\partial}{\partial z}\,\phi 1(x,\,z,\,t))\,(\frac{\partial^3}{\partial z^2\,\partial t}\,\phi 1(x,\,z,\,t))$$

$$
\begin{aligned}
&+2\,(\frac{\partial^2}{\partial z^2}\,\phi 1(x,\,z,\,t))\,(\frac{\partial^2}{\partial z\,\partial t}\,\phi 1(x,\,z,\,t)) \\
&+2\,(\frac{\partial}{\partial x}\,\phi 1(x,\,z,\,t))\,(\frac{\partial^3}{\partial z\,\partial x\,\partial t}\,\phi 1(x,\,z,\,t)))\zeta 1(x,\,t) \\
&+2\,(\frac{\partial}{\partial z}\,\phi 1(x,\,z,\,t))\,(\frac{\partial^2}{\partial z\,\partial t}\,\phi 2(x,\,z,\,t)) \\
&+2\,(\frac{\partial}{\partial z}\,\phi 2(x,\,z,\,t))\,(\frac{\partial^2}{\partial z\,\partial t}\,\phi 1(x,\,z,\,t)) \\
&+2\,(\frac{\partial}{\partial x}\,\phi 1(x,\,z,\,t))\,(\frac{\partial^2}{\partial x\,\partial t}\,\phi 2(x,\,z,\,t)) \\
&+2\,(\frac{\partial}{\partial x}\,\phi 2(x,\,z,\,t))\,(\frac{\partial^2}{\partial x\,\partial t}\,\phi 1(x,\,z,\,t)) \\
&+(\frac{\partial^2}{\partial t^2}\,\phi 3(x,\,z,\,t)) + (\frac{\partial}{\partial z}\,\phi 1(x,\,z,\,t))^2\,(\frac{\partial^2}{\partial z^2}\,\phi 1(x,\,z,\,t)) \\
&+(\frac{1}{2}\,g\,(\frac{\partial^3}{\partial z^3}\,\phi 1(x,\,z,\,t)) + \frac{1}{2}\,(\frac{\partial^4}{\partial z^2\,\partial t^2}\,\phi 1(x,\,z,\,t)))\,\zeta 1(x,\,t)^2 = 0
\end{aligned}
\tag{A.24}
$$

However, since ω has been expanded with respect to a, the lowest order combined boundary condition is satisfied only to the second order. At the third order, a residue

$$
-2\,\frac{g^2\,a^3\sin(k\,x-\omega\,t)\,k\,\lambda}{\omega_0} \tag{A.25}
$$

will exist. After adding this residue to the third order combined boundary condition and substituting lower order solutions, we have

$$
-\frac{1}{2}\,\frac{k\,g^2\,a^3\,(4\sin(k\,x-\omega\,t)\,\lambda - 2\,k^2\sin(k\,x-\omega\,t))}{\omega_0} = 0. \tag{A.26}
$$

Consequently,

$$
\lambda = \frac{1}{2}\,k^2 \tag{A.27}
$$

and the dispersion relation up to the second order is derived as

$$
\omega = \sqrt{g\,k}(1 + \frac{1}{2}a^2k^2). \tag{A.28}
$$

Note that the parameter ϵ is no longer needed to order the magnitude and can be taken to be one. The amplitude a are now much smaller than one for the consistency of this theory.

Appendix B

Detailed Derivation from KdV to NLS

The KdV equation can be written in the general form as

$$A_t + \beta\, A\, A_z + \gamma\, A_{zzz} = 0. \tag{B.1}$$

In the following, we will try to derive the narrow-banded solution via the singular perturbation method. The only small parameter is ϵ which represents the wave amplitude. Therefore, every quantity is expanded in ϵ and the slow space and time variables are defined as

$$\zeta = \epsilon(z - c_g t), \tag{B.2}$$

$$\tau = \epsilon^2 t. \tag{B.3}$$

These assumptions are associated with the following chain rules:

$$\frac{\partial}{\partial t} = \frac{\partial}{\partial t} - \epsilon c_g \frac{\partial}{\partial \zeta} + \epsilon^2 \frac{\partial}{\partial \tau}, \tag{B.4}$$

$$\frac{\partial}{\partial z} = \frac{\partial}{\partial z} + \epsilon \frac{\partial}{\partial \zeta}. \tag{B.5}$$

We then assume the solution form of A as

$$A = \epsilon \sum_{q=0}^{\infty} \epsilon^q \sum_{r=0}^{q+1} A_{qr}(\zeta, \tau) E^r + c.c., \tag{B.6}$$

where

$$E(z,t) = e^{i[kz - w(k)t]}. \tag{B.7}$$

After applying the solution form and chain rules, the KdV equation (B.1) can be solved. It should be noted that

$$A_{00} = A_{00}^* = 0$$

because the leading order is assumed to be narrow-banded.

In the following, we will solve the perturbative equation order by order.

$O(\epsilon^1 E^1)$

The lowest-order equation is

$$-i\,A_{01}\,(\,\gamma\,k^3 + \omega\,) = 0, \tag{B.8}$$

hence

$$\omega = -\gamma\,k^3. \tag{B.9}$$

This is the dispersion relation which is quadratic for the variation of wave velocity.

$O(\epsilon^2 E^2)$

The next order equation

$$-6\,i\,\gamma\,k^3\,A_{12} + i\,\beta\,k\,(A_{01})^2 = 0 \tag{B.10}$$

has the solution

$$A_{12} = \frac{\beta}{6\,\gamma\,k^2}\,(A_{01})^2 \tag{B.11}$$

which is known as the second harmonic amplitude.

$O(\epsilon^3 E^0)$

The solution to the $O(\epsilon^3 E^0)$ equation

$$3\,\gamma\,k^2\,(A_{10})_\zeta + \beta\,A_{01}\,(A_{01}^*)_\zeta + \beta\,A_{01}^*\,(A_{01})_\zeta = 0 \tag{B.12}$$

is

$$A_{10} = -\frac{\beta}{3\gamma\,k^2} A_{01} A_{01}^*. \tag{B.13}$$

This is called the long wave amplitude. The minus sign of (B.12) indicates the set-down of the mean water level which is due to the radiation stress.

Note that both second harmonic and long wave are proportional to the quadratic of the lowest-order wave amplitude and inversely proportional to the group velocity.

$\mathrm{O}(\epsilon^3 E^1)$

The perturbative equation of $\mathrm{O}(\epsilon^3 E^1)$ gives the NLS equation

$$i(A_{01})_\tau - 3\gamma k (A_{01})_{\zeta\zeta} + \frac{1}{6}\frac{\beta^2}{\gamma k} A_{01}^* (A_{01})^2 = 0. \tag{B.14}$$

The dispersion coefficient is just $\left(\frac{1}{2}\omega''(k)\right)$ because $\omega = -\gamma k^3$ by equation (B.9).

Let the nonlinear coefficient be the Landau constant ν, i.e.

$$\nu \equiv -\frac{1}{6}\frac{\beta^2}{\gamma k}, \tag{B.15}$$

then

$$\frac{1}{2}\omega''(k) = -\frac{\beta^2}{2\nu} = -\frac{0.1875}{\nu} \tag{B.16}$$

This NLS do not have soliton solutions.

Appendix C

Why Envelope Solitary Wave Does not Exist When $(\omega''(k))(\nu) < 0$?

Solitary wave solutions exist for the NLS equation only when the product $(\omega''(k))(\nu)$ is positive. The reason can be briefly explained, both physically and mathematically, in the following.

Physical Explanation

In quantum mechanics, the nonlinear Schrödinger equation

$$i(A_{01})_\tau + \nu|A_{01}|^2 A_{01} + \frac{1}{2}\omega_2''(k)\,(A_{01})_{\zeta\zeta} = 0 \qquad \text{(C.1)}$$

corresponds to the governing equation of the probability density function with the potential energy proportional to $\left[\text{sgn}(\omega''(k))\nu|A_{01}|^2\right]$.

If $(\nu)\ \left(\omega''(k)\right) < 0$, potential energy < 0 everywhere. There is at least one bound state in which the system is focusing. However, if $(\nu)\ \left(\omega''(k)\right) > 0$, potential energy > 0 everywhere. There is no bound state; hence, the system is defocusing. Therefore, the existence of envelope solitary Kelvin wave is impossible.

Mathematical Explanation

If the envelope solitary wave exists, the envelope moves steadily without change of form. That is, the rate of change of the amplitude

A_{01} should be independent of the zonal coordinate ζ, or

$$\frac{\partial^2}{\partial\zeta\,\partial\tau}A_{01} = 0\,. \tag{C.2}$$

Differentiating the nonlinear Schrödinger equation (5.12) with respect to ζ, we obtain

$$i(A_{01})_{\tau\zeta} + \frac{1}{2}\omega''(k)\,(A_{01})_{\zeta\zeta\zeta} + \nu(|A_{01}|^2 A_{01})_\zeta = 0. \tag{C.3}$$

If the envelope solitary wave exists, this equation is simplified to

$$\frac{1}{2}\omega''(k)\,(A_{01})_{\zeta\zeta\zeta} + \nu(|A_{01}|^2 A_{01})_\zeta = 0 \tag{C.4}$$

by (C.2).

In general, the variable A_{01} is complex. However, to discuss if a solitary wave solution exists, we can assume A_{01} to be real and positive. This assumption is justified because an envelope solitary wave can always be represented by a positive amplitude A_{01} multiplied by a sinusoidal function. When this positive amplitude function A_{01} is imposed on the NLS as the initial condition, the envelope solitary wave can exist if, and only if, the NLS equation can keep A_{01} moving without change of form.

A feature of an envelope solitary wave is that the solution is smooth and localized. This implies $(A_{01})_{\zeta\zeta} > 0$ near the edge of the the envelope and $(A_{01})_{\zeta\zeta} < 0$ near the center of the the envelope. Therefore, on the positive ζ side of the envelope, the dispersive term $(A_{01})_{\zeta\zeta\zeta} > 0$. On the other hand, the amplitude decreases with ζ on the positive ζ side of the envelope, hence the nonlinear term $(|A_{01}|^2 A_{01})_\zeta < 0$. To satisfy equation (C.4), $\left(\frac{1}{2}\omega''(k)\right)$ and ν must be of the same sign.

For the Kelvin-NLS equation, the coefficients $\left(\frac{1}{2}\omega''(k)\right)$ and ν are of different signs. This means in any case equation (C.4) cannot be satisfied and hence the envelope solitary wave does not exist.

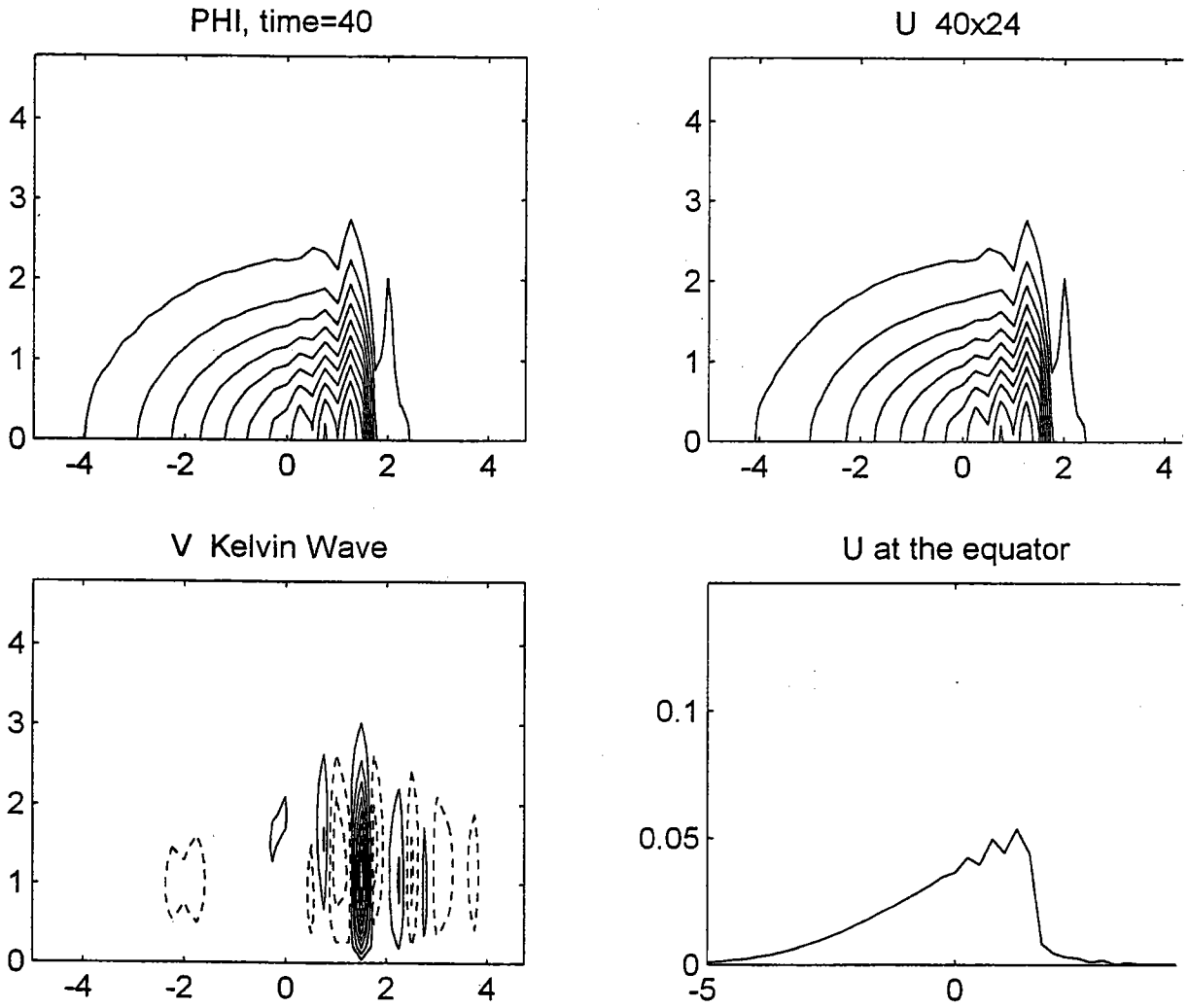

Figure 1: *An equatorial Kelvin wave without shear breaks at t=40*

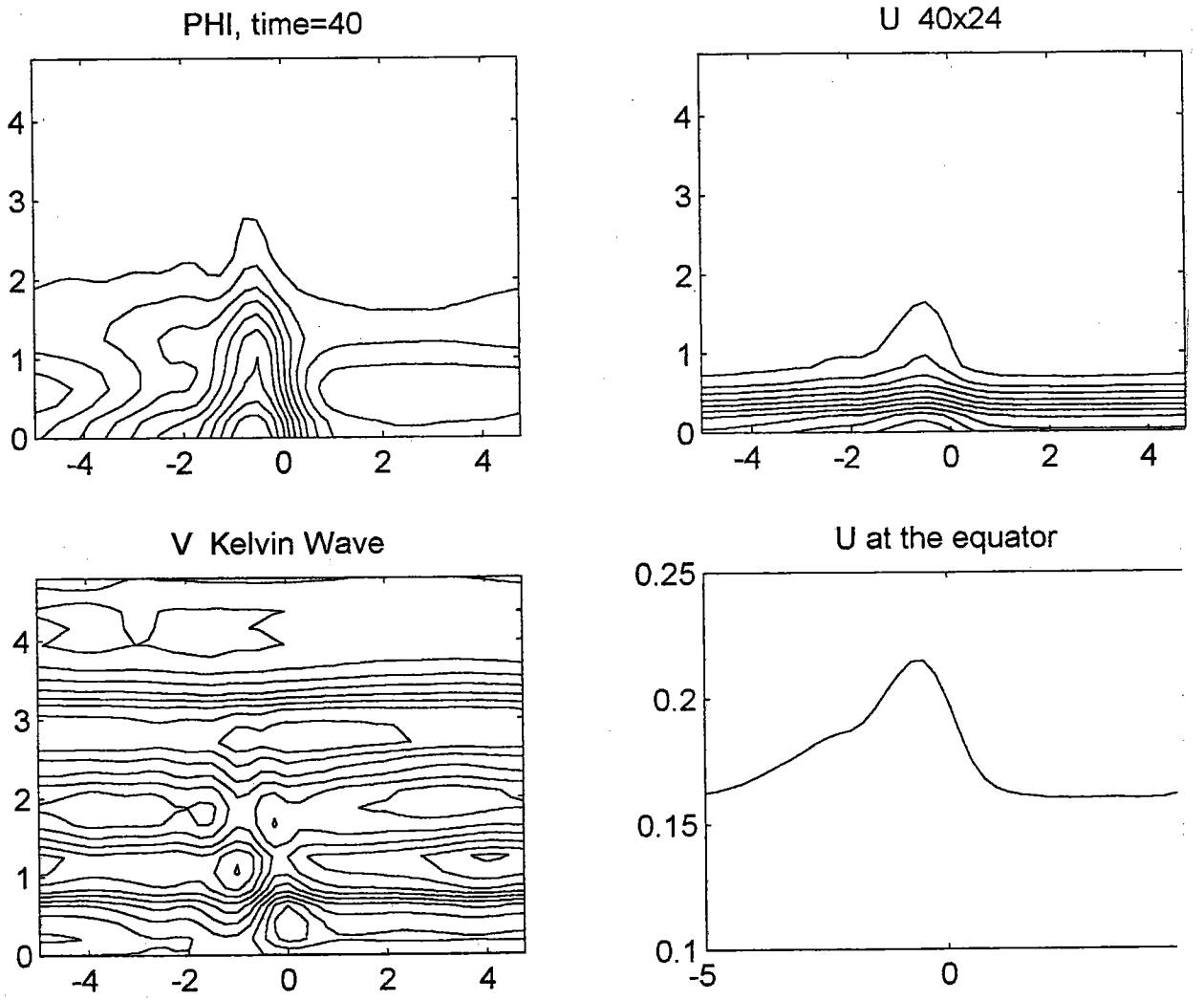

Figure 2: *An equatorial Kelvin wave with shear zonal mean flow does not break at t=40*

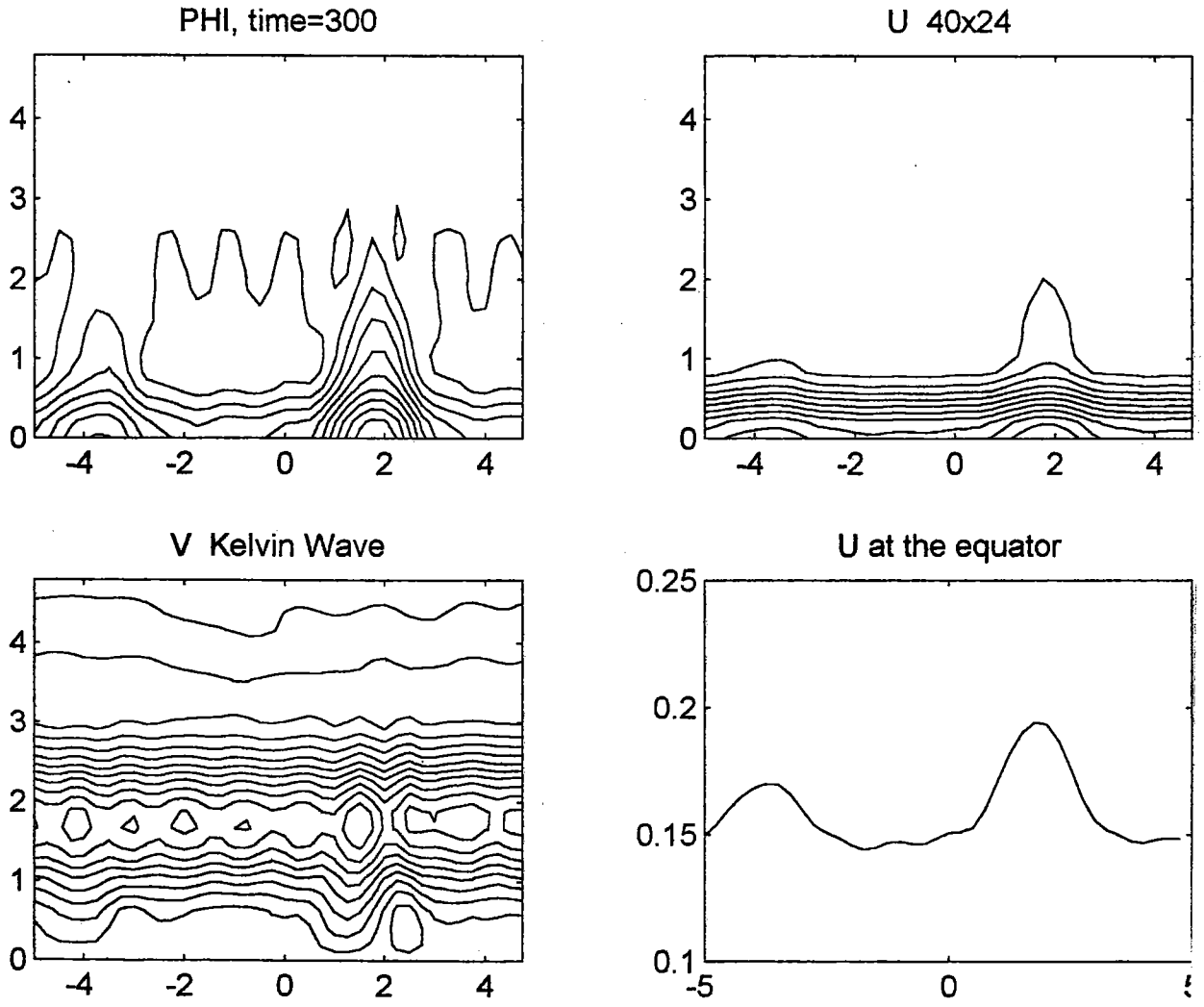

Figure 3: *An equatorial Kelvin wave with shear zonal mean flow evolves into two solitons.*

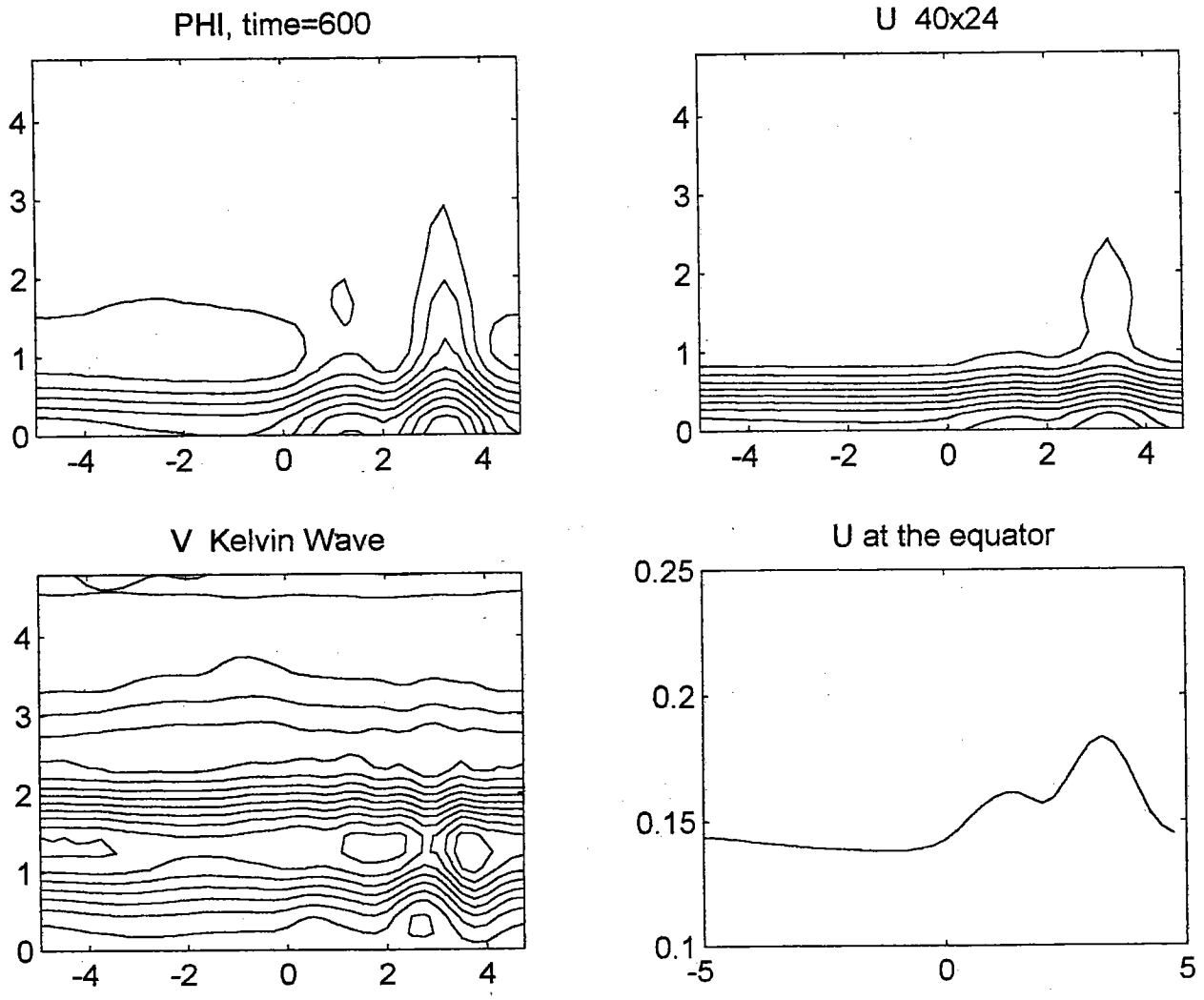

Figure 5: *Interaction of two solitons I*

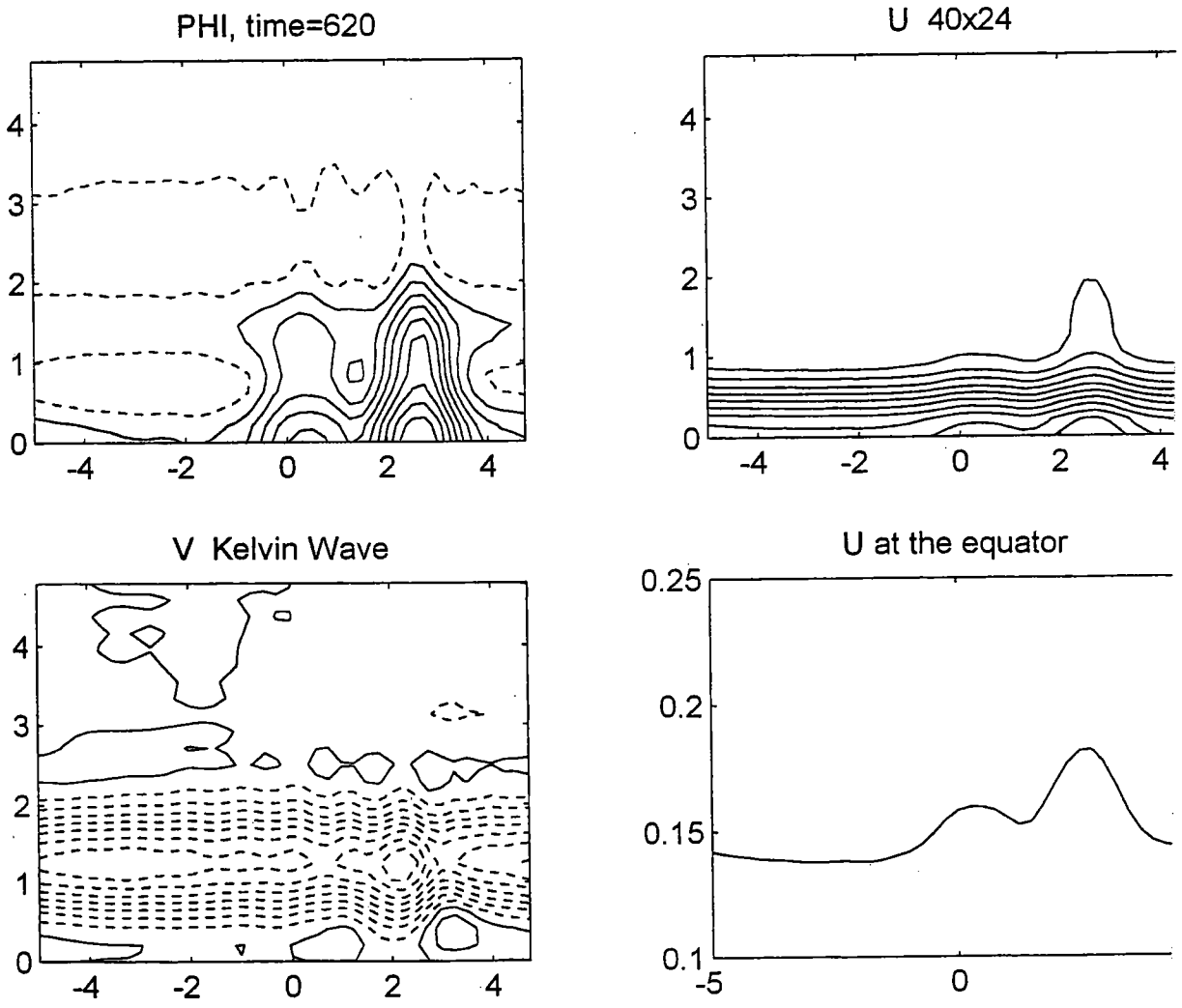

Figure 6: *Interaction of two solitons II*

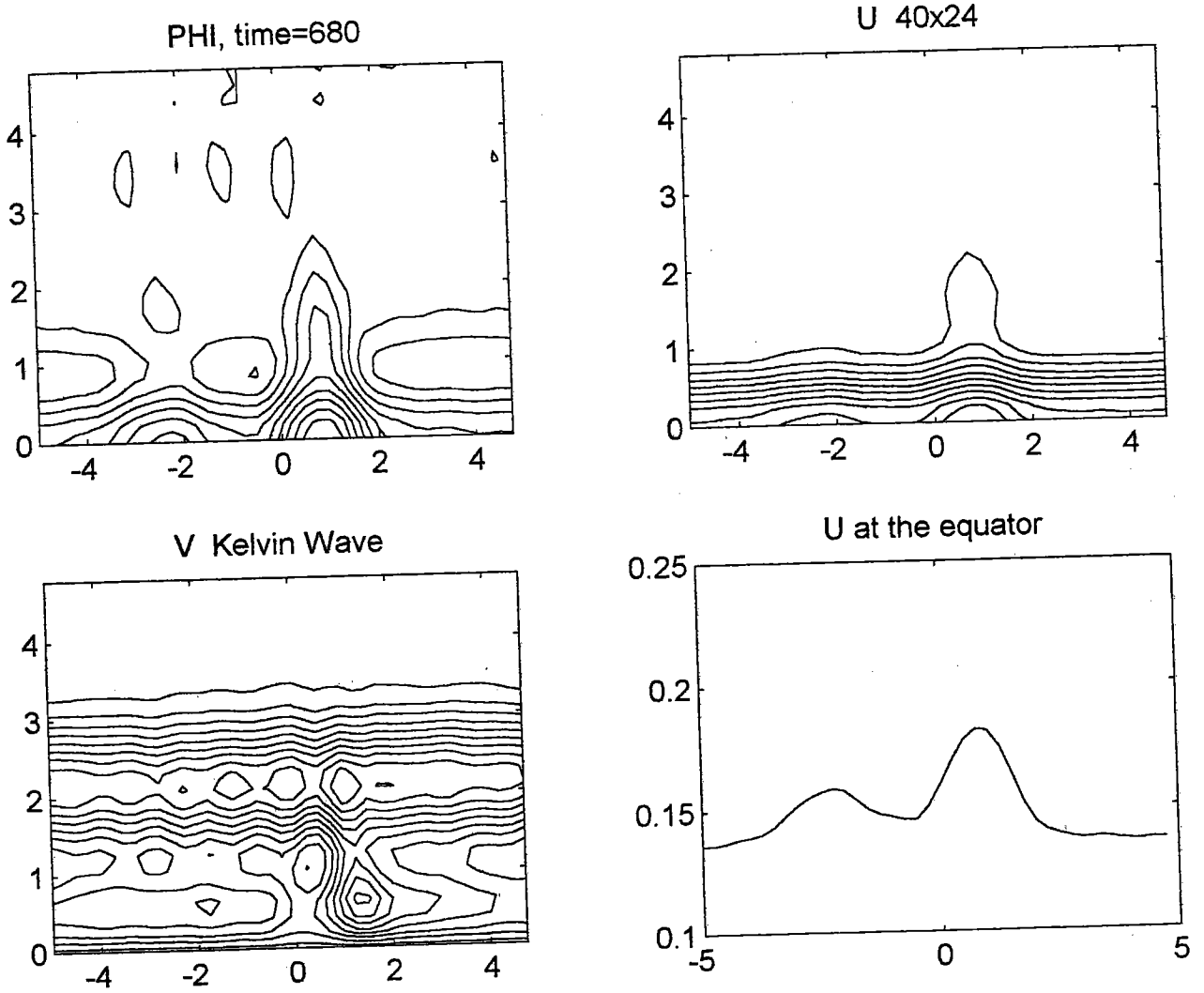

Figure 7: *Interaction of two solitons III*

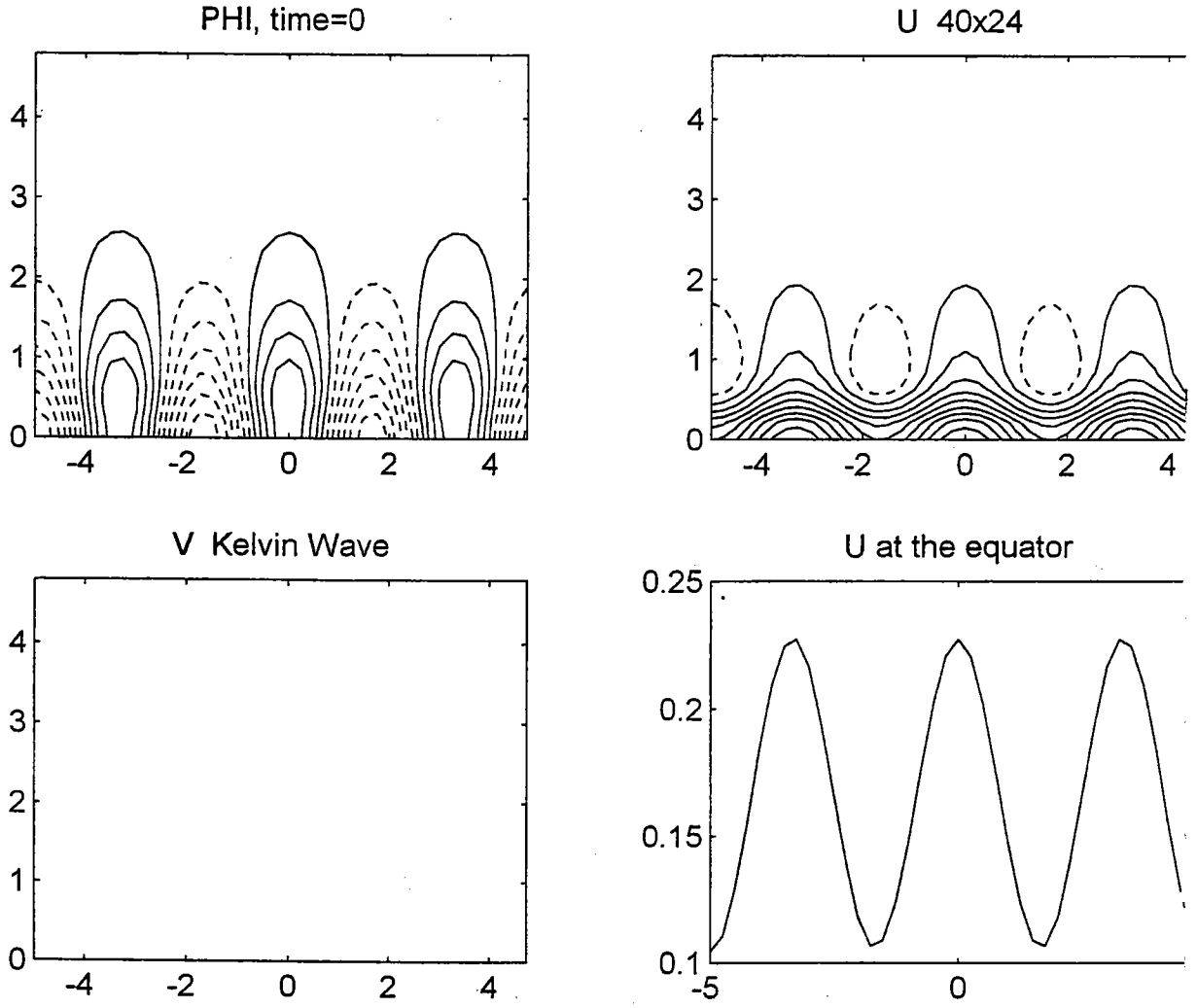

Figure 8: *Initial condition for a wave envelope*

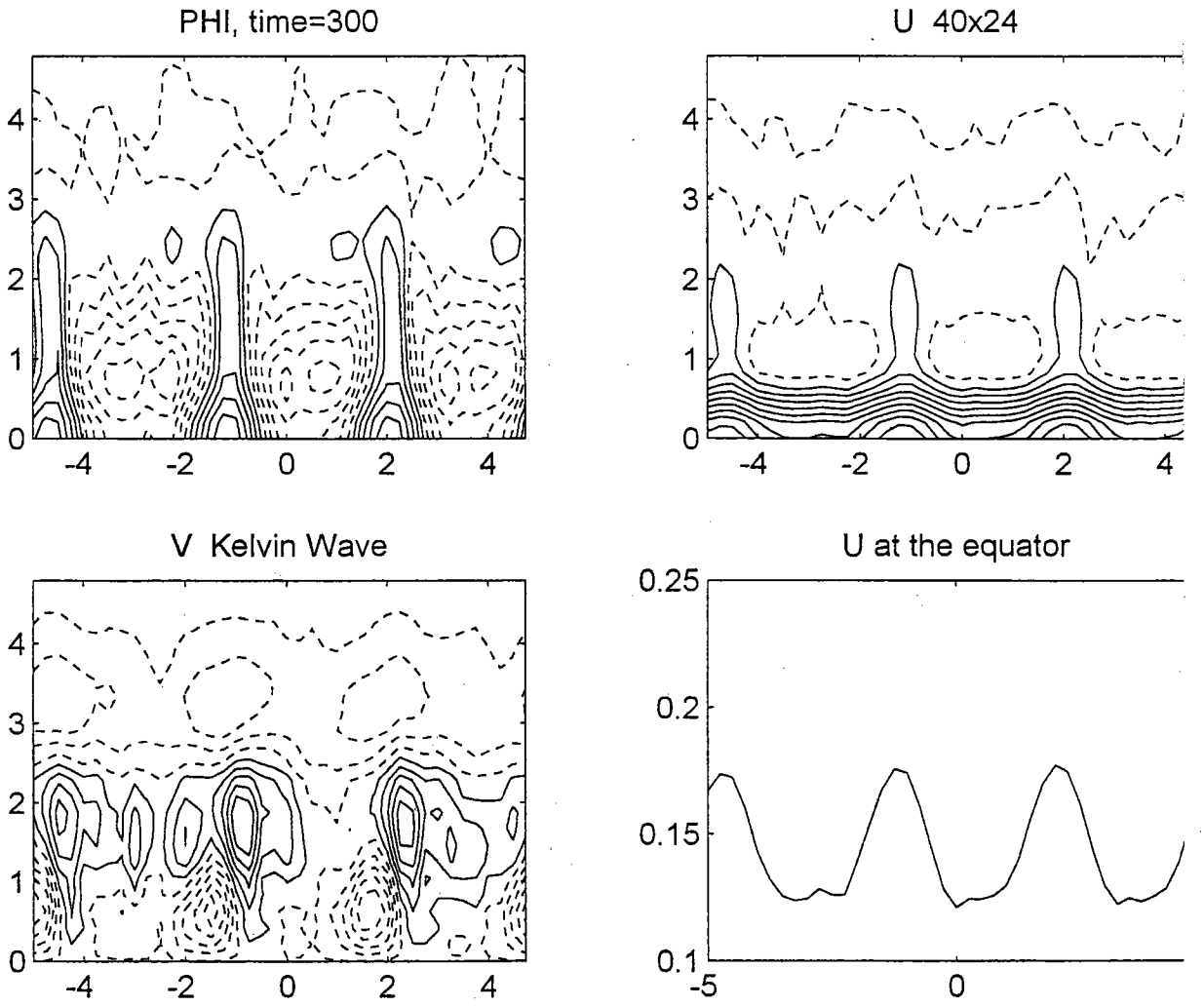

Figure 9: *The wave envelope after t=300*

非線性港池振盪數值模式研究

編輯者：蘇青和、劉立方、蔡丁貴、陳冠宇
發行人：張金機
發行所：台灣省政府交通處港灣技術研究所
台中縣梧棲鎮臨海路 83 號
電　話:：(04)6564216

中華民國 88 年出版，印製 50 本，非賣品